



united
TRIBES OF BRISTOL BAY



June 25, 2020

By Email and Post

Col. Phillip Hibner
District Commander
U.S. Army Corps of Engineers
P.O. Box 6898
JBER, Alaska 99506-0898
drafteis@comments.pebbleprojecteis.com
poaspecialprojects@usace.army.mil

RE: New Technical Information Relevant to the Environmental Review for the Pebble Mine

Dear Colonel Hibner:

We write to you on behalf of the undersigned member organizations (collectively, the “Bristol Bay Defense Alliance (“BBDA”)) regarding the United States Army Corps of Engineers’ (“USACE”) and the cooperating agencies’ environmental review under the National Environmental Policy Act (“NEPA”) for the Pebble Limited Partnership’s (“Pebble”) application to discharge fill material into waters of the United States for the purpose of developing a mine project in the Bristol Bay region of Alaska (the “Proposed Pebble Mine”). Specifically, we write to provide the USACE and the cooperating agencies with significant new information demonstrating that the analysis in the draft Environmental Impact Statement (“DEIS”)—and more recent supporting documentation provided by Pebble—fails to take the required hard look at seismic risks to the Proposed Pebble Mine and its massive tailings storage facilities (“TSFs” or “tailings dams”) and the impacts to the pristine Bristol Bay watershed.

A team of internationally recognized seismologists and geotechnical engineers who have consulted with governments and industry around the world made findings that include:

- The seismic studies conducted for the Proposed Pebble Mine are obsolete and are not adequate as basis for project environmental and permit review. Those studies use seismic models that are no longer in use and also failed to collect information about seismic activity at the location of the mine.
- Pebble’s tailings dam stability analysis drastically understates the risk related to dam stability because it falsely locates the water table in an impossible location far below the

tailings dam embankment. An earthen dam would present even greater stability concerns than a rockfill dam.

- Pebble’s technical proposal violates standard tailings dam construction practices by using waste rock from the mine for construction. The proposed design creates a grave risk of river acidification and metal contamination in the normal operation of the facility.

To further the USACE’s and cooperating agencies’ review, we present a state of the art new analysis by widely recognized seismic experts. The new analysis has been peer reviewed by leading experts and is based on the best available science of the seismic issues at the location of the Proposed Pebble Mine. Given the serious flaws in Pebble’s seismic hazard and tailings dam stability analyses for the Proposed Pebble Mine, this new analysis is the only credible information from which the USACE can evaluate seismic risks and the potential for and significant ecological impacts to the Bristol Bay watershed and its unrivaled salmon fishery from a catastrophic failure of the Proposed Pebble Mine’s massive tailings dams.

Beyond its ecological importance, the Bristol Bay salmon fishery generates immense economic value. Each year, the Bristol Bay commercial sockeye fishery generates revenue of \$1.2 billion and employs nearly 15,000 people in Alaska. The undersigned organizations comprising the BBDA will be directly affected by the Proposed Pebble Mine’s significant environmental impacts on their businesses, community, and way of life.

The BBDA requests that the USACE and the cooperating agencies meaningfully consider the information in this letter and its enclosures by issuing a Supplemental EIS that adequately discloses the seismic risks to the Proposed Pebble Mine’s critical infrastructure, including its massive TSFs, and the likely catastrophic environmental harm that would result.

I. Introduction

TSF failures constitute a significant risk for *any* mining tailings dam in the world, regardless of site-specific geography, geohazards, and ecological values. But the risks posed by the Proposed Pebble Mine are unique, profound, and demand thorough examination by regulators and the public. In the heart of the pristine Bristol Bay watershed—responsible for producing the largest salmon runs in the world and for supporting a world-class, sustainable salmon fishery—Pebble proposes constructing one of the world’s largest copper mines and highest earthen mine tailings impoundments to hold back toxic mine tailings waste in area with significant earthquake and other geohazards hazards. Given this reality, it should go without saying that proper NEPA environmental review of the Proposed Pebble Mine should undertake rigorous analysis of the serious potential for catastrophic failure of the Proposed Pebble Mine’s TSFs and the devastating impacts such failure would have on the sensitive ecosystem and its salmon fishery.

Unfortunately, the record before the USACE is replete with inaccuracies and is not sufficient to support the proper evaluation of the extreme seismicity in the Project area and related risks and impacts to the Proposed Pebble Mine's infrastructure and operations and surrounding environment. It is therefore imperative that the USACE, the U.S. Environmental Protection Agency (EPA) and other cooperating agencies, consider the information contained in this letter and its enclosed technical reports—prepared by world-renowned seismic hazard experts—in evaluating the potential for significant and unacceptable impacts on the Proposed Pebble Mine's TSFs and the Bristol Bay watershed's pristine ecological system, including its unrivaled salmon fisheries.

Below, we provide the following information and analysis to help the USACE, EPA, and the cooperating agencies, conduct the necessary thorough examination of the Proposed Pebble Mine's potential for significant impacts:

- (1) A description of the undersigned organizations comprising the BBDA, their connection to the Bristol Bay watershed and its life-sustaining salmon fishery, and their collective concerns with the Proposed Pebble Mine's unacceptable impacts;
- (2) A summary of the new information in the attached technical reports prepared by world-renowned experts on seismic impacts to infrastructure and geotechnical engineering, which demonstrate that the analysis in the DEIS and its supporting documents dramatically underestimated the potential for catastrophic damage resulting from seismic activity; and,
- (3) In light of this significant new information, we urge the USACE, in coordination with the cooperating agencies, to meet its NEPA obligations and prepare and circulate for public comment a Supplemental EIS that takes the requisite hard look at the likely significant impacts from the Proposed Pebble Mine.

II. BBDA And Its Member Organizations

Collectively, BBDA and its members and supporters live and/or work in Bristol Bay and near the location of the Proposed Pebble Mine and have long-standing interests in the world-class fisheries of Bristol Bay. Below, we introduce each member organization comprising the BBDA and their interests relative to the Proposed Pebble Mine and Bristol Bay's pristine ecosystem and its one-of-a-kind salmon fishery.

Bristol Bay Economic Development Corporation ("BBEDC") is a 501(c)(4) non-profit corporation whose mission is to promote economic growth and opportunities for residents of its member communities through sustainable use of the Bristol Bay and Bering Sea resources. BBEDC undertakes programs and management to foster economic and social benefits for the residents and

communities of Bristol Bay in order to ensure sustainability of the region's renewable natural resources, including its salmon fisheries and other fish stocks and fisheries.

Bristol Bay Native Association, Inc. ("BBNA") is a non-profit corporation serving 31 federally recognized tribes in the Bristol Bay regions in southwest Alaska. BBNA's mission is to advance the social, cultural, and economic interests of the Tribes and Alaska Native people of the Bristol Bay Region, including by prioritizing protection of Bristol Bay's salmon fisheries (commercial, subsistence, and sport) and salmon habitat in all land management decisions.

United Tribes of Bristol Bay ("UTBB") is a tribally chartered consortium of 15 federally recognized tribal governments in Bristol Bay that represent over 80% of the population of Bristol Bay. UTBB's mission is to protect the Yup'ik, Dena'ina, & Alutiiq indigenous way of life from unsustainable development in Bristol Bay.

Bristol Bay Regional Seafood Development Association, Inc. ("BBRSDA") is a 501(c)(6) non-profit corporation with the mission of maximizing the value of the Bristol Bay commercial salmon fishery for the benefit of its members. BBRSDA's membership consists of all 1,863 Bristol Bay salmon driftnet permit holders and is funded by a self-assessment of 1% on the ex-vessel value from driftnet landings. BBRSDA operates a successful branding and marketing program for Bristol Bay Sockeye Salmon which relies heavily on the fishery's abundance and positive reputation for pristine habitat.

Bristol Bay Reserve Association ("BBRA") is a 501(c)(6) non-profit corporation with the mission of promoting the interests of its members who own commercial fishing vessels and participate in the Bristol Bay commercial salmon drift fishery. BBRA has approximately 350 member vessel owners. Approximately 25 percent of the vessels participating in the Bristol Bay commercial salmon drift fishery are BBRA member vessels.

The BBDA's concerns with the Proposed Pebble Mine have been well-documented, including via comment letters submitted during summer 2019 articulating the many inadequacies of the DEIS. The Proposed Pebble Mine poses unacceptable risks to the Bristol Bay watershed and to the Bristol Bay salmon fisheries. The Proposed Pebble Mine would, at minimum, directly impact at least 3,000 acres of wetlands and 24 miles of streams in the Bristol Bay watershed. It would induce salmon avoidance in up to 35 miles of streams and reduce aquatic reproduction in up to 38 miles of streams. As described in the EPA Region 10 Regional Administrator's May 28, 2020 letter to you, stream impacts are more likely to be greater than 100 miles, "along with secondary impacts to 1,647 acres of wetlands and other waters, including 80.3 miles of streams, associated with fugitive dust deposition, dewatering, and fragmentation of aquatic habitats."

Of particular relevance to this letter, a catastrophic failure of the TSFs would have disastrous impacts to the watershed—and well beyond—and its ability to produce its unrivaled salmon runs.

III. Significant New Information Regarding Seismic Risks At The Pebble Mine

The Proposed Pebble Mine and its massive TSFs are located in a highly seismic area. Accordingly, the environmental review for the Proposed Pebble Mine must adequately examine the risk of earthquakes in the Project Area and impacts on the stability of the TSFs, and the likely catastrophic environmental harm that would result from failure of the TSF. As discussed below, the current record before the USACE fails to do so. Therefore, to complete the legally required rigorous environmental review and permitting process for the Proposed Pebble Mine, the USACE must supplement the record with the information below and enclosed.

As part of the comment process for the DEIS, Dr. Thomas O'Rourke and Dr. Izzat M. Idriss—two world-renowned experts on seismic impacts to infrastructure and geotechnical engineering—provided technical reports (via July 1, 2019 comments submitted by BBRA) evaluating the DEIS's analysis and conclusions about seismic risks in the vicinity of the Proposed Pebble Mine and the associated impacts to the Proposed Pebble Mine's infrastructure, including its mine tailings impoundments. Dr. O'Rourke is the Thomas R. Briggs Professor of Engineering, Civil and Environmental Engineering at Cornell University. Dr. O'Rourke has been recognized with the highest international awards in the engineer profession and has been sought out as an expert the federal government as well as countries around the world on the impact of earthquakes on infrastructure and buildings. Dr. Idriss is a professor emeritus of geotechnical engineering at the UC Davis College of Engineering and also taught at UC Berkeley, UCLA, Arizona, and Stanford. Dr. Idriss has won the highest recognition in his profession and is an expert on dams and has been consulted by mining companies around the world for his expertise in earthquake engineering and analysis as well as design, implementation, and review of tailings storage facilities. Drs. O'Rourke's and Idriss's reports identified serious flaws with the methodologies used in the DEIS for assessing the risks and impacts of a failure of the proposed mine tailings impoundment. Dr. O'Rourke's and Dr. Idriss's reports are attached to this letter as **Exhibit A**.

Because of this deficient evaluation, it was—and is—clear that the failure to adequately consider seismic hazards and potential failure of the TSFs constitutes a glaring analytical gap in the DEIS for the Proposed Pebble Mine. Based on the findings and concerns raised in Dr. O'Rourke's and Dr. Idriss's reports, the BBRA engaged two additional seismic hazard experts, Dr. Nick Gregor and Dr. Linda Al Atik, to further evaluate and prepare an analysis of the seismic risks for the Pebble mine based on the best available science and the current industry standards for such an analysis. Attached as **Exhibit B** to this letter is Drs. Gregor's and Al Atik's expert report titled "Seismic Hazard Analysis for the Pebble Mine Project, Southwest Alaska" (hereafter the "2020 Seismic Hazard Analysis"). The study design and analysis by Drs. Gregor and Al Atik were reviewed and approved by Dr. Norm Abrahamson who is perhaps the most widely recognized expert in this field.

To validate the conclusions in the 2020 Seismic Hazard Analysis, Dr. O'Rourke and Dr. Idriss conducted a peer review of that work, which is attached to this letter as **Exhibit C** (the "2020 Seismic Hazard Analysis Peer Review" or "Peer Review report"). For completeness, the 2020 Seismic Hazard Analysis Peer Review includes an evaluation and comparison of the following seismic hazard and TSF stability studies prepared by Knight and Piésold, Ltd. ("KP") on behalf of Pebble:

- (1) A 2013 KP report on seismicity assessment and seismic design that helped formed the basis for the geohazard risk analysis in the DEIS ("2013 KP seismic report");
- (2) A 2019 KP report updating the 2013 KP seismic report, which was prepared in response to a request for information from the USACE and that has not been subject to public review or comment ("2019 KP seismic report"); and,
- (3) A 2019 KP report on TSF embankment stability, which was prepared in response to a request for information from the USACE and that has not been subject to public review or comment ("2019 KP stability report").

The conclusions of the 2020 Seismic Hazard Analysis Peer Review are unequivocal. The Peer Review report demonstrates that Dr. Gregor's and Dr. Al Atik's 2020 Seismic Hazard Analysis is state of the art and should be used to establish target earthquake ground motions for evaluating the seismic performance of all the components of the Proposed Pebble Mine. Moreover, the 2020 Seismic Hazard Analysis supersedes the 2013 and 2019 KP seismic reports in almost every way, demonstrating that the USACE, the EPA, and cooperating agencies, cannot use the KP reports as a sound scientific basis for environmental review of the Proposed Pebble Mine's critical infrastructure and its significant impacts on the surrounding environment. For example:

- The 2013 and 2019 KP seismic reports use out of date information (i.e., information that has not been used in the industry for decades) and apply information an internally inconsistent manner for its earthquake ground motions models;
- The results of the probabilistic seismic hazard analysis presented in the 2013 and 2019 KP seismic reports are not site specific and should not be used for design purposes for any critical structure, including the massive TSFs, at the Pebble mine site;
- The 2013 KP seismic report that serves as the foundation for geohazard risks presented in the DEIS fails to accurately reflect the longer duration of earthquakes in the vicinity of the Pebble mine site and the corresponding risk of liquefaction and damage to earthen structures such as the mine's TSFs.

- The hazard of volcanic eruption, ensuing tsunami, and inundation and damage at the Proposed Pebble Mine's port sites represents a real threat requiring minimum design standards that 2013 and 2019 KP seismic reports fail to address.

Ultimately, the 2020 Seismic Hazard Analysis Peer Review recommends that (1) only the results of the probabilistic and deterministic hazard analyses included in Dr. Gregor's and Dr. Al Atik's 2020 Seismic Hazard Analysis be used for evaluating the Proposed Pebble Mine and, in turn, (2) the results presented in the 2013 and 2019 KP Reports should not be used for the Pebble mine site.

As for the 2019 KP stability report, the 2020 Seismic Hazard Analysis Peer Review presents even more scathing assessment, concluding that "the results of the stability analyses presented in the 2019 KP Memo are unusable to assess the safety of the proposed design." The 2019 KP stability report suggests, without any scientific justification, that the water table at the TSF embankment is much lower than evidence would indicate. As a result, the 2019 KP stability report drastically overstates the stability of the Proposed Pebble Mine's critical infrastructure to earthquakes. To the extent Pebble proposes to use earthfill in addition to or instead of rockfill for tailings dam then the tailings dam will face even greater stability issues. Further, waste rock from the Pebble mine is proposed as rockfill to build the TSF embankment and there appears to be no corresponding analysis of the potential for waste rock to acidify major salmon rivers in the vicinity of the Proposed Pebble Mine. Based on the proposed TSF design, use of potential acid generating material as rockfill is unacceptable.

In short, the seismic risk and TSF stability analyses produced by KP lack scientific rigor, they dramatically underestimate the risk of catastrophic failure of the Proposed Pebble Mine's massive TSFs, and they cannot be relied on to support conclusions on the potential for significant environmental impacts in the NEPA environmental review of the Proposed Pebble Mine and subsequent permitting decisions, including permitting under the Clean Water Act section 404. By contrast, the 2020 Seismic Hazard Analysis is state of the art, is based on the best available science, and must therefore serve as the foundation for a hard look at the Proposed Pebble Mine's significant impacts stemming from seismic events and TSFs failures.

IV. USACE, in Coordination with the EPA and the Cooperating Agencies, Must Issue a Supplemental EIS to Account for this Significant New Information

USACE cannot escape the significance of the information in the attached expert reports by claiming that the DEIS disclosed the possibility of seismic activity and the potential for catastrophic failure of the TSFs. The incontrovertible fact is that the seismic analysis and disclosure in the DEIS and supporting documents (including KP's 2019 reports that have not been subject to public review and comment) is woefully inaccurate and unreliable, resulting in a misleading representation of the associated risks. Put simply, meaningful consideration of the expert reports attached to this letter could not result in the same conclusions as those in the DEIS

based on flawed data and scientifically indefensible methodologies. For USACE to conclude otherwise would be plainly arbitrary and capricious.

NEPA requires the USACE to take a “hard look” at the environmental issues related to the Proposed Pebble Mine and adequately inform the public of its decision-making process. The NEPA process will inform the USACE’s permitting decision under the Clean Water Act, which requires the USACE to evaluate—based on in-depth factual determinations and scientific studies—whether the Proposed Pebble Mine will cause or contribute to significant degradation of the waters of the United States, including significant adverse effects of the discharge of pollutants on fishery areas and economic values. NEPA’s purpose is to ensure that “the agency will not act on incomplete information, only to regret its decision after it is too late to correct.” *Marsh v. Oregon Natural Res. Council*, 490 U.S. 360, 377 (1989). With these statutory obligations in mind, when faced with new information of the character and magnitude in the attached reports, information that contradicts a central element of the DEIS, the USACE cannot avoid analysis of that information in a Supplemental EIS. *See Friends of the Clearwater v. Dombeck*, 222 F.3d 552, 557 (9th Cir. 2000) (requiring agencies to take a “hard look” at whether new information requires a Supplemental EIS).

As a result, the USACE, in coordination with the cooperating agencies, must prepare and solicit comment on a Supplemental EIS that evaluates the seismic risks and impacts of a failure of the proposed mine tailings storage facilities in light of the acceptable scientific methodologies and the best available technical information. Further, this analysis is directly relevant to and necessary for the USACE’s obligations under the Clean Water Act’s section 404(b)(1), guidelines, 40 C.F.R. § 230.10(a), to evaluate and document the potential for impacts in the event of a tailings impoundment failure to support its determination regarding the Least Environmentally Damage Practicable Alternative.

In conclusion, the potential impacts from the construction and operation of the Proposed Pebble Mine on Bristol Bay’s salmon runs and the people that depend upon them, such as the members of the BBDA, are simply too great to ignore accepted scientific methodologies for assessing risks. The new information in attached expert reports makes clear that, at minimum, a more robust analysis of seismic risks, in a Supplemental EIS, is warranted. Otherwise, based on the current record before the USACE, “No Action” is the only justifiable alternative.

* * *

On behalf of undersigned organizations comprising the BBDA, thank you for your consideration of the forgoing comments.

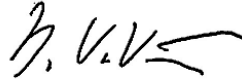
Sincerely,

BRISTOL BAY NATIVE ASSOCIATION



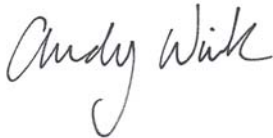
Ralph Andersen
President & CEO

BRISTOL BAY ECONOMIC
DEVELOPMENT CORPORATION



Norm Van Vactor
President & CEO

BRISTOL BAY REGIONAL SEAFOOD
DEVELOPMENT ASSOCIATION



Andy Wink
Executive Director

UNITED TRIBES OF BRISTOL BAY



Robert Heyano
President

BRISTOL BAY RESERVE ASSOCIATION



Robert Kehoe
Executive Director

Attachments:

1. Exhibit A - Drs. O'Rourke's and Idriss's Initial DEIS Comment Reports
2. Exhibit B - Drs. Gregor's and Al Atik's Expert Report titled "Seismic Hazard Analysis for the Pebble Mine Project, Southwest Alaska" (June 2020)
3. Exhibit C - Drs. O'Rourke's and Dr. Idriss's Peer Review Report.

cc: Christopher W. Hladick, Regional Administrator, U.S. EPA, Region 10
Mathew LaCroix, U.S. EPA Region 10, Alaska Operations Office
Shane McCoy, Project Manager, USACE, Alaska District,
Lynne Richmond, Communications and Public Affairs Specialist, Advisory Council on
Historic Preservation
Thomas Tilden, First Chief and Courtenay Carty, Tribal Administrator, Curyung Tribal
Council
George Alexie, President, Nondalton Tribal Council

Kyle Moselle, Large Mine Permitting, Department of Natural Resources, State of Alaska

Nathan Hill, Borough President, Lake and Peninsula Borough

Guy Hayes, Public Affairs, U.S. Department of the Interior, Bureau of Safety and Environmental Enforcement

Don Striker, Acting Regional Director, U.S. Department of the Interior, National Park Service

Stewart Cogswell, Field Supervisor, Anchorage Field Office, U.S. Department of the Interior, Fish and Wildlife Service

Alan Mayberry, Associate Administrator, U.S. Department of Transportation, Pipeline and Hazardous Materials Safety Administration

David Seris, Waterways Management Branch, 17th Coast Guard District, U.S. Coast Guard

**Pebble Mine Geohazard and Tailings Dam Embankments Analyses of
Dr. T. O'Rourke and Dr. Izzat M. Idriss**

(Submitted Summer 2019 During DEIS Public Comment Period)

EXHIBIT A

T.D. O'ROURKE**Geotechnical Consultant**

10 Twin Glens Road, Ithaca, New York 14850
607-272-4029

25 June 2019

TO: Bristol Bay Reserve Association
FROM: Tom O'Rourke
RE: Geohazards Affecting the Pebble Mine Complex

My comments related to geohazards affecting the Pebble Mine Complex are provided as follows:

1. As pointed out by the U.S. Geological Survey [USGS] (2007), Alaska is the most seismically active state in the U.S. The Pebble Mine Project (Project) would involve a very large mining site and transportation facilities, including a deep and expansive mine pit, waste rock piles, tailings storage facilities (TSFs), roadways, pipelines, bridges, port facilities, ore processing units, offices, housing, as well as water and electric distribution and wastewater treatment systems (collectively, the Pebble Mine Complex). By some estimates, the total areal extent of the Project's mine site operations, not including the full Pebble Mine Complex with off-site roads, pipelines, bridges, and port facilities, would cover 19 mi².

A project of this scale and magnitude poses material and significant risks and impacts on important natural resource production and viability, as well as transportation facilities and infrastructure (USGS, 2007). The analysis in the Draft Environmental Impact Statement (DEIS) does not use current data or up-to-date commonly accepted evaluation measures. Unless the DEIS is revised substantially to include the investigations and analyses outlined below, it will not provide an adequate basis to evaluate the risk potential of the Project.

Given the Project's seismic risk, mine size and complexity, and potential detrimental effects on the world's largest salmon run, the DEIS needs to provide an up-to-date evaluation of the regional seismicity, including comprehensive probabilistic seismic and deterministic seismic hazard analyses. The seismic hazard analyses reported in the DEIS are based on ground motion maps that are twelve years old (USGS, 2007), do not include recent seismic activity, and do not include the use of the most recent ground motion prediction equations (GMPEs), known as NGA West (2014). Up-to-date seismicity assessments and GMPEs are generally a prerequisite for the seismic risk assessment of projects with an impact similar to that of the Pebble Mine Complex. In my opinion, it is accepted practice to use up-to-date seismicity analyses and GMPEs to evaluate infrastructure projects with broad life safety and environmental risks, including mines. Since 2015-2016, similar projects have converted to using the most recent GMPEs, which are missing from the DEIS.

2. The TSFs involve very large embankments with projected heights reaching 545 ft that will impound approximately 1.295 billion tons of mine tailings, sludge, and water. To put that into context, the Mount Polley tailings dam embankments in British Columbia, which failed in August 2014, reached a height of approximately 130 feet (U.N. Environment GRID Arendal 2017). The Val di Stava Dam collapse in Italy in 1985 involved tailings dam embankments that were only slightly higher than 110 feet (U.N. Environmental GRID Arendal 2017). Issues related to dam height risk are exacerbated in a seismically active region like Alaska. Simulation results reported by Lynker (2019) show that a breach of a large tailings dam consistent with Pebble Mine Complex operations can inundate waterways in excess of 80 mi. downstream and deposit debris in more than 155 mi. of streams that are mapped as salmon habitat.

Because the consequences of failure are so high, with the immediate release of toxic mining chemicals and wastes, seismic embankment deformation analyses need to take account of up-to-date seismicity and GMPEs as well as the most effective models for ground deformation simulation. The seismic embankment deformation analyses in the DEIS do not include seismicity or GMPEs that are up-to-date. In addition, they are based on simplified sliding block models, semi-empirical predictive relationships, and general empirical methods that do not account explicitly for the liquefaction behavior of soil. Soil liquefaction occurs when saturated soil loses its shear strength and stiffness under applied stress, such as earthquake-induced transient ground motion, and behaves as a liquid.

In contrast, the seismic risk assessment of dams operated by the Los Angeles Department of Water and Power is performed by simulating liquefaction-induced soil deformation using models that account explicitly for soil strength and stiffness loss during pore water pressure buildup in response to seismic motion. In some cases, as many as three different models are used. The employment of different models accounts for uncertainty with respect to the actual liquefaction behavior of soil, and allows for comparison of the collective results that, in turn, enhances the engineer's understanding of the deformation process. In my opinion, the use of current seismic data and GMPEs is the commonly accepted professional standard for evaluation of a critical dam.

The simplified methods employed in the DEIS lead to an estimate of embankment crest settlement on the order of 4 ft under Maximum Credible Earthquake (MCE) conditions. These results are used to conclude that the settlement magnitude is not enough to compromise functionality of the filter zones in the proposed tailings dam embankment nor reduce the crest elevation below the maximum allowable water level behind the dam. In my judgement, the DEIS cannot substantiate these conclusions unless it performs adequate modeling using up-to-date seismicity assessments and GMPEs, consistent with those discussed and recommended in this report.

One problem apparently not addressed in the DEIS is that embankment crest settlement leads to transverse cracks in the dam. If this cracking extends below the water level behind the dam, pathways for flow and erosion will exist with the potential to erode through and overtop the dam. In addition to comparing crest settlement with the minimum freeboard, the analyses should also evaluate the reduction in horizontal soil stress parallel to the longitudinal axis of the dam to

determine if enough soil stress exists to resist transverse crack formation. This type of analysis cannot be performed with the simplified models used in the DEIS. Without this evaluation and more rigorous seismic hazard and embankment deformation analyses, the DEIS assessment of the proposed tailings dam is not sufficient to assess seismic risk.

3. Soil liquefaction is a major threat to the many transportation systems and collocated infrastructure planned for the Project, including roads, bridges, culverts, port facilities, and pipelines for transporting various materials including gas, diesel, and water. During the 1964 Alaska earthquake there was widespread failure of railroad embankments and bridges founded on liquefiable soils. The most recent 30 November 2018 Anchorage Alaska earthquake provides evidence for embankment failure at Vine Road in Wasilla, Alaska, underlain by organic peat deposits (GEER, 2019).

The Project will involve as many as 86 mi. of gravel surface access roads. It is estimated that, along the roadways, there may be four pipelines that would carry copper concentrate, water, natural gas, and diesel fuel. The roads and pipelines will cross many streams, rivers, and wetlands that are often underlain by liquefiable soils. Many streams and river crossings will be wide enough to require a bridge, which may be used to carry the pipelines. Experience during past earthquakes, including those in Alaska, show that bridges will fail or deform excessively from liquefaction-induced soil movements. Such failure or deformation may also damage the pipelines. Since the pipelines are collocated, the failure of one can undermine and damage the adjacent lines, thus increasing the overall risk of pipeline failure and release of contents. Because these locations are stream, wetland, and river crossings, the loss of toxic contents will enter waterways immediately with direct impact on salmon runs and associated habitat.

Loss of bearing due to liquefaction of underlying soils will result in road embankment settlement and lateral ground deformation. Such deformation will also affect the integrity of pipelines in proximity to the failed road embankment. The DEIS needs to analyze and evaluate adequately the many impacts on natural resources and transportation infrastructure associated with liquefaction.

4. Seismicity is not the only issue that could affect the Project's infrastructure. The high annual rainfall around the area of the proposed Pebble Mine Complex, in combination with steep mountainous slopes and the absence of significant vegetation at higher elevations, increases the risk and frequency of intense storm runoff. The roadways are exposed to these runoff events, which can lead to washouts of culverts at smaller stream crossings and undermining of bridges at larger water bodies. The washout of a culvert will be accompanied by erosion of the roadway and the undermining of pipelines located nearby and parallel to the roadway. The deformation and/or failure of a bridge will also induce damage to pipelines carried by the bridge, with the potential for release of toxic contents directly into salmon runs. The 2019 tailings dam collapse in the Brazilian state of Minas Gerais is an example of what heavy rainfalls can do to mine infrastructure. In that case, heavy rains led to dam failure, releasing significant amounts of toxic mine wastes and mud, contaminating a major stretch of the Paraopeba River, and killing over 100 people.

5. There have been many tailings dam failures worldwide (e.g., U.N. Environment GRID Arendal, 2017 and 2019; Rico et al., 2007). In view of these problems, the DEIS should identify and address tailings dam failures that have occurred worldwide in a discussion on the vulnerability of tailings dams and the major and most common causes of failure. The DEIS should place the proposed Pebble Mine Complex tailings dam embankments and other infrastructure in the proper context of international experience with these projects, and explain why the proposed dam and infrastructure would not be susceptible to similar types of failures. This assessment should include a discussion and evaluation of the residual risks associated with the tailings dam after cessation of mining operations and closure of the impoundment. The risk of a tailings dam failure and the release of toxic mine wastes will continue after termination of mining operations, and this risk should be addressed and quantified in the DEIS.

The significance of tailings dam behavior is broadly recognized in the engineering community. Indeed, the importance of managing and accounting appropriately for mine wastes is a topic receiving special attention from the National Academies of Sciences, Engineering, and Medicine's Committee on Geological and Geotechnical Engineering (COGGE), which is holding a meeting on June 27, 2019 in Washington, DC, to discuss managing mine waste risks, including a session on managing mine tailings. In its description of the topic, COGGE points out that impoundments containing mining wastes and other particulate materials placed by hydraulic sluicing fail at ten times the frequency of modern engineered dams.

If you have any questions or seek additional clarification regarding my review comments, please contact me directly.

Sincerely,

A handwritten signature in black ink that reads "T. D. O'Rourke". The signature is written in a cursive style with a long horizontal line extending to the left of the first letter.

T. D. O'Rourke

References:

Geotechnical Extreme Events Reconnaissance Association [GEER] (2019), "Geotechnical Engineering Reconnaissance of the 30 November 2018 M 7.0 Anchorage, Alaska Earthquake", Eds. K.W. Franke and R.D. Koehler, *GEER-059*, 2 January, 2019.

Lynker Technologies, LLC (2019), "A Model Analysis of Flow and Deposition from a Tailings Dam at the Proposed Pebble Mine", *LYNK-2018-179*, report submitted to The Nature Conservatory, Juneau, AL.

Rico, M., G. Benito, A.R. Salgueiro, A. Diez-Herrero, and H.G. Pereira (2007), "Reported Tailings Dam Failures: A Review of the European Incidents in the Worldwide Context", *Journal of Hazardous Materials*, Elsevier B.V., Vol. 152, pp 846-852.

U.N. Environment GRID Arendal (2017), "Mine Tailings Storage: Safety Is No Accident", <http://www.grida.no/publications/383>, last accessed 17 June 2019.

U.N. Environment GRID Arendal (2019), "Mine Tailings Storage: Safety Is No Accident", <http://www.grida.no/resources/11424>, last accessed 17 June 2019.

U.S. Army Corps of Engineers (2019), "Pebble Project EIS, Draft Environmental Impact Statement", <https://pebbleprojecteis.com/documents/eis>, last accessed 24 June 2019.

USGS (2007) "Revision of Time-Independent Probabilistic Seismic Hazard Maps for Alaska" by Wesson, R.L., O.S. Boyd, C.S. Mueller, C.G. Bufe, A.D. Frankel, and M.D. Petersen, *Open-File Report 2007-1043*.

July 1, 2019

To: Bristol Bay Reserve Association

From: I. M. Idriss

Subject: *Review of Selected Portions of the Draft Environmental Impact Statement (DEIS) for the Pebble Mine Complex Related to the Tailings Dam Embankments*

To prepare this Report, I went over a number of documents provided to me by Bristol Bay Reserve Association, consisting of relevant sections of the "Draft Environmental Impact Statement (DEIS)", and other reference documents in the DEIS, prepared by AECOM/Knight Piésold in 2018/2019 on behalf of the United States Army Corps of Engineers for the proposed Pebble Mine Complex (Project). The documents provided include:

- Section 3.15 – Geohazards
- Section K3.15 – Geohazards
- Section 4.15 – Geohazards
- Section K4.15 – Geohazards
- Section 4.27.6 – Tailings Release
- Section 4.27.7 – Untreated Contact Water Release
- Section 4.27.8 – Cumulative Effects
- AECOM, Pebble EIS-Phase Failures Modes and Effects Analysis Workshop Report (December 2018)
- Appendix B – Alternatives Development Process
- Appendix N – Project Description
- Knight Piésold, RE: RFI 008 Response – Embankment Static and Seismic Stability – 2018
- Other subsections and figures related to the tailings dam embankments

Based on my brief review of these documents, I have prepared summary comments regarding:

1. Seismic sources and earthquake ground motions
2. Geologic features that may impact stability and/or seepage
3. Embankments
 - a. Foundation soils
 - b. Drainage
 - c. Embankment zoning/construction
4. Stability – static and seismic
5. Deformation Analyses
6. Additional Observations
7. Closing Remarks

This Report covers, to the extent possible, what is (or is not) included in the documents you sent me, and the adequacy/completeness of the information provided.

1. Seismic Sources and Earthquake Ground Motions

The seismicity of the area needs to be brought up to date and the currently acceptable procedures should be adopted to produce the relevant seismic input parameters. The latter include the calculation of target spectra and appropriate accelerograms that are compatible with the target spectra. These spectra and associated accelerograms are usually obtained for a "rock outcrop" at the site and then used to evaluate the seismic performance of the various facilities at the site.

The use of the peak ground acceleration alone, as suggested in the DEIS, is inappropriate.

The DEIS includes a table designated as "Seismicity – Mine Site" that lists the seismic sources and provides values of peak ground acceleration for a number of earthquake events considered by Knight Piésold in the evaluation of the performance of the embankments during earthquakes.

The distance from the seismic source to the mine site in this table is listed as "epicentral distance", a metric that has not been used in earthquake ground motions models (GMMs) for more than four decades. This raises concern about the adequacy of the GMMs used for calculating the values listed in the table, a copy of which is presented below for ease of reference.

Seismicity – Mine Site

Earthquake Source Type	Earthquake Source Name	Source/Fault Mechanism	Maximum Magnitude (Mw)	Epicentral Distance (miles)	Focal Depth (miles)	Maximum Acceleration ¹	
						Median (g)	Median + 1 S.D. (g)
Interface Subduction ²	Alaska-Aleutian Megathrust	Thrust	9.2 (8.5)	120	25	0.08	0.14
Intraslab Subduction	Intraslab Event ³	In-slab	7.5	110	40	0.05	0.11
			8.0	110	40	0.09	0.16
	Deep Intraslab Event ³	In-slab	7.5	50	80	0.15	0.28
8.0			50	80	0.26	0.48	
Shallow Crustal Fault ⁴	Lake Clark Fault (Mapped)	Strike-slip	7.5	22	3	0.12	0.20
		Reverse (Thrust)	7.5	22	3	0.14	0.25
	Lake Clark Fault (Hypothetical Extension)	Strike-slip	7.5	7.5	3	0.26	0.44
		Reverse (Thrust)	7.5	7.5	3	0.27	0.46
	Castle Mountain Fault	Strike-slip	7.3	174	3	< 0.01	0.01
	Bruin Bay Fault	Reverse (Thrust)	8.0	60	3	0.07	0.12
	Border Ranges Fault	Strike-slip	8.0	130	3	0.02	0.04
	Kodiak Island / Narrow Cape Faults	Strike-slip	7.5	190	3	<0.01	0.01
	Telaquana Fault	Strike-slip	7.0	40	3	0.06	0.09
	Mulchatna Fault	Strike-slip	6.5	55	3	0.03	0.05
Denali Fault	Strike-slip	8.0	125	3	0.03	0.05	
Maximum Background Earthquake		Strike-slip	6.5	< 1	7.5	0.31	0.56
		Reverse (Thrust)	6.5	< 1	7.5	0.35	0.61

Table reproduced from the DEIS.

2. Geologic Features that May Impact Stability and/or Seepage

The portions of the DEIS that cover geologic features that could impact the integrity of the tailings embankments and other Project infrastructure are inadequate to support a conclusion that instability is not an issue or that seepage, enhanced by such features, has been adequately addressed. The DEIS needs to expand the geologic features analysis and discussion to show that those features will not lead to instability or seepage that threatens the Project infrastructure.

3. Embankments

There will be a number of embankments constructed as part of this Project, including those needed to contain the bulk tailings and those to contain pyritic tailings. Portions of these embankments will be supported on "rock" and portions will be supported on "soils" after removing portions of the existing soils prior to construction of the embankment. It is not clear what criteria will be used for the latter.

The embankments cross sections I found in the portions of the DEIS I reviewed are more of a "cartoon" rather than a useful engineering cross section that depicts the various zones of the embankment (core, shell, filter and drainage layers) and underlying foundation layers (soil layers, rock). The maximum section of the bulk tailings storage facility (TSF) is included in the DEIS and is shown below to illustrate the inadequacy/incompleteness of the information provided for review.

Far more details are required, including extent (depth and width) and material properties, for each embankment zone and for each foundation soil layer. In addition, the key properties of the underlying rock units need to be provided and analyzed in the DEIS.

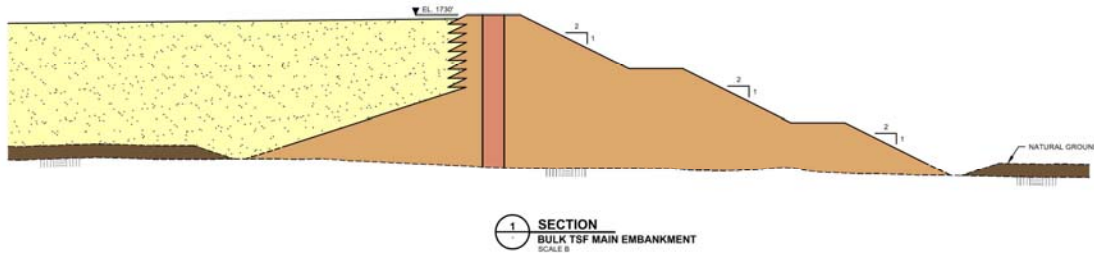


Figure reproduced from the DEIS.

The "Christmas-tree" upstream zone of the section of the bulk TSF embankment, shown in the figure above, requires unique details to be successful, such as: (i) adequate beach; (ii) upstream filters; (iii) minimum width and compaction of the upstream shell and of the filters; (iv) minimum width of core; and (v) appropriate geochemical/geotechnical characteristics of the core materials; etc. None of these details are included in the DEIS.

There are a number of instances in which the DEIS states that various zones will be constructed (e.g., filters, core, etc.) and properly controlled. However, important details and cross sections needed to explain the construction and functioning parts of the dam are not included in the DEIS. Additional information and details of the construction are required to clarify what is being considered, how the proposed controls will be implemented, and how they will function safely during mining operations.

The most unusual item in the DEIS is the statement in Section 4.15 (page 4.15-5) that "(a static FoS of 1.1 or greater is considered stable) [*sic*]"; FoS being factor of safety. I am not aware of that criterion ever being acceptable in any project I ever worked on. The DEIS provides no justification for how would such a minimum FoS be acceptable on this Project.

In my opinion, the information and analyses included in the DEIS regarding TSF embankment design and function are not sufficient to judge the adequacy or acceptability of the proposed design.

4. Stability

The DEIS discusses the static stability for selected sections of the embankments, but provides no information about the zoning, material description, or material properties that are needed to assess the adequacy of the information included in the DEIS.

The use of the so-called "pseudo-static" approach to assess the seismic stability of a slope is inadequate, particularly using the acceleration values listed in the table above to represent the driving force affecting the slope. I could find no explicit statement, in the portions of DEIS I reviewed, that defines where these acceleration values apply.

Normally, a seismic hazard evaluation results in developing target spectra and associated accelerograms to be considered as the rock outcrop motions at the site. The forces applied to the facility (e.g., the TSF embankment section) is calculated using appropriate dynamic analysis procedures. Occasionally it is acceptable in preliminary analyses to use "applicable" simplified procedures to estimate these forces. It is not clear what was done in the DEIS.

Liquefaction of the tailings also needs to be considered in assessing the seismic stability of the TSF embankments. I found nothing explicit about this issue in the DEIS.

5. Deformations Analyses

The approach used in the DEIS is not applicable to the embankments at this site.

Once an appropriate seismic hazard evaluation has been completed for this site and the target spectra and associated accelerograms have been adequately established, a proper nonlinear dynamic analysis, incorporating up to date constitutive models for each zone of the embankments and the foundation layers, can be used to estimate the deformations and deformation patterns of each embankment section. The DEIS needs to include this evaluation and its results. Without it, the DEIS lacks sufficient information from a geotechnical engineering perspective to make a sound judgement about the adequacy of the embankment design.

6. Additional Observations

Pyritic TSF: The DEIS states that the impoundment for this TSF will be lined and that drains will be installed below the liners. It is difficult to assume that the construction will be perfect, or even adequate, and that no puncture will occur in the liners. Therefore, it is important to incorporate defensive measures to control the inevitable leakage from the impoundment and to provide means to collect the seepage and direct it to where it could be appropriately treated. The DEIS, however, does not include this.

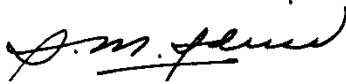
Particular Items of Concern: The DEIS includes four items, in particular, that preclude a proper and sufficient evaluation of the Project's infrastructure, including the tailings dam embankments; these items are:

- a. Implying that peak acceleration is sufficient to describe the seismic input;
- b. Not specifying the location of the seismic input;
- c. Proposing that "a static FoS of 1.1 or greater is considered stable"; and
- d. Neglecting to include proper cross sections of any of the embankment-foundation layouts under consideration.

7. Closing Remarks

The DEIS for the Pebble Mine lacks up-to-date and a number of the currently acceptable procedures to obtain: (i) the relevant seismic input parameters; (ii) key geologic features that could impact the integrity of the tailings embankments and other Project infrastructure; (iii) useful engineering cross sections that depict the embankment (core, shell, filter and drainage layers) and underlying foundation layers (soil layers, rock); (iv) appropriate static and seismic analyses of embankment stability; (v) proper assessment of earthquake-induced embankment deformations; and (vi) essential defensive measures to control, collect, and treat inevitable impoundment leakage. In addition, the DEIS is constrained by four factors that preclude a proper and sufficient evaluation of the Project, including the implication that peak acceleration is sufficient to characterize seismic input, lack of location for seismic input, proposal that a minimum static FoS of 1.1 is considered stable, and absence of proper embankment-foundation cross sections.

Sincerely,

A handwritten signature in black ink, appearing to read "I. M. Idriss", with a horizontal line underneath the name.

I. M. Idriss

**Dr. Nick Gregor and Dr. Linda Al Atik, “Seismic Hazard Analysis for
the Pebble Mine Project, Southwest Alaska” (June 2020)**

With Cover Letter by Dr. Norm Abrahamson

EXHIBIT B

June 1, 2020

To: Nick Gregor
From: Norm Abrahamson

Subject: Review of "Seismic Hazard Analysis for the Pebble Mine Project, Southwest Alaska", dated May 20, 2020

Overall, the report is a high-quality seismic hazard analysis that provides the deterministic and probabilistic hazard results for the Pebble Mine Project. The methods used in the report follow best practice in seismic hazard analysis. The May 20, 2020 version of the report adequately addresses my comments on earlier drafts of the report. A summary of my review of the final report is given below.

For the seismic source characterization, the models for the crustal faults, background zones, and subduction zone are based on up-to-date data and current methodologies. The seismic hazard is controlled by the slab events which is common for this site/source geometry of the subduction zone. Given that the slab events control the hazard at the site, the results can be sensitive to the modeling of the slab earthquakes in the PSHA. The approach used in this report captures the finite-fault geometries of the slab events and is an improvement over the widely used point-source approach.

The selection of the ground-motion models (GMMs) can have a significant effect on the hazard. For crustal earthquakes, the report uses equal weights for the five NGA-W2 models. For subduction earthquakes, the report uses the three alternative branches of the 2016 BCHydro model and the new Kuehn et al (2020) NGA-SUB model. Most of the weight is given to the BCHydro model. Given that the NGA-SUB models have just been released, and this project is one of the first applications and revisions may still be made to the NGA-SUB models, using a low weight on the new NGA-SUB model is appropriate at this time. As the new NGA_SUB models become stable over the next year, updates to the hazard at the Pebble Mine site should consider larger weights to these new GMMs.

In conclusion, the UHS and deterministic spectra developed in the report are appropriate to use as reference rock spectral for the seismic evaluation of the Pebble Mine sites. As noted in the report, when applying these results, the site conditions at the Pebble Mine project sites should be determined and the hazard results adjusted to the site-specific site condition if needed.



Norman Abrahamson

Seismic Hazard Analysis for the Pebble Mine Project, Southwest Alaska

Prepared for:

K&L Gates

Prepared by:

Nick Gregor and Linda Al Atik

May 20th, 2020

Table of Contents

1. Introduction.....	1
1.1 Previous SHA studies	4
2. Seismic Source Characterization	5
2.1 Regional Tectonics.....	5
2.2 Seismicity.....	7
2.3 Crustal Fault Sources	14
2.4 Subduction Interface Sources.....	25
2.5 Subduction Slab Sources	29
2.6 Crustal Host Zone	36
3. Ground-Motion Characterization	38
3.1 Crustal Ground-Motion Models	38
3.2 Subduction Ground-Motion Models	40
4. Probabilistic Seismic Hazard Analysis (PSHA)	51
4.1 Methodology	51
4.2 PSHA Results – Main TSF Site Location.....	51
4.3 PSHA Results – Pyritic TSF Site Location.....	83
4.4 PSHA Results – South TSF Site Location	90
4.5 PSHA Results Summary	96
5. Deterministic Seismic Hazard Analysis (DSHA).....	101
5.1 Methodology	101
5.2 DSHA Results – Main TSF Site Location	102
5.3 DSHA Results – Pyritic TSF Site Location	108
5.4 DSHA Results – South TSF Site Location	111
5.5 DSHA Summary	114
6. Summary and Conclusions	115
7. References.....	119
Appendix A – Modeling the Slab Seismic Source in Southern Alaska for PSHA programs	A-1

List of Tables

Table 1.	Selected site locations for the Main, Pyritic and South TSF sites.	1
Table 2.	Period of completeness for USGS earthquake catalog.	10
Table 3.	Seismic source characteristics for the crustal faults used in the analysis. Weights for multiple values are indicated in brackets.	23
Table 4.	Seismic source parameters for Alaska-Aleutian subduction zone sources used in the analysis.	29
Table 5.	Seismic source parameters for slab subduction zone sources used in the analysis. Weights for multiple values are indicated in brackets.	36
Table 6.	Seismic source parameters for crustal host zone. Weights for multiple values are indicated in brackets.	38
Table 7.	UHS for the Main TSF site location for $V_{S30} = 760$ m/sec.	60
Table 8.	Fractile UHS for the Main TSF site location for $V_{S30} = 760$ m/sec at the 5,000-yr return period level.	70
Table 9.	Fractile UHS for the Main TSF site location for $V_{S30} = 760$ m/sec at the 10,000-yr return period level.	71
Table 10.	Modal peak bin values (magnitude and distance) for the Main TSF site location for $V_{S30} = 760$ m/sec at the 5,000-yr and 10,000-yr return period levels.	74
Table 11.	UHS for the Pyritic TSF site location for $V_{S30} = 760$ m/sec.	84
Table 12.	Fractile UHS for the Pyritic TSF site location for $V_{S30} = 760$ m/sec at the 5,000-yr return period level.	85
Table 13.	Fractile UHS for the Pyritic TSF site location for $V_{S30} = 760$ m/sec at the 10,000-yr return period level.	86
Table 14.	UHS for the South TSF site location for $V_{S30} = 760$ m/sec.	90
Table 15.	Fractile UHS for the South TSF site location for $V_{S30} = 760$ m/sec at the 5,000-yr return period level.	91
Table 16.	Fractile UHS for the South TSF site location for $V_{S30} = 760$ m/sec at the 10,000-yr return period level.	92
Table 17.	Comparison of PGA ground-motion values from the Knight-Piesold (2013) study and this current SHA study.	100
Table 18.	Event parameters for the DSHA scenario events for the Main TSF site location.	102
Table 19.	Median and 84 th percentile ground motions from the DSHA scenarios for the Main TSF site location.	104
Table 20.	Event parameters for the DSHA scenario events for the Pyritic TSF site location.	108
Table 21.	Median and 84 th percentile ground motions from the DSHA scenarios for the Pyritic TSF site location.	109
Table 22.	Event parameters for the DSHA scenario events for the South TSF site location.	111
Table 23.	Median and 84 th percentile ground motions from the DSHA scenarios for the South TSF site location.	112
Table 24.	PSHA UHS and controlling slab 84 th percentile spectra for the reference site conditions of $V_{S30} = 760$ m/sec for the Main TSF site location.	116

Table 25. PSHA UHS and controlling slab 84 th percentile spectra for the reference site conditions of $V_{S30} = 760$ m/sec for the Pyritic TSF site location.	117
Table 26. PSHA UHS and controlling slab 84 th percentile spectra for the reference site conditions of $V_{S30} = 760$ m/sec for the South TSF site location.	118

List of Figures

Figure 1. Overview map of the proposed Pebble Mine project in Southwest Alaska. Three TSF embankments are indicated on the map (Main Embankment, Pyritic Area E embankment, and South Embankment). (Source: Pebble Partnership, 2018).....	2
Figure 2. Schematic showing the elements of a probabilistic seismic hazard analysis (Source: Earthquake Engineering Research Institute, 1989).....	3
Figure 3. Generalized tectonic environment for Alaska and the approximate rupture zones for the large historical earthquakes associated with the interface subduction zones and major crustal faults (Source: Wesson et al., 2008).	6
Figure 4. Location of two historical significant slab events crustal faults (Source: Abers and Mann, 2018).	6
Figure 5. USGS seismicity catalog (through 2004) for events within the project region.....	8
Figure 6. Seismicity catalog (since January 1, 2005) for events within the project region.....	9
Figure 7. Calculated recurrence curve for the USGS catalog (orange line) and the updated project catalog (solid blue line) over all depths (a) and ratio of recurrence curves for the project catalog over USGS catalog (b).	11
Figure 8. Calculated recurrence curve for the USGS catalog (orange line) and the updated project catalog (solid blue line) for depths less than 50 km (a) and ratio of recurrence curves for the project catalog over USGS catalog (b).....	12
Figure 9. Calculated recurrence curve for the USGS catalog (orange line) and the updated project catalog (solid blue line) depths greater than or equal to 50 km (a) and ratio of recurrence curves for the project catalog over USGS catalog (b).	13
Figure 10. Characterized crustal fault used in the SHA.	15
Figure 11. Segmentation of the Alaska-Aleutain subduction zone for large interface earthquakes (Source: Wesson et al., 2008).	26
Figure 12. Top and bottom fault traces for the three closest segments of the Alaska-Aleutian subduction zone source model used in the analysis.	27
Figure 13. Relocated earthquakes from Ratchkovski and Hansen (2002) shown in map view (a) and cross sections closest to the project site (b).....	30
Figure 14. Virtual slab faults and seismicity from the project catalog for events separated by 50 – 100 km (a) and 100 – 150 km (b) with events from each subsection plotted with separate colors.	33
Figure 15. Virtual slab faults and seismicity from the project catalog for events separated by 150 – 200 km with events associated with each subsection plotted with different colors.	34
Figure 16. Crustal host areal source zone and all events with depths less than 50 km shown both with variable size for magnitude (purple circles) and depth (open circles).	38
Figure 17. GMM logic tree for crustal events showing the different branches and associated weights; μ and σ are median predication and epistemic standard deviation of the natural-logarithmic values of the ground-motion parameter of interest.	40
Figure 18. Selected interface data for the KBCG model from Alaska for the two sub-regions of Alaska (Kodiak+Prince William Sounds) and Aleutian.	43
Figure 19. Median spectra for the suite of evaluated interface subduction models.	44
Figure 20. Total aleatory sigma from the evaluated interface subduction models.....	44

Figure 21. Selected slab data for the KBCG model from Alaska for the two sub-regions of Alaska (Kodiak+Prince William Sounds) and Aleutian.45

Figure 22. Median spectra for the suite of evaluated interface subduction models for hypocentral depth of 60 km and magnitude 7 (a) and 8 (b).46

Figure 23. Median spectra for the suite of evaluated interface subduction models for hypocentral depth of 110 km and magnitude 7 (a) and 8 (b).47

Figure 24. Total aleatory sigma from the evaluated slab subduction models.....48

Figure 25. GMM logic tree for subduction events showing the different models and associated weights.49

Figure 26. Mean hazard curves from the individual seismic sources and the total hazard curve for PGA (a) and 0.2 sec (b) for the Main TSF site location.....53

Figure 27. Mean hazard curves from the individual seismic sources and the total hazard curve for 0.5 (a) and 1 sec (b) for the Main TSF site location.....54

Figure 28. Mean hazard curves from the individual seismic sources and the total hazard curve for 3 sec for the Main TSF site location.55

Figure 29. Fraction contribution to the total hazard from the individual seismic sources for PGA (a) and 0.2 sec (b) for the Main TSF site location.56

Figure 30. Fraction contribution to the total hazard from the individual seismic sources for 0.5 (a) and 1 sec (b) for the Main TSF site location.57

Figure 31. Fraction contribution to the total hazard from the individual seismic sources for 3 sec for the Main TSF site location.....58

Figure 32. UHS spectra for the Main TSF site location ($V_{S30} = 760$ m/sec) plot log-linear (a) and log-log (b).59

Figure 33. Mean magnitude values for the Main TSF site location ($V_{S30} = 760$ m/sec).61

Figure 34. Mean distance values for the Main TSF site location ($V_{S30} = 760$ m/sec).61

Figure 35. Mean epsilon values for the Main TSF site location ($V_{S30} = 760$ m/sec).62

Figure 36. Mean magnitude values from the slab source for depth ranges of 50 – 75 km (a) and 100 – 125 km (b) for the Main TSF site location ($V_{S30} = 760$ m/sec).....63

Figure 37. Mean distance values from the slab source for depth ranges of 50 – 75 km (a) and 100 – 125 km (b) for the Main TSF site location ($V_{S30} = 760$ m/sec).....64

Figure 38. Mean epsilon values from the slab source for depth ranges of 50 – 75 km (a) and 100 – 125 km (b) for the Main TSF site location ($V_{S30} = 760$ m/sec).....65

Figure 39. Fractile hazard curves for PGA (0.01 sec) (a) and 0.2 sec (b) for the Main TSF site location.67

Figure 40. Fractile hazard curves for 0.5 sec (a) and 1 sec (b) for the Main TSF site location...68

Figure 41. Fractile hazard curves for 3 sec for the Main TSF site location.69

Figure 42. Fractile UHS for the Main TSF site location for 5,000-yr return period hazard level plotted log-linear (a) and log-log (b).72

Figure 43. Fractile UHS for the Main TSF site location for 10,000-yr return period hazard level plotted log-linear (a) and log-log (b).73

Figure 44. Deaggregation binned contribution as a function of magnitude and distance for the Main TSF site location, 475-yr hazard level and PGA (0.01 sec) (a) and 0.2 sec (b).75

Figure 45. Deaggregation binned contribution as a function of magnitude and distance for the Main TSF site location, 475-yr hazard level and 0.5 sec (a) and 1 sec (b).76

Figure 46. Deaggregation binned contribution as a function of magnitude and distance for the Main TSF site location, 475-yr hazard level and 3 sec.	77
Figure 47. Deaggregation binned contribution as a function of magnitude and distance for the Main TSF site location, 5,000-yr hazard level and PGA (0.01 sec) (a) and 0.2 sec (b).	78
Figure 48. Deaggregation binned contribution as a function of magnitude and distance for the Main TSF site location, 5,000-yr hazard level and 0.5 sec (a) and 1 sec (b).	79
Figure 49. Deaggregation binned contribution as a function of magnitude and distance for the Main TSF site location, 5,000-yr hazard level and 3 sec.	80
Figure 50. Deaggregation binned contribution as a function of magnitude and distance for the Main TSF site location, 10,000-yr hazard level and PGA (0.01 sec) (a) and 0.2 sec (b).	81
Figure 51. Deaggregation binned contribution as a function of magnitude and distance for the Main TSF site location, 10,000-yr hazard level and 0.5 sec (a) and 1 sec (b).	82
Figure 52. Deaggregation binned contribution as a function of magnitude and distance for the Main TSF site location, 10,000-yr hazard level and 3 sec.	83
Figure 53. UHS spectra for the Pyritic TSF site location ($V_{S30} = 760$ m/sec) plot log-linear (a) and log-log (b).	87
Figure 54. Fractile UHS for the Pyritic TSF site location for 5,000-yr return period hazard level plotted log-linear (a) and log-log (b).	88
Figure 55. Fractile UHS for the Pyritic TSF site location for 10,000-yr return period hazard level plotted log-linear (a) and log-log (b).	89
Figure 56. UHS spectra for the South TSF site location ($V_{S30} = 760$ m/sec) plot log-linear (a) and log-log (b).	93
Figure 57. Fractile UHS for the South TSF site location for 5,000-yr return period hazard level plotted log-linear (a) and log-log (b).	94
Figure 58. Fractile UHS for the South TSF site location for 10,000-yr return period hazard level plotted log-linear (a) and log-log (b).	95
Figure 59. Comparison of mean UHS for the three site locations plotted log-linear (a) and log-log (b).	97
Figure 60. Spectral ratio of UHS from the two TSF site locations relative to the ground motions from the Main TSF site location.	98
Figure 61. Comparison of mean UHS for the Main TSF site location only using the BCHydro GMM for the subduction events plotted log-linear (a) and log-log (b).	99
Figure 62. Spectral ratio (UHS with full BCHydro GMM divided by UHS with GMC model) of UHS for the Main TSF site location using only the BCHydro ground-motion model and the full GMC model for subduction events.	100
Figure 63. Median DSHA scenario events (Main TSF) spectra plotted log-linear (a) and log-log (b).	105
Figure 64. 84 th percentile DSHA scenario events (Main TSF) spectra plotted log-linear (a) and log-log (b).	106
Figure 65. 84 th percentile DSHA scenario events (Main TSF) spectra from the Knight-Piesold (2013) study and the current study plotted log-linear (a) and log-log (b).	107
Figure 66. 84 th percentile DSHA scenario events (Pyritic TSF) spectra from the Knight-Piesold (2013) study and the current study plotted log-linear (a) and log-log (b).	110

Figure 67. 84th percentile DSHA scenario events (South TSF) spectra from the Knight-Piesold (2013) study and the current study plotted log-linear (a) and log-log (b).....113

1. Introduction

A seismic hazard analysis (SHA) study is performed for the Pebble Mine project located in Southwest Alaska. This large proposed surface mining complex is located greater than 300 km southwest of Anchorage and approximately 100 km west of the Cook Inlet. As part of the proposed mining operations, three Tailings Storage Facilities (TSF) are expected to be constructed as shown in Figure 1. The planned heights for these three TSF are 545 feet (Main TSF), 305 – 425 feet (Pyritic TSF) and 300 feet (South TSF) (Pebble Partnership, 2018). For this SHA study, ground motions are estimated for approximate center point locations of the three main TSF locations: Main, Pyritic (Area E), and South, as listed in Table 1. These three site locations are within approximately 8 km of each other and as such the estimated ground motions from these three separate site locations are expected to be similar. A full presentation of the analysis is provided for the Main TSF site location and an abbreviated set of the results is presented for the other two TSF site locations in the report.

Table 1. Selected site locations for the Main, Pyritic and South TSF sites.

TSF	Latitude (North)	Longitude (West)
Main	59.908	-155.417
Pyritic (Area E)	59.897	-155.336
South	59.841	-155.457

Ground motions are developed for the horizontal component of motion based on acceleration response spectra consistent with 5% spectral damping. The development of vertical ground-motion spectra is not included in this study, nor is the development of spectrum compatible time histories. All of the ground-motion estimates are based on an assumed reference site condition of rock material with an average shear wave velocity in the top 30 m (V_{S30}) of 760 m/sec. The selection of this reference rock site condition is based on the limited site-specific material information available for the TSF site locations, the limited applicability of the ground-motion models (GMM) for harder rock site conditions, and the ability to scale ground motions from this common reference site condition to potential hard rock site-specific conditions that might be expected around the Pebble Mine project site. Ground motions developed for reference site conditions with V_{S30} of 760 m/sec can be subsequently adjusted to site-specific conditions through a standard analytical site response study when additional site measurements are obtained. Ground motions in this study are developed for a suite of spectral periods ranging from PGA (0.01 sec) to 10 sec.

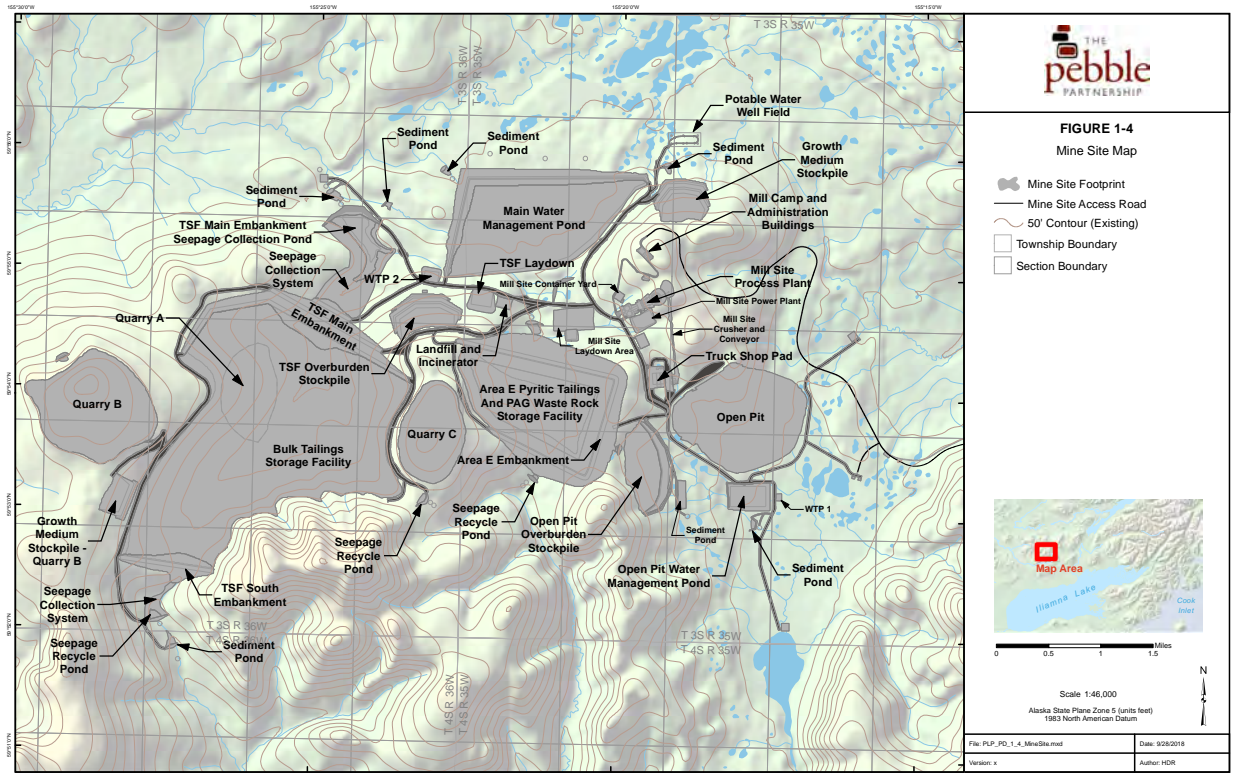


Figure 1. Overview map of the proposed Pebble Mine project in Southwest Alaska. Three TSF embankments are indicated on the map (Main Embankment, Pyritic Area E embankment, and South Embankment). (Source: Pebble Partnership, 2018)

This SHA study follows the current state of practice in performing both a probabilistic seismic hazard analysis (PSHA) and deterministic seismic hazard analysis (DSHA). Following this approach, previous seismic source characterization (SSC) models and as well ground-motion characterization (GMC) models used in previous SHA studies (e.g., Knight-Piesold, 2013, Wesson et al., 2007, 2008) are reviewed and considered in the analysis. In addition, a literature review for both SSC and GMC models is conducted. Note that no field studies are conducted as part of this SHA study.

The basic elements of a SHA are shown in Figure 2 (Earthquake Engineering Research Institute, 1989). The SSC model and the GMC model constitute the input to both the PSHA and DSHA. Note that for the DSHA, the probability density function for magnitude is not required, but rather, the maximum magnitude associated with each seismic source is required. The SSC model defines the earthquake source seismicity and geometry while the GMC model defines the ground-motion scaling as a function of the earthquake source parameters, propagation parameters, and local site conditions.

The primary output of a PSHA study is a set of seismic hazard curves for the ground-motion parameters of interest from which uniform hazard spectra (UHS) are developed using equations given in McGuire (2004) given a specific hazard level (i.e., return period). UHS are developed for

return periods of 475, 1,000, 2,475, 5,000, and 10,000 years for this study. Hazard curves are computed for the mean hazard curves and as well the fractile distribution of hazard curves that allows for the estimate of the uncertainty associated with the mean hazard results. A deaggregation of the seismic hazard using equations given in Bazzurro and Cornell (1999) is used to define controlling events (design earthquake scenarios) and provide an understanding of the controlling seismic sources to the total hazard. These deaggregation results are expected to vary as a function of spectral period and hazard level.

For the DSHA study, the primary output is the response spectrum associated with a given seismic source event consistent with SSC and GMC models. The resulting spectra are computed for the median and 84th percentile cases. Only those scenario events that control the DSHA (i.e., estimate the largest ground motions) are typically considered in a DSHA study.

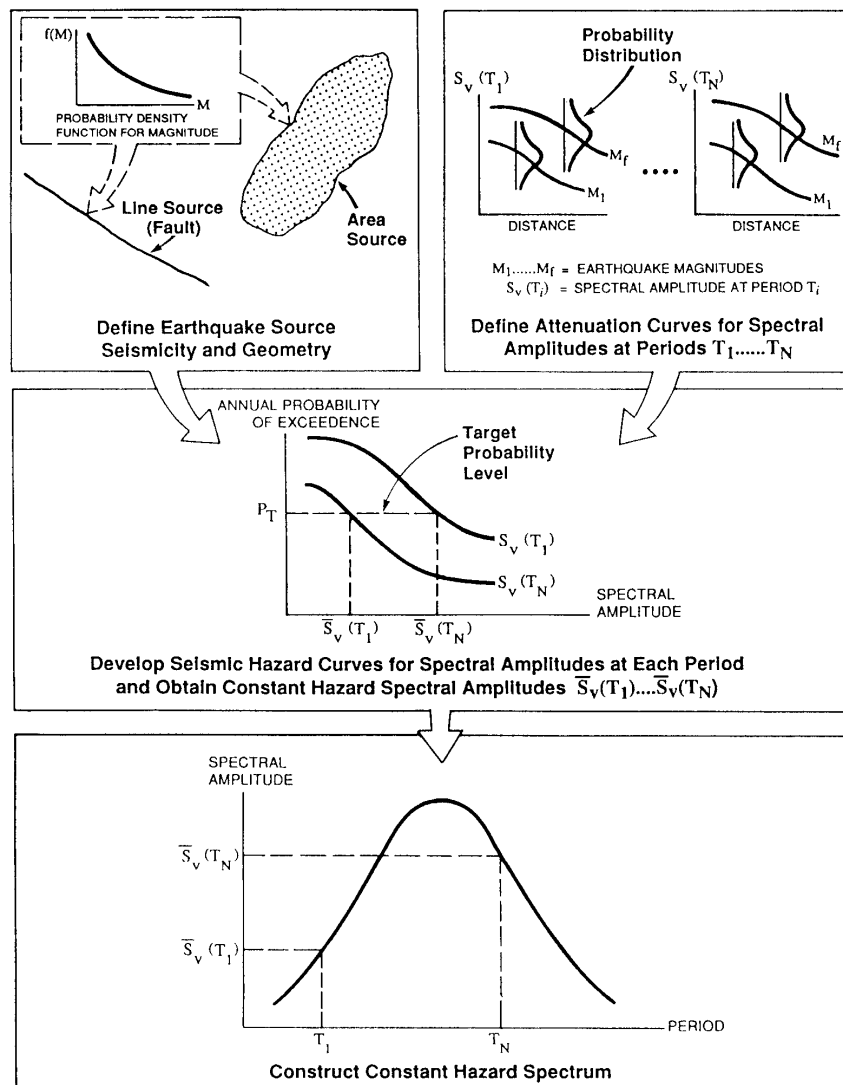


Figure 2. Schematic showing the elements of a probabilistic seismic hazard analysis (Source: Earthquake Engineering Research Institute, 1989).

The PSHA is computed for this study using the HAZ45.2 computer program developed by D. Norm Abrahamson (Abrahamson, 2018). This computer program is validated for calculating seismic hazard by successfully passing the test cases developed as part of the Pacific Earthquake Engineering Research Center (PEER) PSHA code verification project (Hale et al., 2018).

In this report, we present an overview of the SSC and GMC models as developed and implemented in the SHA study. The PSHA results are presented in terms of mean and fractile hazard curves at select spectral periods (i.e., 0.01, 0.2, 0.5, 1.0, and 3.0 sec). Based on the full set of spectral period hazard curves, the uniform hazard spectra (UHS) are presented at a suite of return period levels spanning the range of 475-yr to 10,000-yr. Deaggregation results are also presented in the report for a select suite of spectral periods and hazard levels.

For the DSHA, the computed spectra for the median and 84th percentile cases are provided. These deterministic spectra are calculated for each of the three different seismic sources considered in the analysis: crustal faults, subduction interface events and subduction slab events. In addition, comparisons relative to the UHS spectra are presented in the report.

The resulting PSHA and DSHA ground motions for the reference site condition of rock material with a V_{S30} value of 760 m/sec are presented and compared in this report, however, a recommendation of the applicable design spectra for the TSFs is not included as part of the scope of this report.

1.1 Previous SHA studies

As part of the USGS development of seismic hazard maps for the United States, the most current regional seismic hazard map for the state of Alaska was published in 2007 (Wesson et al., 2007, 2008). Currently the USGS has begun the process of updating this regional map for Alaska, but at this time, any preliminary results based on this update are not available (C. Mueller, personal communication). It is expected that this updating process may require a year or more before it will be completed. Note that the USGS did not perform a DSHA study for the region of Alaska for their 2007 study.

A previous site-specific study by Knight-Piesold (2013) was conducted for the Pebble Mine project. The selected site location used in that study was approximately 2 km west of the selected Pyritic TSF site location, which places it approximately in the center of the Open Pit in Figure 1. This previous study performed both a PSHA and DSHA study for this selected site location. This study relied mainly on the SSC model developed for the USGS 2007 regional seismic hazard map (Wesson et al., 2007) with some additional crustal fault characterizations around the project area (Knight-Piesold, 2013).

For the GMC model, the Knight-Piesold (2013) study employed more current GMMs than those used for the USGS 2007 study. However, these GMMs have subsequently been superseded by more recent GMMs as noted in the technical review of the Knight-Piesold (2013) study

(Parkington, 2018). One of the recommendations from this review was the use of the more current NGA-West2 GMMs for the deterministic analysis of the crustal faults (Parkington, 2018).

In addition to the noted release and suggested use of updated crustal GMMs, more recent subduction GMMs are available and have been used in seismic hazard analysis studies to estimate ground motions from subduction earthquakes than were used in the Knight-Piesold (2013) study.

As part of the development of the SSC and GMC models used in this current SHA study, deviations or differences from this current study and both the USGS (Wesson et al., 2007, 2008) and Knight-Piesold (2013) studies are presented and discussed in the report. In addition, a comparison of the results from these studies is evaluated in the report.

2. Seismic Source Characterization

2.1 Regional Tectonics

The dominant tectonic feature in Southwest Alaska is the seismically active subduction of the Pacific plate beneath the North America plate. This is occurring with a relative plate motion rate of approximate 55 mm/yr (Koehler and Carver, 2018 and references therein) as indicated in Figure 3. Historically, several large interface events have occurred along this approximate 4,000 km Alaska-Aleutian subduction zone with the largest being the 1964 **M9.2** Great Alaska earthquake. The approximate rupture zones for these large historical interface events are shown in Figure 3. Historical events associated with the deeper part of the subducting slab have also been observed in the region with the two most recent events being the 2016 **M7.1** Iniskin earthquake (Abers and Mann, 2018) and the 2018 **M7.1** Anchorage earthquake (Ruppert and Witter, 2020). The earthquake locations of these two deeper and significant slab earthquakes are shown in Figure 4 along with the depth contours for the top of the subducting slab, the approximate rupture area of the 1964 Great Alaska earthquake and regional seismicity. Deep slab events associated with the subducting Pacific plate have been observed down to depths as great as 200 km in the region, although with less frequency than slab events associated with the shallower depths of the subducting plate.

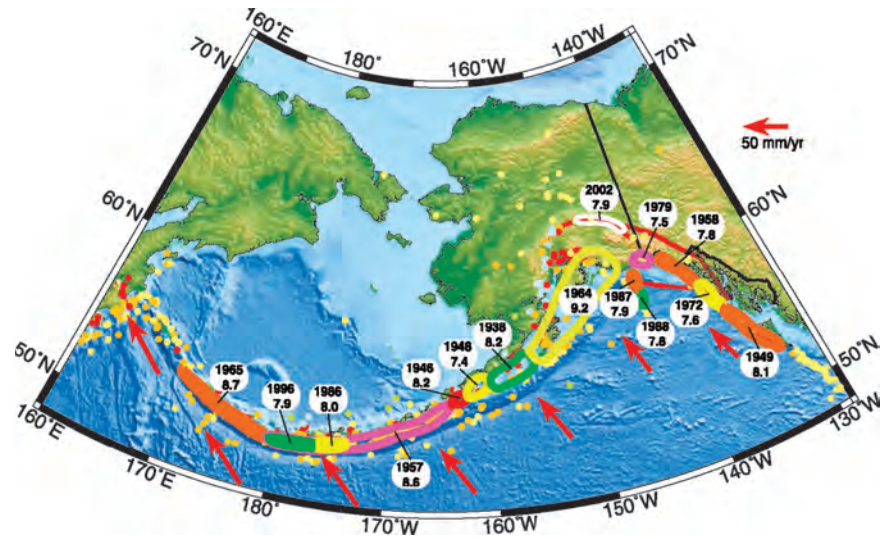


Figure 3. Generalized tectonic environment for Alaska and the approximate rupture zones for the large historical earthquakes associated with the interface subduction zones and major crustal faults (Source: Wesson et al., 2008).

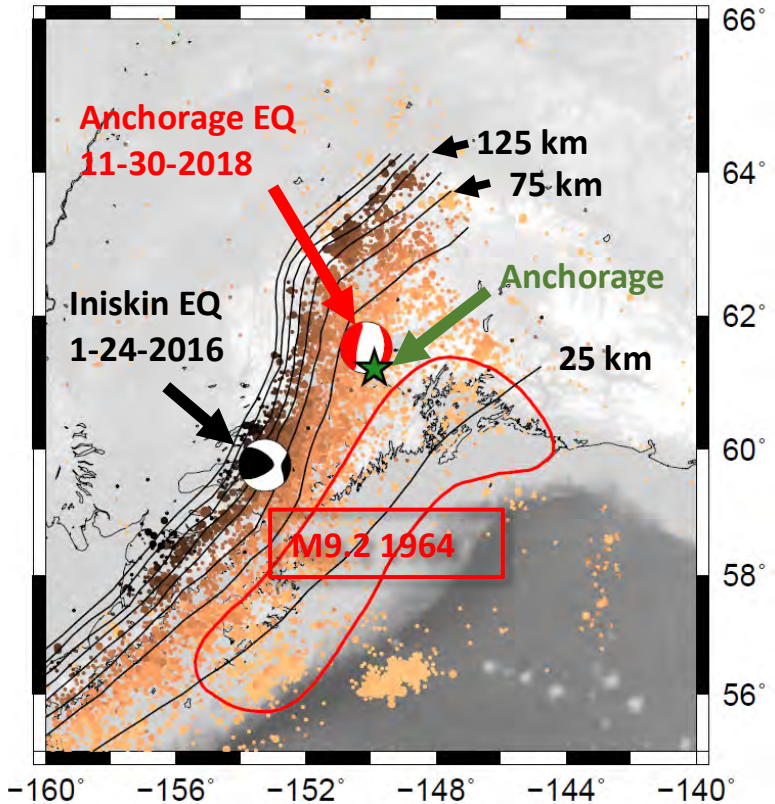


Figure 4. Location of two historical significant slab events crustal faults (Source: Abers and Mann, 2018).

In addition to the subducting plates tectonic feature, several major crustal faults have been identified in Central and Southeast Alaska (Koehler et al., 2012; Koehler et al. 2013, Koehler and Carver, 2018). These crustal faults are common in the backarc region of oblique and rotational plate vector motions as is occurring along the eastern section of the Alaska-Aleutian subduction zone (Elliott and Freymueller, 2018). Specifically, the Denali fault system was the source of the 2002 **M**7.9 Denali earthquake. Given its proximity to the major population centers of Fairbanks and Anchorage and the recent large earthquake, this section of the Denali fault has received more extensive field investigations and studies (e.g., see Haeusler et al., 2016 and references therein) than the extended sections of the fault system to the west which are closer the Pebble project sites. Additional secondary crustal faults have been identified and characterized in the region (Koehler et al., 2012; Koehler et al. 2013, Koehler and Carver, 2018) and are discussed as part of the SSC model development.

2.2 Seismicity

Historically Alaska had recorded a large number of earthquakes given its active tectonic environment. These events are associated with both crustal events and as well both interface and slab subduction events. As part of the USGS regional seismic hazard maps, a compiled historical seismicity catalog was developed which included earthquakes through the end of 2004 (Wesson et al., 2007, 2008). As part of this development, a standard process was applied for the removal of duplicate event listings and the identification of dependent earthquakes. The duplicate removal process followed a ranking of reporting seismicity catalog agencies with the preferred location being selected from the highest ranking reporting catalog agency (Wesson et al., 2007, 2008). For the identification of dependent events, the Gardner and Knopoff (1974) methodology was applied. This USGS seismicity catalog was obtained (C. Mueller, personal communication) and used for events prior to 2005. These events are plotted in Figure 5 for a selected project region between latitudes 52 to 65 degrees north and longitudes -144 to -165 degrees west. The events falling in this project section box are plotted in Figure 5 and are separated based on the depth boundary value of 50 km that was used in the USGS analysis (Wesson et al., 2017, 2018).

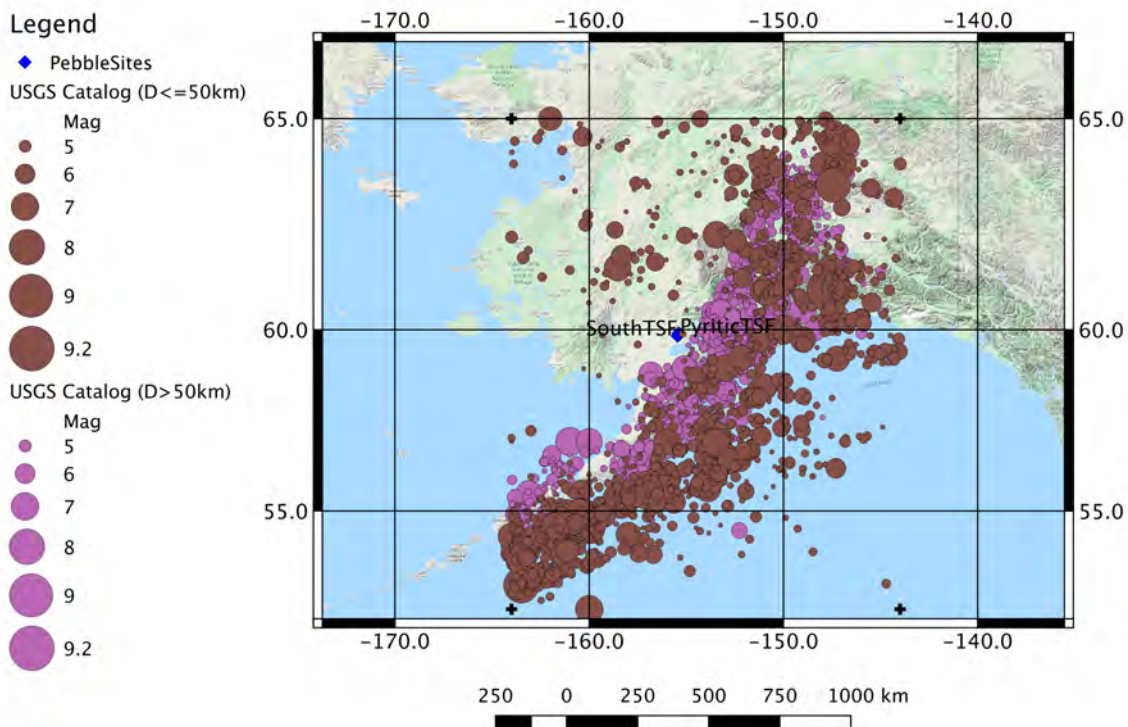


Figure 5. USGS seismicity catalog (through 2004) for events within the project region.

Given the expected occurrence of earthquakes in this region since the end of 2004, a seismicity catalog search from the ANSS Comcat on-line catalog web portal (<https://earthquake.usgs.gov/earthquakes/search/>) is performed for the bounding project box region starting from January 1, 2005 through to March 27, 2020. This search is not performed for the pre-2005 time based on the recommendation from C. Muller (personal communication) that it should be consistent with the USGS 2007 catalog. Given this recent seismicity catalog search, the various magnitude scales are converted to a common moment magnitude scale following the Sipkin (2003) and Utsu (2002) scaling relationships. These relationships are the same relationships used in a recent SHA study in British Columbia Canada (BC Hydro, 2012).

Following the same approach that was used by the USGS, dependent events are identified based on Gardner and Knopoff (1974). The resulting catalog for events since January 1, 2005 is plotted in Figure 6, again separated by the depth boundary of 50 km.

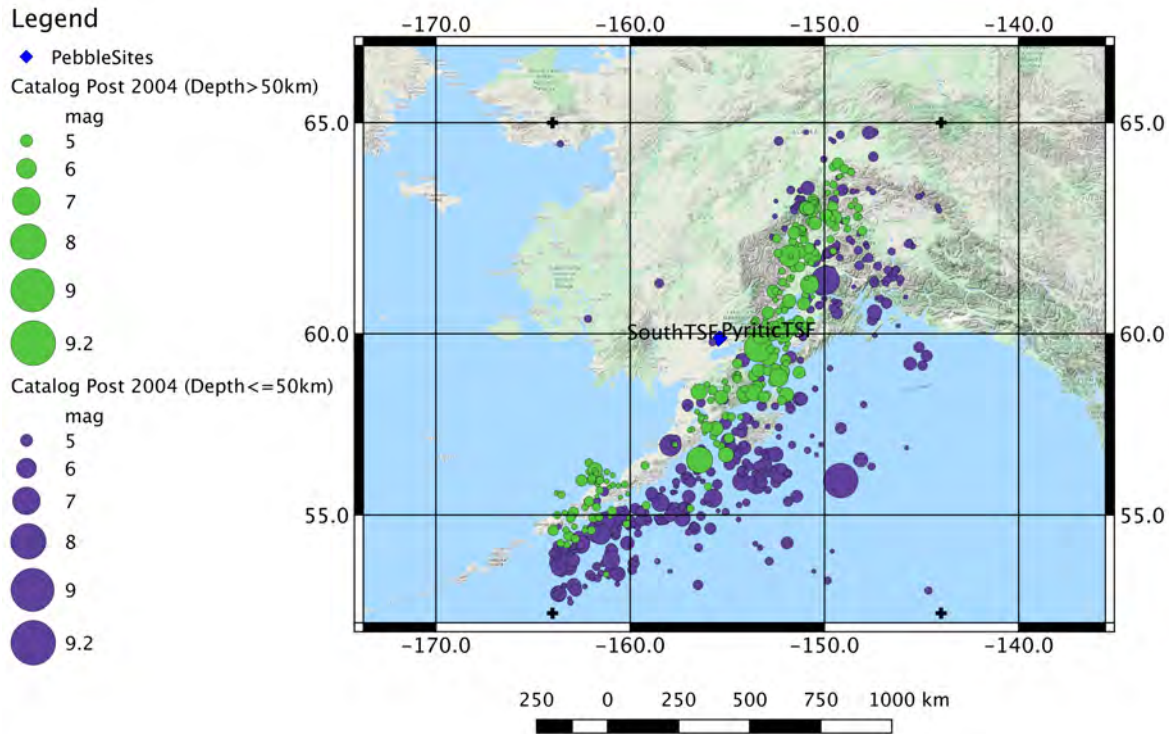


Figure 6. Seismicity catalog (since January 1, 2005) for events within the project region.

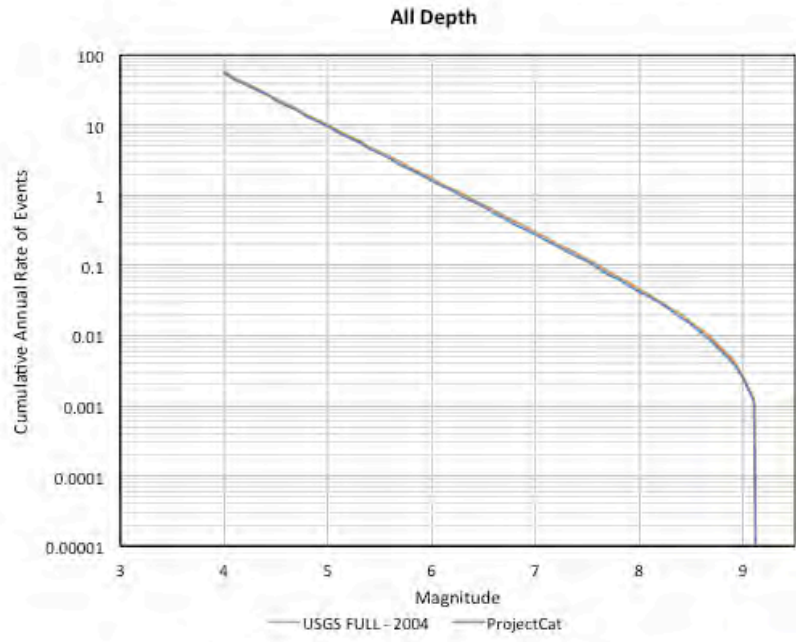
Visually for the active subduction zone, the recent events since January 1, 2005 (Figure 6) show a similar activity rate and geographic distribution to the pre 2005 events (Figure 5). For the interior region of Alaska away from the subduction zone, the more recent events are less populace which can be an artificial visual observation given the shorter time period for the recent events when compared to the full USGS catalog.

The first event in the USGS catalog occurred in 1899. A critical input parameter needed for the estimation of recurrence parameters from an earthquake catalog is the period of completeness. This has been observed to be magnitude dependent and is heavily dependent on the seismic network coverage and or historical accounts for a given region. As expected, the limited historical accounts and later installed seismic instruments networks limit the period of completeness for this region of Alaska. The USGS (Wesson et al., 2007, 2008) estimated the period of completeness as listed in Table 2. Similar period of completeness intervals were estimated from the more recent SHA study for Susitna Dam (Furgo, 2012), and for that study, the same USGS intervals were adopted.

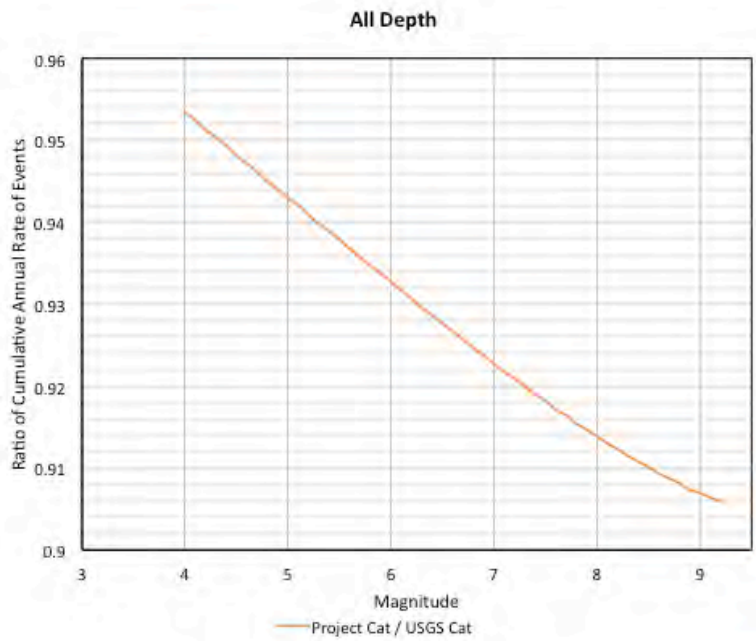
Table 2. Period of completeness for USGS earthquake catalog.

Magnitude	Completeness year
4.5 and greater	1964
6.0 and greater	1932
6.9 and greater	1898

Given the updated seismicity catalog developed for this SHA study, recurrence parameters are estimated following the Weichert (1980) methodology for both the USGS catalog and the full updated catalog. The period of completeness intervals listed in Table 2 are applied in the calculation and recurrence parameters are computed for the full catalog and the depth differentiated catalog. The results are shown in Figure 7 – 9. The top plot in each figure shows the calculated cumulative annual recurrence curve from the USGS catalog (orange lines) and the project catalog (blue line). The bottom plot shows the ratio between the project catalog and the USGS catalog. Based on these comparisons of the recurrence curves, the addition of approximately 15 years of more recent seismicity (project catalog) resulted in a reduction of about 10% or less in the overall recurrence rates of earthquakes in the project region for all depths. For the depths less than 50 km the reduction is slightly larger up to about 14% and less and for the deeper events (i.e., greater or equal to 50 km) the reduction is only about 6%.

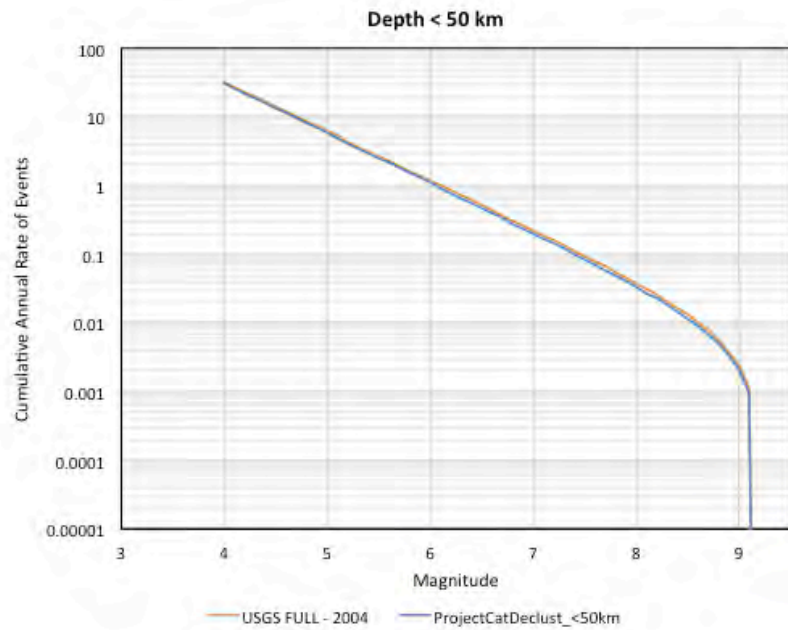


(a)

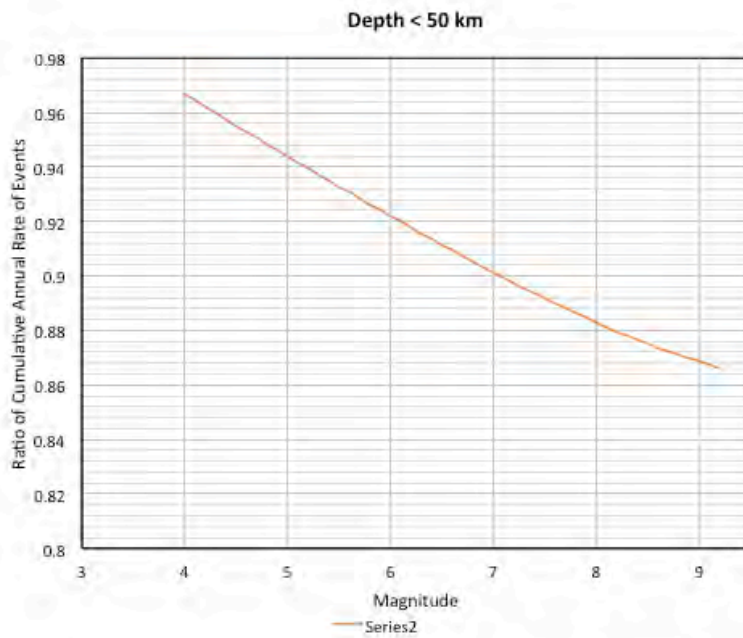


(b)

Figure 7. Calculated recurrence curve for the USGS catalog (orange line) and the updated project catalog (solid blue line) over all depths (a) and ratio of recurrence curves for the project catalog over USGS catalog (b).

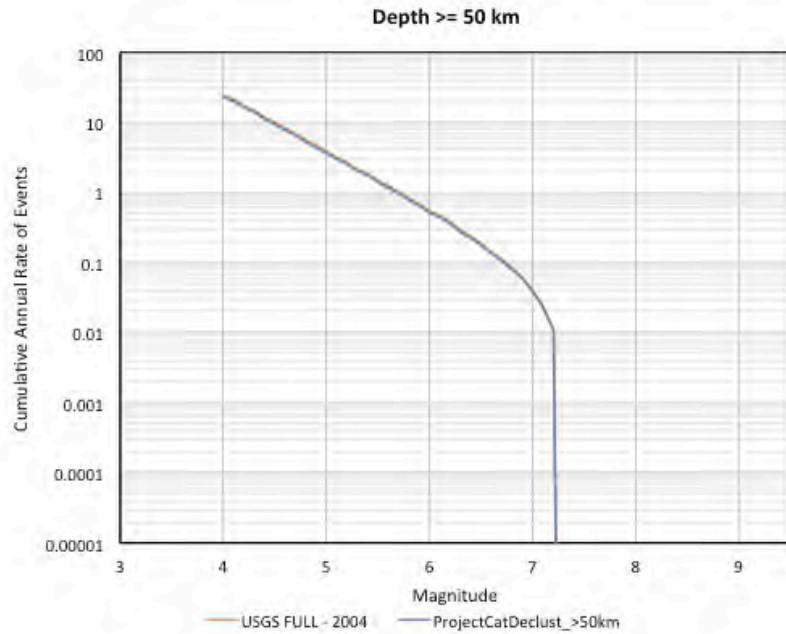


(a)

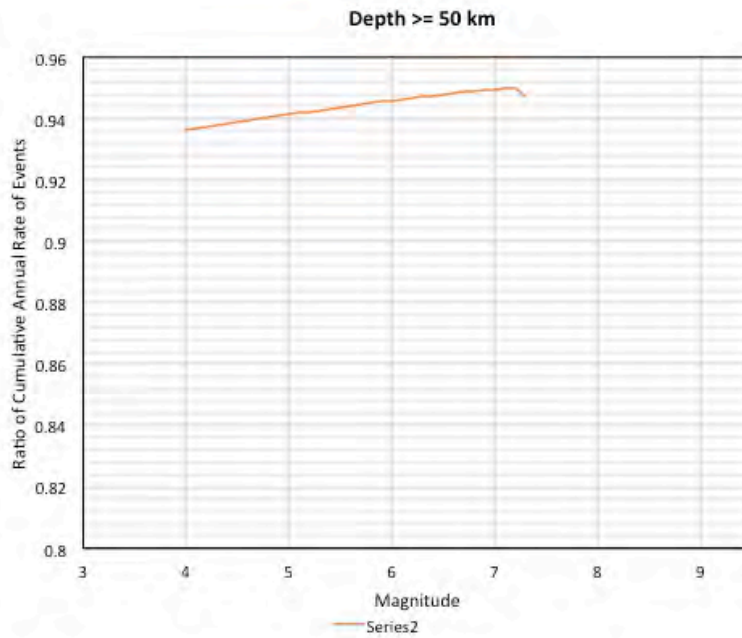


(b)

Figure 8. Calculated recurrence curve for the USGS catalog (orange line) and the updated project catalog (solid blue line) for depths less than 50 km (a) and ratio of recurrence curves for the project catalog over USGS catalog (b).



(a)



(b)

Figure 9. Calculated recurrence curve for the USGS catalog (orange line) and the updated project catalog (solid blue line) depths greater than or equal to 50 km (a) and ratio of recurrence curves for the project catalog over USGS catalog (b).

2.3 Crustal Fault Sources

Given the overall regional tectonics, several crustal faults have been identified in the project region (Wesson et al., 2007, 2008; Koehler et al., 2012; Koehler et al, 2013; Koehler and Carver, 2018). These faults have been characterized based either on field investigations, field mapping and or inferences from geologic, tectonic and historical studies. As noted earlier, for this seismic hazard study, no new field work is conducted, and the characterization and implementation of the crustal faults for the analysis is based on previous seismic hazard studies in the region and published literature. Future studies, which may lead to the identification and characterization of new faults and or refinement of the current faults used in this analysis, may require a reassessment of the seismic hazard results presented in this study. The crustal fault sources used in this analysis are shown in Figure 10 along with the project site location. Additional crustal faults have been identified and characterized in Southern Alaska, but they are not expected to contribute to the overall seismic hazard at the project site location given their large distance from the project site (Wesson et al., 2007, 2008; Fugro, 2012; Koehler et al., 2012; Koehler et al, 2013; Koehler and Carver, 2018). For each of these faults, a discussion is presented on their characterization used for this SHA. Although the Knight-Piesold (2013) study provides a listing of the faults used in their analysis, their report is lacking on the full specific characterization of these specific crustal faults (e.g., slip rate), and thus an assessment cannot fully be made about potential differences in the characterization of these faults. Discussion is provided, however, when direct comparisons between the Knight-Piesold (2013) study and this current SHA study can be made.

For all of the crustal faults, the Youngs and Coppersmith (1984) magnitude recurrence model is applied. This is selected based on the common state of practice for the modeling of crustal faults. The vertical thickness for each fault is assigned to be 15 km. This value is consistent with the assigned vertical thickness of 15 km for the Castle Mountain fault used by the USGS (Wesson et al., 2007) and is also consistent with the average hypocentral depth of about 12 km for crustal events in the area. Given the relatively small contribution to the total hazard from these crustal faults, no epistemic variability was applied to the vertical thickness. All the crustal faults are assumed to be surface rupturing faults, which to be consistent with the USGS model (Wesson et al., 2007).

The estimate of the maximum magnitudes for the crustal faults is based on the magnitude-area scaling relationship of Wells and Coppersmith (1994). For cases in which variable dip angles are assigned, the best estimate dip angle is used in calculating the maximum magnitude. To capture the epistemic uncertainty, the maximum magnitude is varied by +/-0.2 magnitude units with the weights of 0.185, 0.63 and 0.185 selected to represent the 5th, 50th and 95th percentiles. This range is based on the observed range based on different magnitude-area scaling relationships (e.g., see Appendix E of Field et al., 2013).

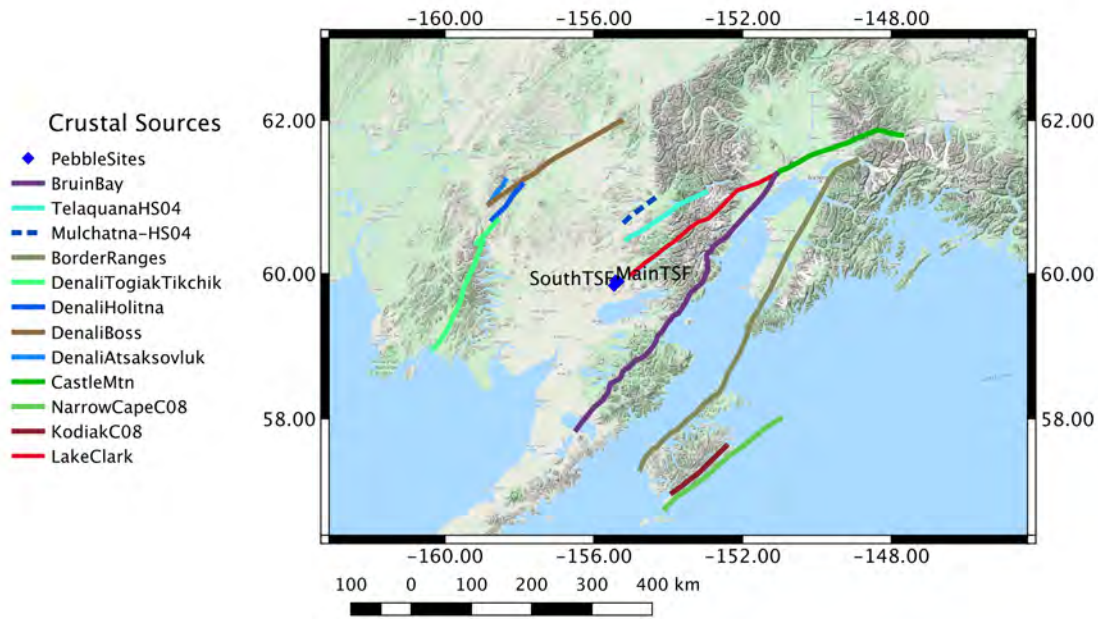


Figure 10. Characterized crustal fault used in the SHA.

Lake Clark Fault

The Lake Clark fault is a right-oblique reverse fault that is mapped from the southwest end of Lake Clark (Haeussler and Saltus, 2004) in a northeasterly direction to the terminus of the western end of the Castle Mountain fault, north of the Cook Inlet. This fault has been identified and mapped in several studies (e.g., Haeussler and Saltus, 2004; Amato et al., 2007; Gillis et al. 2009; Koehler and Reger, 2011), including the Quaternary fault and fold database for Alaska (Koehler et al., 2012). The western trace and terminus of the fault, which is closest to the project site, was refined based on the analysis of aeromagnetic data (Haeussler and Saltus, 2004). In that study, the preferred Lake Clark fault trace was along the northern side of Lake Clark and the end of the fault was approximately located at the southwest end of Lake Clark (Haeussler and Saltus, 2004).

Given the general limited amount of field investigations in this part of Alaska for crustal fault studies due to the remoteness and difficulty in performing such field investigations, there exists a level of uncertainty about the western terminus of the Lake Clark fault. Any western extension of this fault would bring it closer to the project site locations. As noted in the Knight-Piesold (2013) report, personal communications with P. Haeussler indicated that the southwest

extension of the Lake Clark fault was unresolvable given the lack of bedrock exposures in the area but there could be a southern splay towards Iliamna Lake. Two additional field studies (Koehler, 2010; Haeussler and Waythomas, 2011) of the mapped Braid surface scarp south of the project site along the north side of Iliamna Lake concluded that the creation of the scarp was not based on seismic activities. Also noted in the Knight-Piesold (2013) report, a detailed surface geology and geomorphology study was conducted by T. Hamilton for the immediate area around the project site and his findings did not indicate any linear features or disturbance of surficial deposits that would be consistent with seismic fault activity. Based on these studies and conclusions and the acceptance of the Knight-Piesold (2013) characterization, we model the terminus of the Lake Clark fault at the southwest end of Lake Clark, consistent with the findings from Haeussler and Saltus (2004). Any additional future studies which would potentially extend this western terminus of the Lake Clark fault could impact the hazard results provided in this study, and we recommend that a re-analysis be performed in the future based on any updated characterizations of the Lake Clark fault.

Haeussler and Saltus (2004) estimated approximately 26 km of right-lateral offset in the past 34 – 39 Ma for the Lake Clark fault. Previously, Plafker et al. (1975) estimated about 5 km of offset in the last 38.6 Ma and Detterman et al. (1976) estimated about 500 – 1,000 m of vertical uplift of the northwest side of the fault from offset Tertiary strata near the Cook Inlet. These estimates lead to geologic slip rates of 0.67 – 0.76 mm/yr from the Haeussler and Saltus (2004) study and a slower rate of 0.14 mm/yr from the Plafker et al. (1975) study. Koehler and Carver (2018) also note that the Lake Clark fault could be active but with a low slip rate and still remains a poorly characterized fault. To capture this range in the estimated slip rates, four values are assigned. The values of 0.67, 0.715 and 0.76 mm/yr are adopted from the Haeussler and Saltus (2004) study with a total weight of 0.9. The individual weights of 0.27, 0.36, and 0.27 are assigned given the limited data. The central value of 0.715 mm/yr is based on the average of the upper and lower values. The remaining 0.1 weight was assigned to the lower slip rate of 0.14 mm/yr coming from the previous Plafker et al. (1975) study. This assigned 0.1 weight is based on the judgment that the more recent Haeussler and Saltus (2004) study better represented the slip rates than the older study.

The dip angle of this fault is assigned to be 70 degrees with an uncertainty of +/- 15 degrees based on the characterization given in Koehler and Reger (2011). The closest approach of this fault to the Main TSF site location is approximately 25 km with the site being located on the hanging-wall side of this fault.

Based on the mapped length of 262 km, an estimated maximum magnitude of 7.62 is computed based on the Wells and Coppersmith (1994) empirical relationship for magnitude and fault area.

Castle Mountain Fault

The Castle Mountain fault is located northeast of the project site and its western end is at the northeast end of the Lake Clark fault. Given the similar alignment of the fault traces from these

two faults, it has been postulated that these two faults are part of the same system and or connected (Koehler and Reger, 2011); however, no definitive evidence has been shown that this is case. Therefore, for this study, the two faults are treated as separate faults similar to the other seismic hazard studies performed in the region (Fugro, 2012).

The Castle Mountain fault is one of the few crustal faults characterized in the USGS 2007 study for Alaska (Wesson et al., 2007, 2008) in the region around the project site location. Given its relative close location to Anchorage and the observation of recent historical earthquakes associated with this fault, it has received more investigative studies over the years than the other crustal faults in the region (e.g., Labay and Haeussler, 2001; Haeussler et al., 2002; Willis et al., 2007; Koehler and Reger, 2011).

The fault is characterized as an oblique strike-slip fault with a high dip angle that is segmented into eastern and western sections (Willis et al., 2007). The eastern section has a noted dip angle of 75 degrees, dipping to the north, with associated historical events (mb 5.7 and 1984 and magnitude 4.5 in 1996) but no Holocene surface rupture (Willis et al., 2007 and references therein). In contrast, the western section has noted Holocene surface rupture but no associated historical earthquakes (Willis et al., 2007 and references therein).

Preferred slip-rate estimates for the western section of the Castle Mountain fault are 3.0 – 3.2 mm/yr (Willis et al., 2007). The USGS 2007 study (Wesson et al., 2007, 2008) used a slightly lower value of 2.9 mm/yr for the Castle Mountain fault which is a significant increase from the previous state hazard map for Alaska which used an assigned slip rate of 0.5 mm/yr (Wesson et al., 1999). The assigned slip rates for this study are listed in Table 3. The highest and lowest slip rate values of 3.2 and 0.5 mm/yr are selected to capture the range in slip rates each with 50% weight. These are selected given the potential feature that the western section of the Castle Mountain fault is less active (Willis et al., 2007) than the central and eastern section where most of the field work has been performed. This is consistent with the observed decrease in slip rate moving westward along the Denali fault system. Additional variation is not included in the slip rate logic tree for this fault given its distance from the project site and low contribution to the total hazard.

The dip angle of this fault is assigned to be 75 degrees with an uncertainty of +/- 10 degrees. These dip angles are based on general dip angles observed for oblique and strike-slip faults as well as the estimated values from Koehler and Reger (2011) for the Lake Clark fault. The weights for these three values are selected to represent the approximation for the 5th, 50th and 95th percentile distribution. The closest approach for this fault to the Main TSF site location is approximately 286 km. Based on the mapped length of 189 km, an estimated maximum magnitude of 7.47 is computed based on the Wells and Coppersmith (1994) empirical relationship for magnitude and fault area.

Telaquana Fault

The Telaquana fault is mapped parallel to the Lake Clark fault and is located about 35 km to the northwest (Haeussler and Saltus, 2004). Limited information is available for this fault in the published literature and the adopted characterization for this study is based on the characterization from Haeussler and Saltus (2004). This fault is classified as a right-lateral strike-slip fault based on the observed offsets of the magnetic anomalies. Haeussler and Saltus (2004) estimated 10 km (western end) and 11 km (eastern end) of offset in the past 34 – 39 Ma. This translates to a geologic slip rate of between 0.25 – 0.32 mm/yr. The adopted slip rates for the SSC model are listed in Table 3 for the Telaquana fault. These three values are based on the lowest, central, and highest slip rate estimates from the Haeussler and Saltus (2004) study and the assigned weights are selected to represent the 10th, 50th, and 90th percentile given the limited amount of data.

The closest distance from this fault to the Main TSF site location is approximately 63 km. Based on the mapped length of 135 km, an estimated maximum magnitude of 7.31 was computed based on the Wells and Coopersmith (1994) empirical relationship.

Mulchatna Fault

The Mulchatna fault is located north of the Telaquana fault and maps along a similar fault trace azimuth (see Figure 10). This mapped section of the fault is contained in the Plafker et al. (1994) neotectonic map for Alaska (Koehler et al., 2013) database but is not included in the Quaternary fault and fold database (Koehler et al., 2012). Plafker et al. (1994) had this fault identified as being pre-Quaternary. Decker et al. (1994) describe the characterization of the Mulchatna fault as being based on a pronounced aeromagnetic discontinuity.

As part of the Knight-Piesold (2013) study, the Mulchatna fault was included, however, the report does not present the full characterization of this fault which would be needed for a PSHA study (e.g., slip rate or recurrence interval estimates). Given the lack of knowledge for this fault either from the Knight-Piesold (2013) study, published literature (e.g., this fault is not described in the Koehler and Carver, 2018 study), the apparent lack of Quaternary seismic activity, and the expected minimal contribution to the seismic hazard for the project site, this crustal fault source is not included in the analysis. Future studies may provide the opportunity to include this potential crustal seismic source in future seismic hazard studies.

Bruin Bay Fault

The Bruin Bay fault is an identified fault which starts in the southwest of Becharof Lake and is mapped in a northeasterly direction to the approximate location of the Lake Clark and Castle Mountain faults in the northern Cook Inlet area (see Figure 10). This fault represents the northwestern tectonic boundary of the Cook Inlet forearc basin (Betka et al., 2017). Hartsock (1954) first identified the presence of this fault on the Iniskin Peninsula. The fault has been characterized as a reverse fault with variable dip angles ranging between 45 – 80 degrees

dipping to the northwest (Stevens and Crow, 2003 and references therein). Detterman and Reed (1980) noted that the Bruin Bay fault is not defined by a single plane, but rather is observed to be defined by a series of steeply dipping faults which span a range of 6 – 8 km. This is consistent with the Plafker et al. (1994) fault database provided in Koehler et al., (2013). For this seismic study, a singular fault plane is approximated based on these mapped fault traces and other assumed singular fault traces for the Bruin Bay fault (e.g., see Stevens and Crow, 2003; Haeussler and Saltus, 2011; Betka et al., 2017). To capture the uncertainty in the dip of the fault, three dip angles of 50, 65, and 80 degrees were assigned to this fault with the weights of 0.185, 0.63, 0.185 (see Table 3). The dip angles are based on a representative dip angle of 65 degrees for a reverse fault from the Stevens and Crow (2003) study and the range of +/-15 degrees from the Koehler and Reger (2011) study for the Lake Clark fault. The assigned weights are selected to represent the 5th, 50th, and 95th percentile. The closest approach for this fault to the Main TSF site location is approximately 99 km.

Estimates for the slip rate of the Bruin Bay fault are limited and based on long-term geologic offsets. A historical study for the northeastern end of the fault (Barnes, 1966) indicated that the fault is buried under Quaternary deposits except where it is exposed. Schmoll and Yehle (1987) concluded that there is no geologic evidence of activity within the last ~120,000 years (i.e., during the late Pleistocene or Holocene time period). Haeussler et al. (2000) postulate that the northern end of the fault may be associated with Quaternary deformation. More recently, Betka et al. (2017) postulated that the hanging-wall uplift rate associated with the Bruin Bay fault system could be in the range of 0.2 – 0.4 mm/yr based on the offset during the last 31 – 37 Ma. Koehler and Carver (2018) suggest that this fault could be reactivated given the modern stress field in the region. The assigned slip rates of 0.2, 0.3, and 0.4 mm/yr are selected given the estimated range from Betka et al. (2017). The assigned weights of 0.3, 0.4, and 0.3 are selected given the limited data to represent the 10th, 50th and 90th percentile.

Previous seismic hazard studies in the region (Woodward Clyde, 1978) have associated the November 3, 1943 crustal earthquake $M_w=7.2$ as potentially being associated with the Bruin Bay fault. The epicenter location of this event is located about 40 – 50 km north of the Castle Mountain fault and further away from the Bruin Bay fault. A more recent reanalysis of this event and other historical events in the Cook Inlet area (Silwal et al., 2018) does not support this association of the 1943 historical earthquake with the Bruin Bay fault system.

The total mapped length of the Bruin Bay fault is 509.6 km would translate to a maximum magnitude of 7.9. However, given the potential discontinuous nature of the sections of the Bruin Bay fault as mapped in the region, judgment is applied to reduce this total mapped fault length for the calculation of the maximum magnitude. The maximum magnitude is calculated based on the rupture length being equal to ½ of the total fault length and has a value of 7.6.

Border Ranges Fault

The Border Ranges fault represents the arc-forearc boundary of the Alaskan-Aleutian arc (Haeussler and Saltus, 2011; Pavlis and Roeske, 2007) and has been mapped on a large regional

scale as a single structure for over 1,300 km from Kodiak Island eastwards to Baranof Island (e.g., see Figure 1 of Pavlis and Roeske, 2007). On a more focused site-specific area scale, the Border Ranges fault consists of several shorter mapped segments (Plafker et al., 1994) similar to the other mapped faults in the project region. For this seismic hazard study, a single fault plane is selected to approximate the location of the Border Ranges fault (see Figure 10) due to the large distance to the site region.

Field investigations and general studies of this fault are variable along the sections with an increased emphasis and focus on the sections closer to Anchorage (Pavlis and Roeske, 2007 and references therein). Additional studies have also been conducted on the northwest side of Kodiak Island where the fault is exposed (Pavlis and Roeske, 2007 and references therein). This section is the closest to the project site at an approximate distance of 213 km. The fault is characterized as a vertically dipping strike-slip fault consistent with the tectonic evolution of this boundary fault (Stevens and Craw, 2003; Haeussler and Saltus, 2011).

Estimates of the fault activity of the Border Ranges fault have been limited especially in the region around the project site and has been noted to vary significantly along strike (Pavlis and Roeske, 2007). In the Stuart Creek region, which is located east of Anchorage, Pavlis and Roeske (2007) postulate that up to 130 km of displacement has occurred over the last 65 Ma. This would translate to a geologic slip rate of 2 mm/yr. For this seismic analysis, this estimated slip rate of 2 mm/yr is adopted as the central slip rate for the Border Ranges fault. In the region around Kodiak Island, Caver et al. (2008) estimate an overall southwest movement of 3 – 5 mm/yr for the Bering Block and a general regional tectonic GPS movement of 5 – 15 mm/yr. These estimates would be accommodated by the Border Ranges, Kodiak Island, and Narrow Cape faults. The upper and lower slip rates of 1 and 3 mm/yr are selected in combination with the upper and lower slip rates for the Kodiak Island and Narrow Cape faults to approximate the range of values from Carver et al. (2008). The range in total slip rates from the three faults is 3.25 – 11.6 mm/yr, which is slightly lower than the GPS regional range of 5 – 15 mm/yr from Carver et al. (2008) but more consistent with the Bering block specific range of 3 – 5 mm/yr from Carver et al. (2008). The assigned weights of 0.3, 0.4 and 0.3 are judged to be representative of the 10th, 50th, and 90th percentile based on the uncertainty in the data for this source.

Based on the mapped length of approximately 589 km, a maximum magnitude of 7.9 is estimated. However, consistent with the reduction applied for the Bruin Bay fault, the maximum magnitude assigned to the Border Range fault is computed based on the judgment of using ½ of the total mapped fault length. This maximum magnitude is 7.6.

Kodiak Island and Narrow Cape Faults

The Kodiak Island and Narrow Cape faults represent a series of sub-parallel faults around the area of Kodiak Island (Plafker et al., 1994; Koehler et al., 2013). These faults are azimuthally in alignment with the Border Ranges fault and the trench of the Aleutian Subduction zone (see Figure 10). These faults are believed to accommodate compression and flexure of the upper

plate given the on-going subduction tectonic process (Koehler and Caver, 2018). These faults were characterized to be vertically dipping strike-slip faults with the vertical thicknesses of 15 km (Carver et al., 2008).

GPS measurements across Kodiak Island indicate left-lateral displacements on the order of 5 – 15 mm/yr (Carver et al., 2008). This total would be accommodated by the Border Ranges, Kodiak Island and Narrow Cape faults. In addition, Carver et al. (2008) estimated an individual slip rate of 3.3 mm/yr for the Narrow Cape fault. In the USGS 2007 model, the Kodiak Island fault is assigned a slip rate of 1 mm/yr (Wesson et al., 2007). For this study, the central slip rates of 1 mm/yr (Wesson et al., 2007) and 3.3 mm/yr (Carver et al., 2008) are selected for the Kodiak Island and Narrow Cape faults, respectively. A factor of 2 is applied to these central slip rate estimates to reflect the large uncertainty in the data and the resulting range in the combined slip rates from the Border Range, Kodiak Island and Narrow Cape faults. As indicated previously, this range is between 3.25 – 11.6 mm/yr and is slightly lower than the Carver et al. (2008) range of 5 – 15 mm/yr based on the GPS measurements. It is judged that this slightly smaller range is acceptable given the large uncertainties, the limited data, and or the potential for the regional GPS measurements to be representing other faults not included in the fault slip rate combination. The assigned slip rates for the Kodiak Island and Narrow Cape faults are listed in Table 3 along with the weights that are selected based on the limited data.

Based on the mapped length of 115 km for the Kodiak Island fault, an estimated maximum magnitude of 7.24 is computed based on the Wells and Coppersmith (1994) empirical relationship for magnitude and fault area. The Narrow Cape fault is characterized with a total length of 237 km based on a series of mapped fault traces, mainly off shore of Kodiak Island. For the maximum magnitude, $\frac{1}{2}$ of the total fault length is used given the discontinuous nature of the fault, resulting in the same value of 7.24 as for the Kodiak Island fault. These faults are located at distances greater than 300 km from the Main TSF site location.

Denali Fault

The Denali fault is a major crustal fault in southern Alaska and is mapped from the western coast near Bristol Bay continuously to the Baranof Island region south of Juneau. Historically, larger earthquakes have occurred along this fault system with the largest most recent event being the 2002 Denali earthquake (**M7.9**). Given the significance of this large fault system, several investigations have been performed over the years (e.g., see Haeussler et al., 2016 and references therein); however, the level of investigations significantly decrease for the western sections of the fault system given the remoteness of its location.

The project site is located closest to the western segments of the Denali fault system (see Figure 10). Specifically, these segments are the Boss Holitna, Atsakovluk and Togiak-Tikchik segments going from east to west. Geologic slip-rate estimates in the region of the Denali fault that ruptured during the 2002 earthquake fall within the range of 7 – 14 mm/yr (Koehler and Carver, 2018). The limited slip-rate estimates both to the east and west of this region are noted to be lower (Koehler and Carver, 2008). An estimate of about 5 mm/yr has been computed for a

location along the Denali fault at a longitude of -152 degrees. Further to the west, near longitude -154.5, a recent estimate of the slip rate was 3 mm/yr (Haeussler et al., 2016). The observed decrease of the slip rate in the western segments of the Denali fault system (Haeussler et al., 2016) is consistent with the tectonic model of rotation and internal deformation of the southern Alaska block and transfer of slip to faults north of the Alaska Range (Haeussler et al., 2014). As part of the USGS 2007 analysis (Wesson et al., 2007, 2008), the slip rate associated with the western segments of the Denali fault system were tapered down from the peak slip rate values in the central section to a slip rate value of zero at a longitude of -154.7. A recent geodetic study for the state of Alaska estimates slip rates for the western extension of the Denali fault to be 0.5+/-0.4 mm/yr range (Elliot and Freymueller, 2018). Given the observed decrease in the slip rates along the western segments of the Denali fault system, slip rates for the four segments considered in this analysis are assigned to be 0.1, 0.5, and 0.9 mm/yr given the recent geodetic study for the State of Alaska. The weights assigned to these values are 0.3, 0.4, and 0.3 given the limited data.

The Boss and Atsakovluk segments have been classified as showing mid-Quaternary and Quaternary displacement, respectively (Koehler et al., 2013). The Holitna and Togiak-Titchik segments are classified as having pre-Quaternary displacements (Koehler et al., 2013). The Holitna segment is classified as being a northwest dipping reverse fault (Koehler and Carver, 2018), whereas the other faults are not classified and are assumed to be strike-slip in nature consistent with the other segments of the Denali fault system. The Holitna fault is assigned a dip angle of 60 degrees. This single value is selected as a representative value from reverse faults. No uncertainty is placed on this dip angle because of the large distance from the project site to this fault source and its relatively small contribution to the total hazard. All of these segments of the Denali fault system are approximately 200 km away from the Main TSF site location.

The individual fault lengths for each segment are listed in Table 3 along with the estimated maximum magnitude given the fault area.

Table 3. Seismic source characteristics for the crustal faults used in the analysis. Weights for multiple values are indicated in brackets.

Fault	Mechanism	Dip (Direction)	Vertical Thickness (km)¹	Length (km)	Slip Rate (mm/yr)	Magnitude
Lake Clark	Oblique [0.5] ² Reverse [0.5] ²	55 [0.185] 70 [0.63] 85 [0.185] (NW)	15	262.0	0.67 [0.27] 0.715 [0.36] 0.76 [0.27] 0.14 [0.10]	7.42 [0.185] 7.62 [0.63] 7.82 [0.185]
Castle Mountain	Oblique [0.5] Strike-slip [0.5]	65 [0.185] 75 [0.63] 85 [0.185] (NW)	15	189.5	3.2 [0.5] 0.5 [0.5]	7.27 [0.185] 7.47 [0.63] 7.67 [0.185]
Telaquana	Strike-slip	90	15	134.5	0.25 [0.30] 0.285 [0.40] 0.32 [0.30]	7.11 [0.185] 7.31 [0.63] 7.51 [0.185]
Bruin Bay	Reverse	50 [0.185] 65 [0.63] 80 [0.185] (NW)	15	509.6	0.2 [0.30] 0.3 [0.40] 0.4 [0.30]	7.4 [0.185] 7.6 ³ [0.63] 7.8 [0.185]
Border Ranges	Strike-slip	90	15	589.5	1.0 [0.30] 2.0 [0.40] 3.0 [0.30]	7.4 [0.185] 7.6 ³ [0.63] 7.8 [0.185]
Kodiak Island	Strike-slip	90	15	114.9	0.5 [0.30] 1.0 [0.40] 2.0 [0.30]	7.04 [0.185] 7.24 [0.63] 7.44 [0.185]
Narrow Cape	Strike-slip	90	15	236.6	1.7 [0.30] 3.3 [0.40] 6.6 [0.30]	7.04 [0.185] 7.24 ³ [0.63] 7.44 [0.185]
Denali – Boss	Strike-slip	90	15	223.3	0.1 [0.30] 0.5 [0.40]	7.32 [0.185] 7.52 [0.63]

					0.9 [0.30]	7.72 [0.185]
Denali - Holitna	Reverse	45 [0.30] 60 [0.40] 75 [0.30] (NW)	15	66.6	0.1 [0.30] 0.5 [0.40] 0.9 [0.30]	6.87 [0.185] 7.07 [0.63] 7.27 [0.185]
Denali - Atsaksovluk	Strike-slip	90	15	41.3	0.1 [0.30] 0.5 [0.40] 0.9 [0.30]	6.61 [0.185] 6.81 [0.63] 7.01 [0.185]
Denali – Togiak/Tikchik	Strike-slip	90	15	228.2	0.1 [0.30] 0.5 [0.40] 0.9 [0.30]	7.33 [0.185] 7.53 [0.63] 7.73 [0.185]

¹ All crustal faults are assumed to be surface rupturing faults with vertical thickness of 15 km.

² Reverse and oblique fault mechanism are treated the same in the NGA-West2 GMMs.

³ Maximum magnitude computed based on ½ of total fault length.

2.4 Subduction Interface Sources

The main tectonic process that is occurring in region is the on-going subduction of the Pacific plate beneath the North American plate along the Aleutian trench. Convergence rates in the region are about 50 mm/yr (DeMets et al., 1990). However, all of this convergence is not translated directly into seismic displacement, as a poorly constrained amount of slip is being transferred aseismically (Wesson et al., 2007). Historically, several large interface earthquakes have occurred along this subduction zone including the large 1964 **M**9.2 Great Alaska earthquake. The estimated rupture areas for the large historical subduction earthquakes were shown previously in Figure 3.

The SSC model for the subduction interface events used in this study is primarily adopted from the USGS 2007 model (Wesson et al., 2007, 2008). Specific modifications from the USGS 2007 model are discussed. Given the historical seismicity, the modeling of the full Alaskan subduction zone for large interface events is segmented into seven segments as shown in Figure 11 (Wesson et al., 2008). Based on the location of the project site, the seismic hazard analysis will consider the three closest segments: Semidi, Kodiak, and Prince William Sound. The Prince William Sound and Kodiak segments approximate the rupture area from the 1964 Great Alaskan earthquake and are modeled as rupturing together in our model. In addition, the potential for the Kodiak segment to rupture independently from the Prince William Sound segment is considered. The Semidi segment is also modeled as separate rupture.

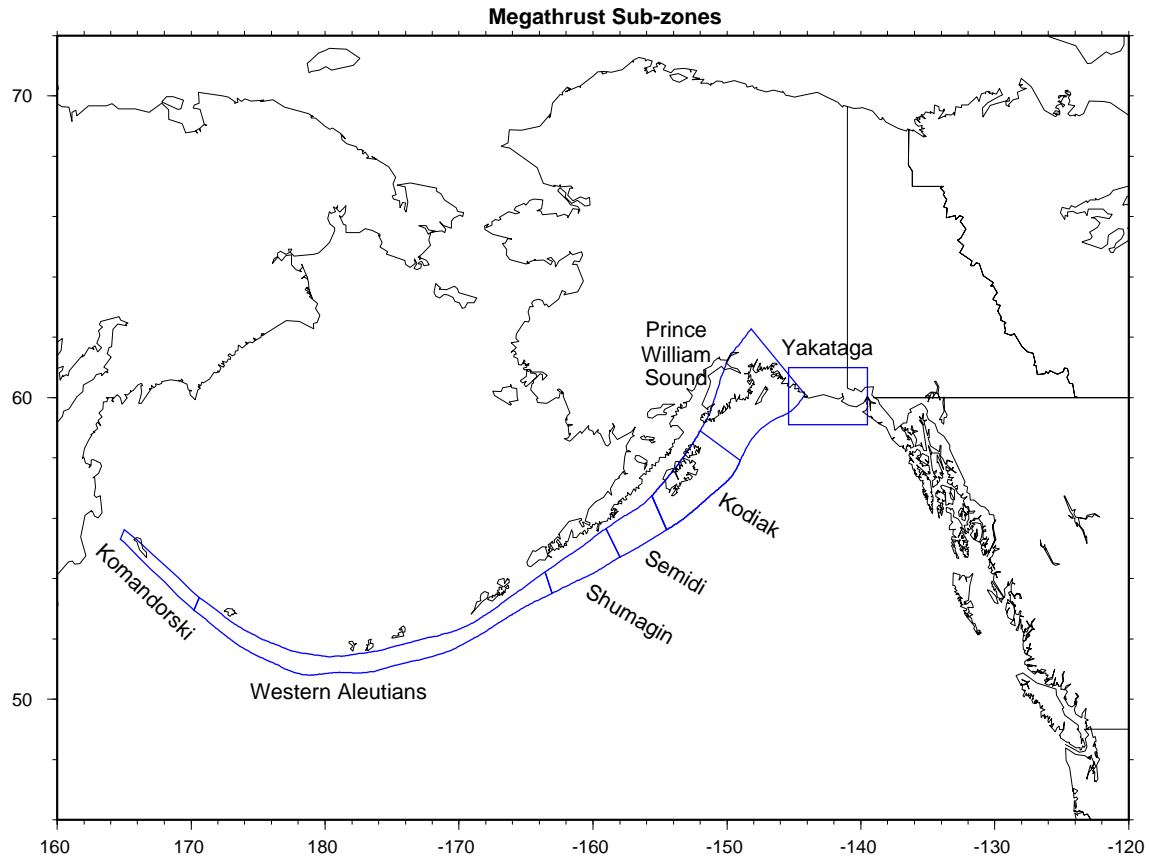


Figure 11. Segmentation of the Alaska-Aleutain subduction zone for large interface earthquakes (Source: Wesson et al., 2008).

Based on the rupture geometry of the subduction zone segments with a variable down-dip width (i.e., variable depth for the bottom of the segment), a singular rectangular fault plane with a constant dip angle would not adequately represent the rupture area. The PSHA program used in this analysis (HAZ45.2) can handle this variable down-dip thickness and has been applied for similar analyses in the Pacific Northwest to handle the variable geometry associated with the Cascadia subduction zone. To implement this geometry, the coordinates (latitude, longitude, and depth) of the top and bottom of the interface source are defined. The PSHA program will create the corresponding 3D shape for the rupture model and compute the necessary distance metrics needed for the ground-motion estimation. The geometry is adopted from the USGS model (Wesson et al., 2007, 2008), and the location of the top and bottom of the modeled interface are shown in Figure 12 for the three closest segments. The upper traces were all placed a depth of 20 km and the bottom traces vary over the range of 33 – 50 km. This upper depth of 20 km was selected based on the inferred rupture area from the 1964 Great Alaska earthquake rather than the shallower depth assumed with the subducting tectonic plate. Note that this shallower depth would be further away from the project site being located in a southeasterly direction. The closest distances from the project site region to the Kodiak segment and the Semidi segment are approximately 225 km and 350 km respectively.

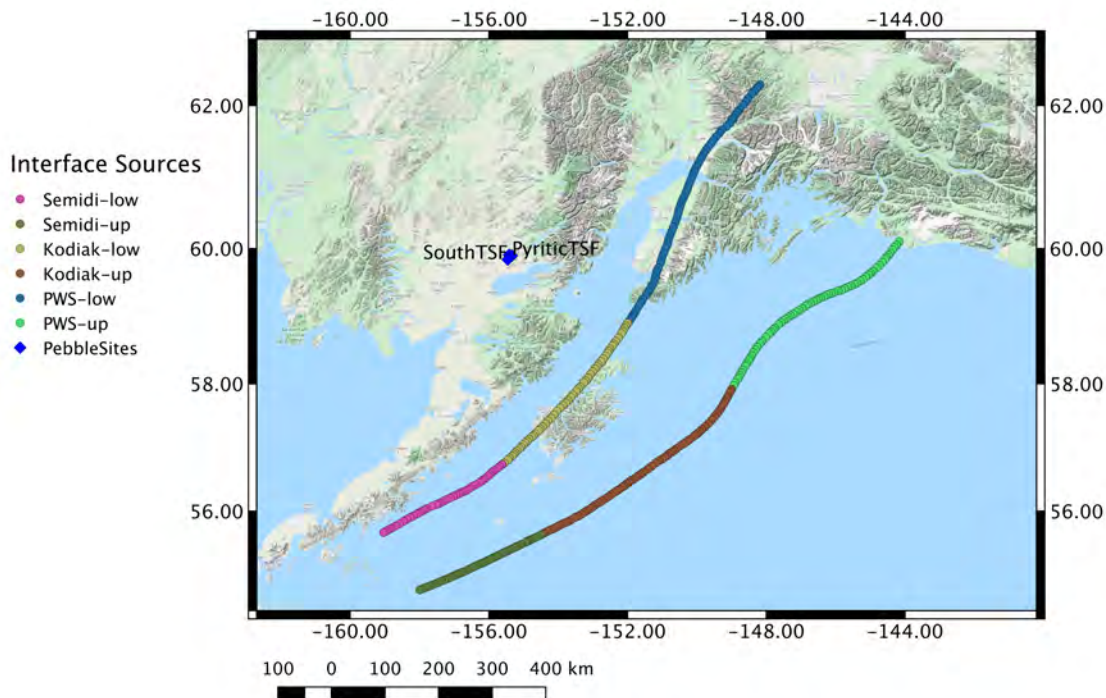


Figure 12. Top and bottom fault traces for the three closest segments of the Alaska-Aleutian subduction zone source model used in the analysis.

The maximum characteristic magnitudes adopted from the USGS 2007 model for the three closest segments are listed in Table 4. The Kodiak segment is modeled as rupturing both independently and with the Prince William Sound segment to replicate the 1964 Great Alaska earthquake. Differing estimates have been presented for the recurrence interval of great megathrust earthquakes in Southern Alaska. Koehler and Carver (2018) estimate a median recurrence interval for the 1964 event of 560 years based on a range between 333 – 875 years. This was based on the analysis of nine events over the last 5,000 years (Koehler and Carver, 2018). Note that the previous USGS 2007 hazard maps and the Knight-Piesold (2013) studies were based on a recurrence interval of 650 years (Wesson et al., 2007, 2008) based on the analysis of six events in the last 3,300 years. For this study, the more recent values from Koehler and Carver (2018) are adopted.

Separate estimates for the recurrence interval of independent rupture of the Kodiak segment have been estimated by Koehler and Carver (2018); however, it is difficult to estimate a robust median value. To account for this uncertainty, the characterization is developed in which the repeat of the 1964 Great Alaska earthquake includes rupture of both the Kodiak and Prince

William Sound segments and an alternative in which the Kodiak and Prince William Sound segments rupture independently. The assigned weights are 90% for the combined rupture and 10% for the separate independent ruptures. The assignment and value of the higher weight (90%) for the full rupture is based on the lack of definitive field investigations that would indicate the Kodiak segment ruptures independently of the combined segments as occurred in the 1964 event. Based on the smaller size associated with the Kodiak segment, a maximum magnitude of 8.8 is assigned which is consistent with the USGS model. Note that for the USGS model, only the combined rupture is considered for the Kodiak and Prince William Sound segments. For these two cases, the magnitude recurrence relationship is modeled as a purely characteristic model as represented by a normal distribution centered on the maximum magnitude and standard deviation of 0.12 magnitude units.

Recurrence interval estimates for the Semidi segment were not developed as part of the USGS 2007 model. Rather, the modeling of large magnitude events (magnitudes in the range of 8 – 8.5) was applied based on the analysis of the seismicity catalog (Wesson et al., 2007, 2008). A truncated Gutenberg-Richter (GR) relationship is used in this study and the parameters are listed in Table 4.

Following the USGS 2007 model and approach, events between magnitudes 7 – 8 are modeled using a truncated GR relationship. The recurrence parameters are listed in the last row in Table 4 and are taken directly from the USGS model. For magnitudes less than 7, the activity rate was based on the recurrence analysis of the seismicity catalog as applied through the smoothed gridded source file (Wesson et al., 2007, 2008). For this study, these smaller magnitude events associated with the distant interface sources (i.e., distances greater than about 300 km) are not expected to contribute significantly to the total hazard at the site and are not included in the SSC model or calculations.

Table 4. Seismic source parameters for Alaska-Aleutian subduction zone sources used in the analysis.

Segment	Largest Historical EQ (Mw, year)	Characteristic Magnitude ²	Recurrence Interval (year)	a-value	b-value
Semidi	8.2 (1938)	8.5	---	2.4	0.710
Kodiak [0.1]	9.2 (1964)	8.8	560 ¹	---	---
Kodiak + Prince William Sound [0.9]	9.2 (1964)	9.2	560 ¹	---	---
Aleutian Zone (M7 – 8)	9.2 (1964)	8.0	---	3.54	0.689

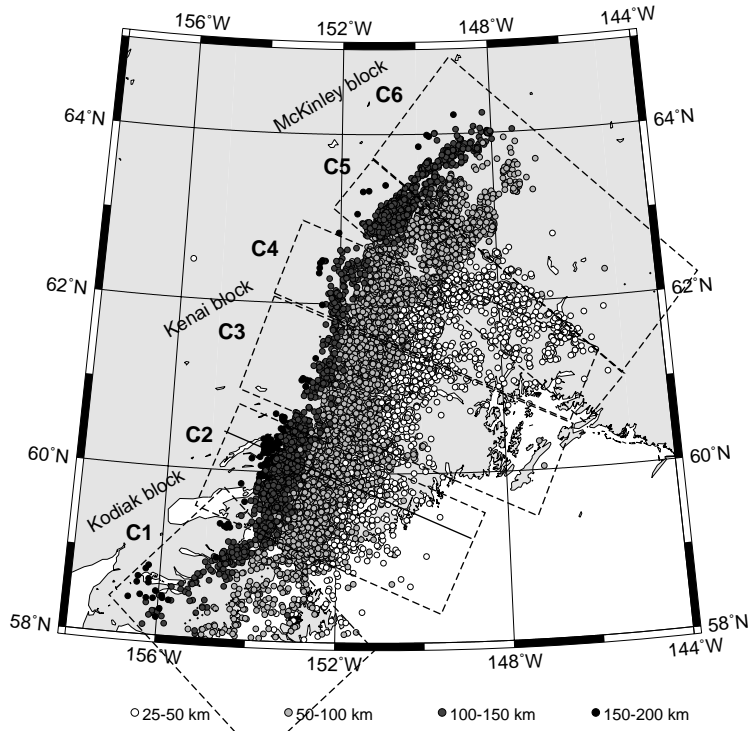
¹ Median recurrence interval with estimate in the range between 333 – 875 years (Koehler and Carver, 2018). For the analysis three discrete recurrence intervals of 333 [0.185], 560 [0.63] and 875 [0.185] years are used.

² Additional epistemic uncertainty of +/-0.2 magnitude units is included in the SSC model with weights of 0.185, 0.63, and 0.185.

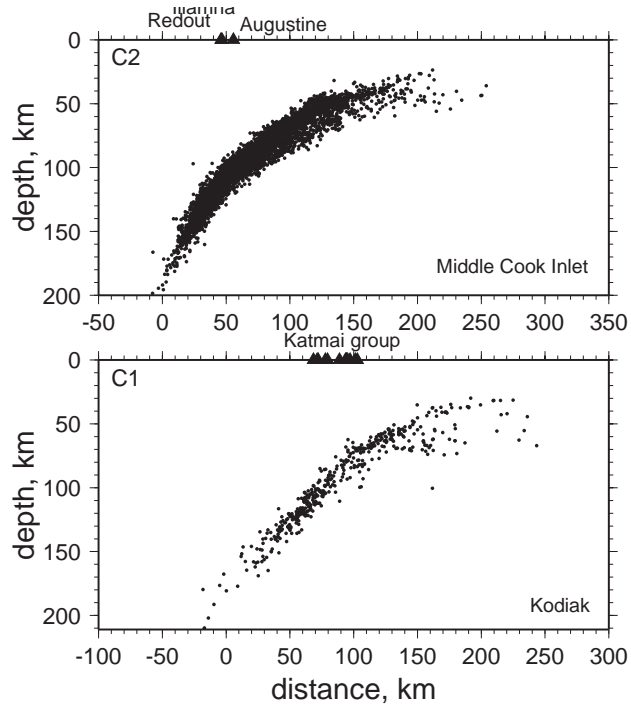
2.5 Subduction Slab Sources

The deeper seismicity associated with the subducting Pacific plate has also historically caused significant earthquakes in the region. Most recently, the November 30, 2018 Anchorage earthquake (M7.1) was located just north of Anchorage with a depth of 47 km. This epicenter was greater than 300 km from the project site locations. An older but closer (i.e., epicentral distance of approximately 117 km) large magnitude slab event occurred on January 24, 2016 (M7.1) and was also associated with the subducting slab. The 2016 event had a hypocentral depth of 129 km. It is also evident from the seismicity plots shown in Figures 5 and 6 that this deeper part of the subducting slab is highly active, and the overall seismic hazard at the project site locations can be expected to be influenced and controlled by these events.

Ratchkovski and Hasen (2002) performed an earthquake relocation methodology in the region which allows for the image of the subducting slab as shown in Figure 13. These relocated events in cross section C1 and C2 are the closest to the Pebble project site and indicate that the subducting slab is seismically active down to depth of approximately 200 km. This deeper section of the slab is about 30 km horizontally from the project site locations.



(a)



(b)

Figure 13. Relocated earthquakes from Ratchkovski and Hansen (2002) shown in map view (a) and cross sections closest to the project site (b).

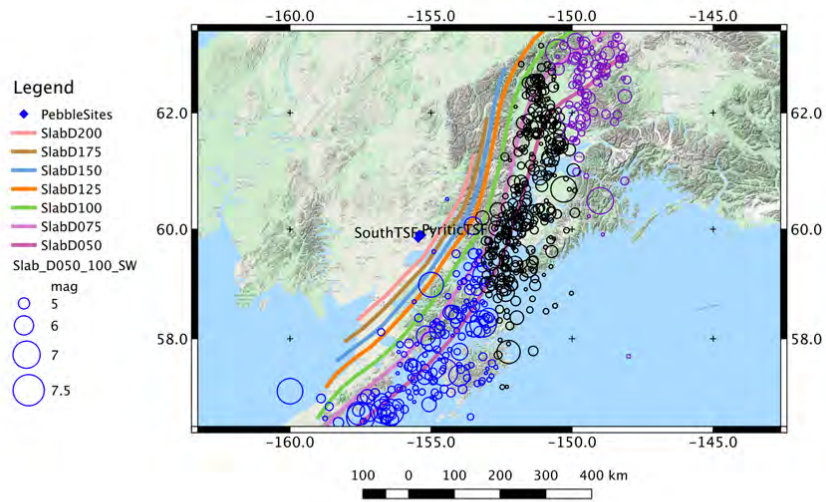
The modeling and implementation of slab seismic sources within a given PSHA program has been observed to cause differences in the resulting hazard given the same characterization of a slab source (Hale et al., 2018). A more detailed presentation of these implementation choices and differences in the estimated hazard for the simple test case provided in Hale et al. (2018) and for the models used for Southern Alaska are presented in Appendix A.

The implementation differences are related to the geometrical representation of the subducting slab and the expected rupture plane for large slab events. Unlike large interface events that rupture along the top of the subducting plate, these deeper slab events are observed to rupture a cross section of the width of the subducting slab. The geometrical representation of the expected ruptures for slab events should be considered in the modeling of the slab seismic sources within any PSHA program. In addition, GMMs for deeper slab events have a noted strong dependence of increasing ground motions for deeper events for the same closest distance (e.g., Abrahamson et al., 2016).

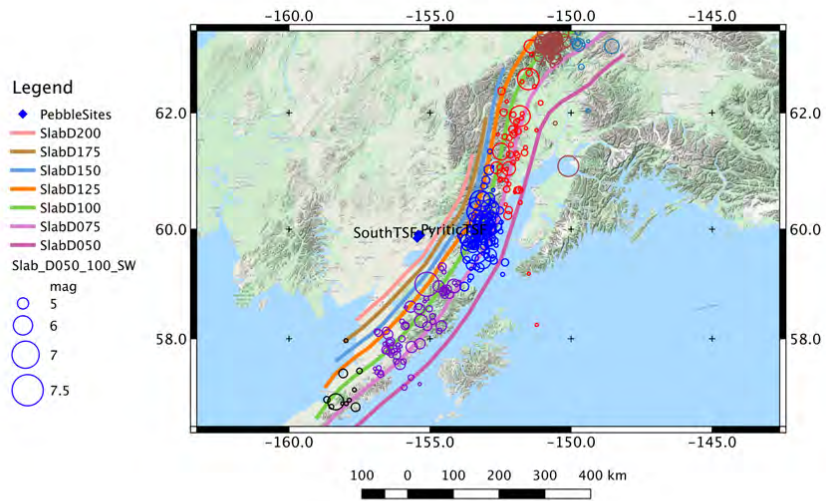
For the USGS model which was also employed in the Knight-Piesold (2013) study, a gridded seismicity approach was implemented. Given the seismicity catalog for depths of 50 km and greater, a smoothing approach was applied to provide activity rates for grid points based on a 0.1x0.1 degree grid spacing. The smoothing distance was 50 km. Given that this approach is based on the occurrence of historical events in the catalog, the resulting variable activity rates are higher in areas in which historical events have occurred and lower in places with limited seismicity. For the USGS model, two separate depth ranges were computed: 50 – 80 km and 80 – 120 km. Based on the documentation, it is not clear if the events occurring with depths greater than 120 km in the area were included in the deeper layer or eliminated in the analysis. These smooth gridded files were then treated as areal points sources within the PSHA programs (i.e., Approach (a) described in Hale et al., 2018).

For the SSC model developed in this SHA study, virtual vertically dipping faults are placed at a series of depths ranging from 50 km to 200 km, every 25 km. These fault traces for the different depth range values are based on the depth contours of the subduction slab global model Version 2.0 (Hayes, 2018). The fault thickness is assigned to be 20 +/-5 km to represent the thickness of the subducting plate based on cross section plots shown in Figure 13 from Ratchkovski and Hansen (2002). The corresponding weights for this thickness variation is 0.185, 0.63 and 0.185 selected to represent the 5th, 50th and 95th percentile. These virtual faults are plotted in Figures 14 and 15 along with the project seismicity catalog. One feature observed with the seismicity associated with the slab events is a non-uniform spatial distribution of events. To capture this feature in the SSC model, the seismicity catalog is separated first by depth ranges of 50 – 100km, 100 – 150 km, and 150 – 250 km. Next within a given depth range, subsections of seismicity based on the observed spatial distribution is selected. For the shallowest depth range of 50 – 100 km there are three selected subsections: SW, Central, and NE. The associated events with each of these subsections are plotted in Figure 14a with different colors.

For the next depth range, a total of six subsections are selected starting with SW01 at the southwestern end of the source through SW06 at the northeastern end of the source. This depth range shows a larger variability in the spatial distribution of events than the previous shallower depth range. The seismicity associated with the six different subsections are indicated in Figure 14b with the different colors. Finally in Figure 15, the seismicity from the deepest depth range of 150 – 250 km is plotted in separate colors indicating the three subsections, SW, Central, and NE.



(a)



(b)

Figure 14. Virtual slab faults and seismicity from the project catalog for events separated by 50 – 100 km (a) and 100 – 150 km (b) with events from each subsection plotted with separate colors.

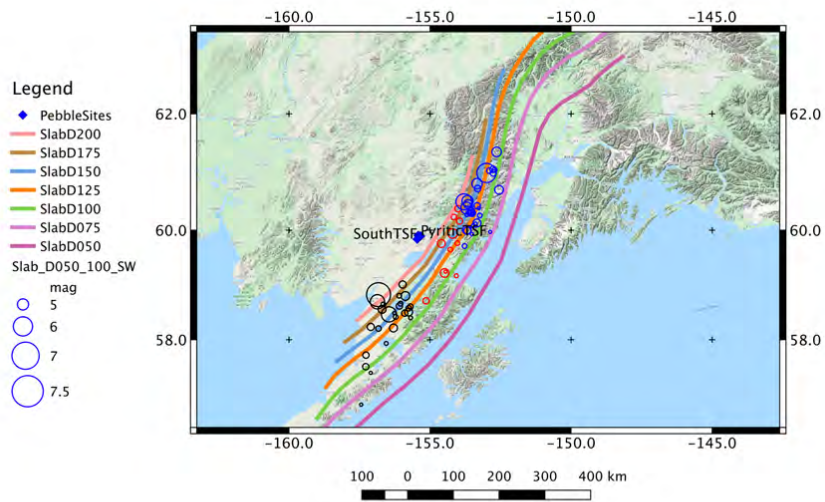


Figure 15. Virtual slab faults and seismicity from the project catalog for events separated by 150 – 200 km with events associated with each subsection plotted with different colors.

For the current SSC model, earthquake recurrence rates are estimated following the Weichert (1980) approach using the project earthquake catalog separated by depth and an additional selection criterion of having events located within the longitudes of -148 to -160 degrees. Although events outside of these longitudes are observed, their greater distance from the project site locations does not necessitate their inclusion for the SSC model development.

Recurrence parameters are estimated for the three specific depth ranges of 50 – 100 km, 100 – 150 km, and 150 – 250 km based on the full geographically sorted earthquake catalog. Based on these estimated recurrence parameters, the activity rates for a given depth range is assigned to the corresponding virtual fault for the associated depth range. A sensitivity analysis is performed on the full earthquake catalog where the recurrence parameters are estimated for the sorted earthquake catalog only using those events through 2004 and compared to the results from the full catalog. The same conclusion is observed that the full catalog including the more recent events does not change the recurrence parameters for the slab model. The additional partitioning of the activity rate within a given depth range is based on the fault lengths associated with each virtual fault and with the ratio of the number of events within a given subsection to the total number of events for all subsections. For the PSHA calculations, these subsection activity rates are assigned to the subsection part of each virtual fault. For the SSC model used in the analysis, the estimated uncertainty in the b-values is incorporated. These values are listed in Table 5.

The differences between this model and the USGS report can be summarized in the following topics. More additional details are discussed in Appendix A. This SSC model assumes that, for a given subsection of the fault (i.e., depth range), the occurrence of events is uniform along the virtual faults, whereas the USGS approach distributes the occurrence of events similar to the observed historical distribution. For the USGS approach, a simplified two-layer model is implemented to approximate the full down-dip extent of the slab whereas the current SSC model approximates the down-dip slab with a set of seven virtual faults. Although these deeper faults have lower activity rates consistent with the observed seismicity, the USGS model does not directly model these events. This deeper part of the slab is closer in horizontal distance to the project site locations, albeit at a deeper depth. Finally, the maximum magnitude assigned to these slab sources is 7.5 for the USGS and both 7.5 and 8.0 for the current SSC model. This increase for the maximum magnitude is consistent with global dataset of slab events (Bozorgnia and Stewart, 2020). The recent 2014 **M**7.96 slab earthquake occurred along the Aleutian slab section well to the west of the project site location. The largest historical event in the slab database for the Alaska subduction section is **M**7.15 and given these historical observations, the assigned weights for the two maximum magnitude values is 50% each.

Given these noted differences and the expected differences based on the implementation and representation of the slab within a PSHA program (Hale et al., 2018), it is expected that the contribution from the slab sources from the current SSC model will be greater than the simplified model used by the USGS. Additional details and discussion are provided in Appendix A to support this expectation.

Table 5. Seismic source parameters for slab subduction zone sources used in the analysis. Weights for multiple values are indicated in brackets.

Slab Fault	Depth Range (km)	Catalog Depth Range (km)	b-value	Act (N>=5) [Subsection]	Maximum Magnitude
Slab_D050	50 – 70	50 – 100	0.7403 [0.185] 0.7872 [0.63] 0.8341 [0.185]	0.41119 [SW] 0.69619 [Central] 0.20409 [NE]	7.5 [0.5] 8.0 [0.5]
Slab_D075	75 – 95	50 – 100	0.7403 [0.185] 0.7872 [0.63] 0.8341 [0.185]	0.42249 [SW] 0.71394 [Central] 0.20929 [NE]	7.5 [0.5] 8.0 [0.5]
Slab_D100	100 – 120	100 – 150	0.8217 [0.185] 0.8926 [0.63] 0.9635 [0.185]	0.01903 [SW01] 0.11418 [SW02] 0.18872 [SW03] 0.08881 [SW04] 0.14590 [SW05] 0.06978 [SW06]	7.5 [0.5] 8.0 [0.5]
Slab_D125	125 – 145	100 – 150	0.8217 [0.185] 0.8926 [0.63] 0.9635 [0.185]	0.01767 [SW01] 0.10601 [SW02] 0.17521 [SW03] 0.08245 [SW04] 0.13545 [SW05] 0.06478 [SW06]	7.5 [0.5] 8.0 [0.5]
Slab_D150	150 – 170	150 – 175	0.7417 [0.185] 0.9317 [0.63] 1.1217 [0.185]	0.02933 [SW] 0.01291 [Central] 0.03637 [NE]	7.5 [0.5] 8.0 [0.5]
Slab_D175	175 – 195	150 – 175	0.7417 [0.185] 0.9317 [0.63] 1.1217 [0.185]	0.02303 [SW] 0.01013 [Central] 0.02856 [NE]	7.5 [0.5] 8.0 [0.5]
Slab_D200	200 - 200	150 – 175	0.7417 [0.185] 0.9317 [0.63] 1.1217 [0.185]	0.01741 [SW] 0.00766[Central] 0.02159 [NE]	7.5 [0.5] 8.0 [0.5]

2.6 Crustal Host Zone

Given the lack of characterized faults in the immediate area around the project site location, the SSC model also considers the potential for events occurring and not associated with any fault. This areal crustal host zone is shown in Figure 16 along with the seismicity with depths less than 50 km. Note that only three of these events had depths greater than 21 km (see Figure 16) being from 1964, 1965, and 1968 and with depths of 33 km, these early hypocenter locations were likely based on a default depth of 33 km used for world-wide seismicity rather than an estimated instrumental depth location. The other remaining seven events have an

average depth of 10.6 km with the deepest being 21 km. The boundaries of this crustal host zone are selected to include the local seismicity in the area with the consideration of the general tectonics and other mapped features in the area. A total of 10 events are located within this crustal host zone and the recurrence parameters are estimated using the same Weichert (1980) methodology. These results are listed in Table 6. Given the limited number of events for this crustal host zone, the uncertainty associated with this source zone is large and taking an upper and lower value would lead to b-values inconsistent with general seismicity studies. Thus, a larger regional crustal catalog is processed to estimate the standard deviation for the b-value. This larger catalog had a total of 76 events. The computed b-value is 0.8981 with a standard deviation of 0.1295. This b-value is similar to the value of 0.9206 computed using the smaller catalog. Similar activity rates are also computed from these two earthquake catalogs. For the analysis, the base b-value of 0.9206 is selected along with an approximate standard deviation from the larger catalog of 0.12. These values are listed in Table 6.

The maximum magnitude for this source is assigned to be 7.25 with the additional epistemic uncertainty of +/-0.2 magnitude units. This maximum magnitude is consistent with the assigned maximum magnitude value of 7.3 used in the USGS SSC model and judgment in taking a slightly larger magnitude than has been historically observed. For the larger regional crustal earthquake catalog, the largest historical event occurred in 1903 and was a magnitude 6.9. The other difference, however, between the two SSC models is again the USGS model uses a smooth gridded approach with a smoothing distance of 75 km. Given the sparse events in the immediate region shown in Figure 16 and the smoothing distance of 75 km, it can be expected that the relative contribution from the crustal host zone in the current SSC model and the USGS gridded source zone would be similar. A sensitivity test run confirmed this expectation.

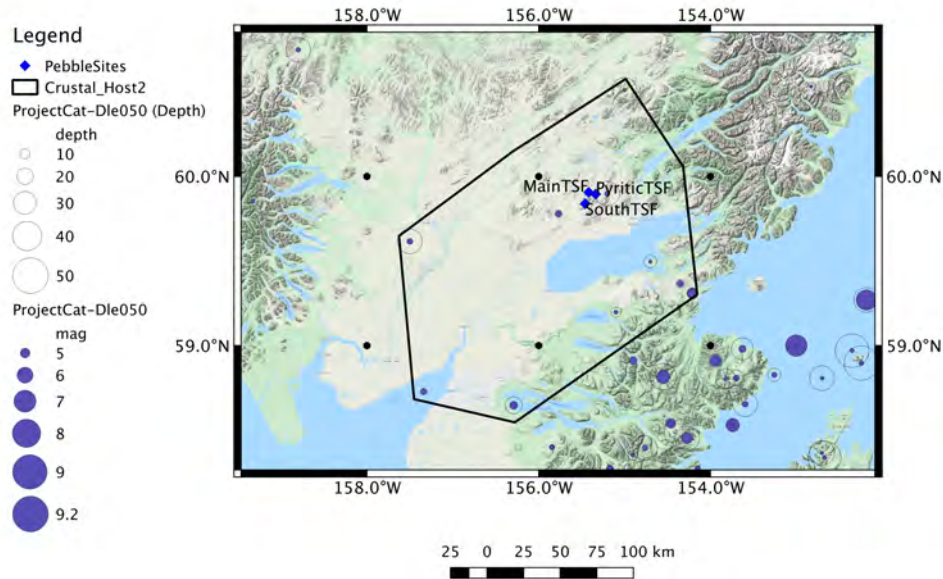


Figure 16. Crustal host areal source zone and all events with depths less than 50 km shown both with variable size for magnitude (purple circles) and depth (open circles).

Table 6. Seismic source parameters for crustal host zone. Weights for multiple values are indicated in brackets.

Source	b-value	Act (N>=5)	Thickness (km)	Maximum Magnitude
Crustal Host	0.72 [0.185]	0.02375	15.0	7.05 [0.185]
	0.92 [0.63]			7.25 [0.63]
	1.12 [0.185]			7.45 [0.185]

3. Ground-Motion Characterization

For both the PSHA and DSHA calculations, GMMs are required. Given the combination of crustal seismic sources and subduction seismic sources, available candidate GMMs are reviewed and ultimately selected for each of these two types of seismic sources. Based on the review of candidate GMMs, the GMC model is developed and is presented in this section of the report.

3.1 Crustal Ground-Motion Models

The development of GMMs for crustal earthquakes in active tectonic regions has significantly evolved during the last decade based on the large increase in the amount of empirical ground-

motion data. Given the history of the previous SHA studies discussed in this report, the suite of GMMs used for crustal events has also evolved. The USGS maps for the Alaska region were based on models from the late 1990s (Wesson et al., 2007). For the more recent Knight-Piesold (2013) study, an update to the GMMs used by the USGS was employed. These newer models were part of the NGA-West1 models that were published in 2008.

The current state of knowledge and practice for crustal GMMs is the more recent NGA-West2 models (Bozorgnia et al., 2014). This suite of GMMs are based on the increased database associated with the NGA-West2 project and GMMs were developed from the same developer teams that were involved in developing the GMMs from the NGA-West1 database. Specifically, five GMMs were developed: Abrahamson et al. (2014) (referred to as ASK14), Boore et al. (2014) (referred to as BSSA14), Campbell and Bozorgnia (2014) (referred to as CB14), Chiou and Youngs (2014) (referred to as CY14) and Idriss (2014) (referred to as ID14). All of these models were defined for the RotD050 component (Boore, 2010) and for spectral damping of 5%. The RotD050 ground-motion is a measure of the amplitude for the average horizontal component and corresponds to the 50th percentile of the response spectra over all rotation angles.

One significant improvement in the GMMs from the 1990s to the current NGA-West2 models is in the classification and characterization of the site response aspect of ground motions. Previously, GMMs were classified based on either “rock” or “soil” site conditions given the limited site information contained in the database for the recording stations. With the improvement of the databases for the NGA-West1 (Chiou et al., 2008) and NGA-West2 (Ancheta et al., 2014) projects, a refined site response function was included based on the time-averaged shear-wave velocity in the top 30 m, defined as the V_{S30} value. Note that the Knight-Piesold (2013) study was for rock site conditions, however, the report does not indicate the V_{S30} value used in the analysis for this generic site condition. As noted earlier, the results presented in this study are for a defined reference site condition with a V_{S30} of 760 m/sec.

Certain NGA-West2 GMMs also include an additional site and basin response term associated with the depth to a shear-wave velocity of 1.0 km/sec (Z1) and 2.5 km/sec (Z2.5). If site-specific information is available for these parameters, they can be used. However, for this study, no site-specific information is available and the default values (i.e., Z1=0.034 km, Z2.5=0.608 km) given the V_{S30} value of 760 m/sec are used in the analysis.

For the ASK14 and CY14 models, the functional form of the models based on an “estimated V_{S30} ” value was implemented in this study. Note that the differences between the estimated and measured V_{S30} flag only impact the aleatory standard deviation of two of the four GMMs (ASK14 and CY14) but does not impact the median ground-motion estimates.

Because the NGA-West2 GMPEs were developed in a collaborative effort with interactions and exchange of ideas among the developers, the NGA-West2 developers recommend that additional epistemic uncertainty be incorporated into the median ground-motion estimates from their GMPEs. The additional epistemic uncertainty model of Al Atik and Youngs (2014), developed as part of the NGA-West2 project is used in this study. This epistemic uncertainty

model is distance-independent but depends on magnitude, style-of-faulting, and spectral period. The logic tree for the ground-motion characterization model is shown in Figure 17.

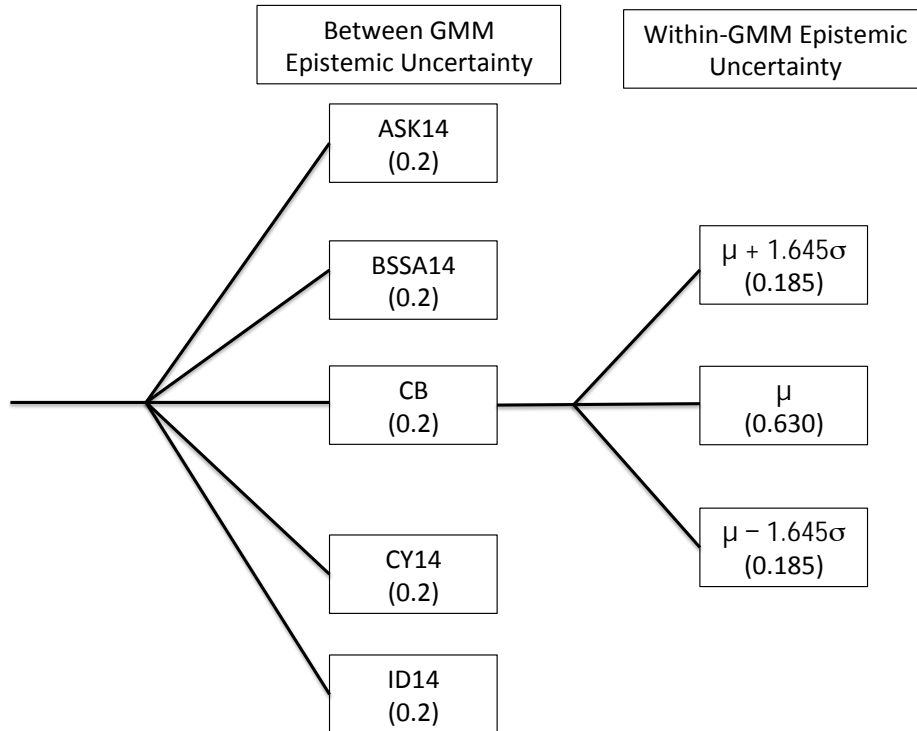


Figure 17. GMM logic tree for crustal events showing the different branches and associated weights; μ and σ are median prediction and epistemic standard deviation of the natural-logarithmic values of the ground-motion parameter of interest.

3.2 Subduction Ground-Motion Models

The development of GMMs for subduction earthquakes has not followed the same rapid community-wide development as models for crustal earthquakes. Similar to the pre NGA-West community development of GMMs, subduction models were published based on developer teams working independently and based on different databases. One of the first large scale efforts to collect a global database of subduction ground motions was performed for the BC Hydro (2012) project. For this project, previous subduction databases (e.g., Youngs et al., 1997; Atkinson and Boore, 2003, 2008) were compiled with additional more recent data. Given this expanded database, a global GMM for subduction earthquakes was developed (Abrahamson et al., 2016).

This newly developed GMM for subduction earthquakes (referred to BChydro) has several functional features which are similar to the functional form for crustal earthquakes. Included in

this was the functional model for the site response, which was based on the V_{S30} parameter similar to the crustal models. Following the time cutoff closure of the subduction database and during the development of the BCHydro GMM, two significant subduction interface events occurred: the 2008 Maule Chile **M**8.8 and the 2010 Tohoku Japan **M**9.0 events. Based on a residual analysis of the data and the initial model, period dependent adjustments were incorporated into the final model to account for these recent large interface events (Abrahamson et al., 2016). In addition, as part of these final adjustments, the magnitude scaling for slab events was modified to have a center magnitude scaling break point at 7.5. For the full BCHydro model, a full logic tree was developed for applications in which other subduction GMMs are not considered. For this study, since additional subduction GMMs are being used in the analysis, the full BCHydro logic is not used, but the epistemic uncertainty branches for the magnitude scaling break point is used.

Recently, the NGA-Subduction program (Bozorgnia et al., 2018) has followed the same community involvement approach successfully performed for crustal models. The database developed for this NGA-Subduction program represents the most current global subduction ground-motion database to date (Bozorgnia and Stewart, 2020). Subduction data was collected from numerous tectonic subduction zones around the world including Alaska. Both the 2008 Maule Chile and the 2010 Tohoku Japan ground-motion data are contained in this global database. In addition to the ground-motion data, the associated metadata for the events and the stations has been compiled although the quality of this additional data varies from region to region, especially for the station information.

Given this newly developed database for subduction earthquakes, several developer teams were involved with the development of GMMs for subduction earthquakes. Similar to the NGA-West program, these developer teams worked in a community environment allowing for the sharing of knowledge during the model development stage. To date, there are two models that have been developed and are in pre-publication: Kuehn et al. (2020) and Parker et al. (2020). These two models are referred to by the author's acronyms KBCG and PSHAB. Given the recent development of these models and their resulting limited use in ground-motion studies, an evaluation of the models in comparison with the BCHydro model (Abrahamson et al., 2016) is performed. The PSHAB model is initially considered as part of this analysis; however, a recent modification of the model is being performed (J. Stewart, personal communication) and based on the unresolved modifications of the model, it is dropped from consideration for this study.

Given the global subduction database, which is comprised of regional sub-datasets, the KBCG developer team constructed both a global model and regionalized models for different subduction zones, one of which is Alaska. The regionalization consists of a regional constant term, regional site amplification term, regionalized anelastic attenuation term, and regionalized magnitude scaling break point value. Both the global versions of this model and their respective Alaska versions are reviewed and considered for inclusion in this SHA study.

In reviewing the data contained in the NGA-Subduction database from Alaska, a large percentage (i.e., 95%) of the V_{S30} information for the stations was based on inferred values

rather than measured values. In addition, the majority of the measured values were for sites located in Anchorage and for stations located away from this large metropolitan area, the assigned V_{S30} values were not robust given the limited geologic and or general information for parts of Alaska (Bozorgnia and Stewart, 2020). It should also be noted that a large amount of the Alaska data is based on recordings from the Temporary Array at significant distances (i.e., several of hundreds of km away from the event) (Bozorgnia and Stewart, 2020). Given this limitation in the data from Alaska, the regionalization of the models may not be robust and is considered as part of the evaluation of the regionalized Alaska models from this new NGA-Subduction model.

Another feature of these subduction GMMs being evaluated, including the BCHydro model, is the formulation of a magnitude scaling break point. For the new NGA-Subduction model, these magnitude scaling break points are defined as a function of the subduction region and specifically, the subducting plate. For example, for interface events for the global model, the value is 7.9 for the KBCG model. However, for the Alaska plate region which includes the Kodiak and Prince William Sound segments of the Alaska-Aleutian subduction zones, this value is 8.6. For the rest of the Alaska-Aleutian subduction zone, the value is 8.0. Given this larger magnitude scaling break value of 8.6 for the KBCG model, higher median ground motions are predicted for the representative **M9.2** Great Alaska earthquake using the Alaska regional model than the global model with the smaller magnitude scaling break point value of 7.9. Additional differences are observed based on the differences between the regionalization of the other features of the model (i.e., constant term, site amplification, and anelastic attenuation).

Given the importance of these magnitude scaling break points, an assessment of their values is performed. The higher **M8.6** value from the KBCG model is based on Campbell (2020) which is based on the age and geometry of the subducting plate in this region of Alaska. Median estimates of this magnitude value fall within the range of 8.3 to 8.9 with the recommended value of 8.6. Based on the limited large magnitude interface data from Alaska, the data does not allow for a better constraint on this value. As an example, the interface data selected for the KBCG model development in Alaska is shown in Figure 18. Additional data from Alaska is contained in the full NGA-Subduction database but the data shown in Figure 18 is the result of applying the selection criteria for the database (Kuehn et al., 2020). The Alaska sub-region (i.e., Kodiak and Prince William Sound segments) only has one earthquake of magnitude 5 (open blue diamonds) with only one station at distances less than 200 km. For the Aleutian segment there is more data but the largest event is a magnitude 7, which is below any magnitude scaling break point. Thus, the data cannot be used to constrain this magnitude break point for Alaska. Note that for the global version, the inclusion of data from events above the magnitude scaling break points allows for the data to constrain the model.

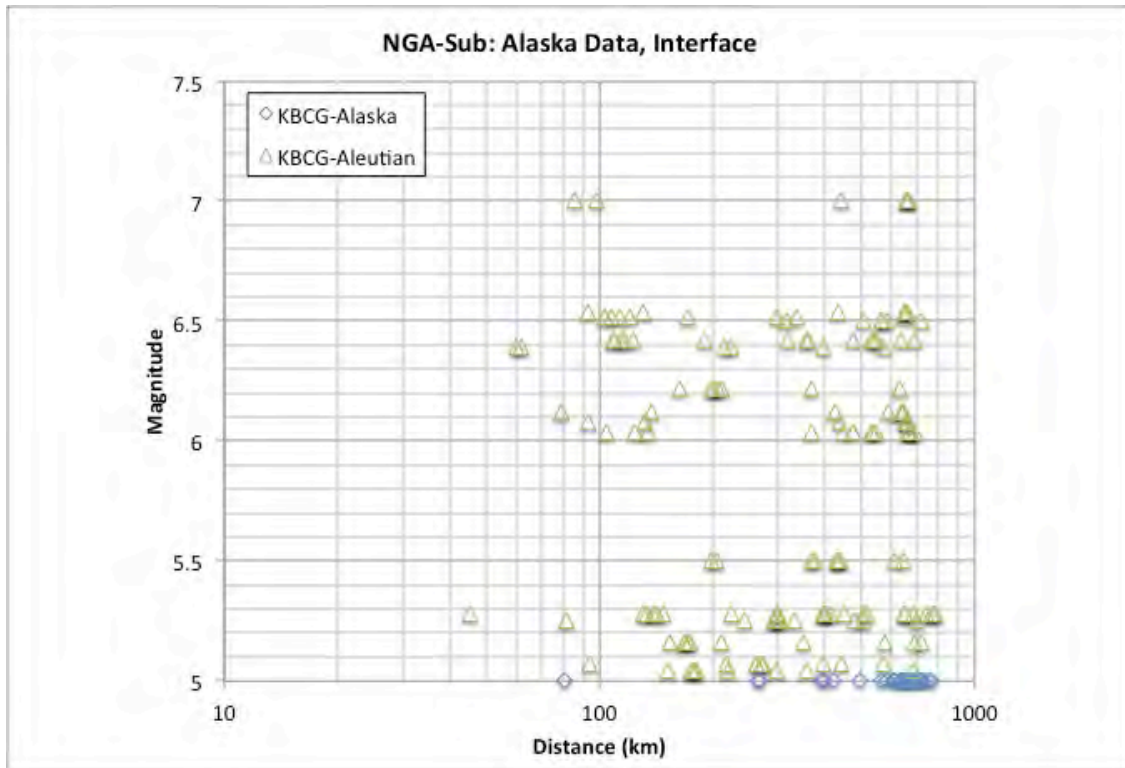


Figure 18. Selected interface data for the KBCG model from Alaska for the two sub-regions of Alaska (Kodiak+Prince William Sounds) and Aleutian.

To further evaluate the subduction interface GMMs, median ground-motion spectra are computed for a representative **M**9.2 earthquake at a distance of 250 km. These spectra are plotted in Figure 19 and are for the reference site condition V_{S30} value of 760 m/sec. The three models for the BChydro (blue lines) are plotted along with the global and two regional models for the KBCG (red lines) model. As previously discussed, the larger magnitude scaling break point value of 8.6 for the Alaska KBCG model (red dashed line) is the cause of these larger median ground motions, especially at the longer spectral periods. In comparing the BChydro model with the global KBCG model, the agreement is favorable for longer spectral periods, but the range is wider for short spectral periods. The new KBCG model has a very different spectral shape than the BChydro model for this scenario. This may reflect regional differences in the ground motions. The BChydro model is a global model from a data set that is dominated by data from Japan which has much stronger short-period ground motions than other regions.

In addition to the comparison for the median ground motions, a comparison of the total aleatory sigma from the evaluated interface models is shown in Figure 20. These sigma models are independent of magnitude, distance, V_{S30} etc. and the new model shows a significant increase in the total sigma relative to the BChydro model for all spectral periods except long periods greater than about 5 – 6 sec.

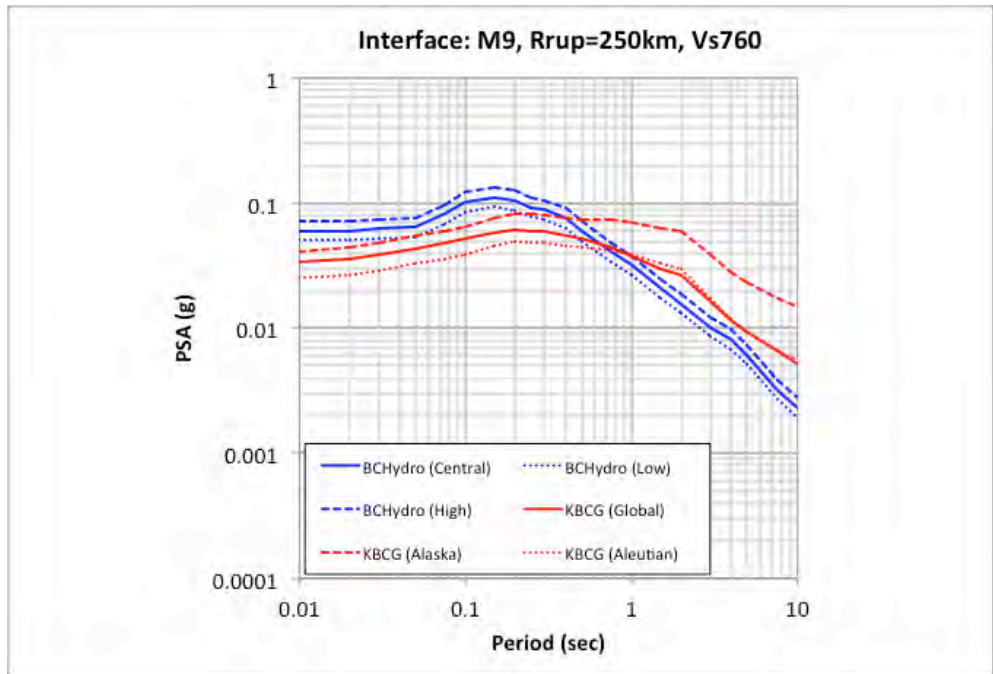


Figure 19. Median spectra for the suite of evaluated interface subduction models.

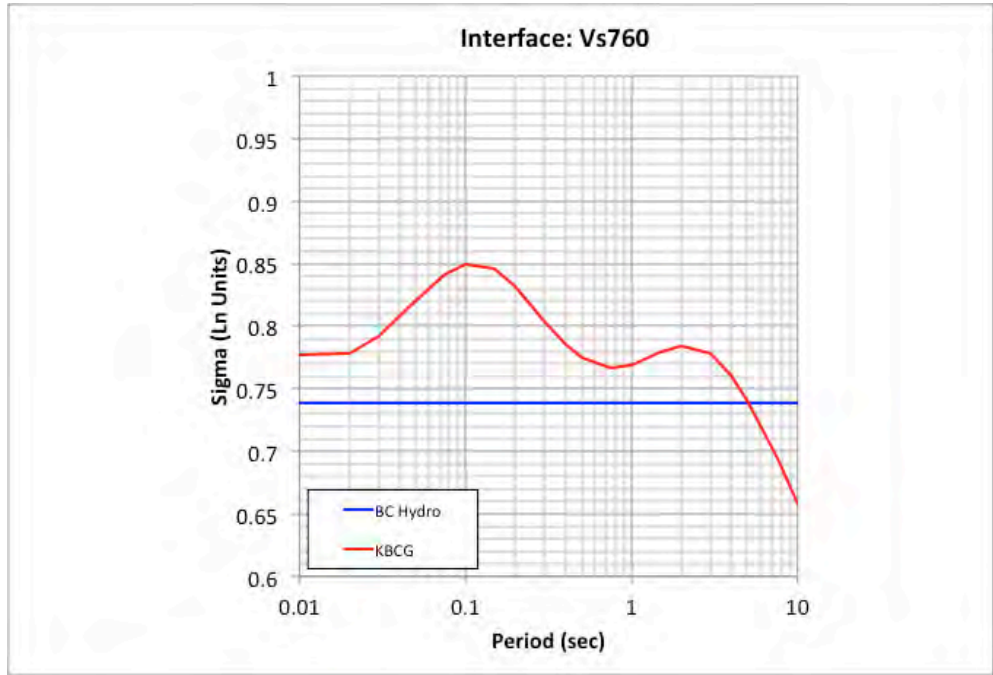


Figure 20. Total aleatory sigma from the evaluated interface subduction models.

Given these evaluations and the assessment of the Alaska data which went into the development of the regionalized models for the KBCG model, only the global versions of this new KBCG model is selected for inclusion in this SHA study.

A similar assessment of the slab models was conducted for this study. The magnitude scaling break points for the KBCG model is 7.6 for the global case, 7.2 for the Alaska case, and 8.0 for the Aleutian case. Note that for the BCHydro model, the recommended central value of the magnitude scaling break point was 7.5 for slab events. The selected slab data used in the KBCG model are plotted in Figure 21. Although there is more data than for the interface case, all of the data fall below the recommended magnitude scaling break point indicating that the data cannot assist in constraining the model.

Based on the preliminary sensitivity analyses of the PSHA, the controlling slab sources are associated with the shallower depths ranges (i.e., 50 – 100 and 100 – 150 km). As a result, four representative median spectra (i.e., two depth/distance values and magnitude 7 and 8) are computed to evaluate the slab subduction models. These spectra are shown in Figure 22 and 23.

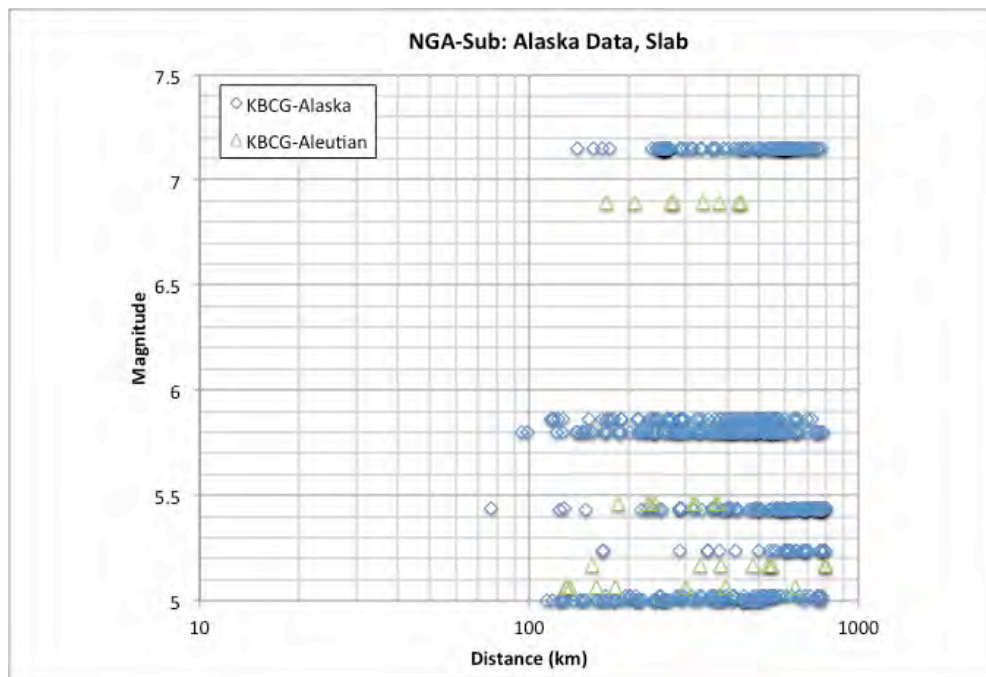


Figure 21. Selected slab data for the KBCG model from Alaska for the two sub-regions of Alaska (Kodiak+Prince William Sounds) and Aleutian.

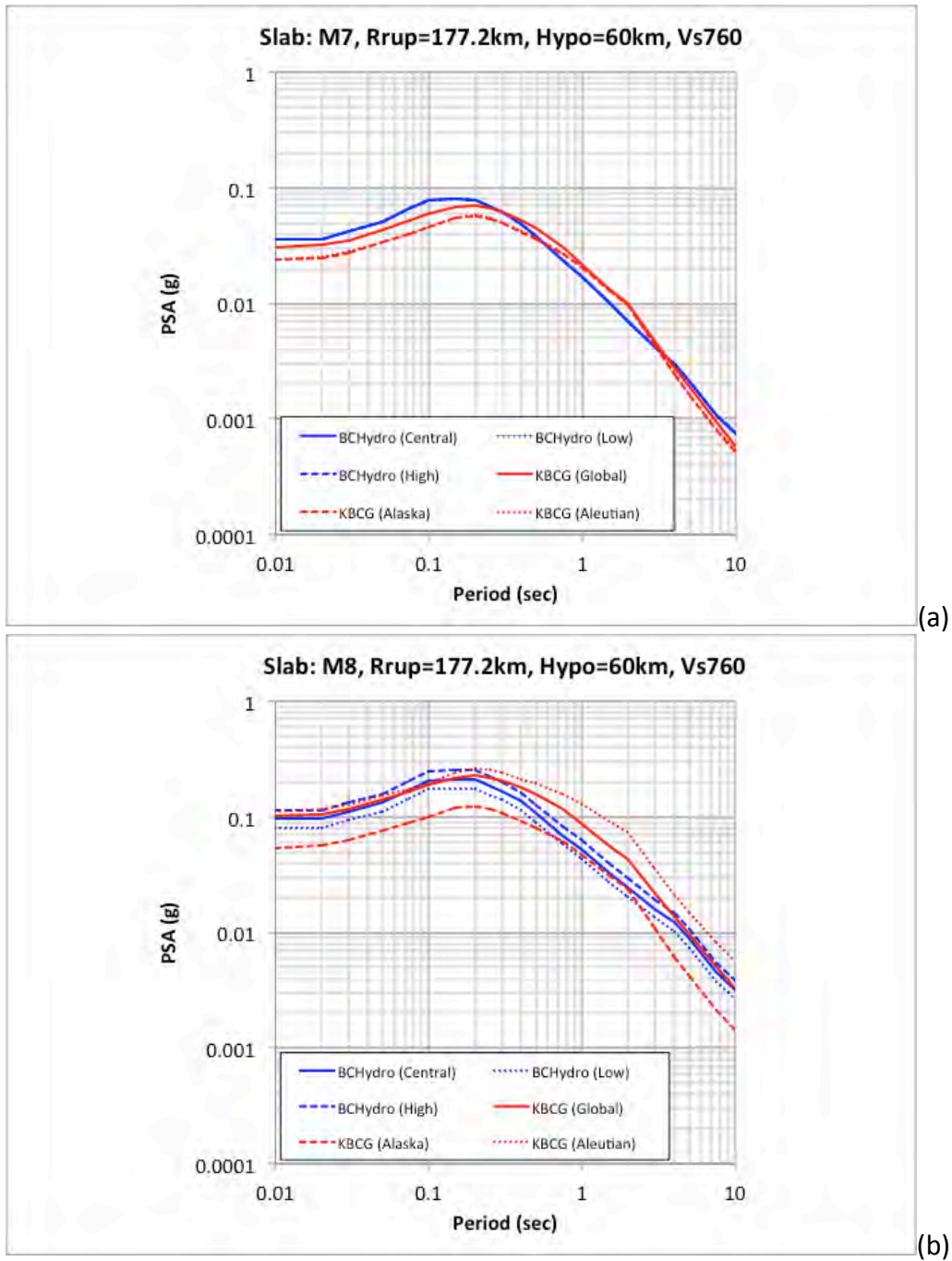


Figure 22. Median spectra for the suite of evaluated interface subduction models for hypocentral depth of 60 km and magnitude 7 (a) and 8 (b).

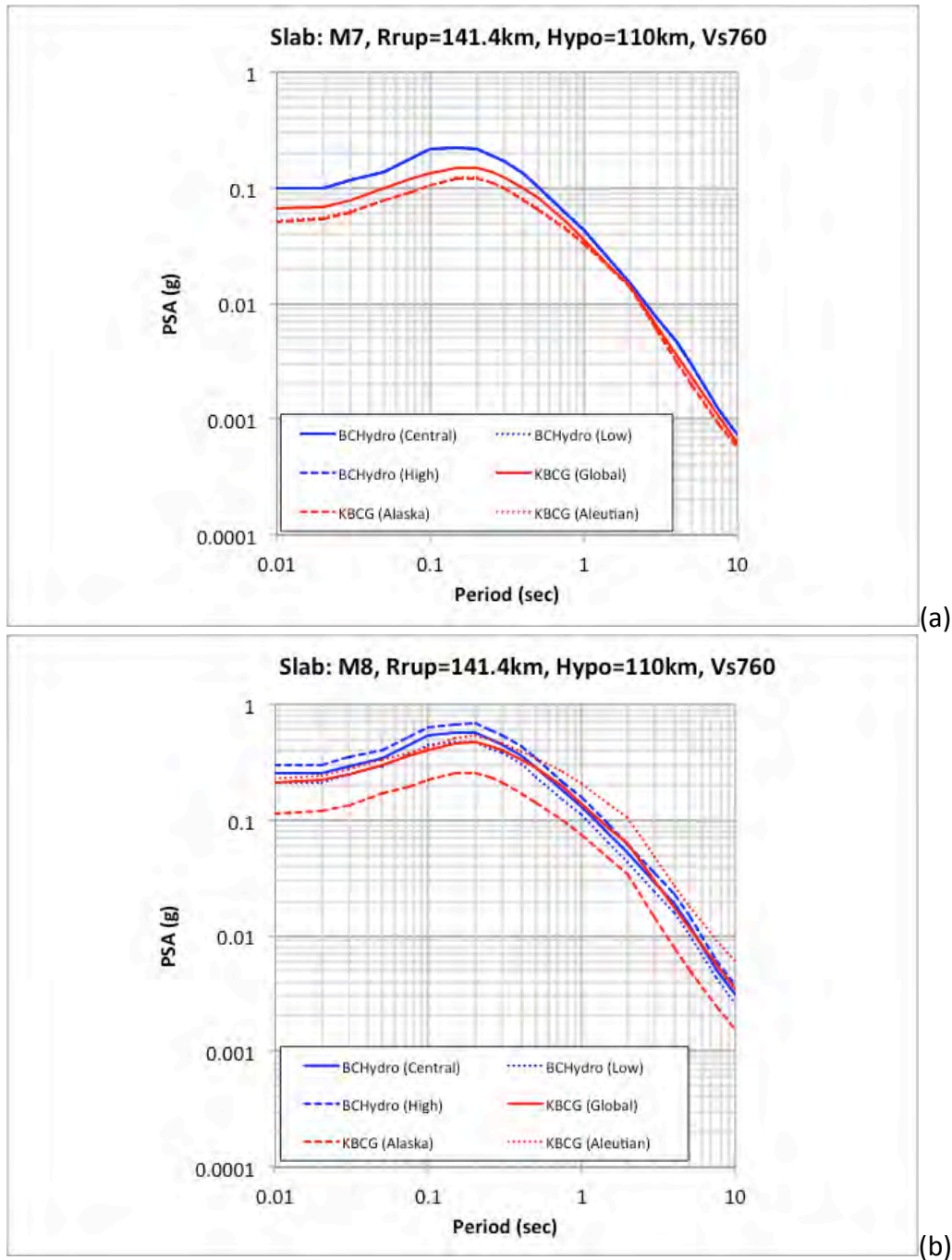


Figure 23. Median spectra for the suite of evaluated interface subduction models for hypocentral depth of 110 km and magnitude 7 (a) and 8 (b).

For the shallower depth case of 60 km, the agreement between the models is favorable for all spectral periods for the magnitude 7 case. For the larger magnitude 8 case, which is above the magnitude scaling break point, the models show a greater divergence for the regional versions but a similar ground-motion estimates for spectral periods up to about one second. For longer spectral periods, the global KBCG model and the BCHydro model show more divergence. For

the deeper cases plotted in Figure 23, a stronger depth dependence of the BCHydro model than modeled in the KBCG model is observed leading to higher ground motions for the BCHydro model. The other observations noted for the previous comparison are applicable for these deeper cases. For the application of the BCHydro GMM, the recommended hypocentral depth limit of 120 km (Abrahamson, et al., 2016) is implemented in the calculations.

The aleatory sigma models for slab events are plotted in Figure 24. Overall, the same observation as noted for the interface case is applicable for the slab case shown in Figure 24.

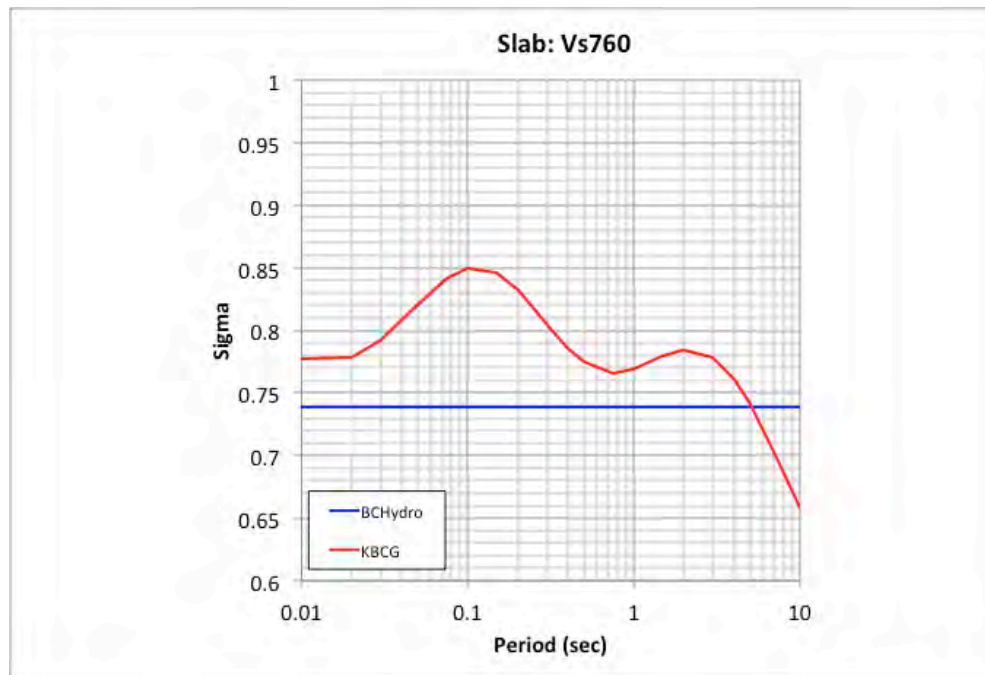


Figure 24. Total aleatory sigma from the evaluated slab subduction models.

Given these evaluations and the assessment of the Alaska data which went into the development of the regionalized slab model, only the global version of the new KBCG NGA-Subduction model is included in the SHA study consistent with the conclusion for the interface version.

The final logic tree for the subduction events (i.e., both interface and slab) is shown in Figure 25. These selected weights consisting of an increased weight for the BCHydro model relative to the new KBCG model is based on the stability and general use of the BCHydro model compared to the newly developed and released GMM and the evaluation observations presented in this report. This lower selected weight of 0.15 for the KBCG model is judged to be acceptable given the limited use of this model in engineering applications at the time of this study. This current study is one of the first studies to consider the new NGA-Subduction model for SHA studies and, as with any new GMM, caution should be used prior to its full adoption for use.

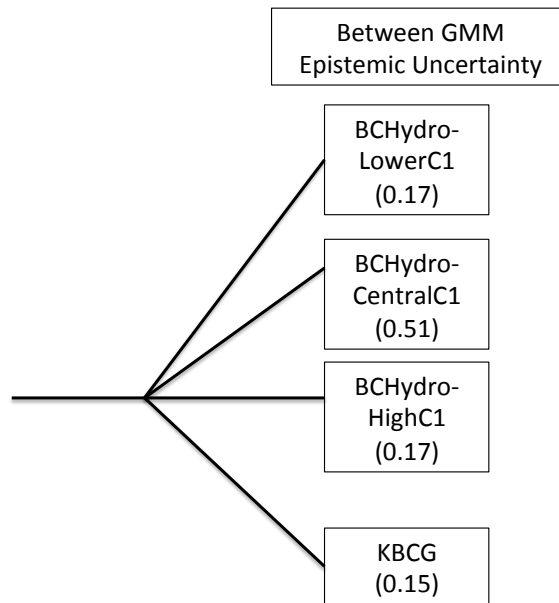


Figure 25. GMM logic tree for subduction events showing the different models and associated weights.

The previous USGS study used the Youngs et al. (1997) and Sadigh et al. (1997) crustal models for interface events with distances less than 70 km and only the Youngs et al. (1997) model for distances greater than 70 km (Wesson et al., 2007). For the slab events, the USGS used the Youngs et al. (1997) and Atkinson and Boore (2003, 2008) models. These older models represent one to two cycles of older GMMs than currently being recommended and used in this study.

For the Knight-Piesold (2013) study, the ground-motion models for interface events were based on the Youngs et al. (1997) and the Atkinson and Boore (2003, 2008) models, which represent an update from the USGS models. Also as noted in the Knight-Piesold (2013), complete saturation (i.e., no increase in the ground-motion estimates for magnitude greater than 8.5) for interface events with magnitude greater than 8.5 was applied for the Atkinson and Boore (2003, 2008) model. Thus in addition to using older GMMs, the estimated ground motions from the characteristic **M**9.2 Great Alaska earthquake would be relatively lower than from other GMMs as a result of the complete saturation magnitude of 8.5 in the Atkinson and Boore (2003, 2008) model.

The other notable difference from the GMMs used in the Knight-Piesold (2013) study and this current study is the classification of the applicable site conditions. For the Knight-Piesold (2013) study, the site condition was classified as “rock” which would be consistent with the classification of the Youngs et al. (1997) model. However, for the Atkinson and Boore (2003, 2008) model, the site classification is consistent with NEHRP site classes ranging from A – E. It is

not clear in the Knight-Piesold (2013) report which specific site classification version of the Atkinson and Boore (2003, 2008) model was used. As noted earlier, the GMMs used in this SHA study are all defined as a function of V_{s30} to capture the site response and a reference site condition of 760 m/sec was selected for this study.

Finally, the selected ground-motion models used in this SHA study are defined for the full broadband spectral period range of 0.01 sec (PGA) to 10 sec. The previous GMMs were more limited in their defined spectral period range with an upper limit of between 3 – 4 sec.

4. Probabilistic Seismic Hazard Analysis (PSHA)

4.1 Methodology

Probabilistic seismic hazard calculations are carried out using the computer program HAZ45.2 (Abrahamson, 2018). This PSHA program follows a standard state of practice approach for probabilistic seismic hazard analysis. It has successfully passed the validation test cases associated with the recent PEER PSHA Validation testing program (Hale et al., 2018).

An epsilon truncation value of 6.0 is used for the PSHA. The minimum magnitude used in the analysis is 5.0. Mean Hazard curves are computed for the three project site location (see Table 1) for the following suite of spectral periods: PGA (0.01 sec), 0.02, 0.03, 0.04, 0.05, 0.075, 0.1, 0.15, 0.2, 0.25, 0.3, 0.4, 0.5, 0.75, 1.0, 1.5, 2.0, 3.0, 4.0, 5.0, 7.5 and 10.0 sec. In addition, fractile hazard curves are computed for these same spectral periods. Based on this suite of mean hazard curves, uniform hazard spectra (UHS) are computed for the suite of five return from 475-yr to 10,000-yr. Estimates of the mean magnitude, distance and epsilon values associated with the set of five return periods are also computed and presented along with select deaggregation results for magnitude and distance bins.

Given the close proximity of the three sites, the general results from the PSHA calculations are similar and the representative plots are fully provided for the Main TSF site location. For the other two site locations (i.e., Pyritic and South TSF) a shorter presentation of the resulting UHS and fractile curves are presented. The deaggregation results are similar for these two sites compared to the results from the Main TSF site location.

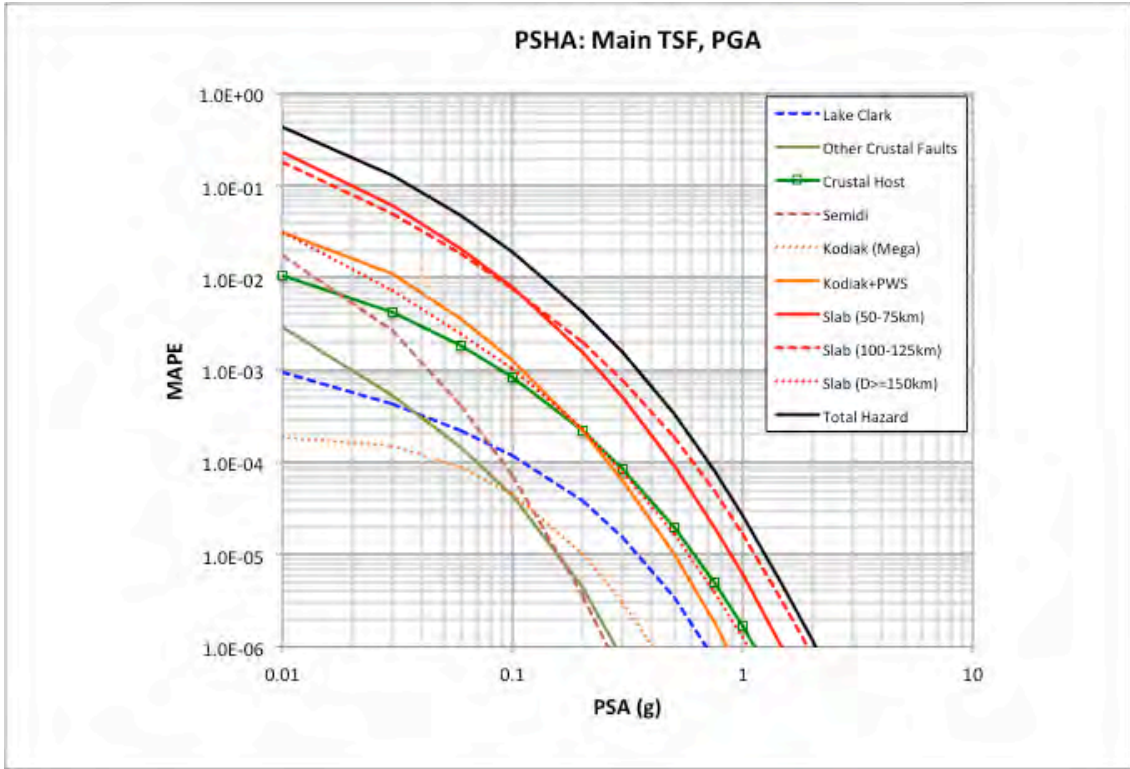
4.2 PSHA Results – Main TSF Site Location

Given the input SSC and GMC model, the mean hazard curves for the Main TSF site location are shown in Figures 26 – 28 for the five spectral periods of PGA (0.01 sec), 0.2, 0.5, 1, and 3 sec. In these plots, the individual hazard curves from the Lake Clark fault, the other crustal faults, the crustal host zone, the Semidi segment of the interface zone, the Kodiak segment for the large magnitude 8.8 event, the full Kodiak and Prince William Sound segment and the various depth ranges for the slab model are plotted. The total mean hazard curve is also shown on these plots.

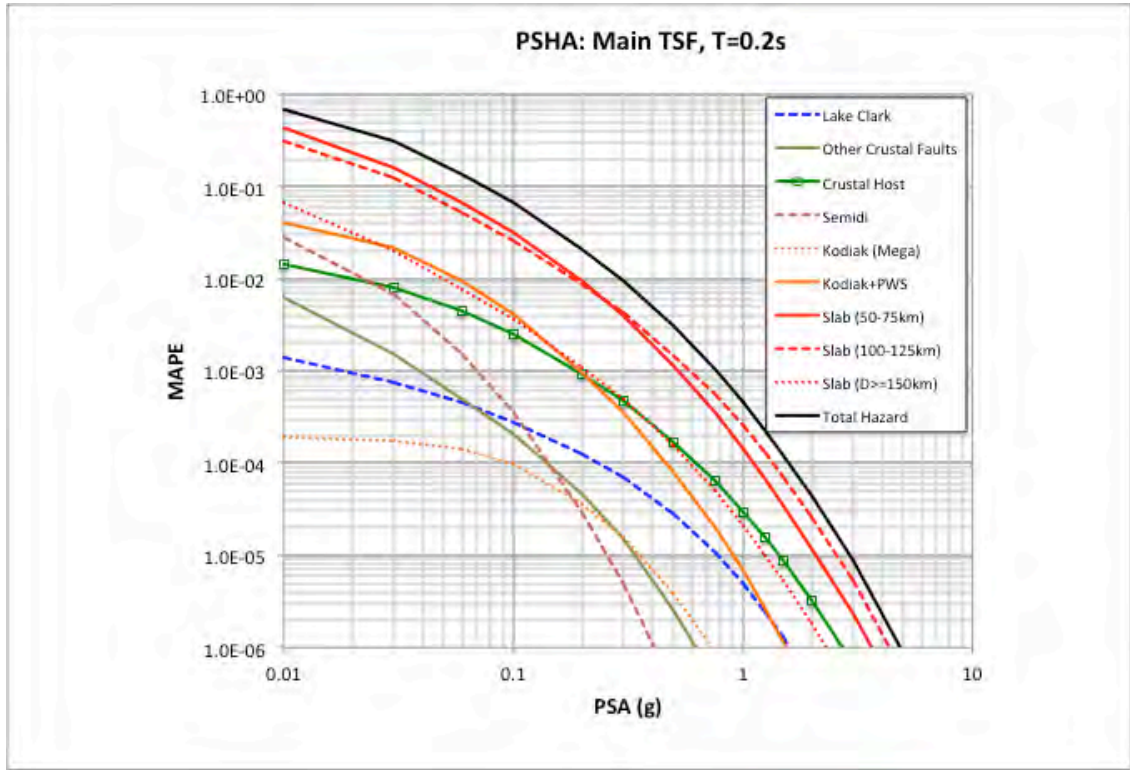
Based on these plots, it is observed that the controlling seismic source is a combination of the slab model for the depth range of 50 – 75 km and 100 – 125 km. For the shorter spectral periods, the stronger depth dependence of the BCHydro ground-motion model (i.e., see Figure 23) is causing the relatively higher contribution for the depth range of 100 – 125 km. For the longer spectral periods, the depth scaling between the BCHydro and KBCG models are more similar leading to the similar contribution from the two depth ranges of 50 – 75 and 100 – 125 km. The deeper slab sources do not contribute as significantly, mainly due to their relatively lower activity rate. At the 1 sec period, the relative contribution from the Kodiak and Prince William Sound source increases, and for spectral periods of 3 sec, its contribution is

approximately equal to the contribution from the two controlling slab sources. The other sources are not significant contributors to the total seismic hazard at the Main TSF site location.

Figures 29 – 31 show the fraction contribution to the total hazard separated by seismic sources. These curves are plotted as a function of mean annual probability of exceedance between the range of 1.0×10^{-2} to 1.0×10^{-4} . These plots also show that the main contribution to the total hazard is coming from the slab sources with depths less than or equal to 125 km. For short periods up to 1 sec, this contribution is approximately 80% of the total hazard. At the longer spectral period of 3 sec, the contribution from slab source reduces to about 60%, the contribution from the interface sources stays constant at about 20%, and the contribution from crustal sources increases to about 20%.



(a)



(b)

Figure 26. Mean hazard curves from the individual seismic sources and the total hazard curve for PGA (a) and 0.2 sec (b) for the Main TSF site location.

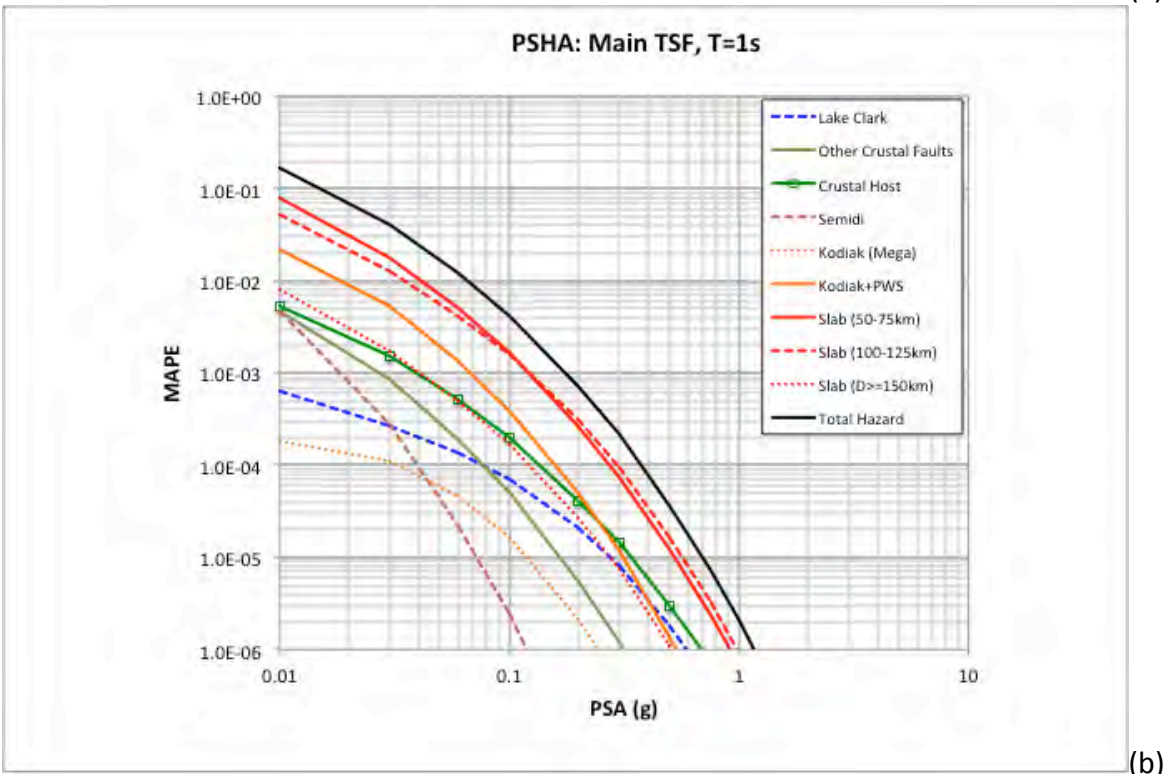
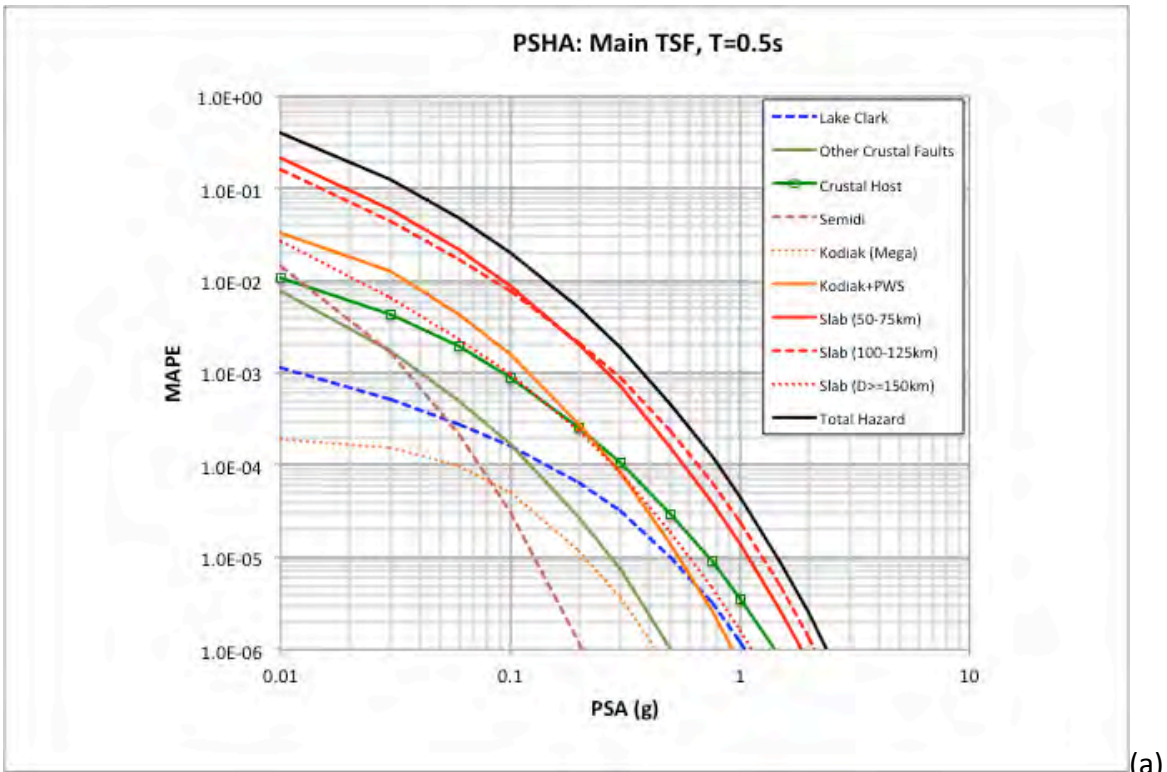


Figure 27. Mean hazard curves from the individual seismic sources and the total hazard curve for 0.5 (a) and 1 sec (b) for the Main TSF site location.

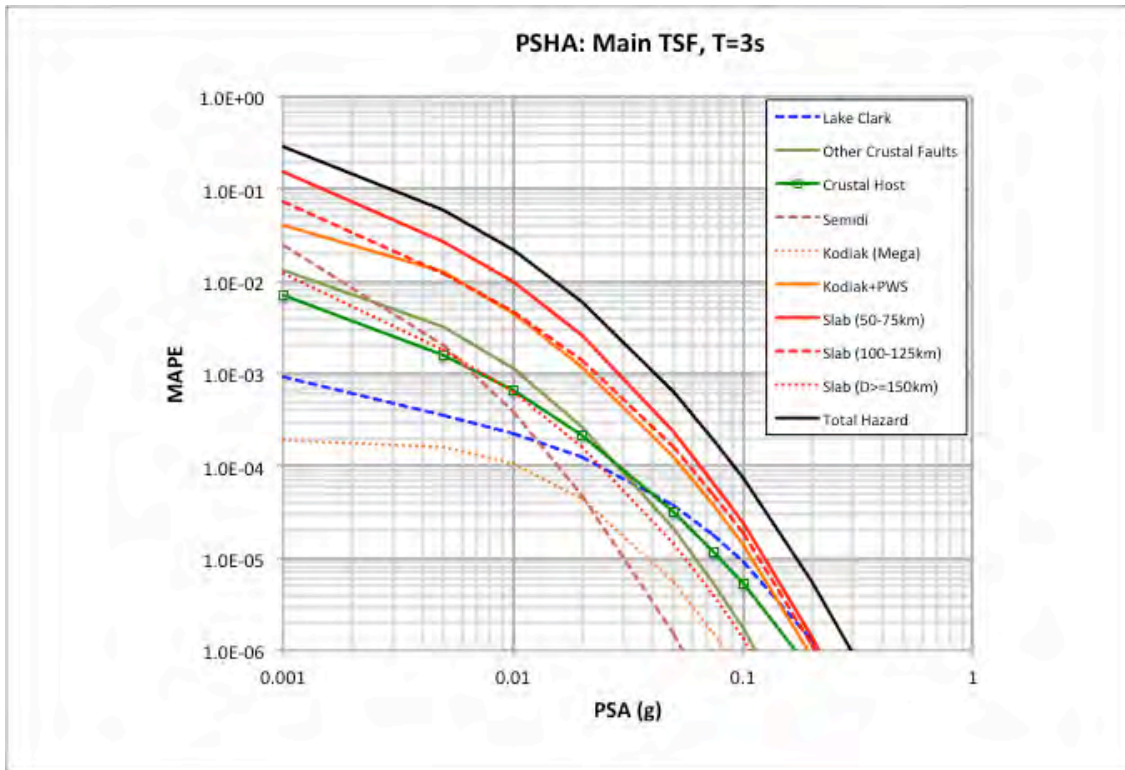
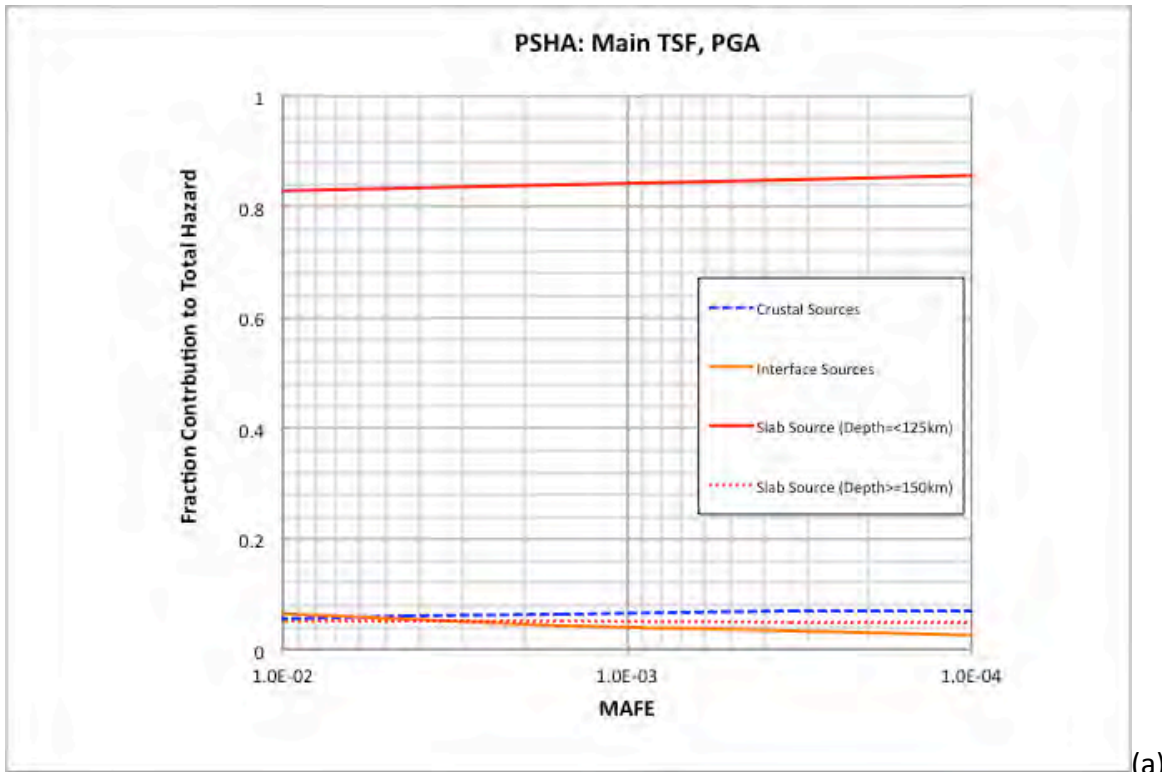
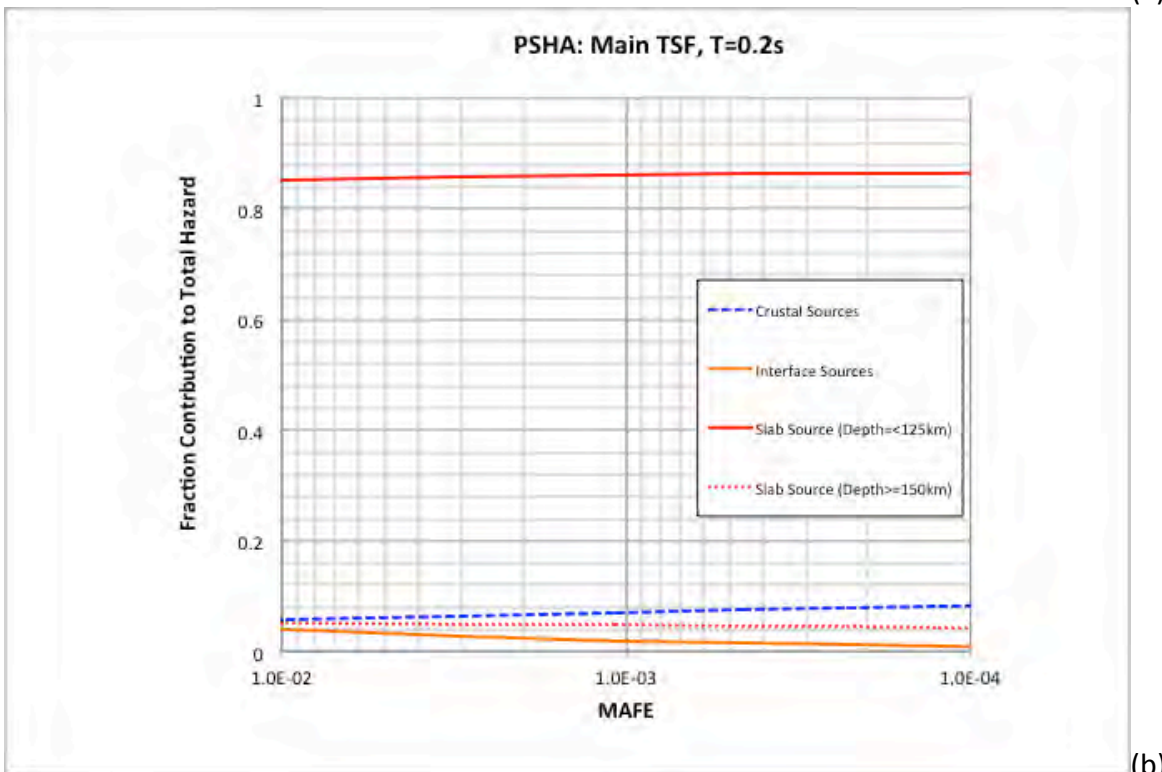


Figure 28. Mean hazard curves from the individual seismic sources and the total hazard curve for 3 sec for the Main TSF site location.

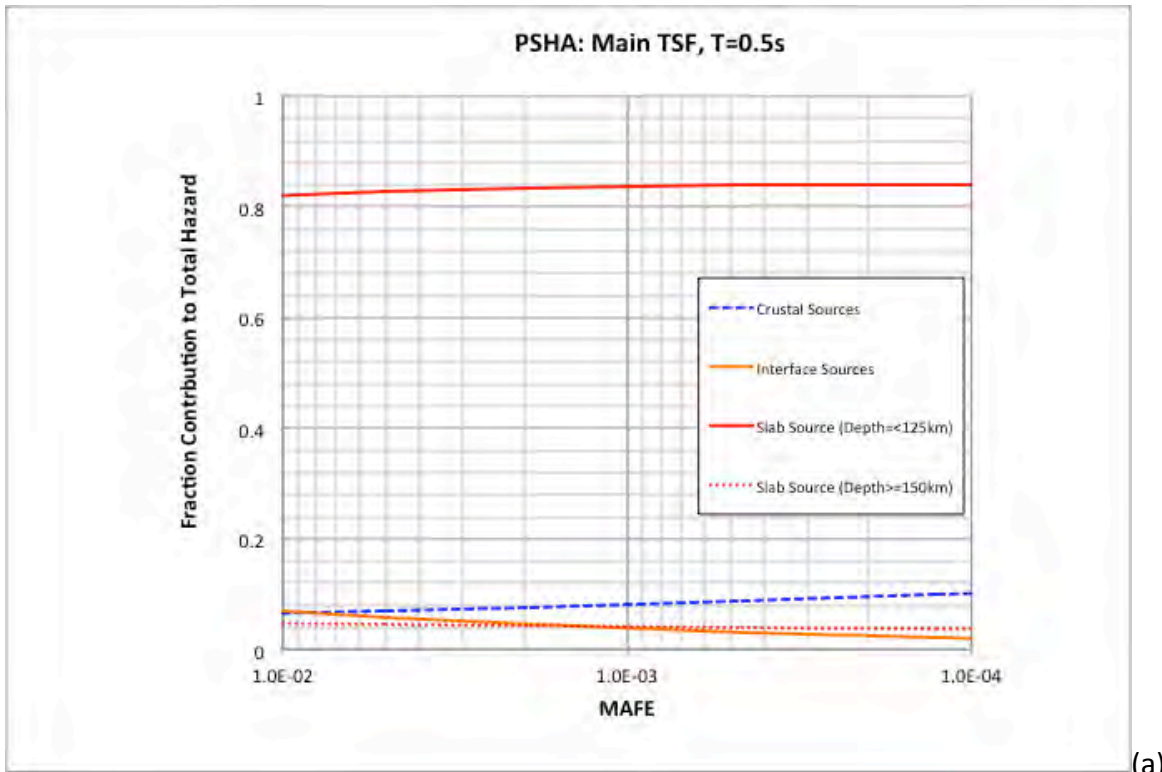


(a)

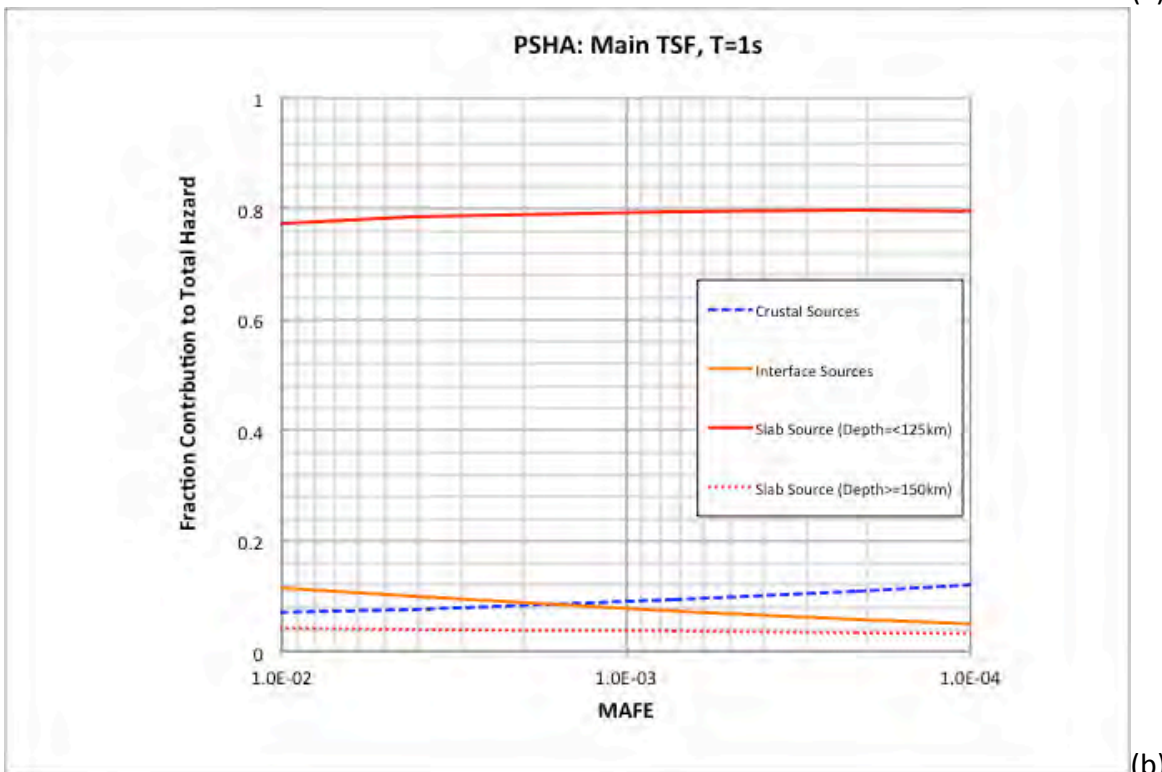


(b)

Figure 29. Fraction contribution to the total hazard from the individual seismic sources for PGA (a) and 0.2 sec (b) for the Main TSF site location.



(a)



(b)

Figure 30. Fraction contribution to the total hazard from the individual seismic sources for 0.5 (a) and 1 sec (b) for the Main TSF site location.

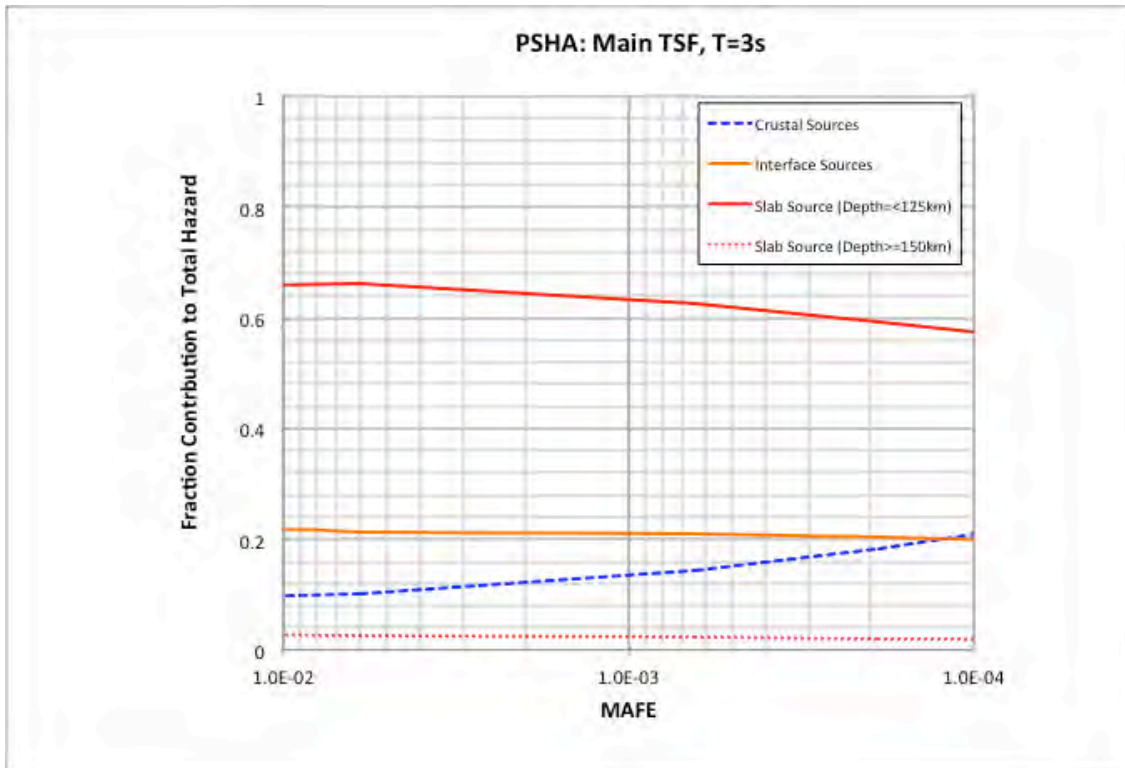


Figure 31. Fraction contribution to the total hazard from the individual seismic sources for 3 sec for the Main TSF site location.

Based on these mean hazard curves, the UHS is computed for return periods of 475, 1,000, 2,475, 5,000 and 10,000 years. These results for the Main TSF are shown in Figure 32 and listed in Table 7. Overall, the spectral shape of the UHS does not change as a function of hazard level which indicates that the controlling seismic source is similar across multiple spectral periods and the suite of return period levels. This observation is also supported by the deaggregation results that are presented later in this report.

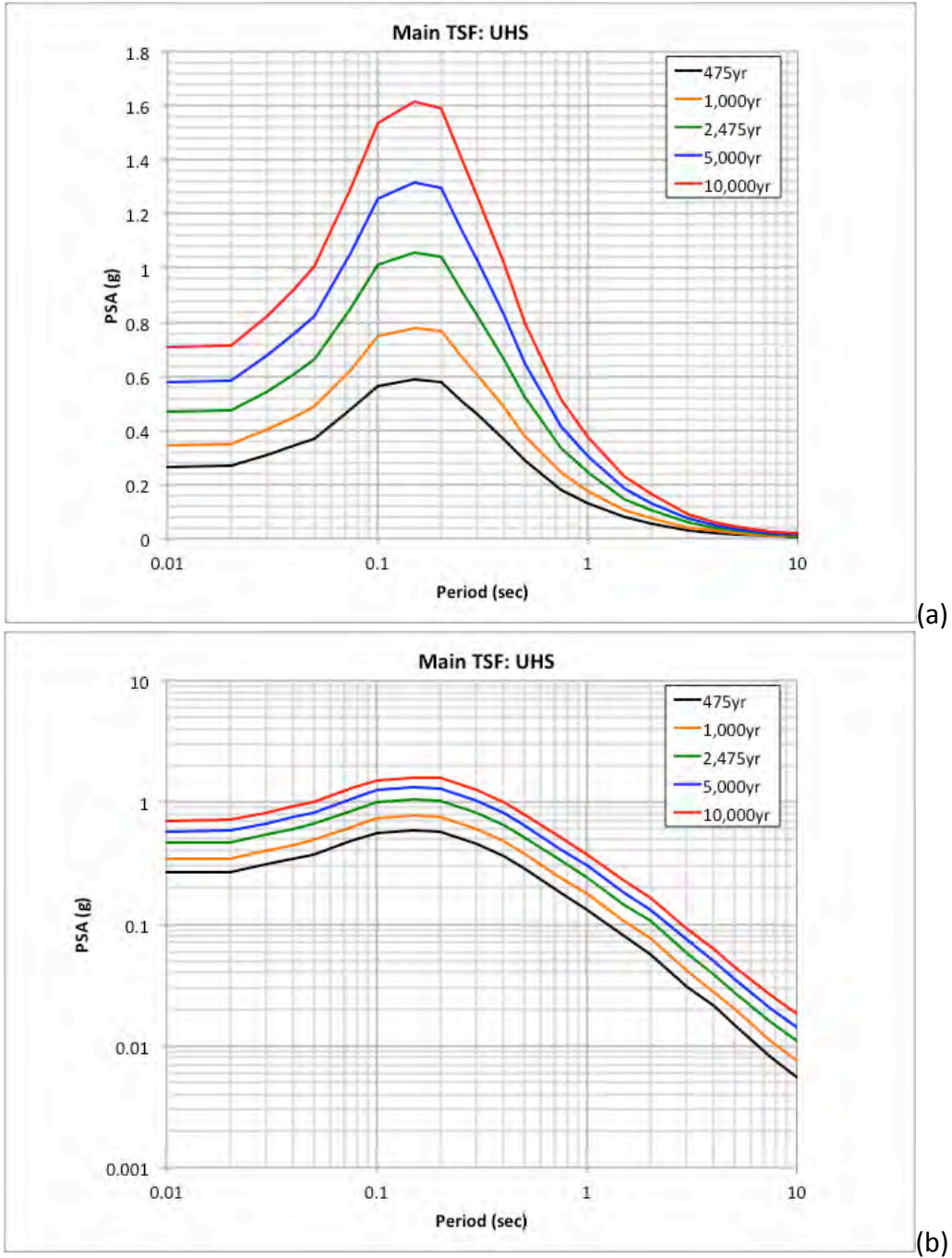


Figure 32. UHS spectra for the Main TSF site location ($V_{S30} = 760$ m/sec) plot log-linear (a) and log-log (b).

Table 7. UHS for the Main TSF site location for $V_{S30} = 760$ m/sec.

Period (sec)	475yr UHS (g)	1,000yr UHS (g)	2,475yr UHS (g)	5,000yr UHS (g)	10,000yr UHS (g)
0.010	0.2653	0.3461	0.4688	0.5790	0.7067
0.020	0.2673	0.3489	0.4735	0.5849	0.7148
0.030	0.3089	0.4017	0.5456	0.6757	0.8248
0.040	0.3417	0.4492	0.6078	0.7586	0.9237
0.050	0.3695	0.4898	0.6611	0.8234	1.0084
0.075	0.4776	0.6257	0.8508	1.0591	1.2955
0.100	0.5653	0.7466	1.0111	1.2561	1.5334
0.150	0.5880	0.7785	1.0583	1.3186	1.6132
0.200	0.5771	0.7655	1.0415	1.2983	1.5889
0.250	0.5100	0.6711	0.9167	1.1442	1.4040
0.300	0.4563	0.6022	0.8231	1.0279	1.2603
0.400	0.3649	0.4858	0.6592	0.8235	1.0108
0.500	0.2882	0.3785	0.5212	0.6486	0.7989
0.750	0.1817	0.2422	0.3322	0.4151	0.5148
1.000	0.1310	0.1756	0.2422	0.3051	0.3724
1.500	0.0799	0.1062	0.1447	0.1839	0.2276
2.000	0.0567	0.0765	0.1056	0.1319	0.1641
3.000	0.0307	0.0416	0.0583	0.0737	0.0910
4.000	0.0213	0.0279	0.0388	0.0500	0.0616
5.000	0.0150	0.0205	0.0279	0.0355	0.0450
7.500	0.0080	0.0110	0.0156	0.0204	0.0261
10.000	0.0055	0.0075	0.0109	0.0141	0.0182

The mean magnitude, distance and epsilon values as a function of spectral period and return period hazard levels are shown in Figures 33 – 35. Consistent with the slab events controlling the seismic hazard, the mean magnitude and distance parameters are in the magnitude 7.5 range at distances about 150 km. For the longer spectral periods, the increase in the mean magnitude and mean distance values are based on the increase of the relative contribution from the larger magnitude and more distant interface events associated with the Kodiak and Prince William Sound segments. The observed decrease in the mean distance for the spectral period of 7.5 sec at the longer return period hazard level is based on the relative increase in the contribution from the local Lake Clark fault. With this increase to the contribution from the closer local fault, the mean distance value is decreased. The mean epsilon values in the range of 1.5 to 2 are also consistent with the slopes of the hazard curves being approximately equal to -3.

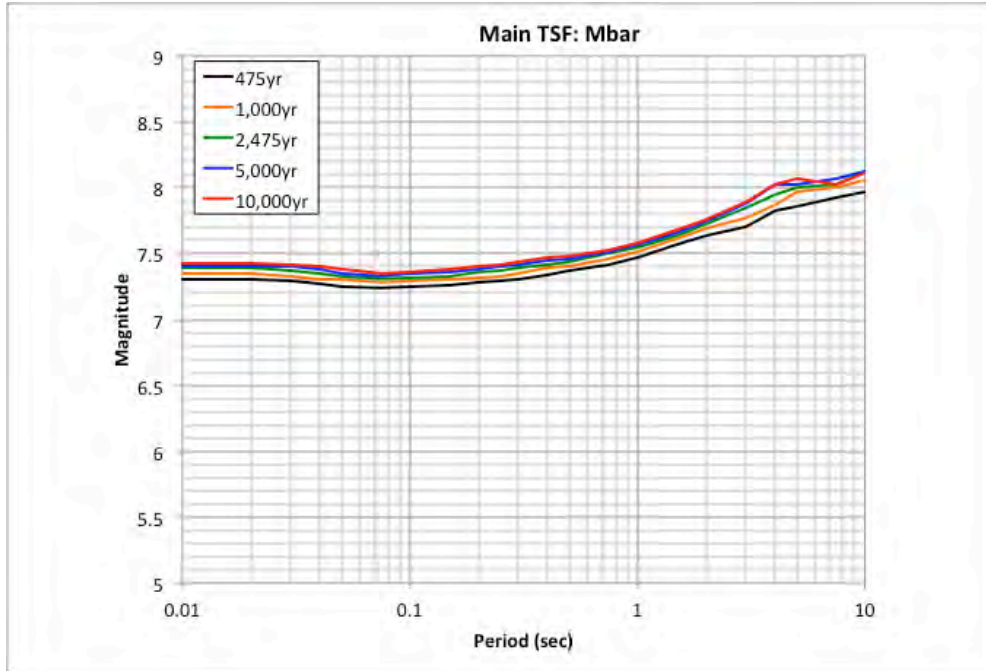


Figure 33. Mean magnitude values for the Main TSF site location ($V_{S30} = 760$ m/sec).

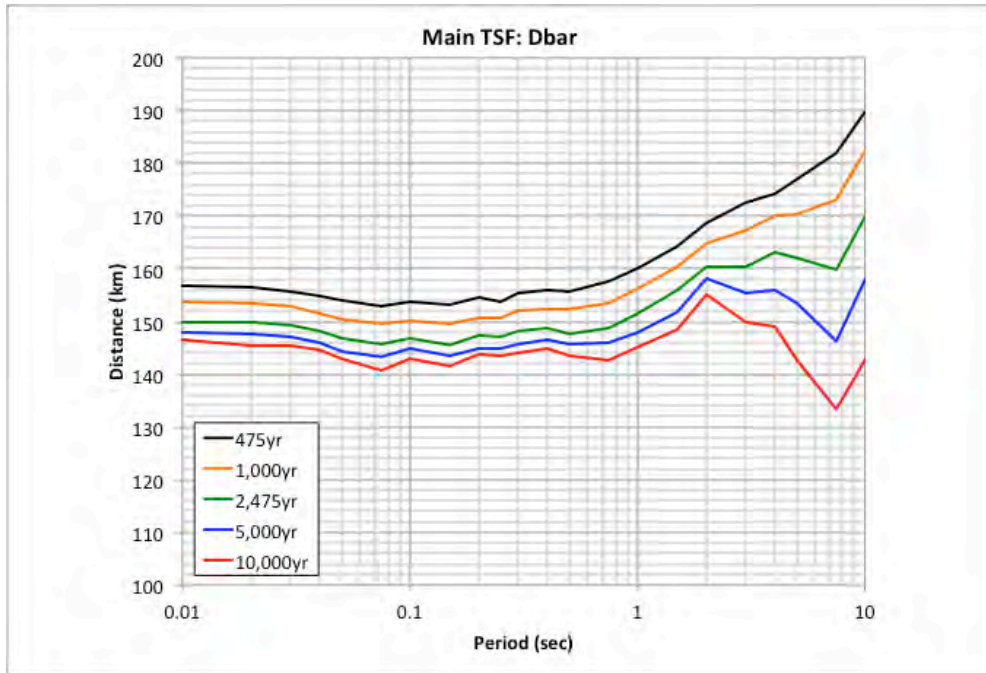


Figure 34. Mean distance values for the Main TSF site location ($V_{S30} = 760$ m/sec).

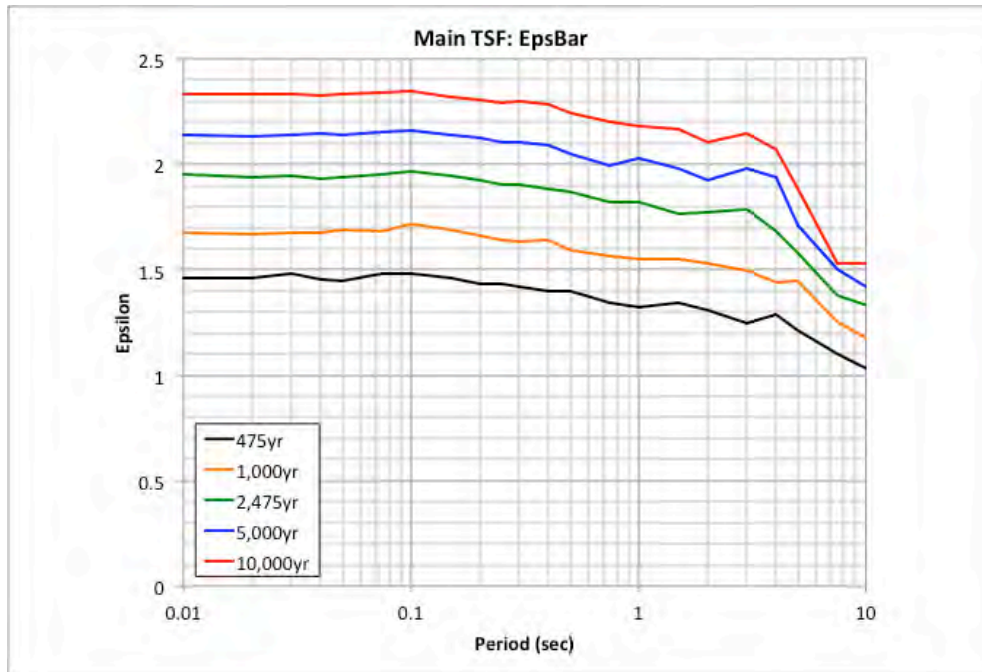
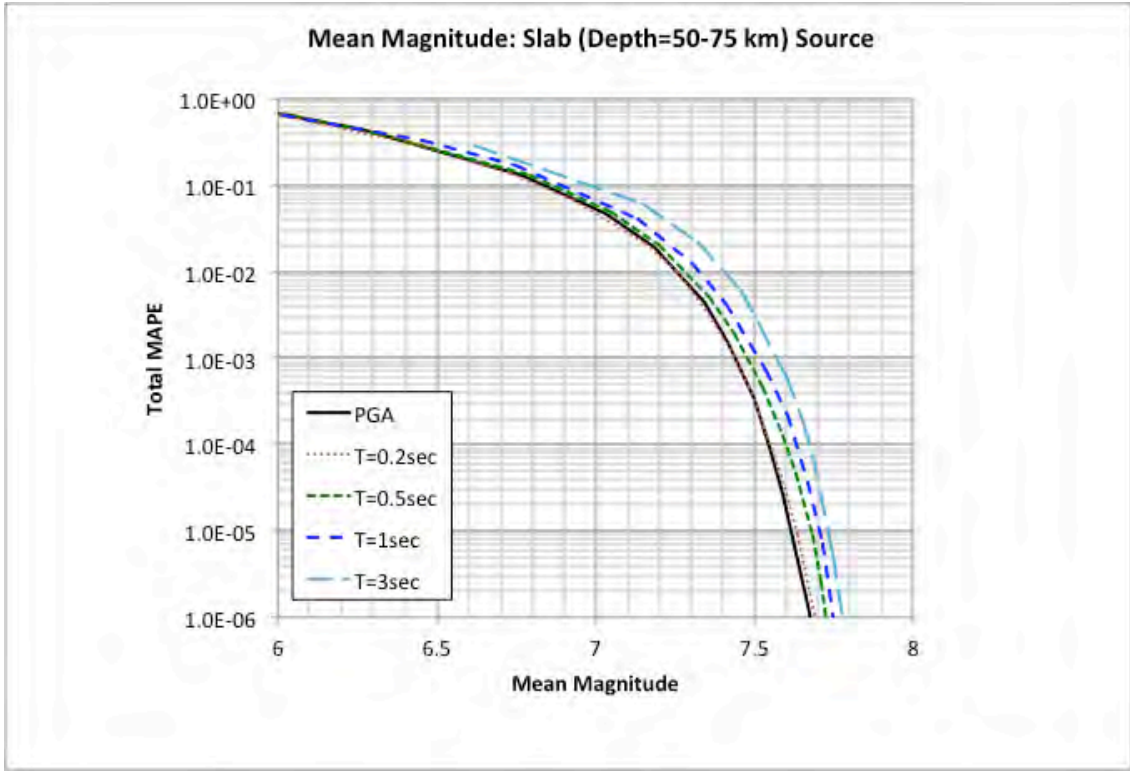
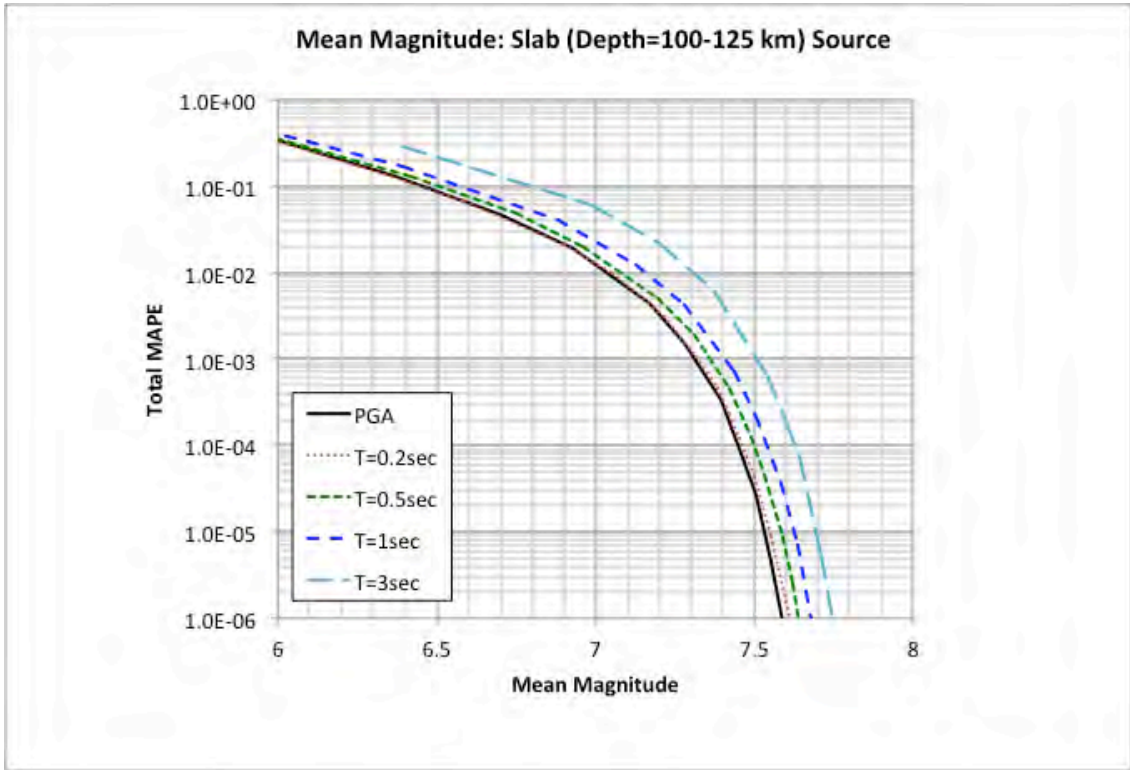


Figure 35. Mean epsilon values for the Main TSF site location ($V_{S30} = 760$ m/sec).

Given the controlling nature of the slab sources for the two depth ranges of 50 – 75 km and 100 – 125 km (i.e., see the hazard curve plots in Figures 26 – 28), the mean magnitude, distance, and epsilon values for each of these two seismic sources are presented. Figure 36 shows the mean magnitude values from the slab sources with the depth ranges of 50 – 75 km (a) and 100 – 125 km (b) for PGA and spectral periods of 0.2, 0.5, 1, and 3 seconds. The mean distance results are shown in Figure 37 and the mean epsilon values are plotted in Figure 38. These results are plotted as a function of the total hazard curve values. These results indicate that the mean events from these two controlling slab sources are rather consistent across the spectral period range with magnitudes in the 7.4 – 7.65 range, distances in the 150 – 170 km range and epsilon values in the 2 – 2.7 range for the 5,000-yr and 10,000-yr return period levels.

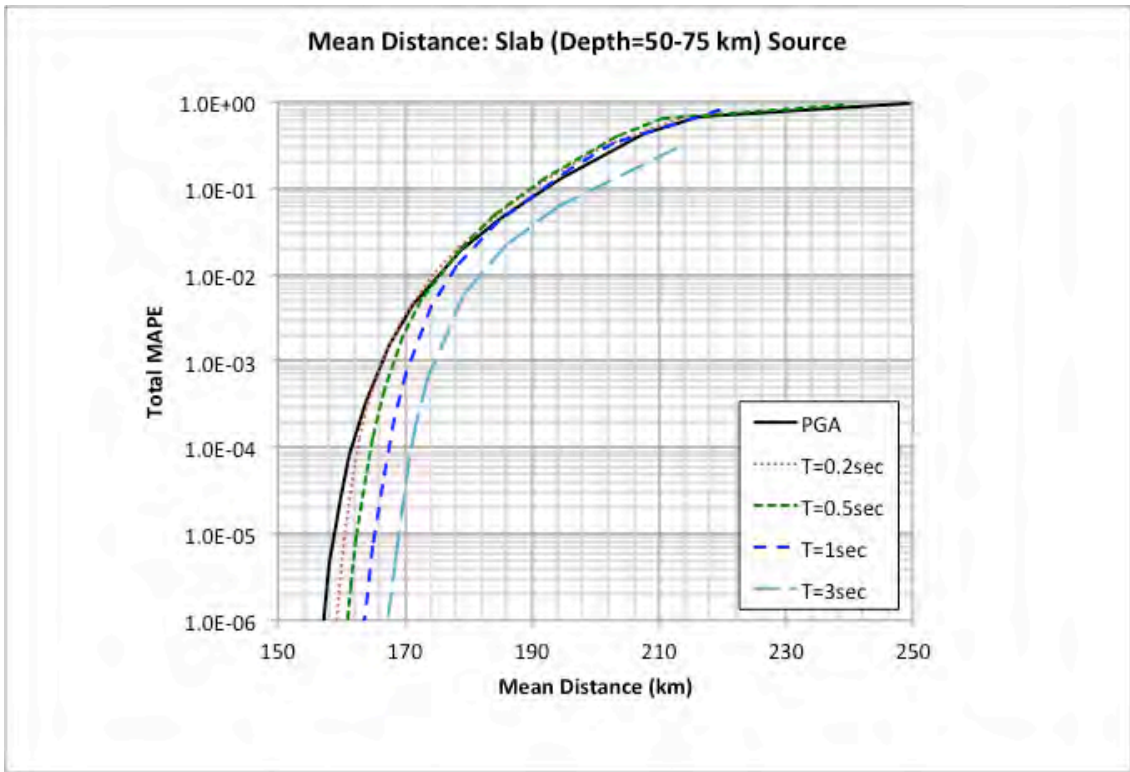


(a)

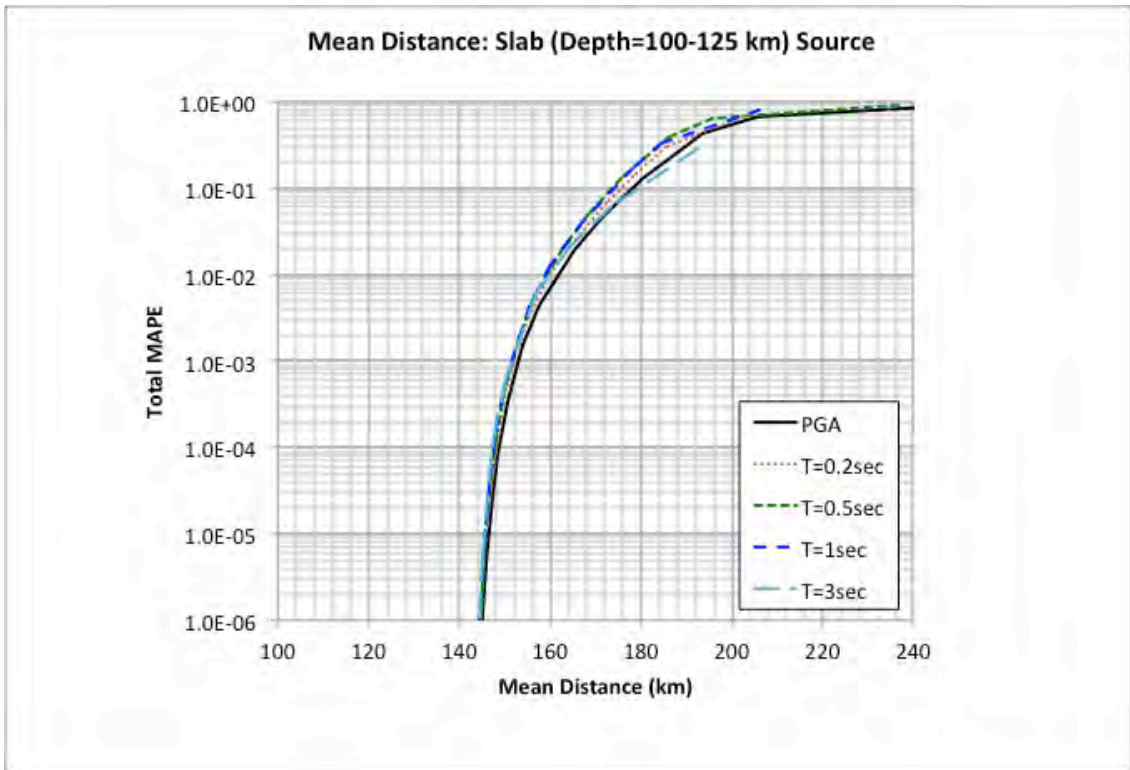


(b)

Figure 36. Mean magnitude values from the slab source for depth ranges of 50 – 75 km (a) and 100 – 125 km (b) for the Main TSF site location ($V_{S30} = 760$ m/sec).

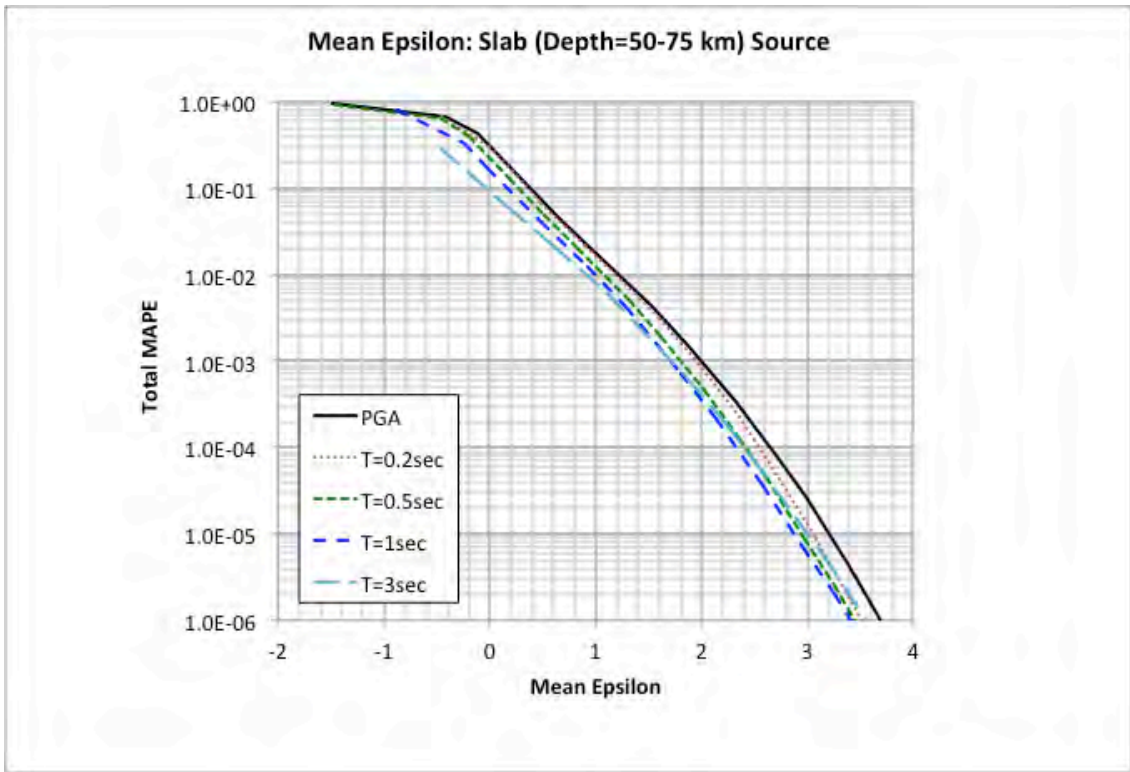


(a)

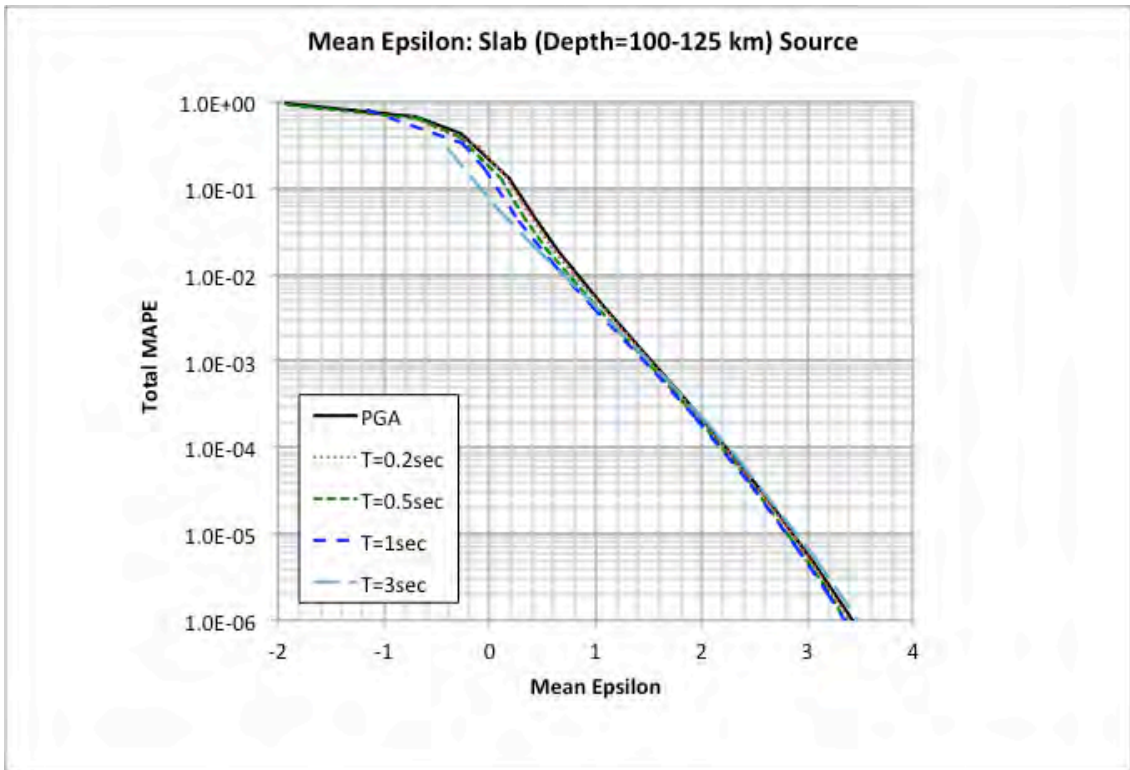


(b)

Figure 37. Mean distance values from the slab source for depth ranges of 50 – 75 km (a) and 100 – 125 km (b) for the Main TSF site location ($V_{S30} = 760$ m/sec).



(a)



(b)

Figure 38. Mean epsilon values from the slab source for depth ranges of 50 – 75 km (a) and 100 – 125 km (b) for the Main TSF site location ($V_{S30} = 760$ m/sec).

The fractile hazard curves for the same five representative spectral periods are plotted in Figures 39 and 41. These observed fractile distributions are based on the uncertainty contained within the SSC and GMC models. The larger dispersion observed for the longer spectral periods is a result of the larger dispersion of the subduction GMMs at these longer spectral periods (e.g., see Figure 22 and 23). Fractile UHS are provided in Tables 8 and 9 for the longer return periods of 5,000-yr and 10,000-yr, respectively. These fractile UHS are also plotted in Figures 42 and 43. For the 95th percentile UHS, the increase at the 2 sec spectral period is a result of the feature of the KBCG GMM which shows an increase in the ground-motions for a spectral period of 2 sec relative to the 1.5 and 3 sec periods (e.g., see Figures 22, 23 and 19).

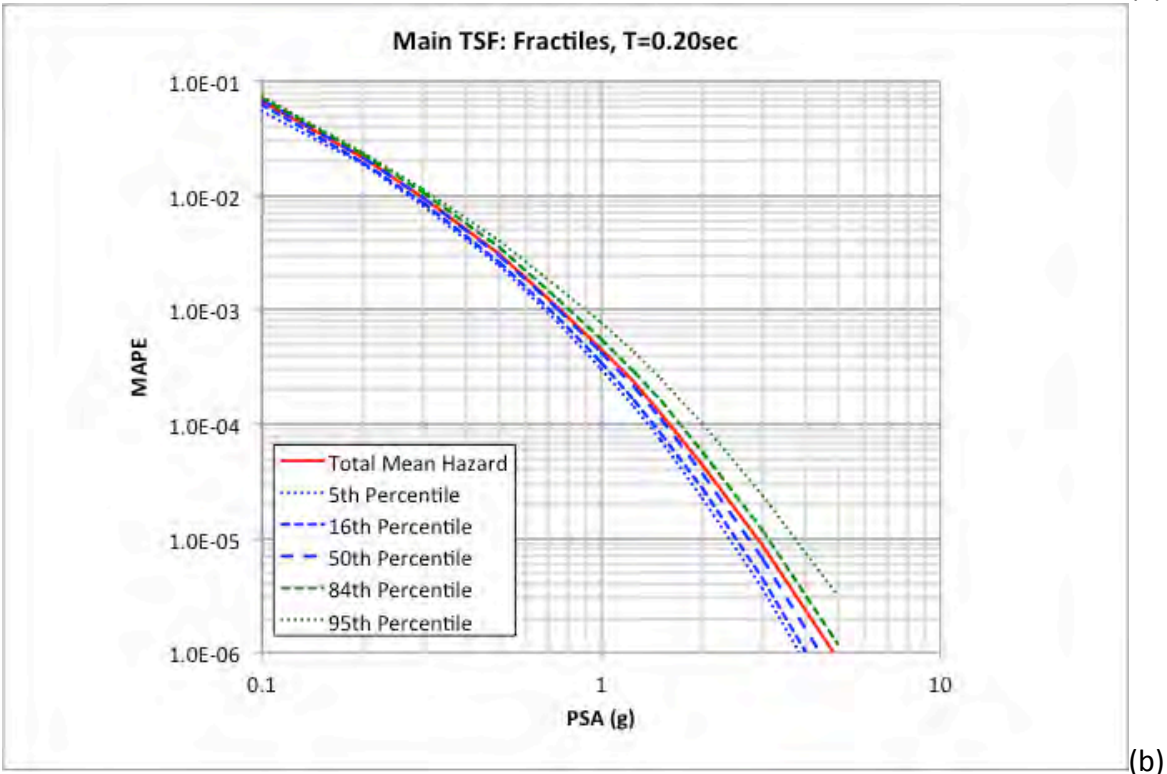
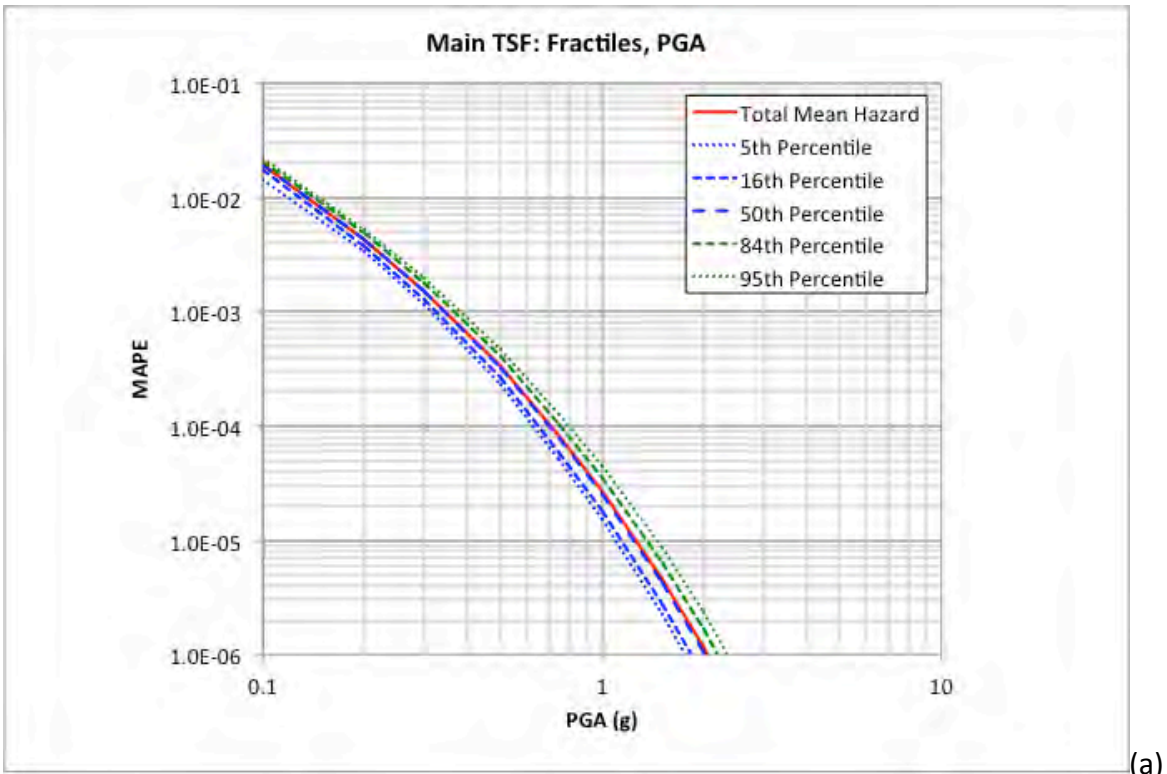
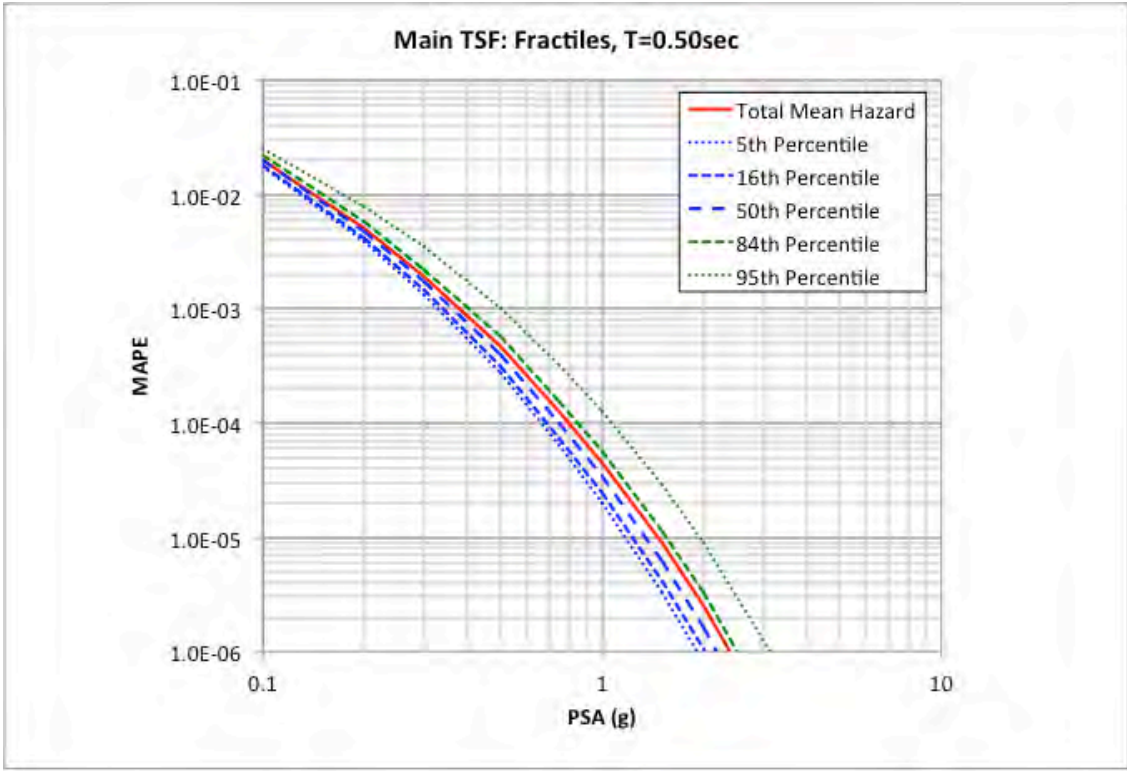
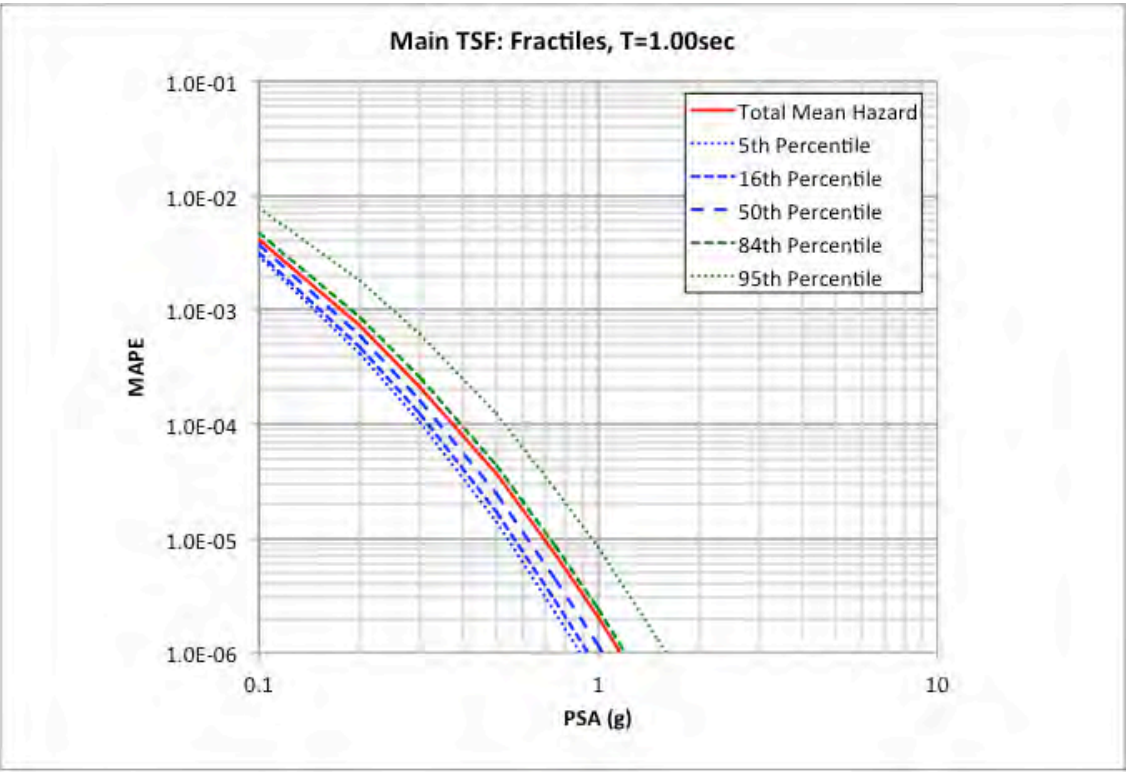


Figure 39. Fractile hazard curves for PGA (0.01 sec) (a) and 0.2 sec (b) for the Main TSF site location.



(a)



(b)

Figure 40. Fractile hazard curves for 0.5 sec (a) and 1 sec (b) for the Main TSF site location.

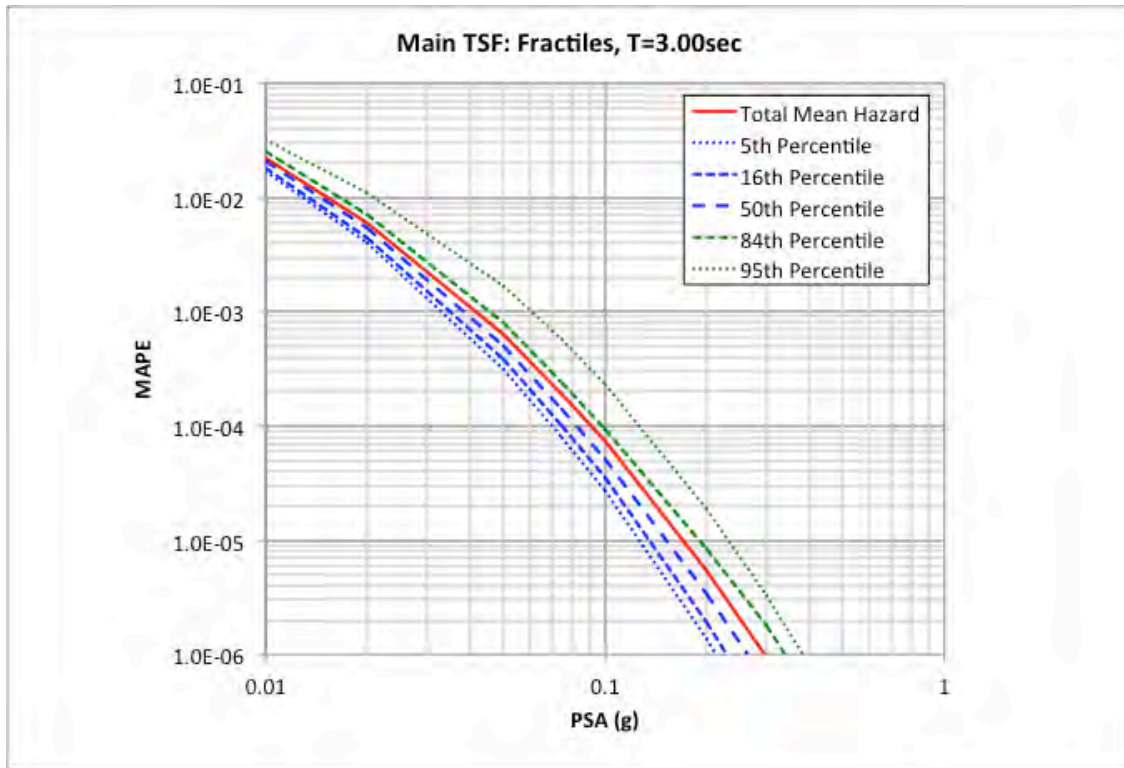


Figure 41. Fractile hazard curves for 3 sec for the Main TSF site location.

Table 8. Fractile UHS for the Main TSF site location for $V_{S30} = 760$ m/sec at the 5,000-yr return period level.

Period (sec)	Mean 5,000-yr UHS (g)	5th 5,000-yr UHS (g)	16th 5,000-yr UHS (g)	50th 5,000-yr UHS (g)	84th 5,000-yr UHS (g)	95th 5,000-yr UHS (g)
0.010	0.5790	0.5191	0.5383	0.5743	0.6159	0.6498
0.020	0.5849	0.5218	0.5407	0.5774	0.6231	0.6690
0.030	0.6757	0.6011	0.6235	0.6674	0.7213	0.7721
0.040	0.7586	0.6681	0.6934	0.7437	0.8075	0.8959
0.050	0.8234	0.7243	0.7522	0.8017	0.8786	1.0110
0.075	1.0591	0.9371	0.9718	1.0370	1.1290	1.2660
0.100	1.2561	1.1160	1.1570	1.2360	1.3370	1.4620
0.150	1.3186	1.1520	1.1960	1.2810	1.4120	1.6320
0.200	1.2983	1.1290	1.1740	1.2620	1.3930	1.6010
0.250	1.1442	0.9863	1.0260	1.1010	1.2300	1.4590
0.300	1.0279	0.8830	0.9187	0.9901	1.1030	1.3020
0.400	0.8235	0.7066	0.7368	0.7925	0.8832	1.0470
0.500	0.6486	0.5456	0.5673	0.6110	0.6939	0.8699
0.750	0.4151	0.3388	0.3527	0.3802	0.4380	0.5886
1.000	0.3051	0.2463	0.2575	0.2792	0.3210	0.4275
1.500	0.1839	0.1418	0.1489	0.1623	0.1910	0.2743
2.000	0.1319	0.0992	0.1042	0.1130	0.1316	0.2101
3.000	0.0737	0.0572	0.0606	0.0668	0.0791	0.1044
4.000	0.0500	0.0391	0.0421	0.0474	0.0557	0.0636
5.000	0.0355	0.0276	0.0297	0.0339	0.0407	0.0455
7.500	0.0204	0.0138	0.0153	0.0194	0.0245	0.0282
10.000	0.0141	0.0094	0.0104	0.0133	0.0170	0.0196

Table 9. Fractile UHS for the Main TSF site location for $V_{S30} = 760$ m/sec at the 10,000-yr return period level.

Period (sec)	Mean 10,000-yr UHS (g)	5th 10,000-yr UHS (g)	16th 10,000-yr UHS (g)	50th 10,000-yr UHS (g)	84th 10,000-yr UHS (g)	95th 10,000-yr UHS (g)
0.010	0.7067	0.6250	0.6500	0.6994	0.7560	0.7987
0.020	0.7148	0.6281	0.6530	0.7033	0.7650	0.8240
0.030	0.8248	0.7308	0.7593	0.8127	0.8802	0.9507
0.040	0.9237	0.8100	0.8398	0.9004	0.9903	1.1080
0.050	1.0084	0.8743	0.9078	0.9747	1.0750	1.2460
0.075	1.2955	1.1340	1.1770	1.2620	1.3850	1.5770
0.100	1.5334	1.3520	1.4020	1.5030	1.6360	1.8140
0.150	1.6132	1.3960	1.4500	1.5560	1.7270	2.0340
0.200	1.5889	1.3690	1.4250	1.5350	1.7060	1.9930
0.250	1.4040	1.1950	1.2460	1.3430	1.5100	1.8030
0.300	1.2603	1.0710	1.1160	1.2060	1.3540	1.6110
0.400	1.0108	0.8565	0.8924	0.9662	1.0820	1.2850
0.500	0.7989	0.6620	0.6910	0.7505	0.8519	1.0700
0.750	0.5148	0.4113	0.4301	0.4675	0.5400	0.7254
1.000	0.3724	0.3017	0.3147	0.3401	0.3924	0.5281
1.500	0.2276	0.1741	0.1836	0.2017	0.2345	0.3357
2.000	0.1641	0.1194	0.1257	0.1374	0.1621	0.2572
3.000	0.0910	0.0701	0.0747	0.0823	0.0977	0.1263
4.000	0.0616	0.0489	0.0526	0.0587	0.0694	0.0786
5.000	0.0450	0.0338	0.0368	0.0427	0.0522	0.0578
7.500	0.0261	0.0171	0.0191	0.0243	0.0320	0.0378
10.000	0.0182	0.0114	0.0126	0.0170	0.0222	0.0257

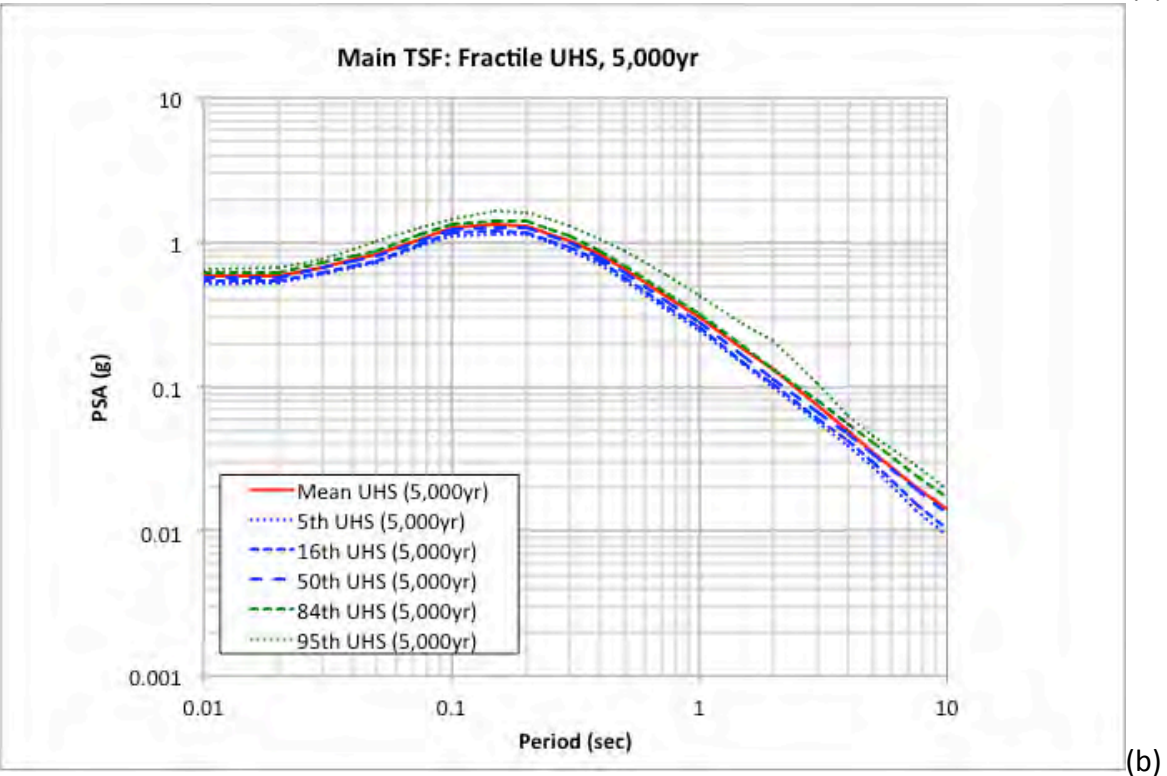
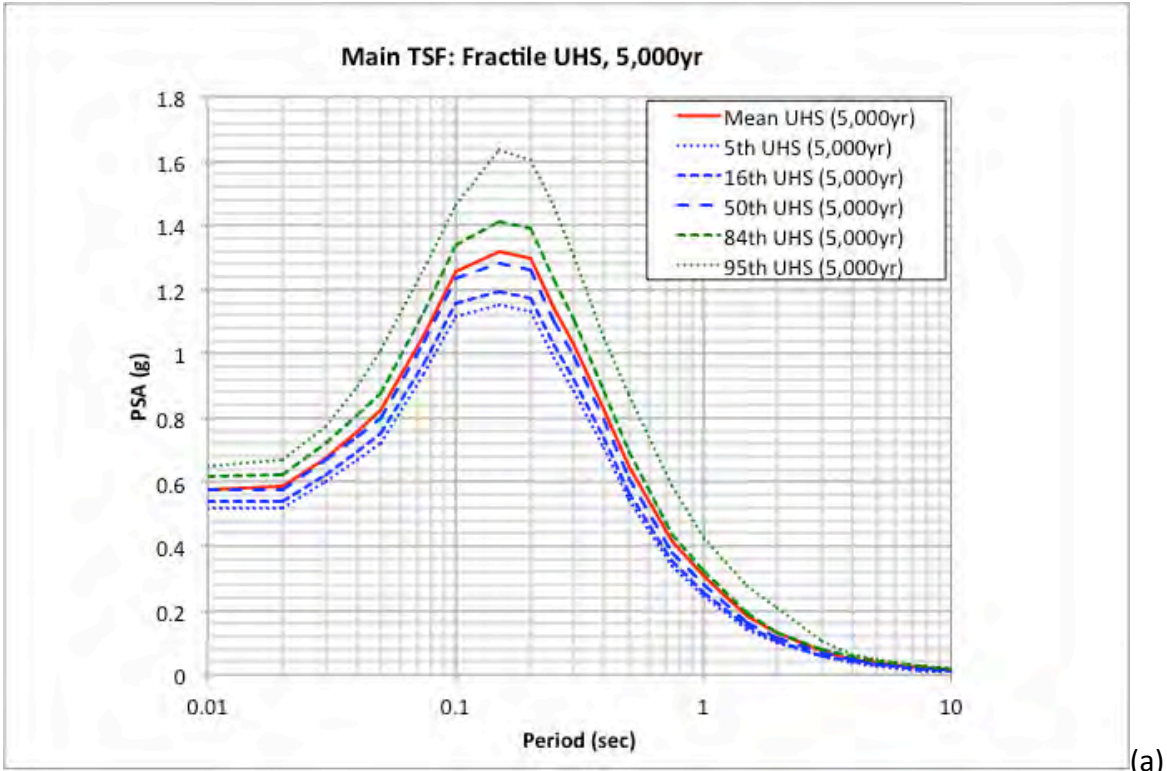
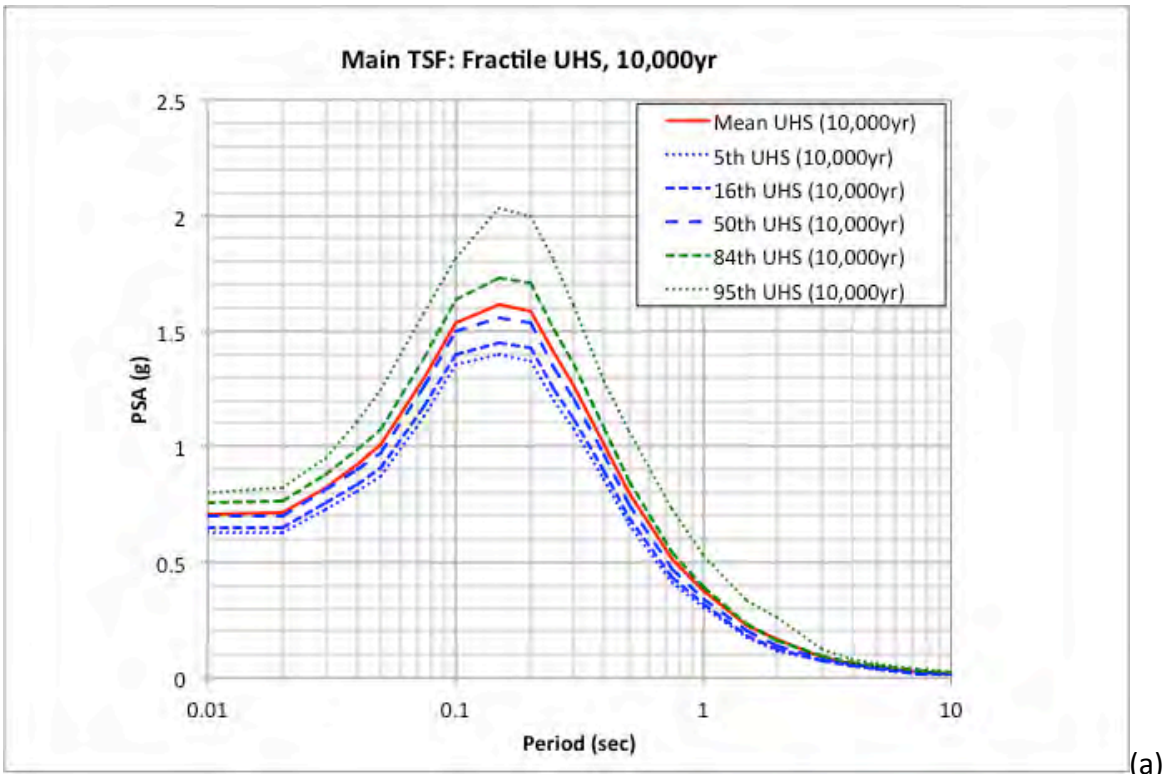
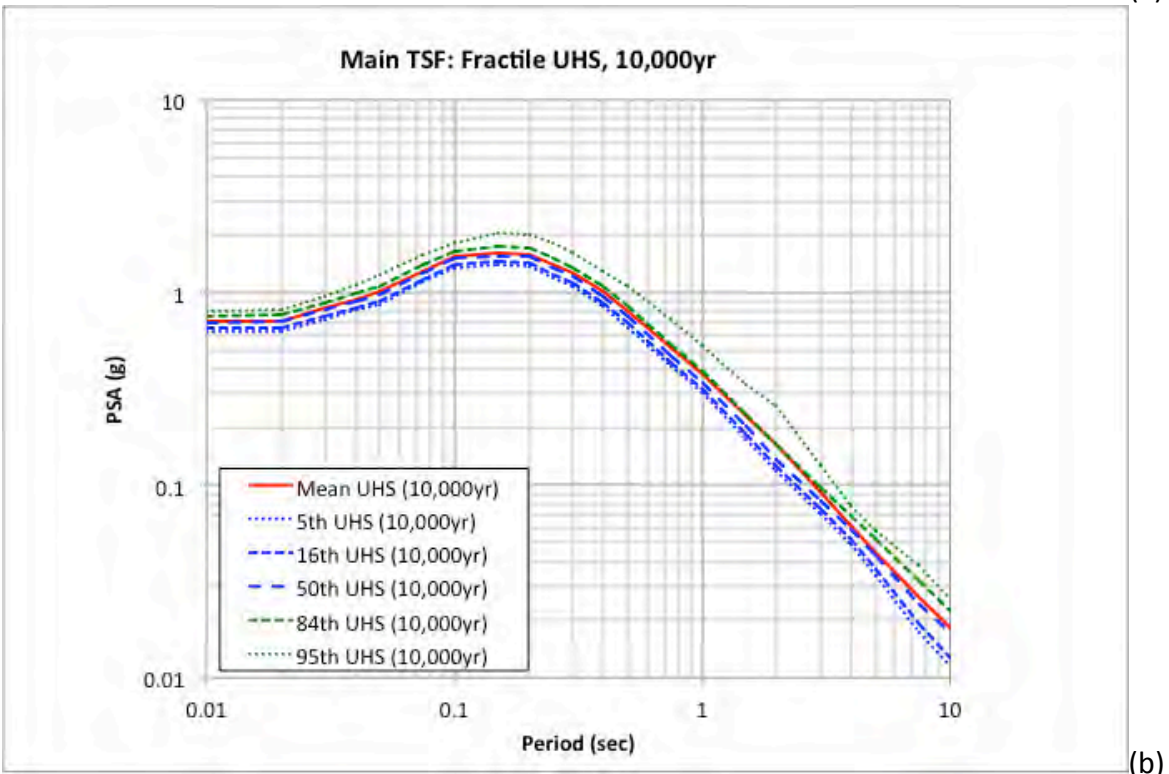


Figure 42. Fractile UHS for the Main TSF site location for 5,000-yr return period hazard level plotted log-linear (a) and log-log (b).



(a)



(b)

Figure 43. Fractile UHS for the Main TSF site location for 10,000-yr return period hazard level plotted log-linear (a) and log-log (b).

The binned deaggregation for the Main TSF site location for the hazard levels of 475, 5,000 and 10,000 years are plotted in Figures 44 – 52 for the representative five spectral periods of PGA (0.01 sec), 0.2, 0.5, 1, and 3 sec. These results are consistent with the previous hazard curve plots showing that the main contribution is from the slab seismic source with magnitudes in the 7 – 8 range and distances in the 100 – 200 km range. For the longer spectral periods of 1 and 3 sec, the relative contribution from the larger ($M > 8.5$) and more distant ($R > 200$ km) interface seismic source and the local Lake Clark fault (i.e., magnitudes 7.5 – 8.0 and distances 20 – 50 km) increases.

The modal peak bin values for the 5,000-yr and 10,000-yr cases are listed in Table 10. These results are also consistent with the previous plots and observations.

Table 10. Modal peak bin values (magnitude and distance) for the Main TSF site location for $V_{S30} = 760$ m/sec at the 5,000-yr and 10,000-yr return period levels.

Period (sec)	5,000-yr Modal Deaggregation	10,000-yr Modal Deaggregation
PGA (0.01)	Mag: 7.0 – 7.5 Distance: 110 – 150 km	Mag: 7.5 – 8.0 Distance: 110 – 150 km
0.2	Mag: 7.0 – 7.5 Distance: 110 – 150 km	Mag: 7.5 – 8.0 Distance: 110 – 150 km
0.5	Mag: 7.5 – 8.0 Distance: 110 – 150 km	Mag: 7.5 – 8.0 Distance: 110 – 150 km
1.0	Mag: 7.5 – 8.0 Distance: 150 – 200 km	Mag: 7.5 – 8.0 Distance: 150 – 200 km
3.0	Mag: 7.5 – 8.0 Distance: 150 – 200 km	Mag: 7.5 – 8.0 Distance: 150 – 200 km

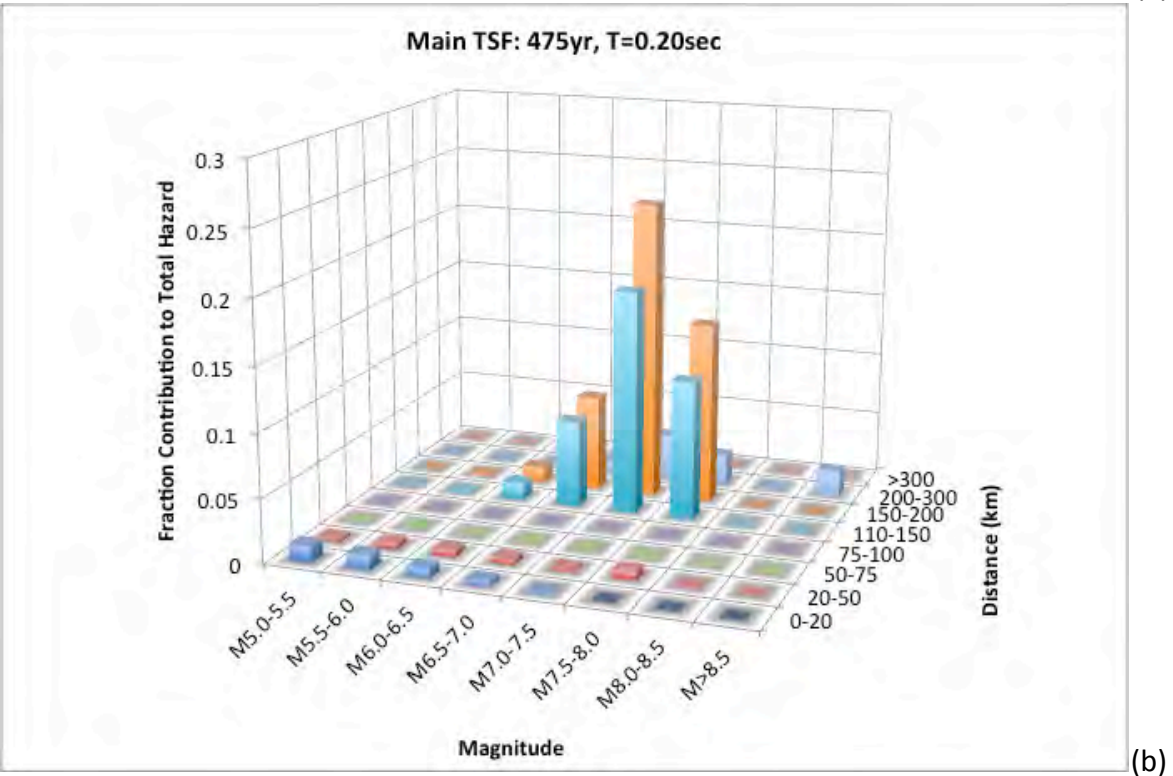
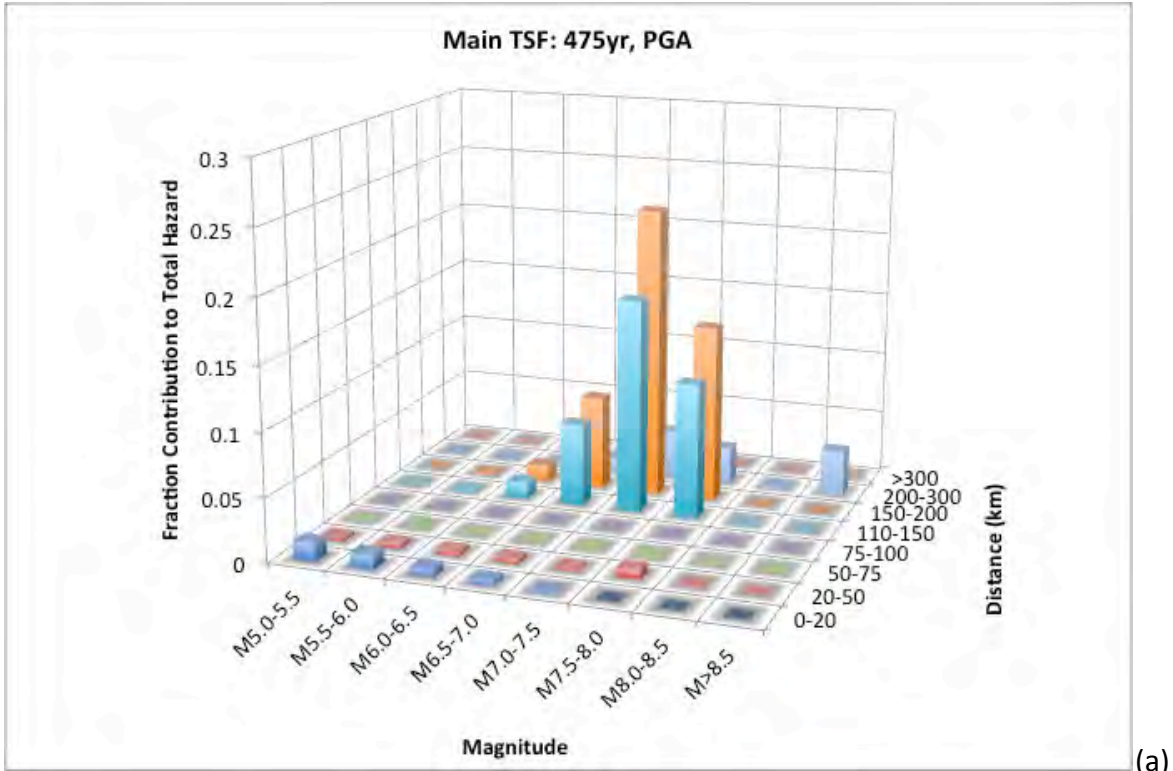
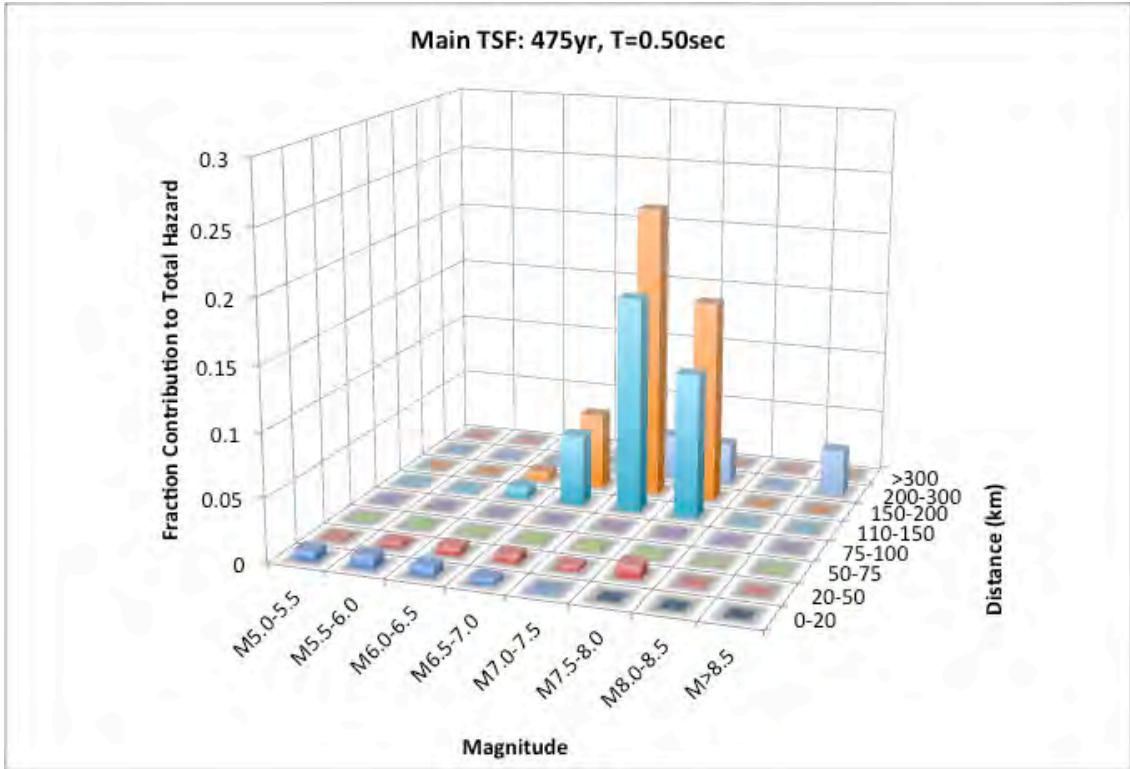
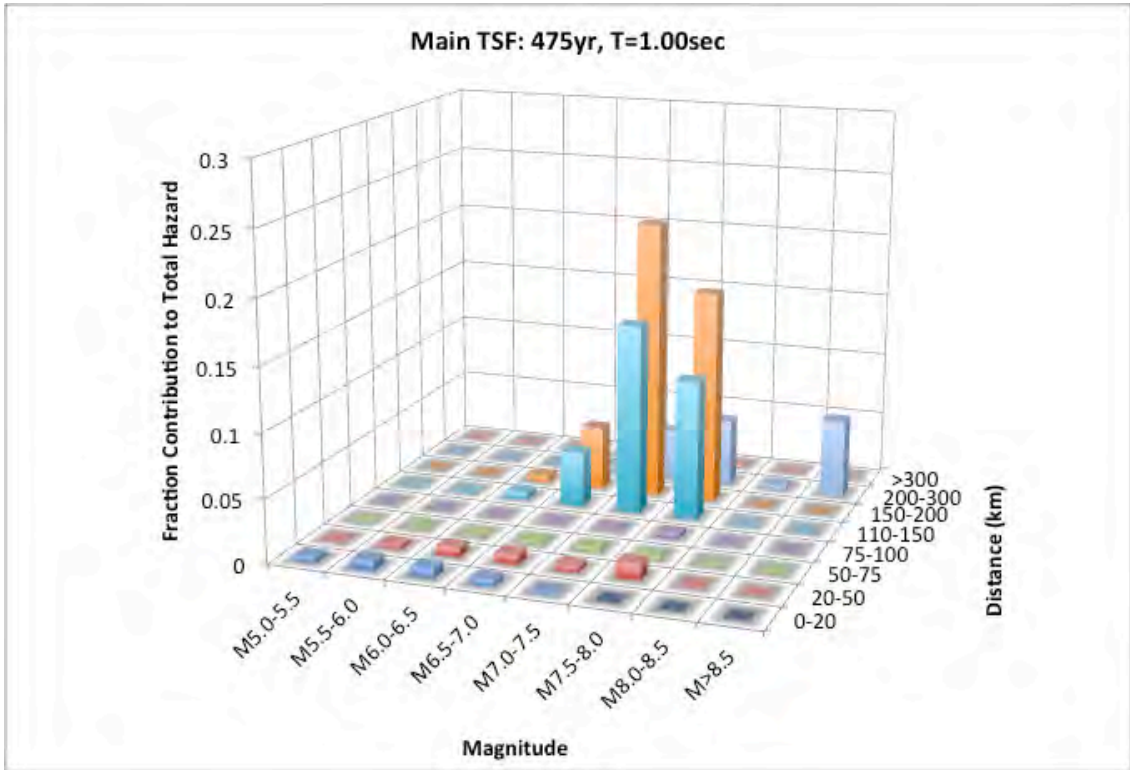


Figure 44. Deaggregation binned contribution as a function of magnitude and distance for the Main TSF site location, 475-yr hazard level and PGA (0.01 sec (a) and 0.2 sec (b).



(a)



(b)

Figure 45. Deaggregation binned contribution as a function of magnitude and distance for the Main TSF site location, 475-yr hazard level and 0.5 sec (a) and 1 sec (b).

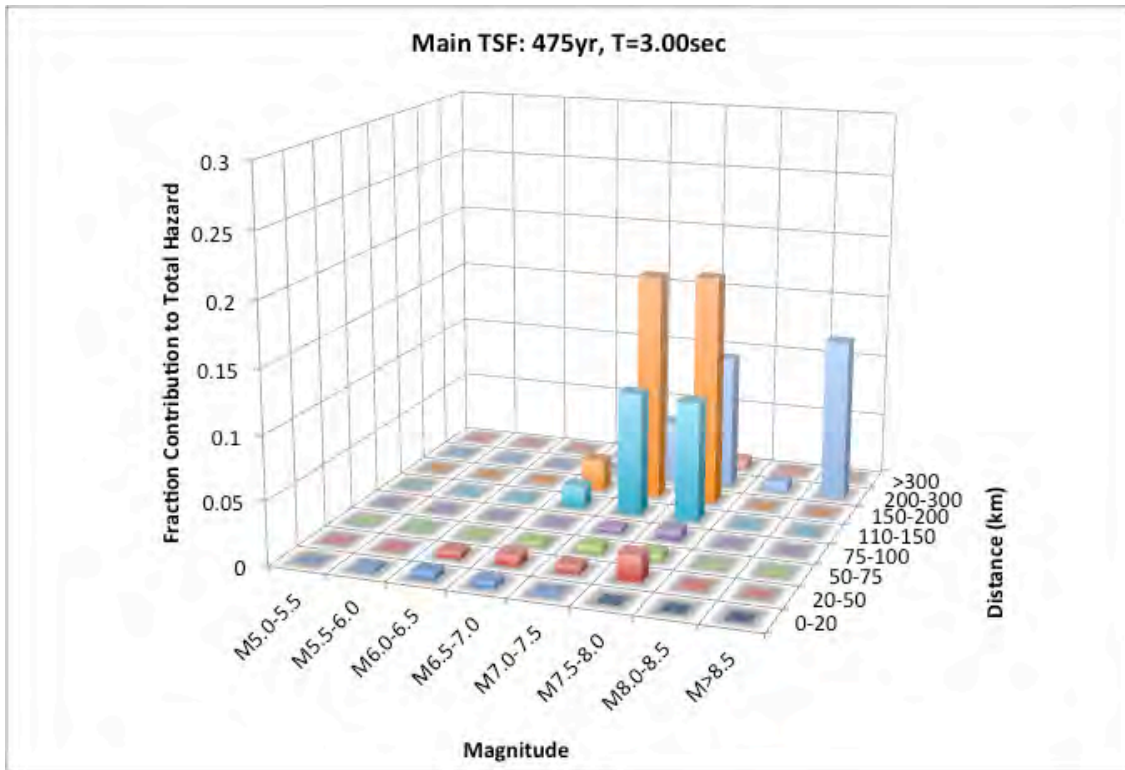


Figure 46. Deaggregation binned contribution as a function of magnitude and distance for the Main TSF site location, 475-yr hazard level and 3 sec.

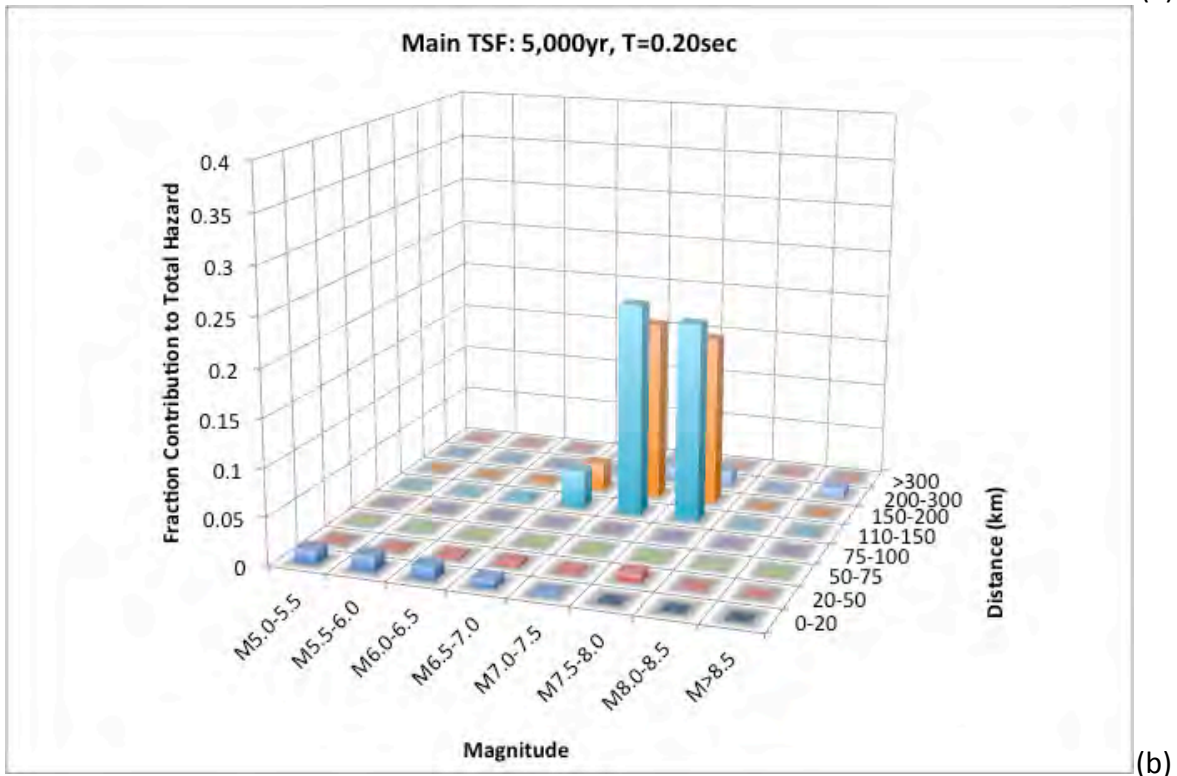
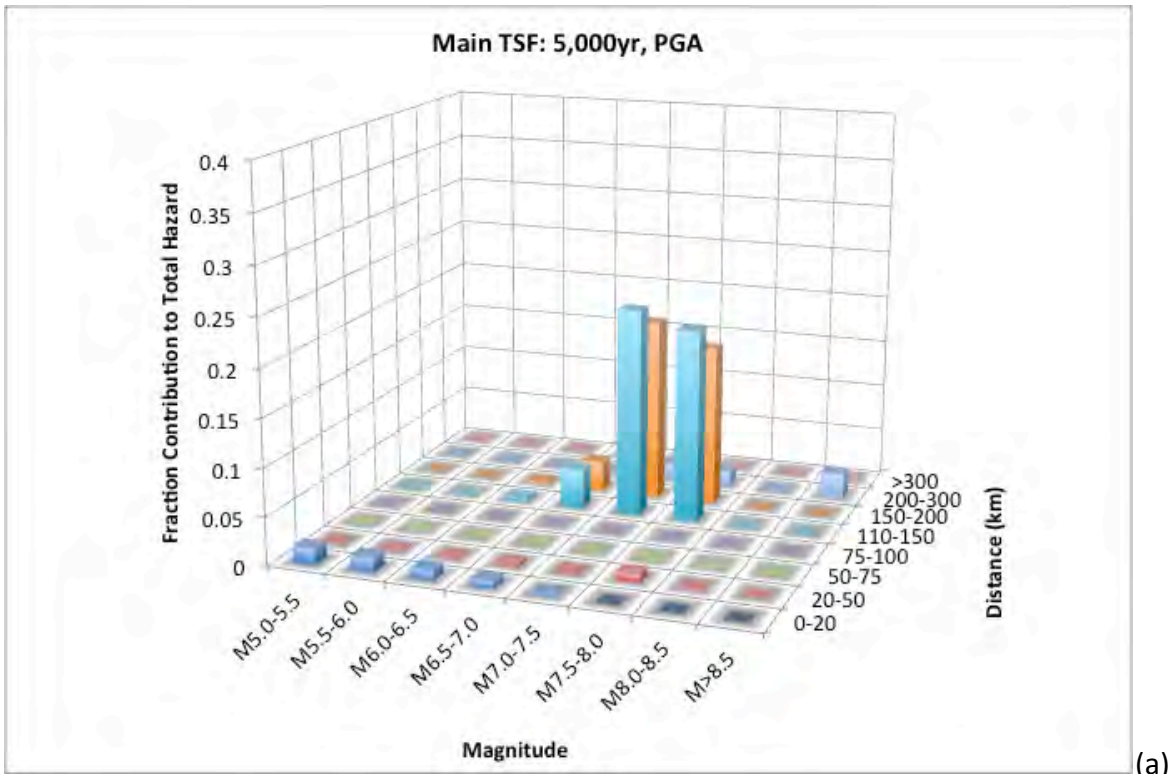


Figure 47. Deaggregation binned contribution as a function of magnitude and distance for the Main TSF site location, 5,000-yr hazard level and PGA (0.01 sec) (a) and 0.2 sec (b).

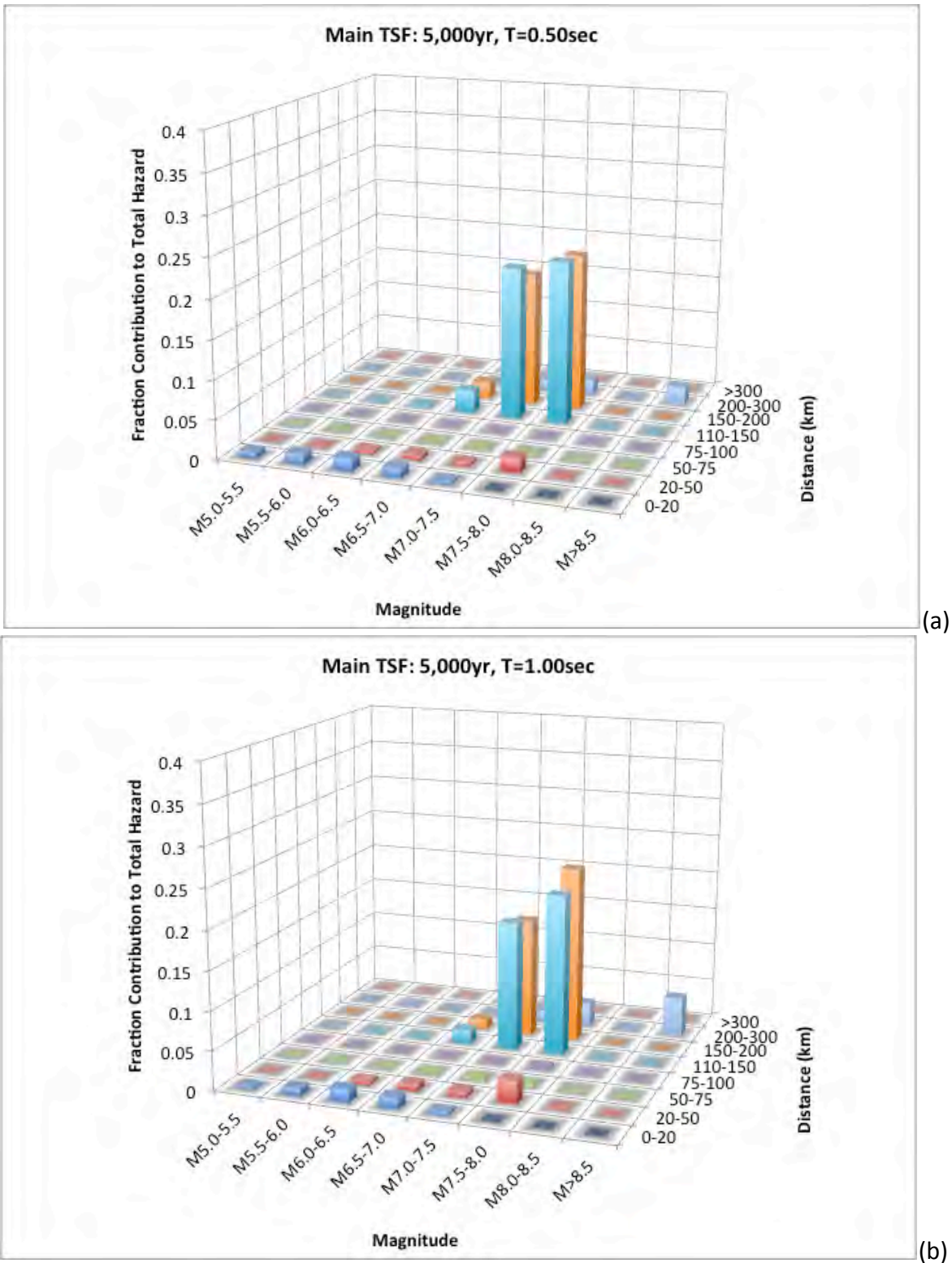


Figure 48. Deaggregation binned contribution as a function of magnitude and distance for the Main TSF site location, 5,000-yr hazard level and 0.5 sec (a) and 1 sec (b).

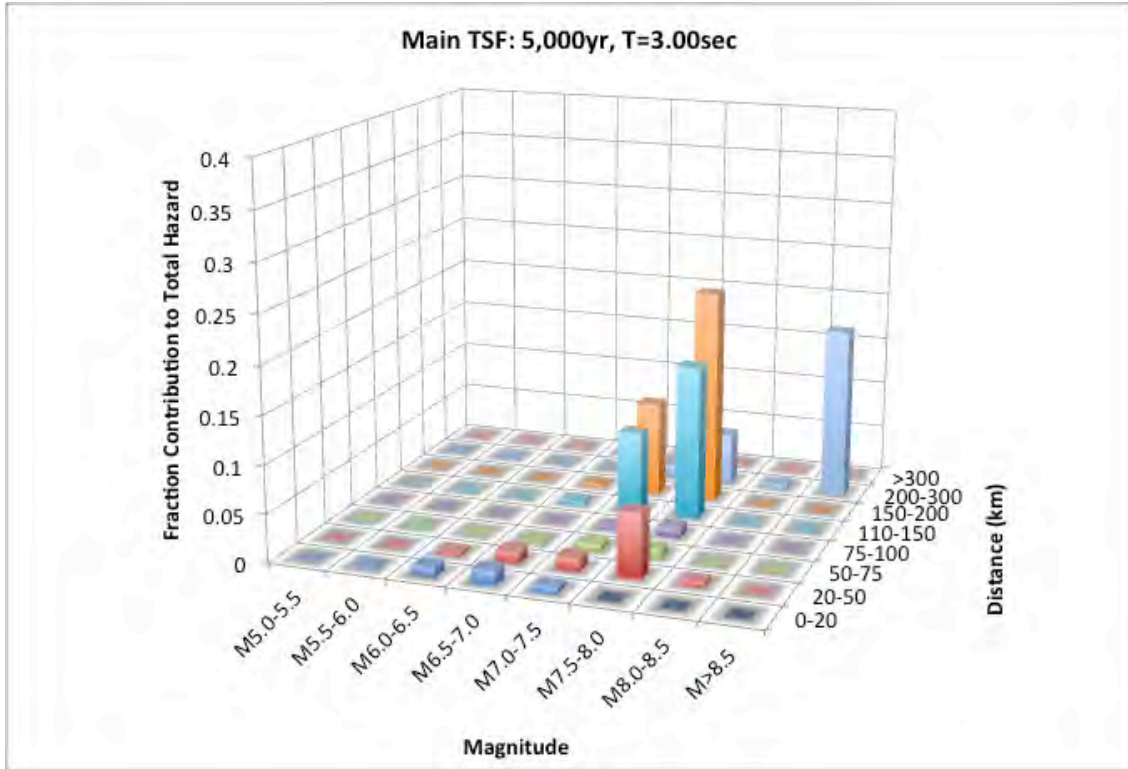


Figure 49. Deaggregation binned contribution as a function of magnitude and distance for the Main TSF site location, 5,000-yr hazard level and 3 sec.

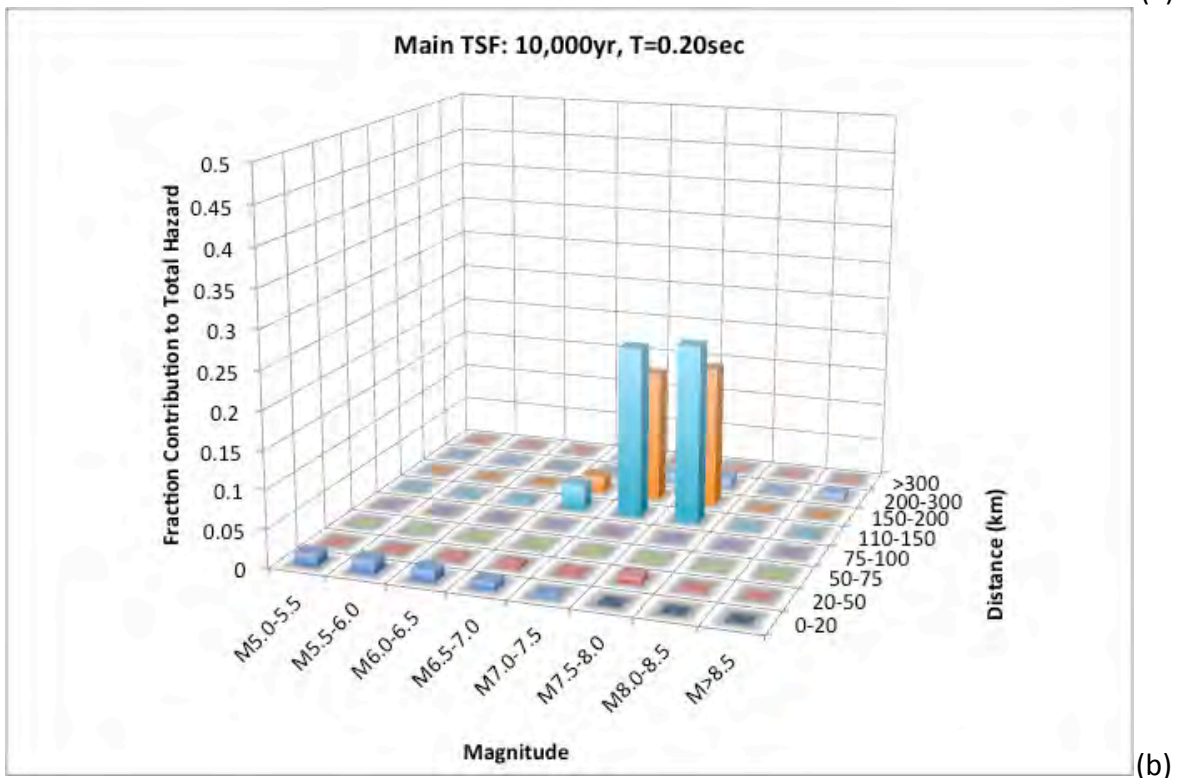
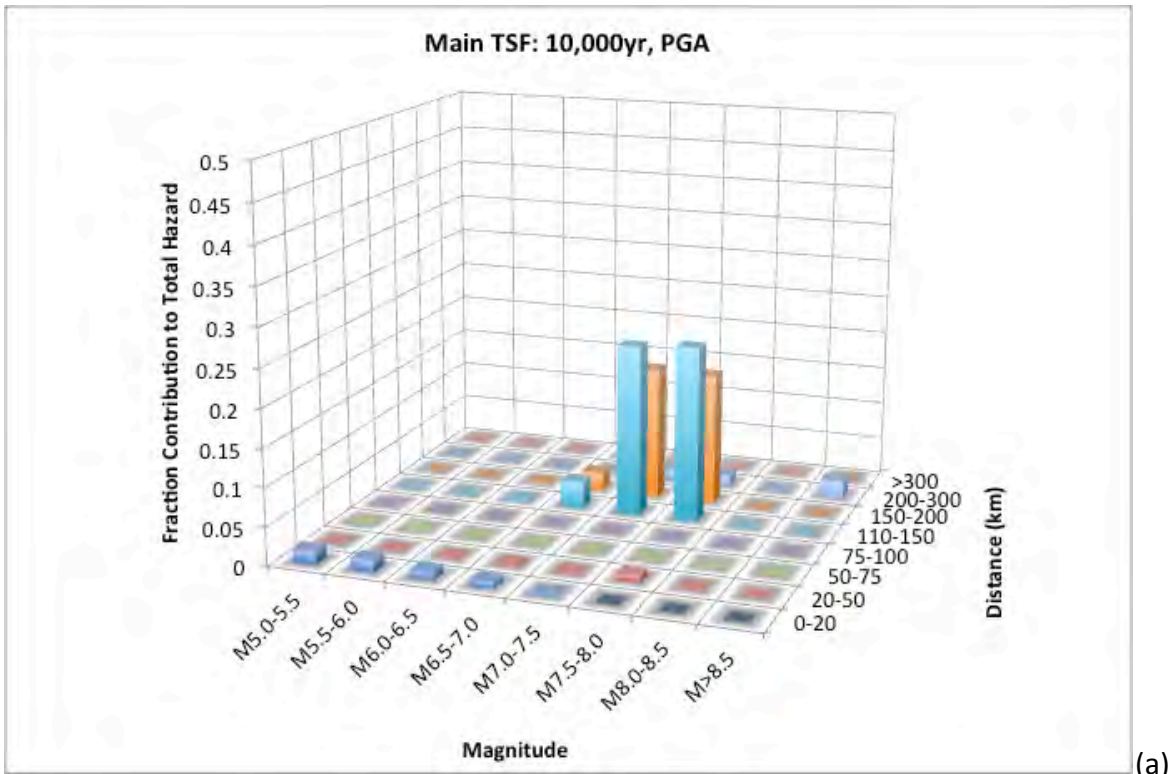
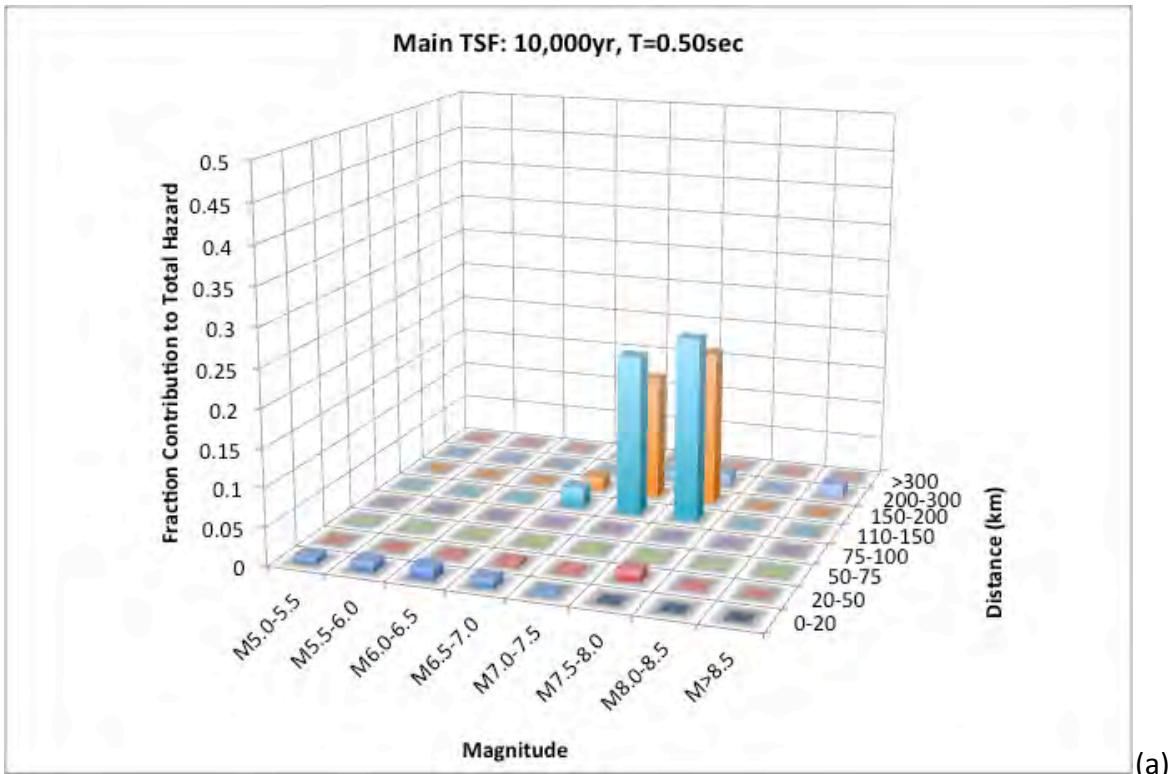
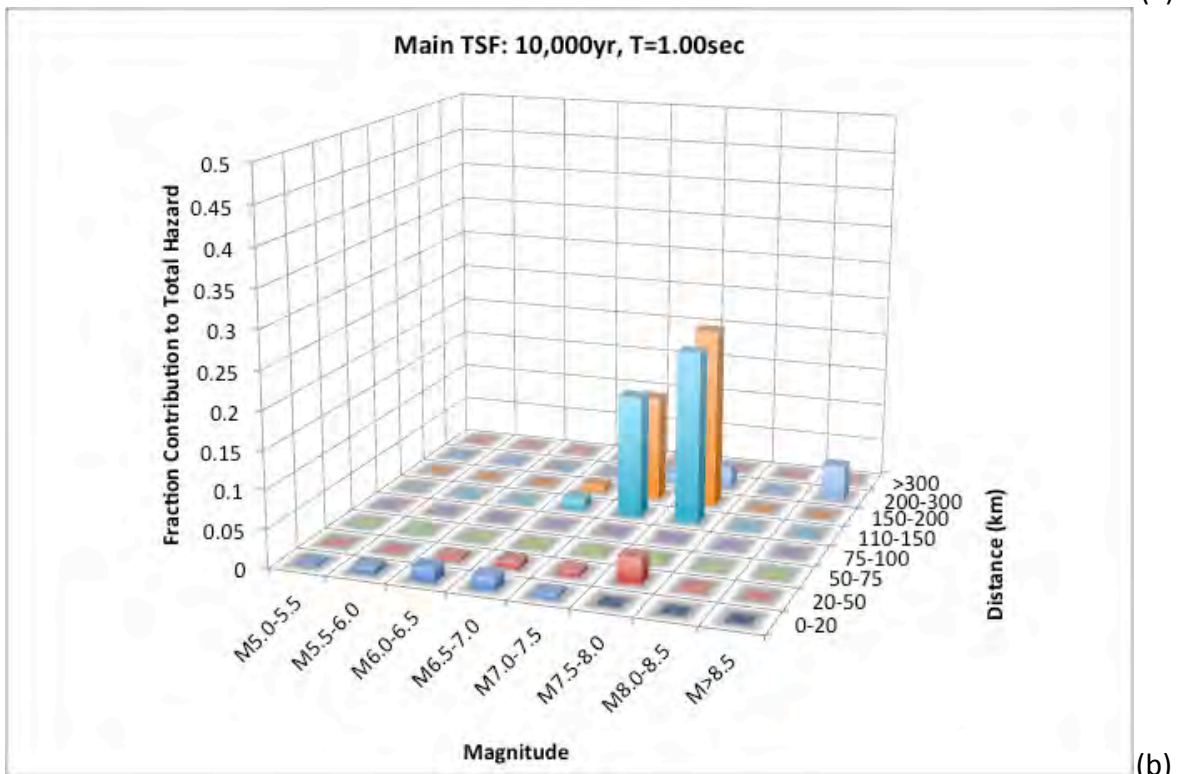


Figure 50. Deaggregation binned contribution as a function of magnitude and distance for the Main TSF site location, 10,000-yr hazard level and PGA (0.01 sec) (a) and 0.2 sec (b).



(a)



(b)

Figure 51. Deaggregation binned contribution as a function of magnitude and distance for the Main TSF site location, 10,000-yr hazard level and 0.5 sec (a) and 1 sec (b).

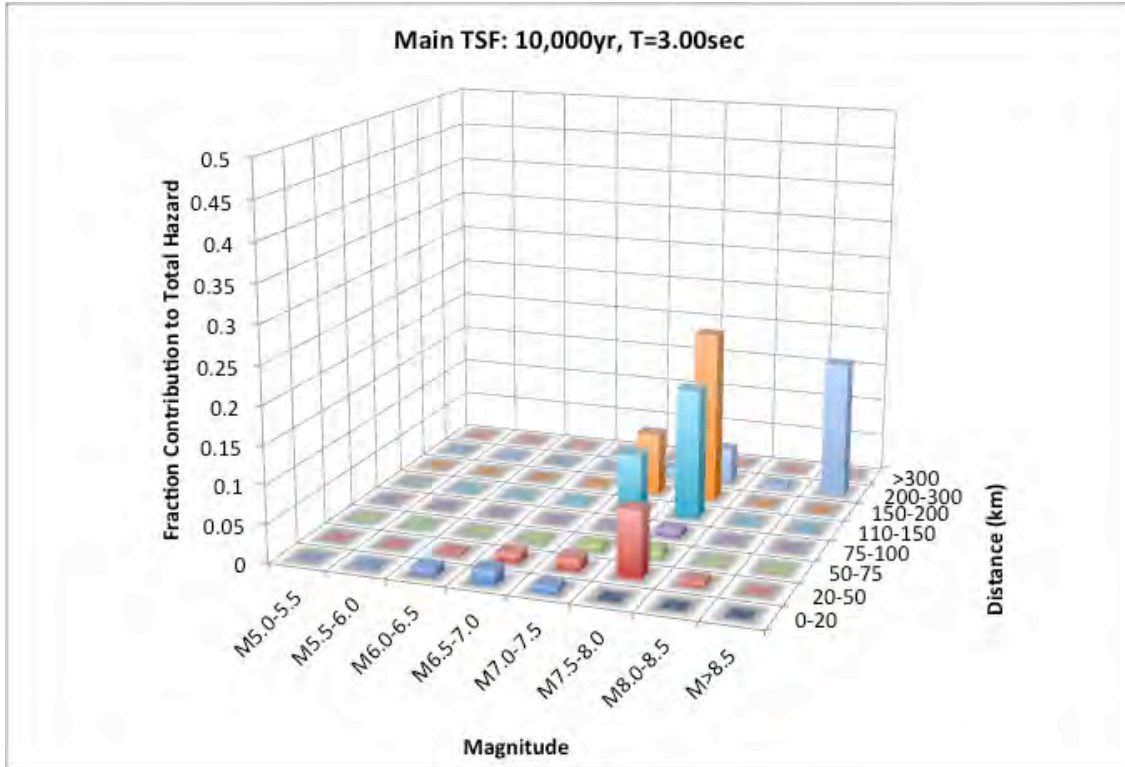


Figure 52. Deaggregation binned contribution as a function of magnitude and distance for the Main TSF site location, 10,000-yr hazard level and 3 sec.

4.3 PSHA Results – Pyritic TSF Site Location

As noted earlier and shown in Figure 1, the Pyritic TSF site location is located east of the Main TSF site location. This site is located slightly closer to the controlling slab seismic source and as such the UHS ground motions would be expected to be slightly larger (see Section 4.5 for the comparison). The overall contribution from the individual sources and the fractile distribution are expected to be similar to the results observed for the Main TSF site location.

The UHS based on the mean hazard curves are listed in Table 11 and plotted in Figure 53 for the Pyritic site location. The fractile UHS for the 5,000 and 10,000-yr return period hazard levels are listed in Tables 12 and 13 and plotted in Figures 54 and 55.

Table 11. UHS for the Pyritic TSF site location for $V_{s30} = 760$ m/sec.

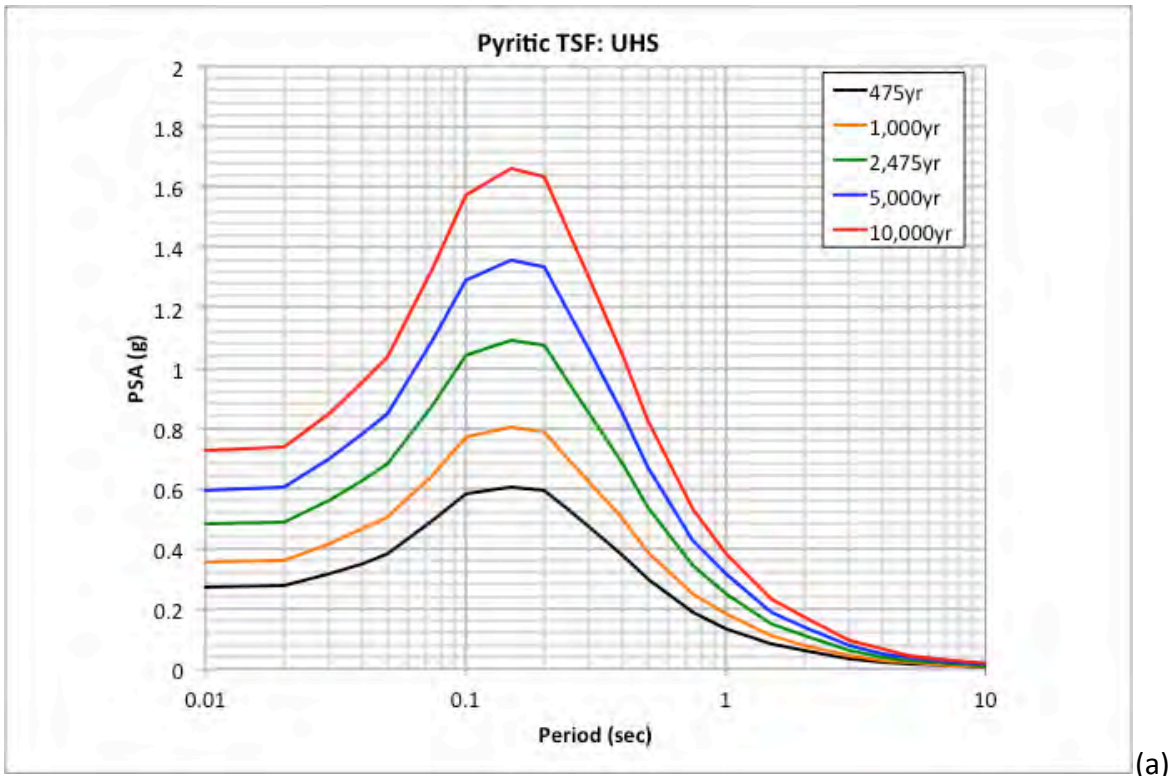
Period (sec)	475-yr UHS (g)	1,000-yr UHS (g)	2,475-yr UHS (g)	5,000-yr UHS (g)	10,000-yr UHS (g)
0.010	0.2729	0.3555	0.4828	0.5949	0.7273
0.020	0.2751	0.3584	0.4878	0.6011	0.7360
0.030	0.3171	0.4132	0.5605	0.6954	0.8477
0.040	0.3511	0.4627	0.6252	0.7795	0.9507
0.050	0.3800	0.5043	0.6805	0.8467	1.0358
0.075	0.4925	0.6440	0.8753	1.0892	1.3323
0.100	0.5813	0.7675	1.0394	1.2913	1.5760
0.150	0.6054	0.8009	1.0895	1.3578	1.6607
0.200	0.5942	0.7876	1.0722	1.3368	1.6357
0.250	0.5245	0.6920	0.9450	1.1792	1.4470
0.300	0.4708	0.6202	0.8474	1.0580	1.2972
0.400	0.3756	0.5013	0.6794	0.8479	1.0396
0.500	0.2974	0.3900	0.5363	0.6688	0.8228
0.750	0.1878	0.2496	0.3420	0.4283	0.5300
1.000	0.1349	0.1814	0.2496	0.3137	0.3838
1.500	0.0821	0.1090	0.1490	0.1898	0.2344
2.000	0.0583	0.0786	0.1084	0.1357	0.1693
3.000	0.0316	0.0429	0.0599	0.0759	0.0939
4.000	0.0218	0.0287	0.0400	0.0515	0.0636
5.000	0.0154	0.0210	0.0287	0.0366	0.0466
7.500	0.0082	0.0112	0.0160	0.0209	0.0269
10.000	0.0056	0.0077	0.0111	0.0145	0.0187

Table 12. Fractile UHS for the Pyritic TSF site location for $V_{S30} = 760$ m/sec at the 5,000-yr return period level.

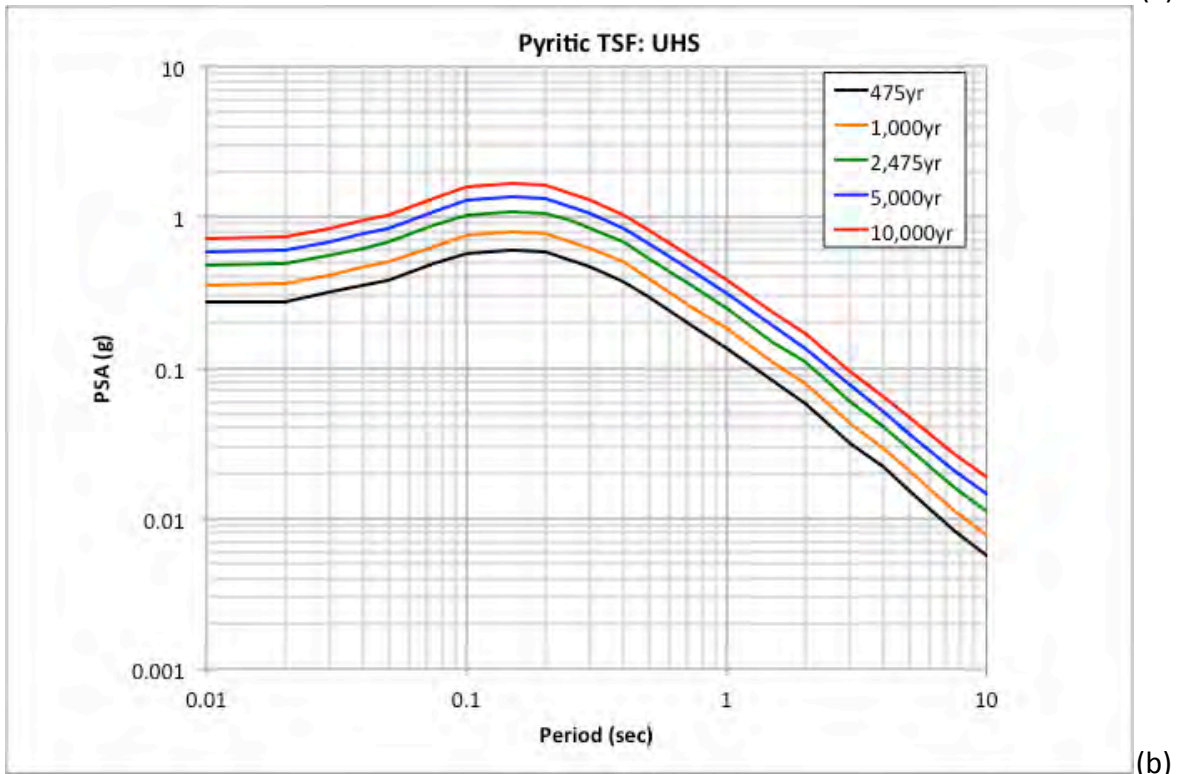
Period (sec)	Mean 5,000-yr UHS (g)	5th 5,000-yr UHS (g)	16th 5,000-yr UHS (g)	50th 5,000-yr UHS (g)	84th 5,000-yr UHS (g)	95th 5,000-yr UHS (g)
0.010	0.5949	0.5325	0.5521	0.5894	0.6332	0.6708
0.020	0.6011	0.5350	0.5545	0.5924	0.6410	0.6933
0.030	0.6954	0.6174	0.6404	0.6857	0.7430	0.7984
0.040	0.7795	0.6865	0.7126	0.7629	0.8300	0.9325
0.050	0.8467	0.7447	0.7711	0.8219	0.9034	1.0490
0.075	1.0892	0.9633	0.9989	1.0640	1.1620	1.3170
0.100	1.2913	1.1470	1.1890	1.2690	1.3760	1.5190
0.150	1.3578	1.1850	1.2300	1.3150	1.4540	1.6950
0.200	1.3368	1.1620	1.2070	1.2960	1.4340	1.6630
0.250	1.1792	1.0150	1.0540	1.1320	1.2660	1.5160
0.300	1.0580	0.9080	0.9448	1.0170	1.1350	1.3520
0.400	0.8479	0.7279	0.7581	0.8141	0.9094	1.0840
0.500	0.6688	0.5609	0.5834	0.6286	0.7149	0.9014
0.750	0.4283	0.3486	0.3630	0.3915	0.4517	0.6080
1.000	0.3137	0.2538	0.2654	0.2879	0.3300	0.4418
1.500	0.1898	0.1461	0.1534	0.1674	0.1973	0.2830
2.000	0.1357	0.1020	0.1070	0.1162	0.1355	0.2159
3.000	0.0759	0.0590	0.0624	0.0689	0.0815	0.1071
4.000	0.0515	0.0405	0.0436	0.0491	0.0574	0.0653
5.000	0.0366	0.0285	0.0307	0.0351	0.0421	0.0469
7.500	0.0209	0.0143	0.0158	0.0200	0.0252	0.0291
10.000	0.0145	0.0097	0.0107	0.0137	0.0174	0.0201

Table 13. Fractile UHS for the Pyritic TSF site location for $V_{S30} = 760$ m/sec at the 10,000-yr return period level.

Period (sec)	Mean 10,000-yr UHS (g)	5th 10,000-yr UHS (g)	16th 10,000-yr UHS (g)	50th 10,000-yr UHS (g)	84th 10,000-yr UHS (g)	95th 10,000-yr UHS (g)
0.010	0.7273	0.6420	0.6677	0.7187	0.7762	0.8240
0.020	0.7360	0.6450	0.6705	0.7225	0.7859	0.8537
0.030	0.8477	0.7515	0.7786	0.8336	0.9056	0.9868
0.040	0.9507	0.8309	0.8616	0.9240	1.0170	1.1510
0.050	1.0358	0.8973	0.9319	1.0010	1.1030	1.2960
0.075	1.3323	1.1650	1.2090	1.2940	1.4250	1.6380
0.100	1.5760	1.3880	1.4400	1.5410	1.6830	1.8870
0.150	1.6607	1.4350	1.4910	1.5970	1.7770	2.1110
0.200	1.6357	1.4080	1.4650	1.5760	1.7560	2.0680
0.250	1.4470	1.2300	1.2800	1.3790	1.5520	1.8740
0.300	1.2972	1.1010	1.1460	1.2400	1.3930	1.6710
0.400	1.0396	0.8807	0.9178	0.9941	1.1120	1.3330
0.500	0.8228	0.6817	0.7118	0.7709	0.8766	1.1070
0.750	0.5300	0.4239	0.4434	0.4823	0.5554	0.7514
1.000	0.3838	0.3102	0.3237	0.3500	0.4042	0.5442
1.500	0.2344	0.1797	0.1896	0.2074	0.2416	0.3456
2.000	0.1693	0.1229	0.1295	0.1416	0.1673	0.2649
3.000	0.0939	0.0724	0.0771	0.0849	0.1009	0.1298
4.000	0.0636	0.0507	0.0543	0.0607	0.0717	0.0808
5.000	0.0466	0.0350	0.0382	0.0443	0.0538	0.0597
7.500	0.0269	0.0178	0.0198	0.0250	0.0330	0.0391
10.000	0.0187	0.0118	0.0131	0.0176	0.0229	0.0264

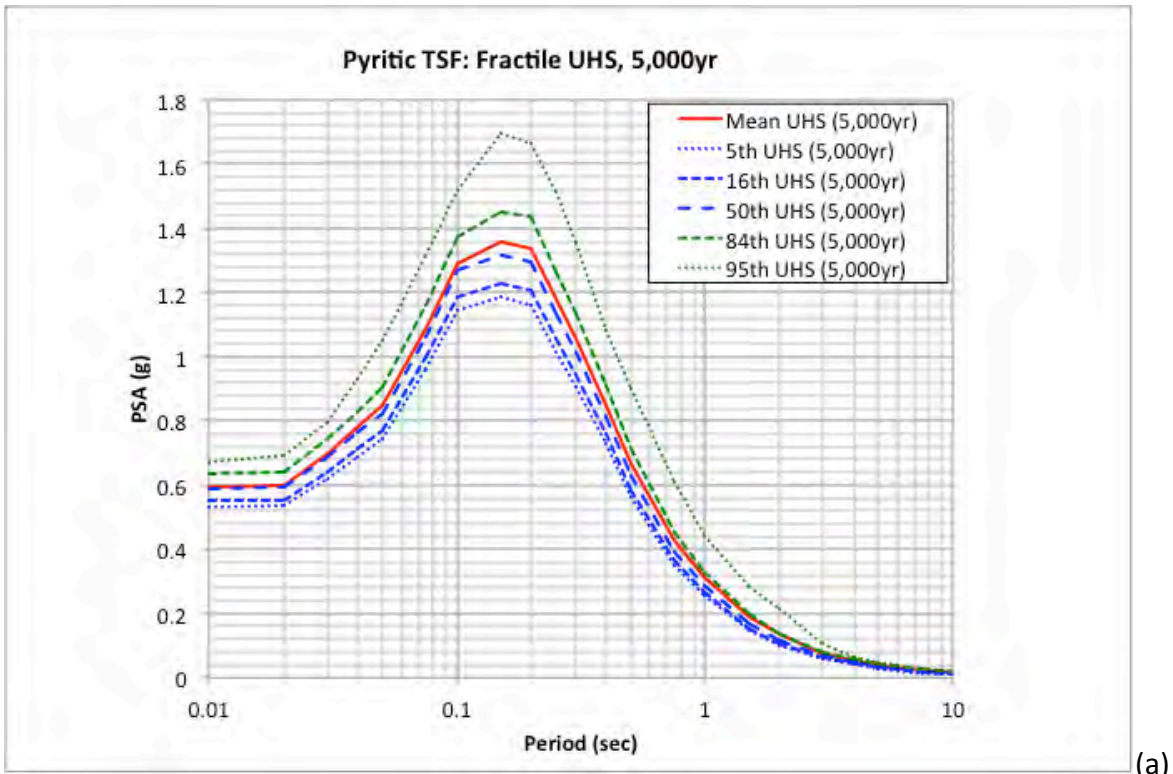


(a)

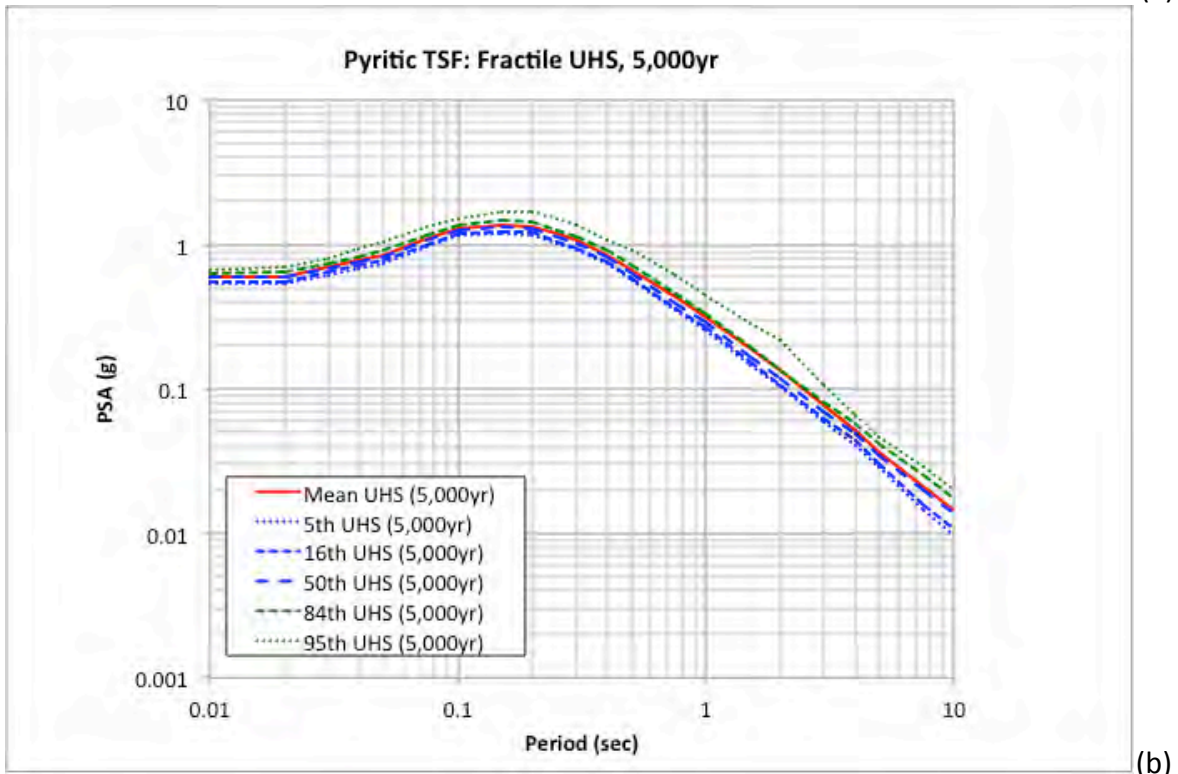


(b)

Figure 53. UHS spectra for the Pyritic TSF site location ($V_{S30} = 760$ m/sec) plot log-linear (a) and log-log (b).

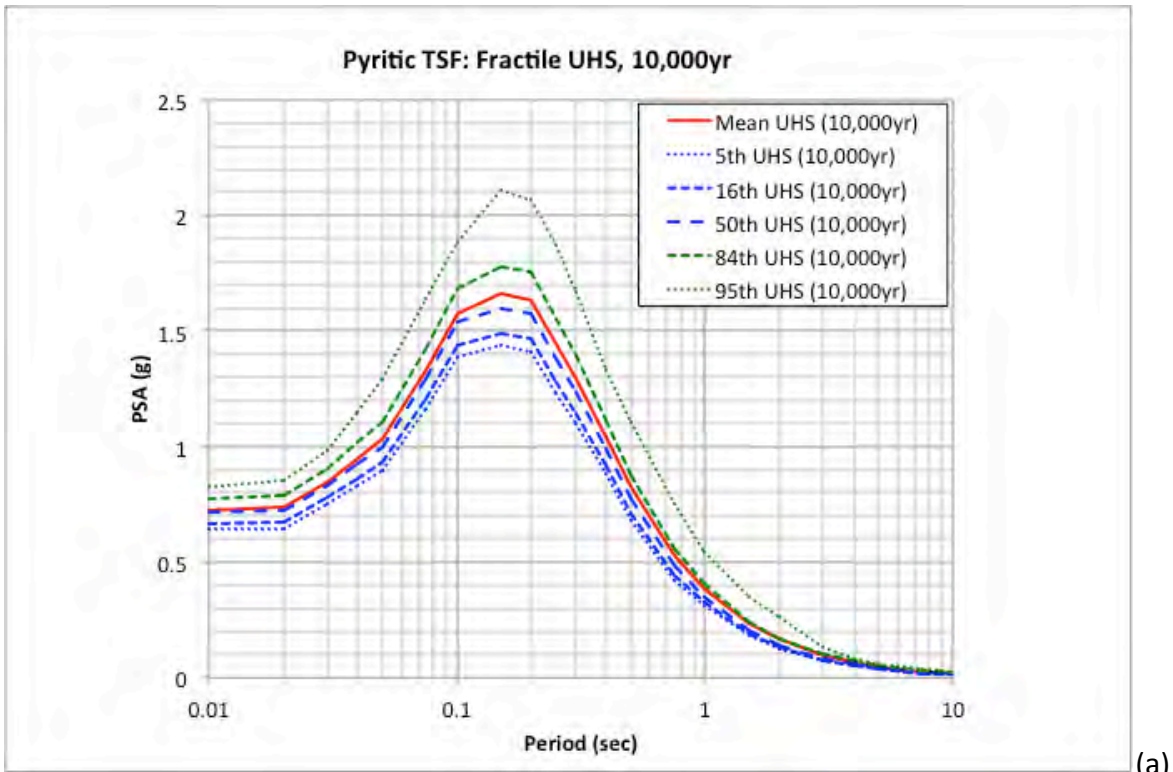


(a)

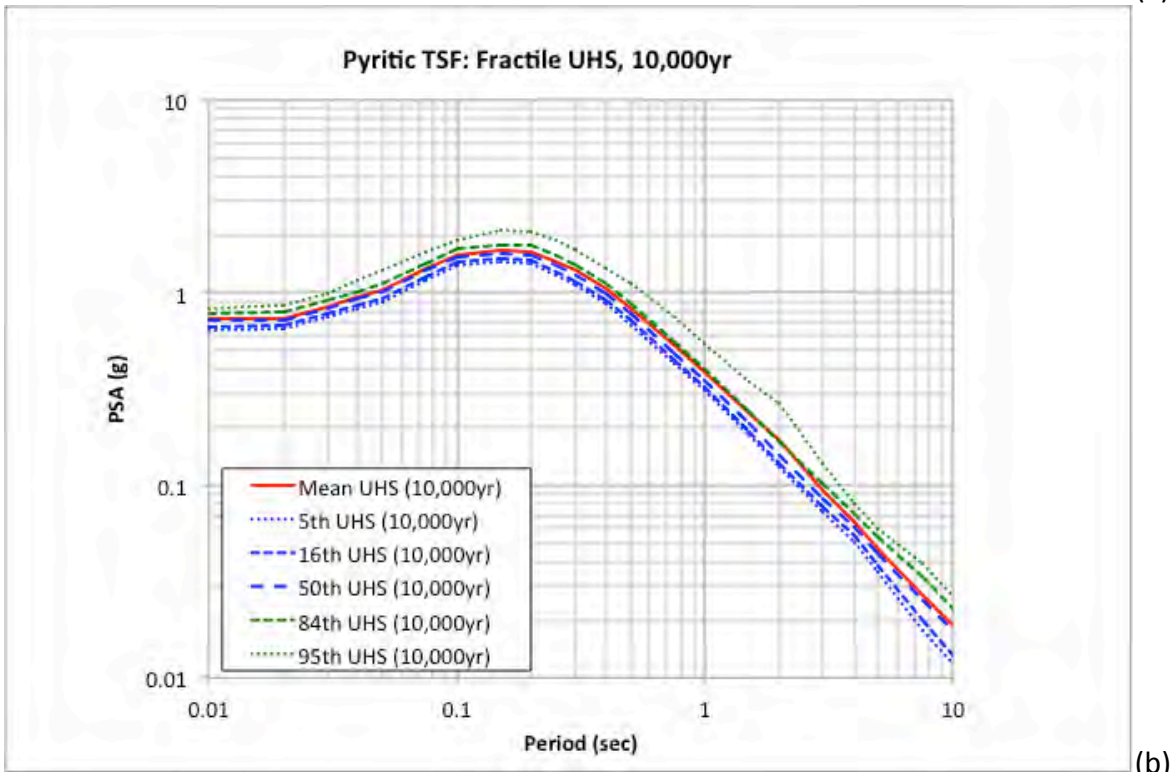


(b)

Figure 54. Fractile UHS for the Pyritic TSF site location for 5,000-yr return period hazard level plotted log-linear (a) and log-log (b).



(a)



(b)

Figure 55. Fractile UHS for the Pyritic TSF site location for 10,000-yr return period hazard level plotted log-linear (a) and log-log (b).

4.4 PSHA Results – South TSF Site Location

As noted earlier and shown in Figure 1, the South TSF site is located southwest of the Main TSF site location. This site is located slightly closer to the controlling slab seismic source and as such the UHS ground motions would be expected to be slightly larger or similar (see Section 4.5 for the comparison). The overall contribution from the individual sources and the fractile distribution would be expected to be similar to the results observed for the Main TSF site location.

The UHS based on the mean hazard curves are listed in Table 14 and plotted in Figure 56 for the South site location. The fractile UHS for the 5,000 and 10,000-yr return period hazard levels are listed in Tables 15 and 16 and plotted in Figures 57 and 58.

Table 14. UHS for the South TSF site location for $V_{S30} = 760$ m/sec.

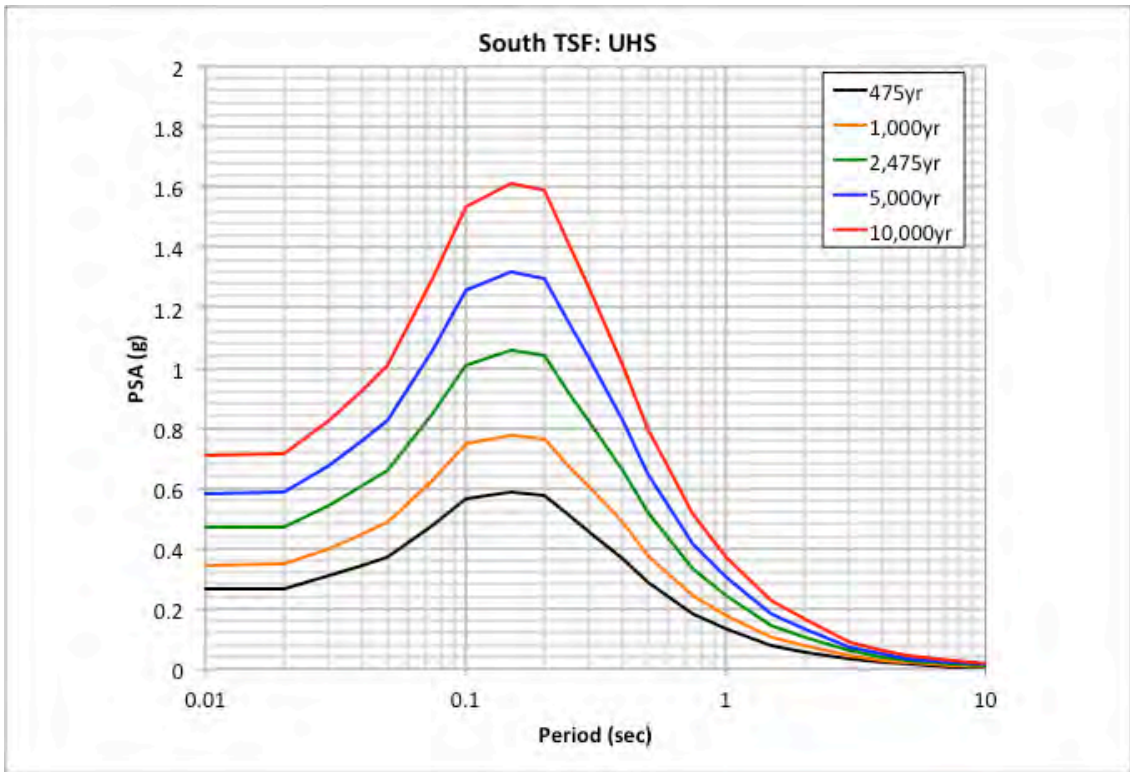
Period (sec)	475-yr UHS (g)	1,000-yr UHS (g)	2,475-yr UHS (g)	5,000-yr UHS (g)	10,000-yr UHS (g)
0.010	0.2646	0.3456	0.4684	0.5790	0.7072
0.020	0.2667	0.3484	0.4731	0.5849	0.7153
0.030	0.3082	0.4010	0.5452	0.6756	0.8254
0.040	0.3409	0.4483	0.6073	0.7585	0.9243
0.050	0.3686	0.4888	0.6604	0.8233	1.0089
0.075	0.4762	0.6245	0.8500	1.0590	1.2963
0.100	0.5639	0.7452	1.0103	1.2561	1.5343
0.150	0.5866	0.7773	1.0577	1.3188	1.6145
0.200	0.5757	0.7643	1.0409	1.2985	1.5904
0.250	0.5088	0.6699	0.9160	1.1443	1.4051
0.300	0.4551	0.6011	0.8223	1.0277	1.2610
0.400	0.3640	0.4848	0.6584	0.8231	1.0108
0.500	0.2873	0.3777	0.5205	0.6480	0.7985
0.750	0.1812	0.2417	0.3317	0.4145	0.5142
1.000	0.1307	0.1753	0.2418	0.3045	0.3717
1.500	0.0797	0.1060	0.1443	0.1833	0.2269
2.000	0.0566	0.0764	0.1054	0.1315	0.1635
3.000	0.0306	0.0415	0.0581	0.0733	0.0904
4.000	0.0213	0.0278	0.0386	0.0497	0.0611
5.000	0.0150	0.0204	0.0277	0.0351	0.0444
7.500	0.0080	0.0109	0.0155	0.0202	0.0256
10.000	0.0055	0.0075	0.0108	0.0140	0.0180

Table 15. Fractile UHS for the South TSF site location for $V_{S30} = 760$ m/sec at the 5,000-yr return period level.

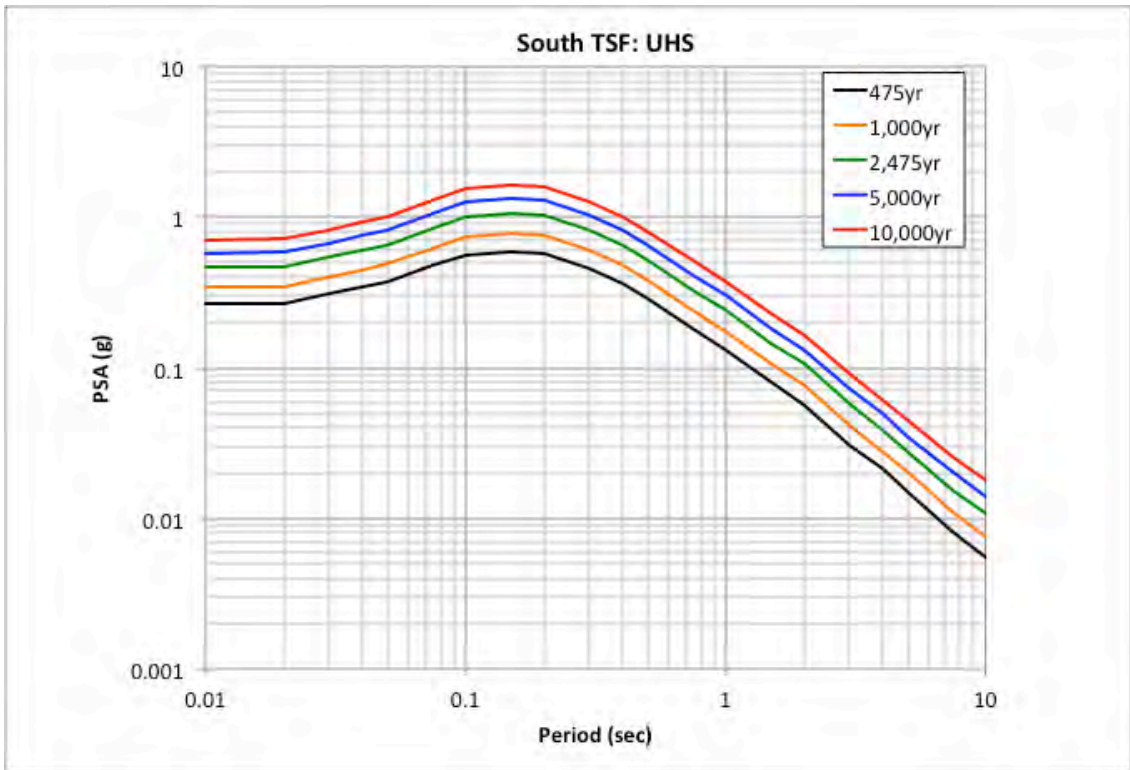
Period (sec)	Mean 5,000-yr UHS (g)	5th 5,000-yr UHS (g)	16th 5,000-yr UHS (g)	50th 5,000-yr UHS (g)	84th 5,000-yr UHS (g)	95th 5,000-yr UHS (g)
0.010	0.5790	0.5192	0.5383	0.5743	0.6156	0.6496
0.020	0.5849	0.5217	0.5405	0.5773	0.6231	0.6700
0.030	0.6756	0.6012	0.6233	0.6672	0.7213	0.7730
0.040	0.7585	0.6679	0.6930	0.7433	0.8075	0.8984
0.050	0.8233	0.7237	0.7516	0.8010	0.8785	1.0130
0.075	1.0590	0.9365	0.9713	1.0360	1.1290	1.2690
0.100	1.2561	1.1160	1.1570	1.2360	1.3380	1.4650
0.150	1.3188	1.1520	1.1950	1.2800	1.4120	1.6350
0.200	1.2985	1.1290	1.1740	1.2620	1.3930	1.6040
0.250	1.1443	0.9862	1.0250	1.1010	1.2290	1.4610
0.300	1.0277	0.8827	0.9181	0.9892	1.1030	1.3040
0.400	0.8231	0.7060	0.7361	0.7917	0.8826	1.0480
0.500	0.6480	0.5448	0.5664	0.6099	0.6922	0.8706
0.750	0.4145	0.3380	0.3519	0.3792	0.4368	0.5887
1.000	0.3045	0.2457	0.2567	0.2784	0.3200	0.4277
1.500	0.1833	0.1412	0.1482	0.1616	0.1900	0.2743
2.000	0.1315	0.0987	0.1037	0.1125	0.1308	0.2101
3.000	0.0733	0.0569	0.0602	0.0663	0.0787	0.1044
4.000	0.0497	0.0388	0.0417	0.0470	0.0554	0.0633
5.000	0.0351	0.0274	0.0295	0.0335	0.0403	0.0452
7.500	0.0202	0.0137	0.0152	0.0192	0.0242	0.0277
10.000	0.0140	0.0093	0.0103	0.0131	0.0169	0.0194

Table 16. Fractile UHS for the South TSF site location for $V_{S30} = 760$ m/sec at the 10,000-yr return period level.

Period (sec)	Mean 10,000-yr UHS (g)	5th 10,000-yr UHS (g)	16th 10,000-yr UHS (g)	50th 10,000-yr UHS (g)	84th 10,000-yr UHS (g)	95th 10,000-yr UHS (g)
0.010	0.7072	0.6255	0.6504	0.6998	0.7562	0.7992
0.020	0.7153	0.6284	0.6532	0.7036	0.7654	0.8262
0.030	0.8254	0.7313	0.7596	0.8132	0.8808	0.9533
0.040	0.9243	0.8102	0.8398	0.9006	0.9909	1.1120
0.050	1.0089	0.8744	0.9076	0.9744	1.0750	1.2500
0.075	1.2963	1.1340	1.1770	1.2620	1.3860	1.5820
0.100	1.5343	1.3520	1.4030	1.5030	1.6380	1.8210
0.150	1.6145	1.3970	1.4510	1.5560	1.7280	2.0410
0.200	1.5904	1.3700	1.4260	1.5360	1.7080	2.0000
0.250	1.4051	1.1960	1.2460	1.3430	1.5100	1.8090
0.300	1.2610	1.0720	1.1160	1.2060	1.3530	1.6160
0.400	1.0108	0.8562	0.8920	0.9656	1.0820	1.2880
0.500	0.7985	0.6611	0.6900	0.7495	0.8500	1.0720
0.750	0.5142	0.4103	0.4289	0.4662	0.5387	0.7259
1.000	0.3717	0.3010	0.3138	0.3391	0.3912	0.5284
1.500	0.2269	0.1731	0.1825	0.2007	0.2333	0.3358
2.000	0.1635	0.1187	0.1249	0.1365	0.1609	0.2573
3.000	0.0904	0.0695	0.0740	0.0815	0.0969	0.1261
4.000	0.0611	0.0485	0.0521	0.0581	0.0687	0.0782
5.000	0.0444	0.0335	0.0364	0.0421	0.0515	0.0569
7.500	0.0256	0.0170	0.0189	0.0238	0.0313	0.0366
10.000	0.0180	0.0114	0.0126	0.0168	0.0218	0.0251

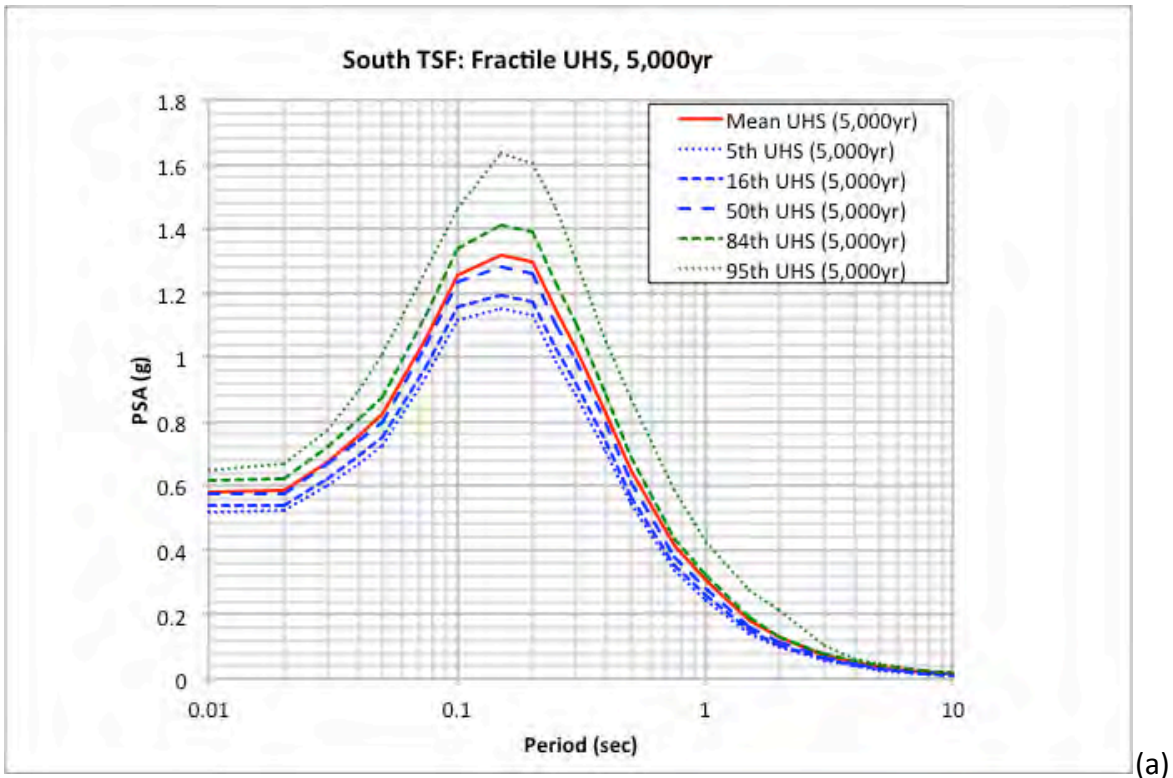


(a)

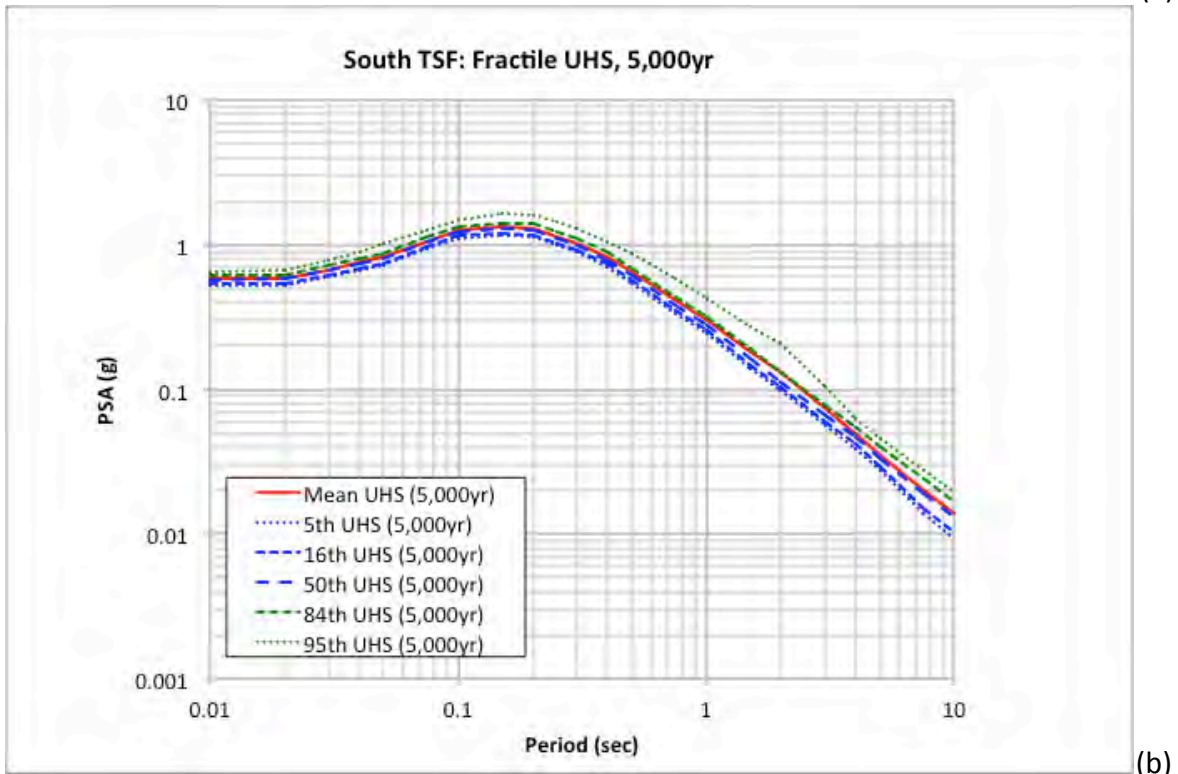


(b)

Figure 56. UHS spectra for the South TSF site location ($V_{S30} = 760$ m/sec) plot log-linear (a) and log-log (b).

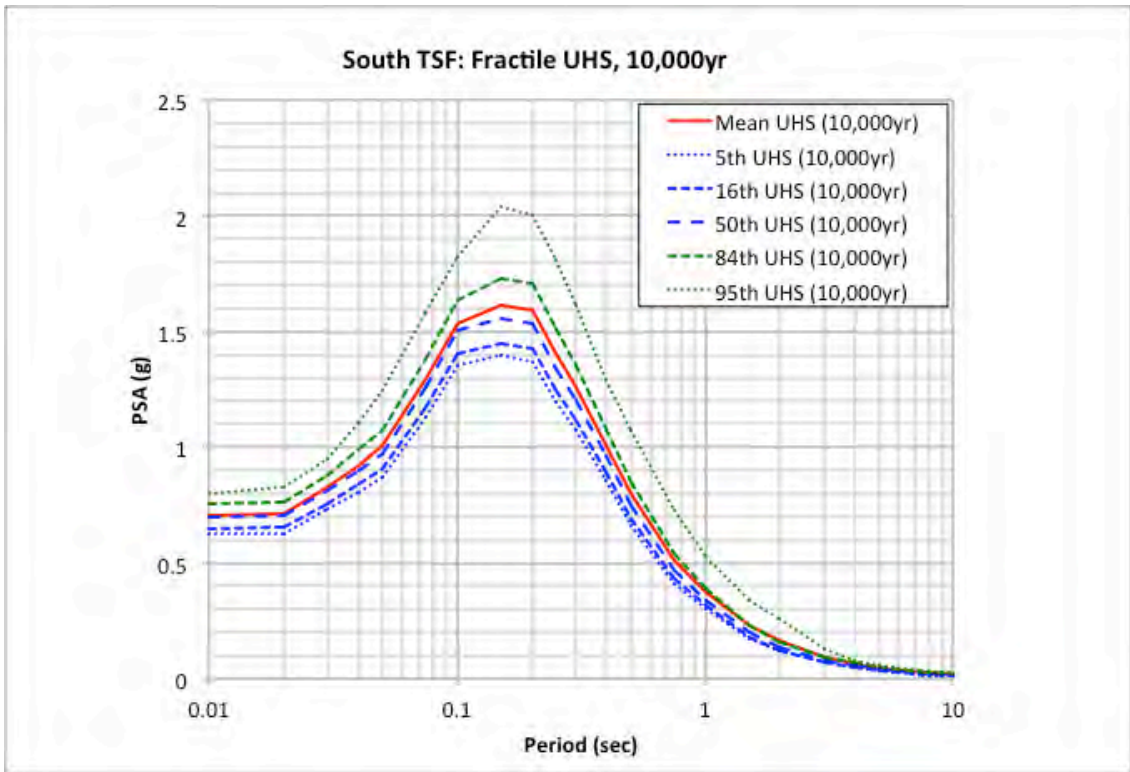


(a)

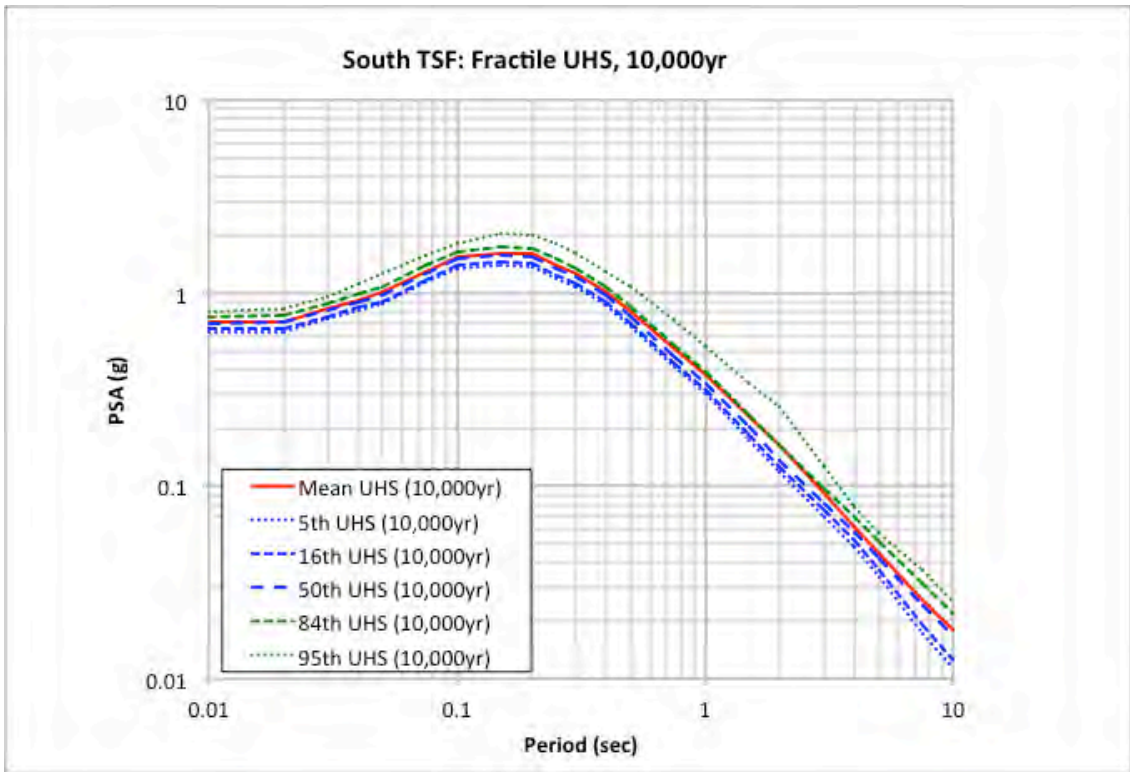


(b)

Figure 57. Fractile UHS for the South TSF site location for 5,000-yr return period hazard level plotted log-linear (a) and log-log (b).



(a)

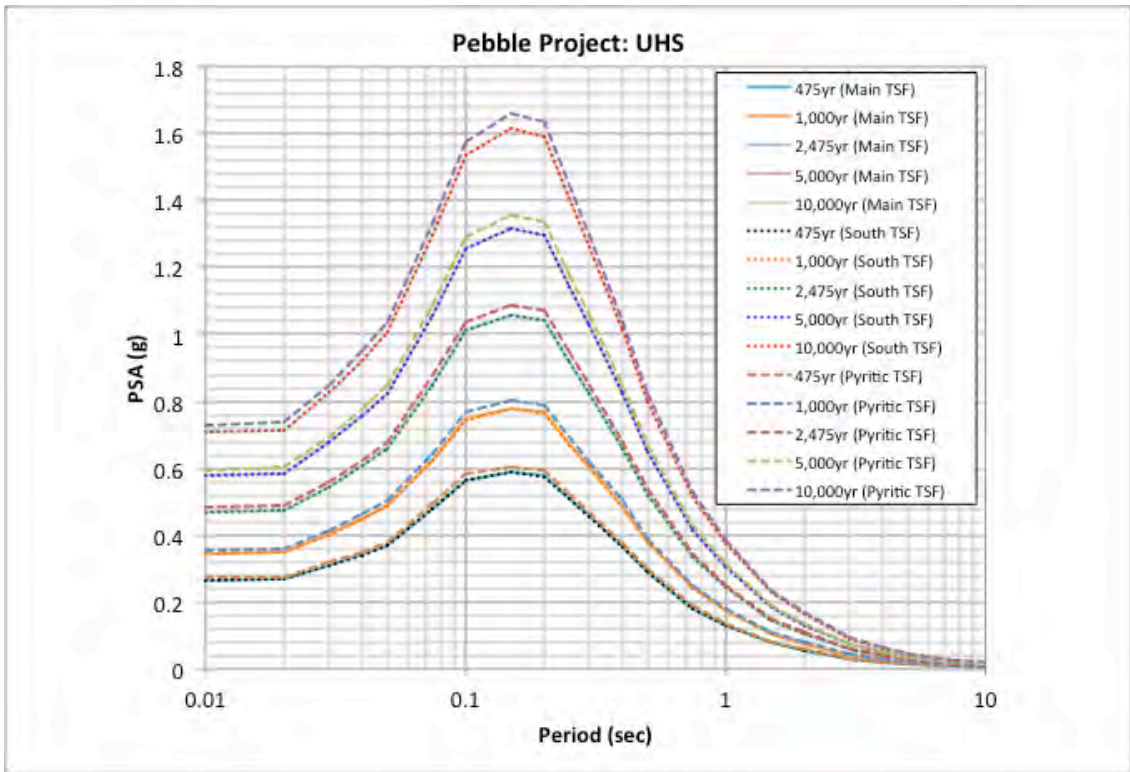


(b)

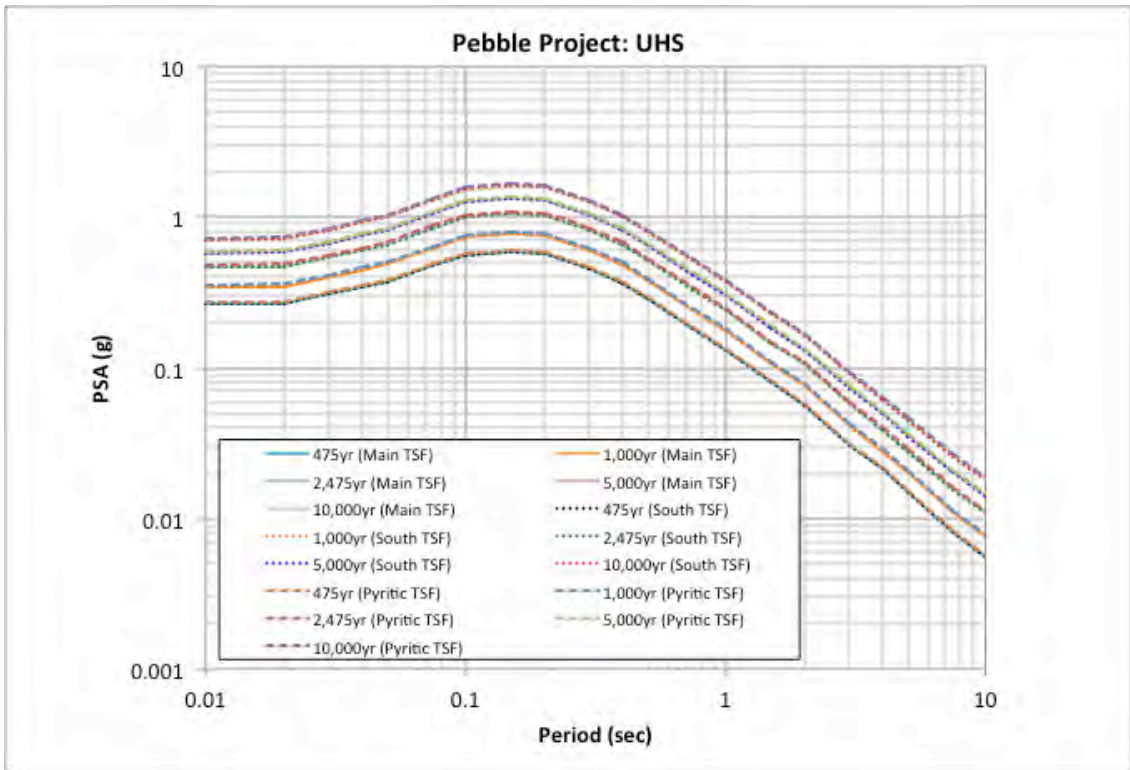
Figure 58. Fractile UHS for the South TSF site location for 10,000-yr return period hazard level plotted log-linear (a) and log-log (b).

4.5 PSHA Results Summary

Given the close proximity of the three TSF site locations, the calculated ground motions at the three sites are expected to be well within the uncertainty of any PSHA calculation. Individual results are given in Table 7 (Main TSF), Table 11 (Pyritic TSF) and Table 14 (South TSF) for the suite of five return period levels. A comparison of these spectra is plotted in Figure 59. The spectral ratio of the UHS from the three site locations relative to the ground motions from the Main TSF location is shown in Figure 60. Given the slightly closer location of the Pyritic TSF site to the controlling seismic sources, these ground motions are larger than the ground motions for the Main TSF site by approximately 3% or less. Thus, the results from the Pyritic TSF site location could be taken as the envelope ground motions for the three sites if the use of the three individual site-specific ground motions is not necessary for future analyses.



(a)



(b)

Figure 59. Comparison of mean UHS for the three site locations plotted log-linear (a) and log-log (b).

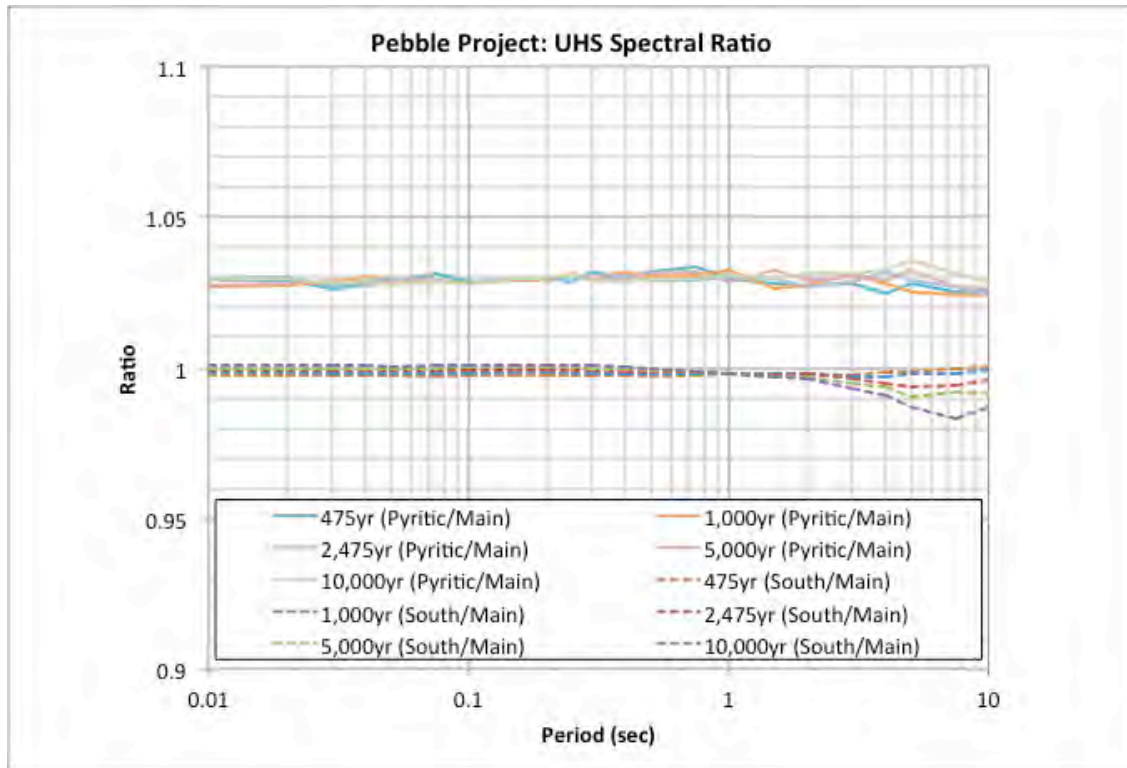
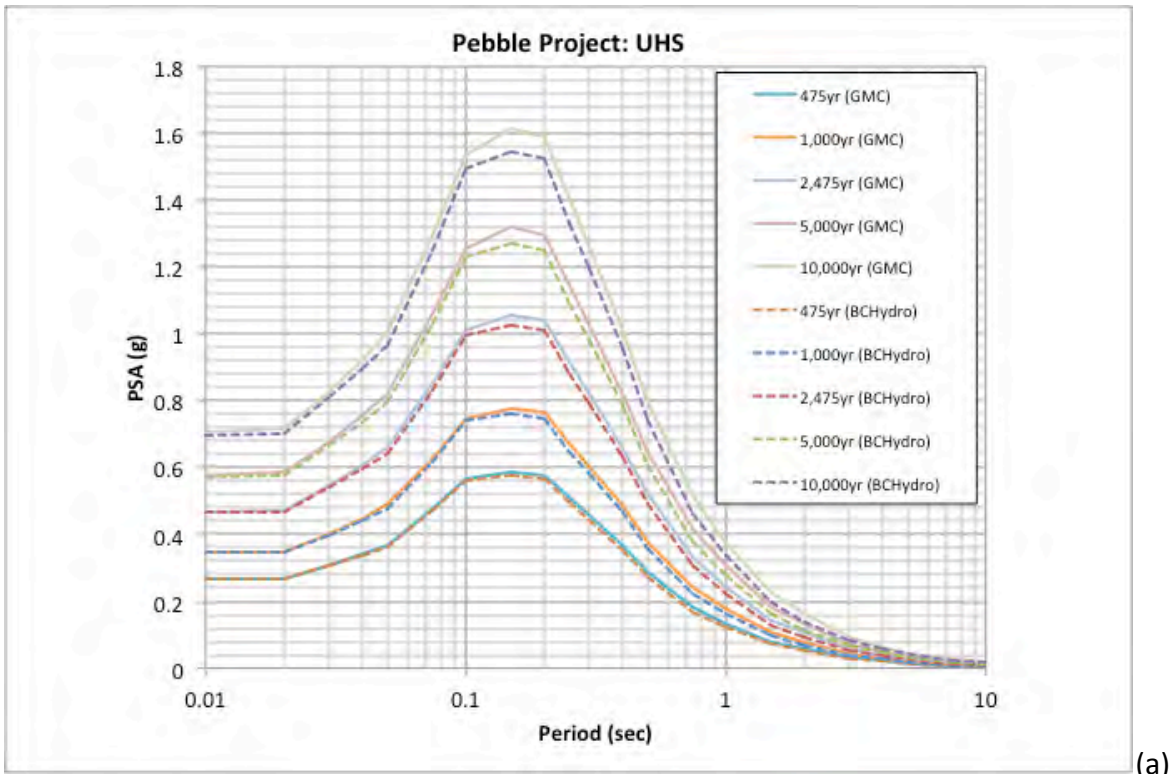


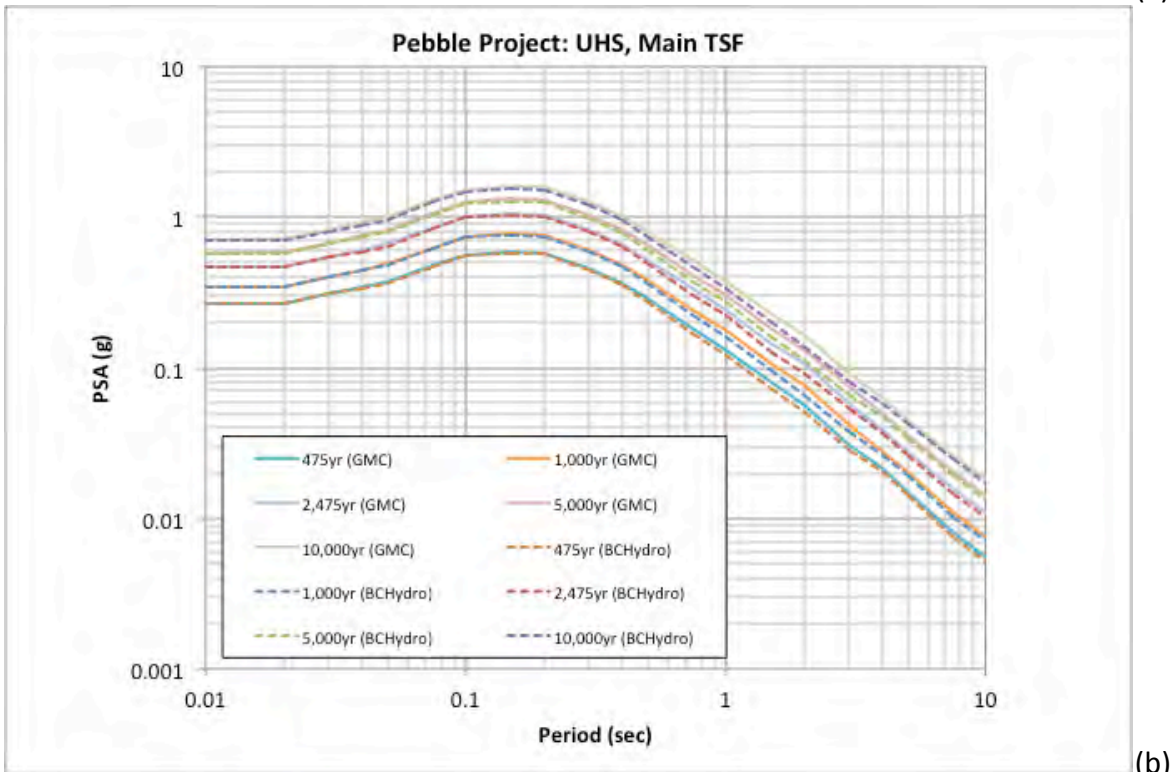
Figure 60. Spectral ratio of UHS from the two TSF site locations relative to the ground motions from the Main TSF site location.

An additional sensitivity analysis is performed to assess the impact of the new NGA-Subduction GMM on the hazard results. UHS are computed for the Main TSF site location using the same SSC model but assigning full weight to the BC Hydro ground-motion model. The same weighting for the crustal events is applied in both calculations. The comparison of the resulting spectra is shown in Figure 61 with the resulting spectral ratio plotted in Figure 62.

These results show that with the inclusion of the new KBCG GMM from the NGA-Subduction program with 15% weight, the resulting ground motions increase on the order of about 15% or less (i.e., spectral ratio of less than 1 in Figure 62). For spectral periods less than about 0.4 sec, the increase is on the order of 5% or less. This is a result of the BCHydro GMM having higher median ground motion estimates but lower aleatory sigma than the KBCG model (e.g., see Figures 22, 23, and 24). For longer spectral periods, the increase is larger, in the 10 – 15% range, with the largest occurring at 2 sec. As noted earlier, this peak difference between the results is driven by the increase from the KBCG GMM for the spectral period of 2 sec.



(a)



(b)

Figure 61. Comparison of mean UHS for the Main TSF site location only using the BCHydro GMM for the subduction events plotted log-linear (a) and log-log (b).

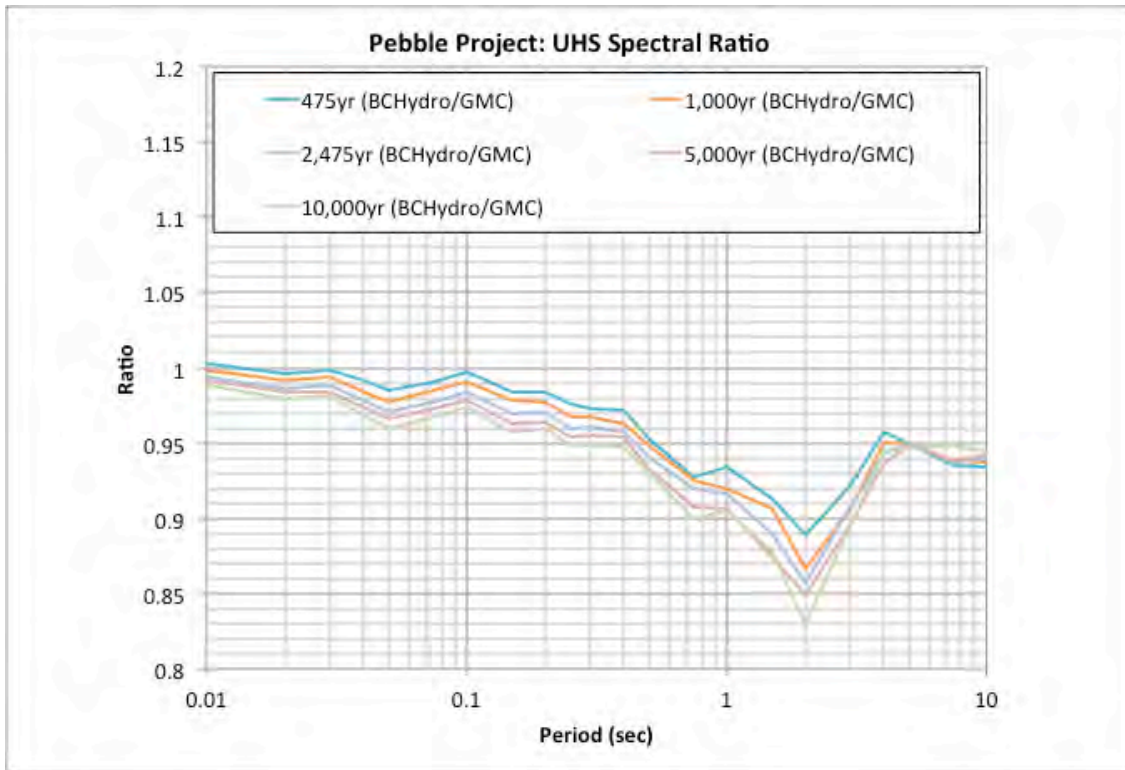


Figure 62. Spectral ratio (UHS with full BCHydro GMM divided by UHS with GMC model) of UHS for the Main TSF site location using only the BCHydro ground-motion model and the full GMC model for subduction events.

Only the PGA ground-motion values from the Knight-Piesold (2013) PSHA study are provided in their report. These values are listed in Table 17 along with the corresponding results from this study and the ratio of the ground motions. As listed, the ratio indicates an increase in the PGA values by a factor of slightly less than 2. Primarily, these observed differences can be attributed to several factors including the difference in ground-motion models and the difference in the slab source modeling used in the PSHA. A more detailed explanation of the causes for these differences is not possible based on the limited documentation provided in the Knight-Piesold (2013) report.

Table 17. Comparison of PGA ground-motion values from the Knight-Piesold (2013) study and this current SHA study.

Return Period (yr)	KP (2013) PGA (g)	Main TSF PGA (g)	Ratio (Current/KP)
475	0.14	0.2653	1.89
1,000	0.19	0.3461	1.82
2,475	0.25	0.4688	1.88
5,000	0.31	0.5790	1.87
10,000	0.38	0.7067	1.86

5. Deterministic Seismic Hazard Analysis (DSHA)

5.1 Methodology

A standard DSHA methodology approach is used for the calculation that is consistent with the SSC and GMC models used in the PSHA. For the DSHA, the largest characteristic magnitude associated with each seismic source is considered along with the closest distance to the project site locations. Both median and 84th percentile ground-motion spectra are computed for the controlling DSHA cases. Specifically, DSHA spectra are computed for the Lake Clark fault, the slab events and the repeat of the 1964 **M9.2** Great Alaska earthquake. For each of the three site locations, a DSHA calculation is performed given the slightly different distances for each controlling seismic source.

For the Lake Clark fault, the DSHA magnitude is 7.62 with a reverse mechanism. Note that the NGA-West2 GMMs do not differentiate between oblique and reverse mechanism ground motions. All three TSF site locations are identified as being on the hanging wall of the Lake Clark fault and off the end of the fault. Following the FERC recommendations (Idriss et al., 2018), the ground motions for these hanging wall sites are computed not including the two GMMs (i.e., BSSA14 and ID14) that do not explicitly account for the effects of being located on the hanging wall. The remaining three crustal GMMs are assigned equal weights. For the Knight-Piesold (2013) study, a slightly smaller magnitude of 7.5 was used for the DSHA calculation.

For the slab seismic source, ground motions were computed for each of the virtual faults used to represent the down going slab. Given these virtual faults, the median and 84th percentile ground motions are controlled by the slab virtual faults at the depths of 100 and 125 km. For both cases, a maximum magnitude of 8.0 is used based on the SSC model. This is the same DSHA magnitude assigned in the Knight-Piesold (2013) study. For the BCHydro GMM, the recommended maximum hypocentral depth of 120 km is used.

For the interface event, a repeat of the 1964 **M9.2** Great Alaska earthquake is selected. The distances are computed based on the closest distance to Kodiak segment of the subduction zone. Both the BCHydro and KBCG subduction GMMs contain a magnitude scaling break point where the scaling of ground motion (i.e., increase of ground motions with increasing magnitudes) decreases above the magnitude scaling point leading to an effect of saturation in the estimation of ground motions from large earthquakes. This scenario **M9.2** event is above the two magnitude scaling break points. For complete saturation, the magnitude scaling above the break point is assumed to be flat (i.e., no increase in ground motions for larger magnitude events). The two empirical models have a reduction in the magnitude scaling but not complete saturation. For the Knight-Piesold (2013) study, a complete saturation maximum magnitude of 8.5, rather than the **M9.2** associated with this historical event, was used in calculated the DSHA ground motions (i.e., following this approach, the same ground motions would be estimated for a magnitude 8.5 event as a magnitude 9.2 event given the same distance).

5.2 DSHA Results – Main TSF Site Location

For the Main TSF site location, the necessary GMM parameters for the four DSHA scenario cases are listed in Table 18. The same suite of GMMs and their assigned weights that were used for the PSHA are applied for the DSHA calculation. The resulting weighted average median and 84th percentile (i.e., median plus one sigma) response spectra are listed in Table 19 and plotted in Figures 63 and 64. Also for comparison, the UHS for the suite of return periods are plotted in these figures. For spectral periods equal to or less than 2 sec, the controlling DSHA spectra is from the slab events. For longer spectral periods, the Lake Clark spectrum is the controlling event. The median spectra from the slab events is approximately equal to the 475-yr UHS for spectral periods up to 2 sec. At periods beyond 2 sec, the Lake Clark median spectrum increases relative to the UHS return period levels.

For the comparison plot of the 84th percentile spectra, the UHS for return periods of 2,475, 5,000 and 10,000 years are also plotted in Figure 64. The controlling DSHA spectra from the slab events are approximately equal to the 5,000-yr UHS for spectral periods up to 2 sec. For the longer spectral periods, the Lake Clark DSHA spectrum is similar to the 10,000-yr UHS.

Table 18. Event parameters for the DSHA scenario events for the Main TSF site location.

Parameter	Lake Clark Fault	Slab Fault (Depth=100 km)	Slab Fault (Depth=125km)	Interface Event
Magnitude	7.62	8.0	8.0	9.2
Rupture Distance (km)	25.3	138.1	143.4	226.5
R _x Distance (km)	6.38	---	---	---
R _{jb} Distance (km)	24.7	---	---	---
R _{hypo} (km)	---	145.5	152.2	---
Ry0 (km)	23.7	---	---	---
Hypocenter Depth (km)	7.5	110	135 ¹	30
Top of Rupture (km)	0	100	125	20
Dip	70	---	---	---
Fault Width (km)	16.0	---	---	---
Hanging Wall/Foot Wall	Hanging Wall	---	---	---
V _{S30} (m/sec)	760	760	760	760
Z ₁ (km)	0.034	---	---	---
Z ₂₅ (km)	0.608	---	---	---
Mechanism	Reverse	Slab	Slab	Interface

¹ Maximum recommended hypocentral depth of 120 km is used for the BChydro GMM.

DSHA spectra were computed and listed in the Knight-Piesold (2013) report. Spectra were computed for the Lake Clark fault, slab and interface events as well as a maximum background earthquake located directly beneath the site. This background event was assigned a magnitude of 6.5 and assumed to be located directly beneath the project site. The corresponding spectrum

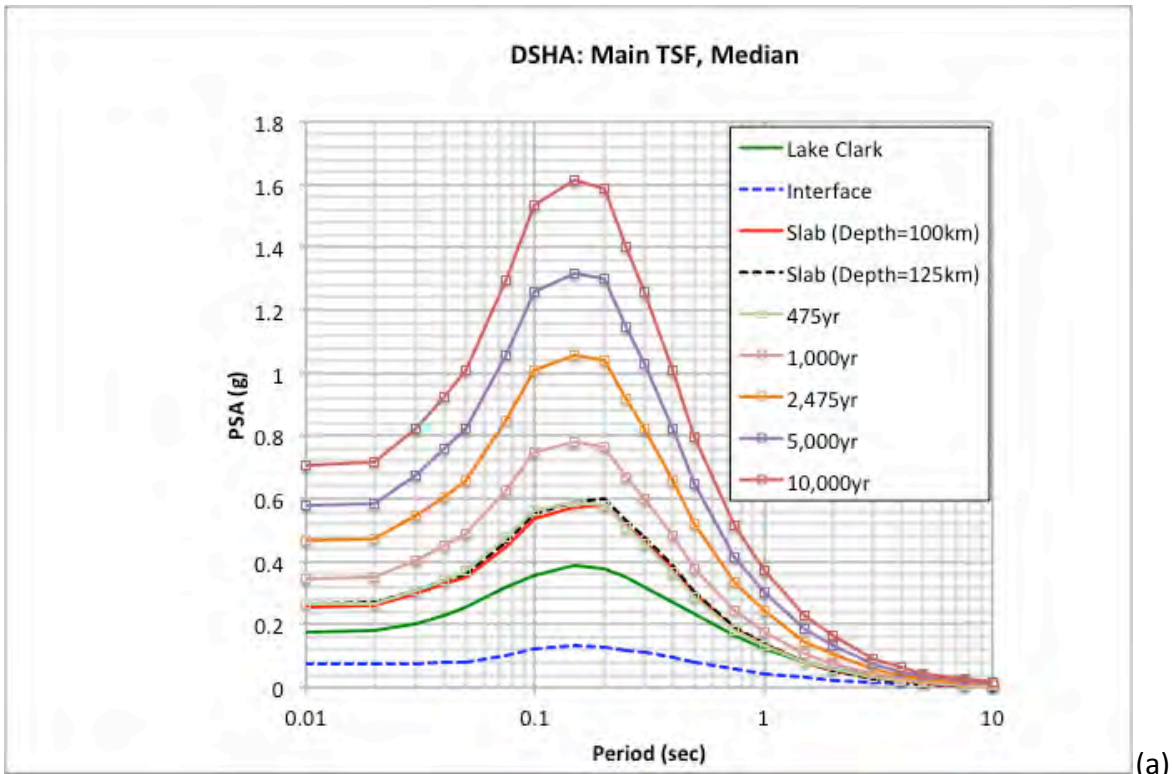
controls the Knight-Piesold (2013) DSHA spectra for periods up to 1.5 sec. At longer spectral periods, the ground motions from the slab sources control the results. The selection of this background event would not be supported based on the deaggregation results from the current PSHA study. Note that given the suite of ground-motion models used in the Knight-Piesold (2013) study, the spectra were only computed up to a spectral period of 3 sec.

A comparison of the 84th percentile DSHA spectra from the Knight-Piesold (2013) study and the DSHA and UHS from this current study is provided in Figure 65. The controlling 84th percentile DSHA spectra from Knight-Piesold (2013) study (i.e., background source event) envelopes the results from this study and is approximately equal to the 5,000-yr UHS for spectral periods less than about 0.2 sec and the 10,000-yr UHS for longer spectral periods. As listed in the Knight-Piesold (2013) report (i.e., see Table 3.3), two slab events are modeled – shallow and deep. The hypocentral depth for these two events are listed as 40 and 80 miles respectively which converts to depths of 64 and 129 km. In addition, the epicentral distances assigned to these two events are 177 and 80 km. These assigned distances and depths are consistent with the general geometry and location of the project site and the typical depths for slab earthquakes.

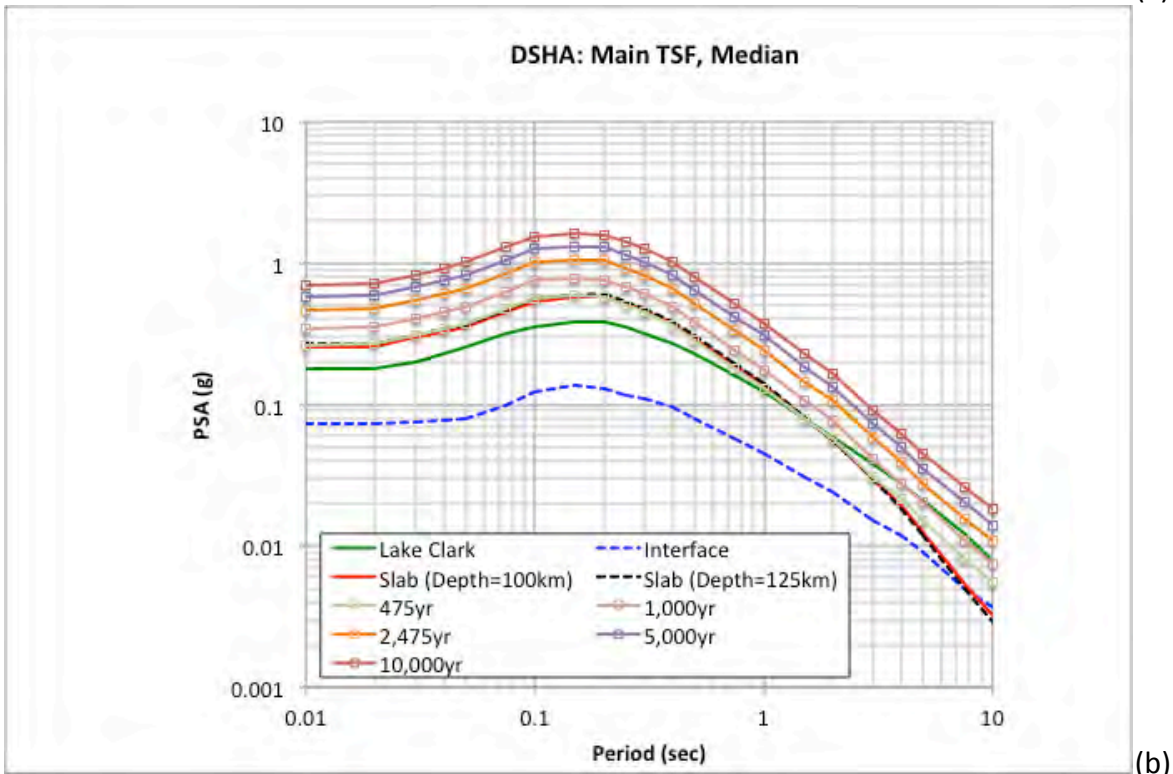
One critical observation of the Knight-Piesold (2013) results for the slab spectra is that the spectral shapes for the slab and interface events are not consistent with the empirical spectral shape of subduction ground motions given the current empirical database. For the slab events, the unfavorable behavior of the Atkinson and Boore (2003) model for these large magnitude deep earthquakes is contributing to the uncharacteristic spectral shapes. The Atkinson and Boore (2003) model was assigned 50% of the total weight in the Knight-Piesold (2013) study with the other 50% being assigned to the Youngs et al. (1997) model. Similarly the behavior of the Atkinson and Boore (2003) model for the large distance interface event is contributing to observed results with the shift in the spectral peak to longer spectral periods.

Table 19. Median and 84th percentile ground motions from the DSHA scenarios for the Main TSF site location.

Period (sec)	Lake Clark Median (g)	Lake Clark 84 th (g)	Slab (D=100km) Median (g)	Slab (D=100km) 84 th (g)	Slab (D=125km) Median (g)	Slab (D=125km) 84 th (g)	Interface Median (g)	Interface 84 th (g)
0.010	0.1775	0.3209	0.2570	0.5403	0.2671	0.5614	0.0724	0.1520
0.020	0.1813	0.3285	0.2587	0.5443	0.2688	0.5651	0.0727	0.1527
0.030	0.2011	0.3675	0.2975	0.6269	0.3087	0.6499	0.0757	0.1593
0.040	0.2291	0.4218	0.3278	0.6922	0.3395	0.7165	0.0777	0.1638
0.050	0.2563	0.4743	0.3516	0.7439	0.3638	0.7690	0.0789	0.1666
0.075	0.3196	0.6013	0.4488	0.9517	0.4638	0.9823	0.0992	0.2099
0.100	0.3553	0.6747	0.5354	1.1356	0.5538	1.1732	0.1222	0.2583
0.150	0.3884	0.7434	0.5720	1.2137	0.5915	1.2533	0.1348	0.2850
0.200	0.3793	0.7284	0.5800	1.2285	0.6009	1.2711	0.1290	0.2725
0.250	0.3507	0.6738	0.5130	1.0851	0.5312	1.1224	0.1156	0.2441
0.300	0.3192	0.6185	0.4622	0.9759	0.4786	1.0097	0.1109	0.2337
0.400	0.2704	0.5282	0.3747	0.7892	0.3879	0.8165	0.0973	0.2047
0.500	0.2315	0.4569	0.2953	0.6213	0.3048	0.6409	0.0793	0.1668
0.750	0.1627	0.3283	0.1884	0.3960	0.1936	0.4067	0.0567	0.1192
1.000	0.1213	0.2471	0.1376	0.2892	0.1409	0.2960	0.0452	0.0951
1.500	0.0797	0.1633	0.0804	0.1693	0.0816	0.1719	0.0305	0.0642
2.000	0.0593	0.1215	0.0556	0.1172	0.0558	0.1177	0.0237	0.0501
3.000	0.0379	0.0773	0.0300	0.0632	0.0295	0.0621	0.0152	0.0322
4.000	0.0277	0.0558	0.0192	0.0403	0.0185	0.0388	0.0119	0.0251
5.000	0.0212	0.0428	0.0125	0.0263	0.0119	0.0248	0.0091	0.0190
7.500	0.0121	0.0246	0.0054	0.0111	0.0049	0.0102	0.0050	0.0104
10.000	0.0079	0.0159	0.0032	0.0067	0.0029	0.0060	0.0037	0.0075

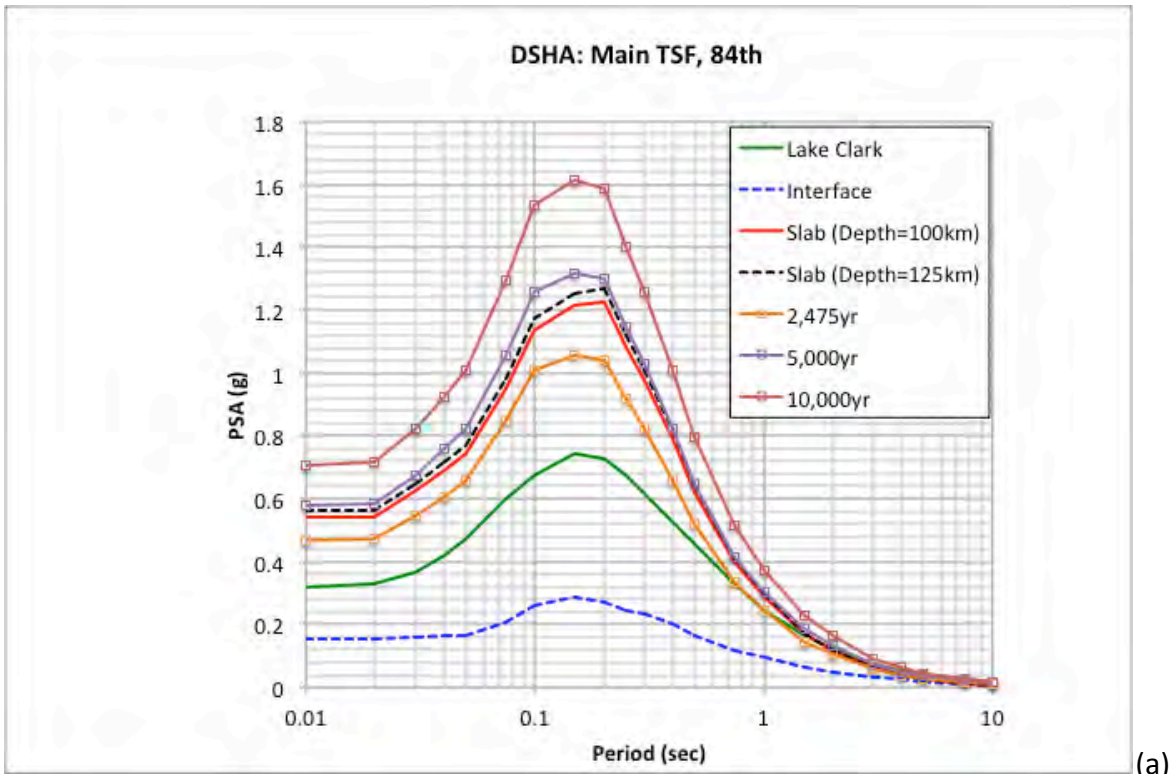


(a)

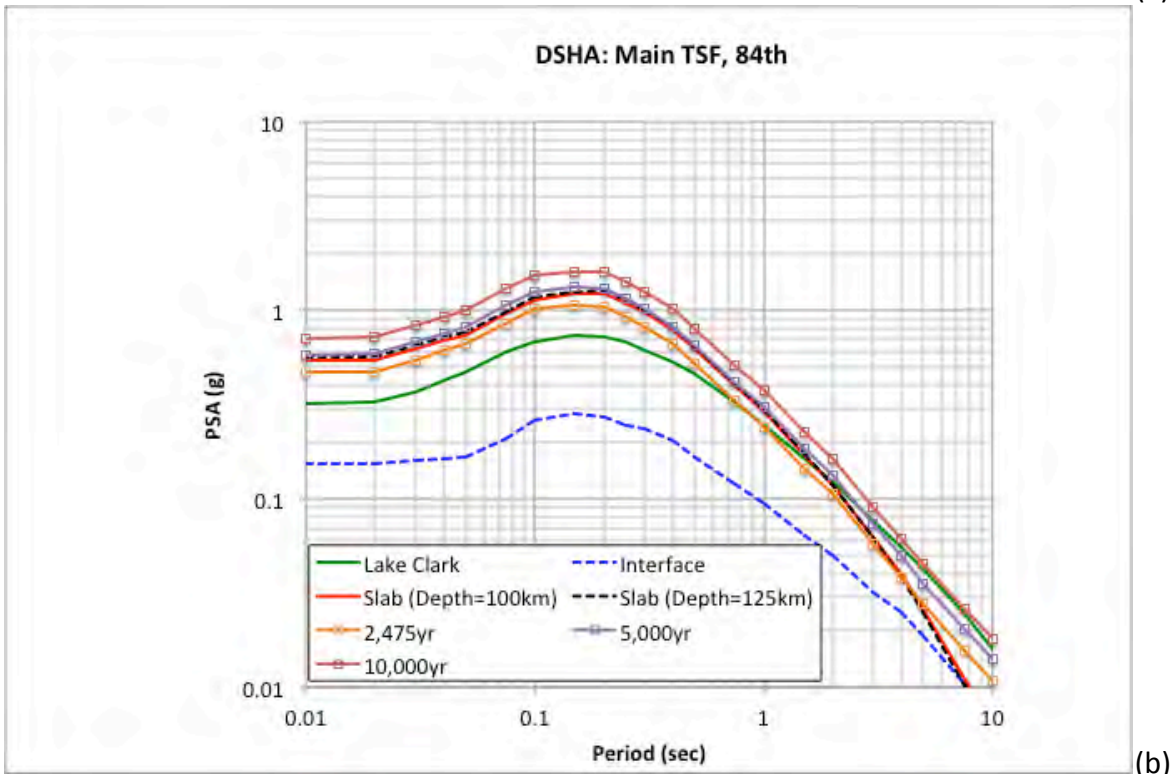


(b)

Figure 63. Median DSHA scenario events (Main TSF) spectra plotted log-linear (a) and log-log (b).

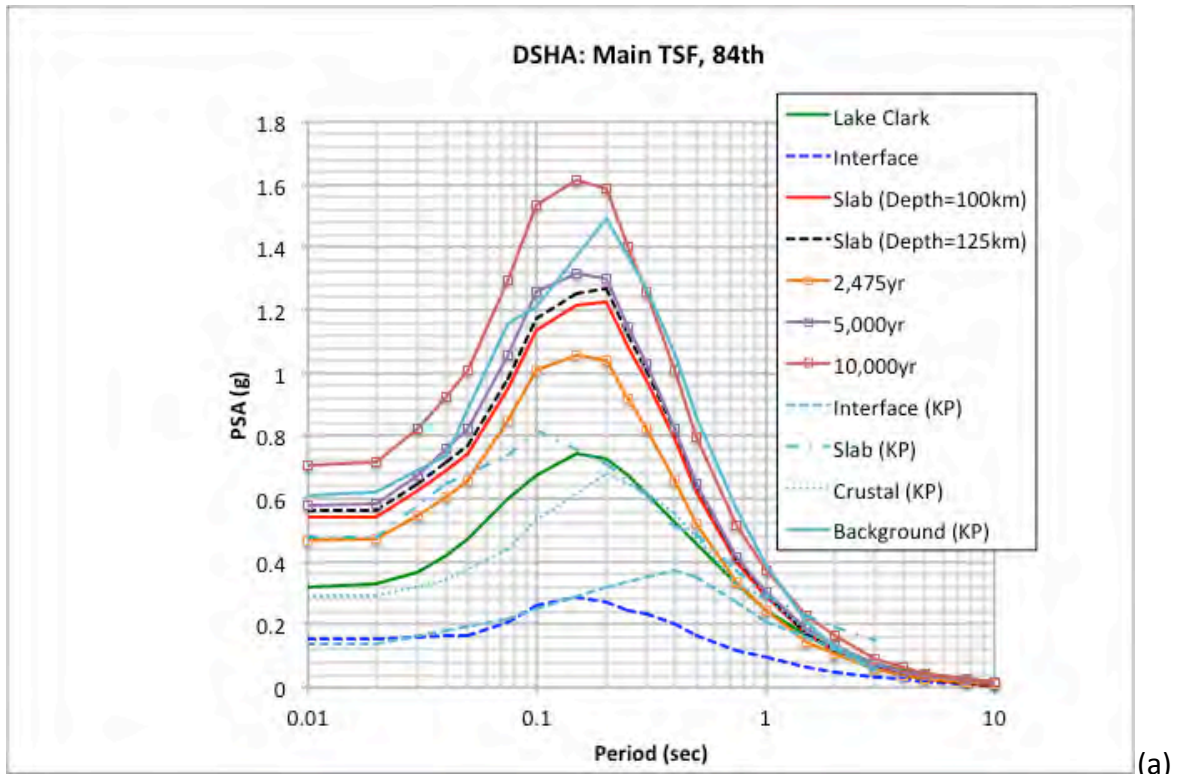


(a)

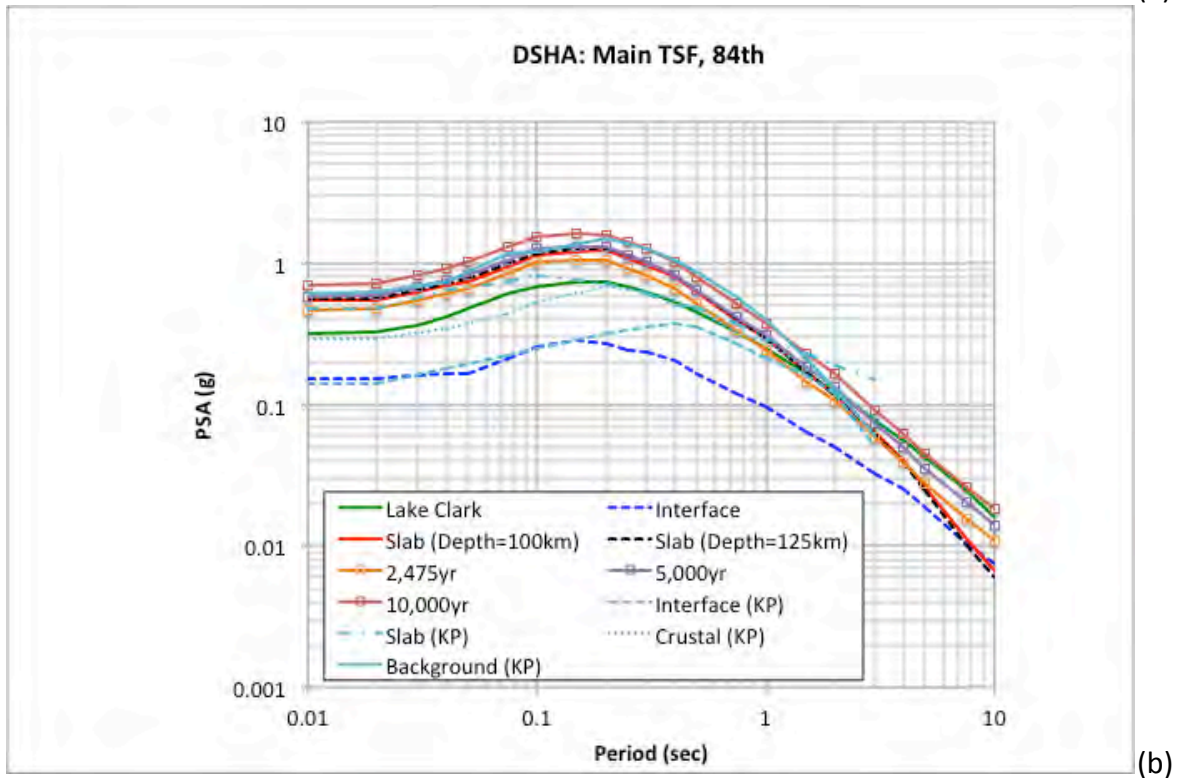


(b)

Figure 64. 84th percentile DSHA scenario events (Main TSF) spectra plotted log-linear (a) and log-log (b).



(a)



(b)

Figure 65. 84th percentile DSHA scenario events (Main TSF) spectra from the Knight-Piesold (2013) study and the current study plotted log-linear (a) and log-log (b).

5.3 DSHA Results – Pyritic TSF Site Location

For the Pyritic TSF site location, the necessary GMM parameters for the four DSHA scenario cases are listed in Table 20. The same suite of GMMs and their assigned weights that were used for the PSHA are applied for the DSHA calculation. The resulting weighted average median and 84th percentile (i.e., median plus one sigma) ground-motion spectra are listed in Table 21. Given the close proximity of the three TSF locations, these spectral values are similar to the previous results presented for the Main TSF site location. A summary comparison of these 84th percentile spectra for the Pyritic TSF site location from this study and the Knight-Piesold (2013) study is shown in Figure 66 with the UHS for this Pyritic TSF site location. The same observations as noted for the Main TSF site location are applicable to the results for the Pyritic TSF site location.

Table 20. Event parameters for the DSHA scenario events for the Pyritic TSF site location.

Parameter	Lake Clark Fault	Slab Fault (Depth=100 km)	Slab Fault (Depth=125km)	Interface Event
Magnitude	7.62	8.0	8.0	9.2
Rupture Distance (km)	21.8	135.0	141.3	222.1
R _x Distance (km)	2.7	---	---	---
R _{jb} Distance (km)	21.7	---	---	---
R _{hypo} (km)	---	142.6	150.2	---
Ry0 (km)	21.0	---	---	---
Hypocenter Depth (km)	7.5	110	135 ¹	30
Top of Rupture (km)	0	100	125	20
Dip	70	---	---	---
Fault Width (km)	16.0	---	---	---
Hanging Wall/Foot Wall	Hanging Wall	---	---	---
V _{S30} (m/sec)	760	760	760	760
Z ₁ (km)	0.034	---	---	---
Z ₂₅ (km)	0.608	---	---	---
Mechanism	Reverse	Slab	Slab	Interface

¹ Maximum recommended hypocentral depth of 120 km is used for the BChydro GMM.

Table 21. Median and 84th percentile ground motions from the DSHA scenarios for the Pyritic TSF site location.

Period (sec)	Lake Clark Median (g)	Lake Clark 84 th (g)	Slab (D=100km) Median (g)	Slab (D=100km) 84 th (g)	Slab (D=125km) Median (g)	Slab (D=125km) 84 th (g)	Interface Median (g)	Interface 84 th (g)
0.010	0.1979	0.3578	0.2658	0.5589	0.2732	0.5741	0.0743	0.1561
0.020	0.2023	0.3664	0.2676	0.5631	0.2749	0.5780	0.0747	0.1569
0.030	0.2246	0.4102	0.3077	0.6484	0.3156	0.6646	0.0778	0.1637
0.040	0.2561	0.4711	0.3389	0.7159	0.3471	0.7326	0.0798	0.1683
0.050	0.2867	0.5302	0.3635	0.7693	0.3719	0.7861	0.0811	0.1713
0.075	0.3586	0.6738	0.4642	0.9845	0.4743	1.0045	0.1021	0.2160
0.100	0.3990	0.7571	0.5538	1.1749	0.5663	1.1998	0.1256	0.2657
0.150	0.4375	0.8371	0.5926	1.2576	0.6055	1.2831	0.1389	0.2936
0.200	0.4267	0.8194	0.6013	1.2736	0.6154	1.3020	0.1330	0.2809
0.250	0.3935	0.7558	0.5317	1.1247	0.5440	1.1494	0.1193	0.2519
0.300	0.3572	0.6920	0.4787	1.0107	0.4899	1.0336	0.1145	0.2413
0.400	0.3023	0.5904	0.3879	0.8170	0.3970	0.8357	0.1006	0.2118
0.500	0.2585	0.5102	0.3057	0.6431	0.3119	0.6559	0.0822	0.1728
0.750	0.1813	0.3657	0.1950	0.4098	0.1980	0.4161	0.0589	0.1238
1.000	0.1355	0.2758	0.1422	0.2990	0.1441	0.3028	0.0469	0.0987
1.500	0.0888	0.1820	0.0829	0.1747	0.0834	0.1756	0.0316	0.0666
2.000	0.0661	0.1354	0.0573	0.1208	0.0570	0.1201	0.0246	0.0519
3.000	0.0423	0.0864	0.0309	0.0651	0.0301	0.0633	0.0158	0.0333
4.000	0.0310	0.0624	0.0197	0.0415	0.0188	0.0395	0.0123	0.0259
5.000	0.0237	0.0479	0.0129	0.0270	0.0121	0.0253	0.0094	0.0196
7.500	0.0134	0.0272	0.0055	0.0114	0.0050	0.0104	0.0052	0.0107
10.000	0.0086	0.0175	0.0033	0.0069	0.0030	0.0061	0.0038	0.0077

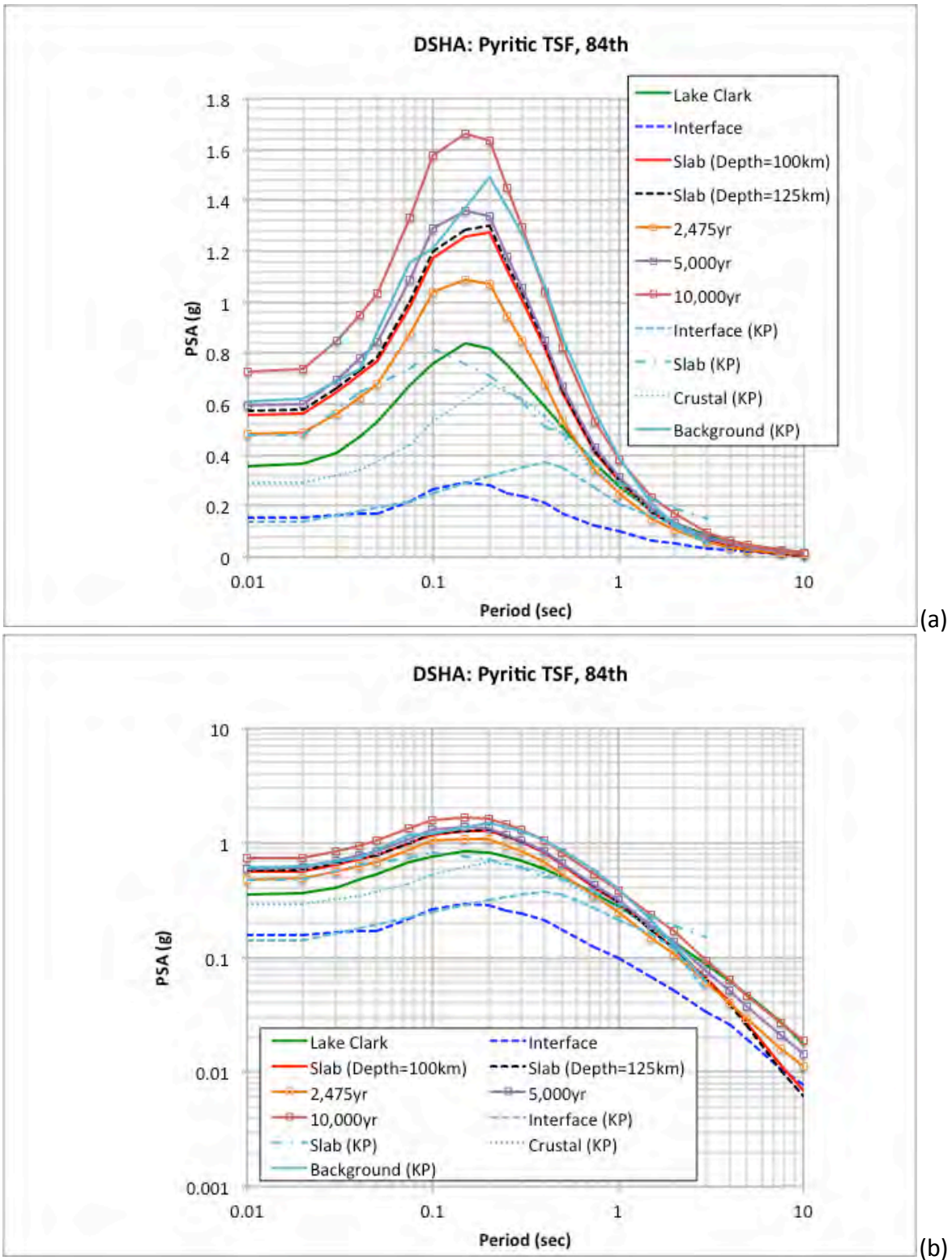


Figure 66. 84th percentile DSHA scenario events (Pyritic TSF) spectra from the Knight-Piesold (2013) study and the current study plotted log-linear (a) and log-log (b).

5.4 DSHA Results – South TSF Site Location

For the South TSF site location, the necessary GMM parameters for the four DSHA scenario cases are listed in Table 22. The same suite of GMMs and their assigned weights that were used for the PSHA are applied for the DSHA calculation. The resulting weighted average median and 84th percentile (i.e., median plus one sigma) ground-motion spectra are listed in Table 23. Given the close proximity of the three TSF locations, these spectral values are similar to the previous results presented for the Main TSF site location. A summary comparison of these 84th percentile spectra for the South TSF site location from this study and the Knight-Piesold (2013) study is shown in Figure 67 with the UHS for this South TSF site location. The same observations as noted for the Main TSF site location are applicable to the results for the South TSF site location with one exception. For the longer spectral periods (i.e., greater than about 2 seconds), the 84th percentile DSHA spectrum from the Lake Clark fault is approximately equal to the 5,000-yr UHS rather than the 10,000-yr UHS for the other two sites. This reduction in the comparison is based on the slightly larger distance for the South TSF site location than the other two TSF site locations from the Lake Clark fault.

Table 22. Event parameters for the DSHA scenario events for the South TSF site location.

Parameter	Lake Clark Fault	Slab Fault (Depth=100 km)	Slab Fault (Depth=125km)	Interface Event
Magnitude	7.62	8.0	8.0	9.2
Rupture Distance (km)	30.8	136.7	142.2	224.9
R _x Distance (km)	1.8	---	---	---
R _{jb} Distance (km)	30.8	---	---	---
R _{hypo} (km)	---	144.2	151.1	---
Ry0 (km)	30.0	---	---	---
Hypocenter Depth (km)	7.5	110	135 ¹	30
Top of Rupture (km)	0	100	125	20
Dip	70	---	---	---
Fault Width (km)	16.0	---	---	---
Hanging Wall/Foot Wall	Hanging Wall	---	---	---
V _{S30} (m/sec)	760	760	760	760
Z ₁ (km)	0.034	---	---	---
Z ₂₅ (km)	0.608	---	---	---
Mechanism	Reverse	Slab	Slab	Interface

¹ Maximum recommended hypocentral depth of 120 km is used for the BChydro GMM.

Table 23. Median and 84th percentile ground motions from the DSHA scenarios for the South TSF site location.

Period (sec)	Lake Clark Median (g)	Lake Clark 84 th (g)	Slab (D=100km) Median (g)	Slab (D=100km) 84 th (g)	Slab (D=125km) Median (g)	Slab (D=125km) 84 th (g)	Interface Median (g)	Interface 84 th (g)
0.010	0.1504	0.2721	0.2609	0.5485	0.2704	0.5684	0.0646	0.1381
0.020	0.1535	0.2783	0.2627	0.5526	0.2722	0.5722	0.0651	0.1395
0.030	0.1700	0.3107	0.3020	0.6364	0.3125	0.6580	0.0676	0.1452
0.040	0.1932	0.3560	0.3327	0.7027	0.3437	0.7253	0.0694	0.1501
0.050	0.2156	0.3996	0.3568	0.7552	0.3682	0.7783	0.0709	0.1545
0.075	0.2678	0.5045	0.4556	0.9663	0.4696	0.9945	0.0879	0.1929
0.100	0.2971	0.5650	0.5435	1.1530	0.5607	1.1878	0.1059	0.2315
0.150	0.3239	0.6204	0.5812	1.2332	0.5992	1.2697	0.1180	0.2568
0.200	0.3171	0.6093	0.5895	1.2485	0.6088	1.2880	0.1158	0.2516
0.250	0.2948	0.5667	0.5213	1.1026	0.5382	1.1372	0.1064	0.2315
0.300	0.2694	0.5222	0.4695	0.9914	0.4848	1.0229	0.1036	0.2246
0.400	0.2288	0.4472	0.3806	0.8016	0.3929	0.8270	0.0925	0.1996
0.500	0.1964	0.3878	0.2999	0.6309	0.3087	0.6491	0.0774	0.1667
0.750	0.1387	0.2799	0.1913	0.4021	0.1961	0.4119	0.0576	0.1244
1.000	0.1033	0.2104	0.1397	0.2936	0.1426	0.2998	0.0464	0.0998
1.500	0.0681	0.1397	0.0815	0.1717	0.0826	0.1739	0.0324	0.0698
2.000	0.0508	0.1040	0.0563	0.1188	0.0564	0.1190	0.0257	0.0554
3.000	0.0325	0.0663	0.0304	0.0641	0.0298	0.0628	0.0164	0.0352
4.000	0.0238	0.0478	0.0194	0.0408	0.0187	0.0392	0.0126	0.0267
5.000	0.0182	0.0367	0.0127	0.0266	0.0120	0.0251	0.0096	0.0203
7.500	0.0106	0.0214	0.0054	0.0112	0.0050	0.0103	0.0055	0.0114
10.000	0.0069	0.0141	0.0033	0.0068	0.0029	0.0061	0.0040	0.0080

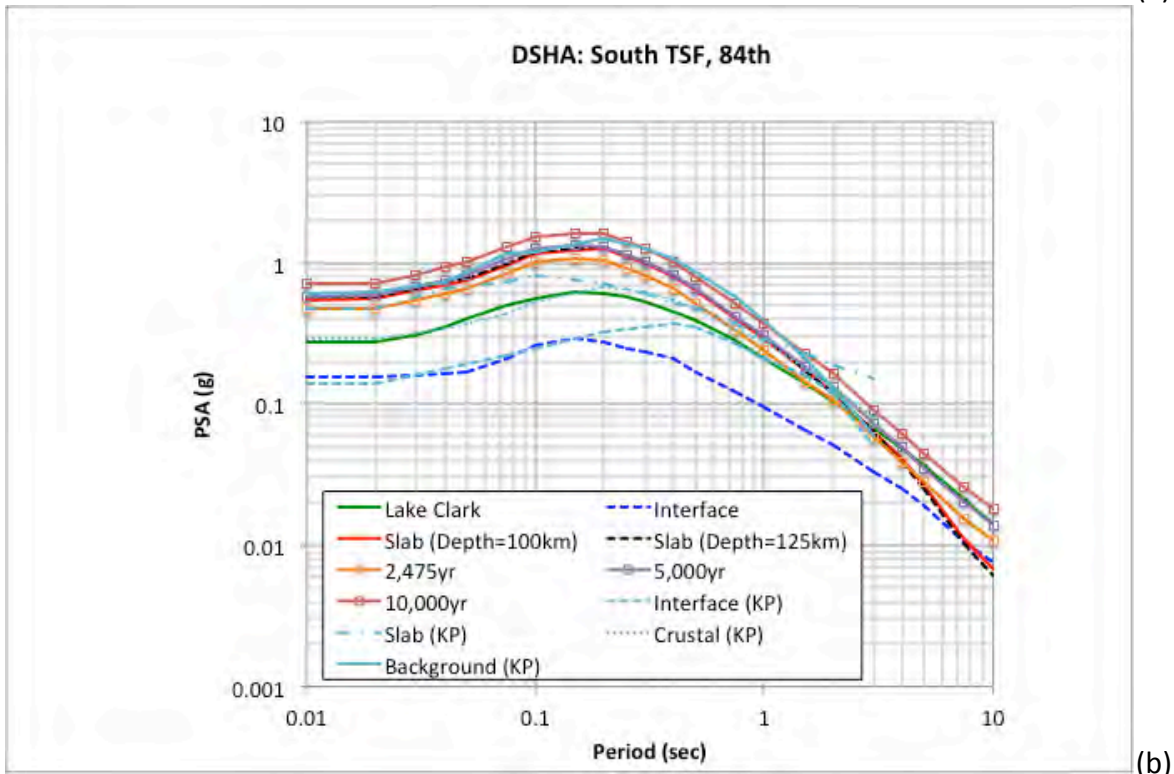
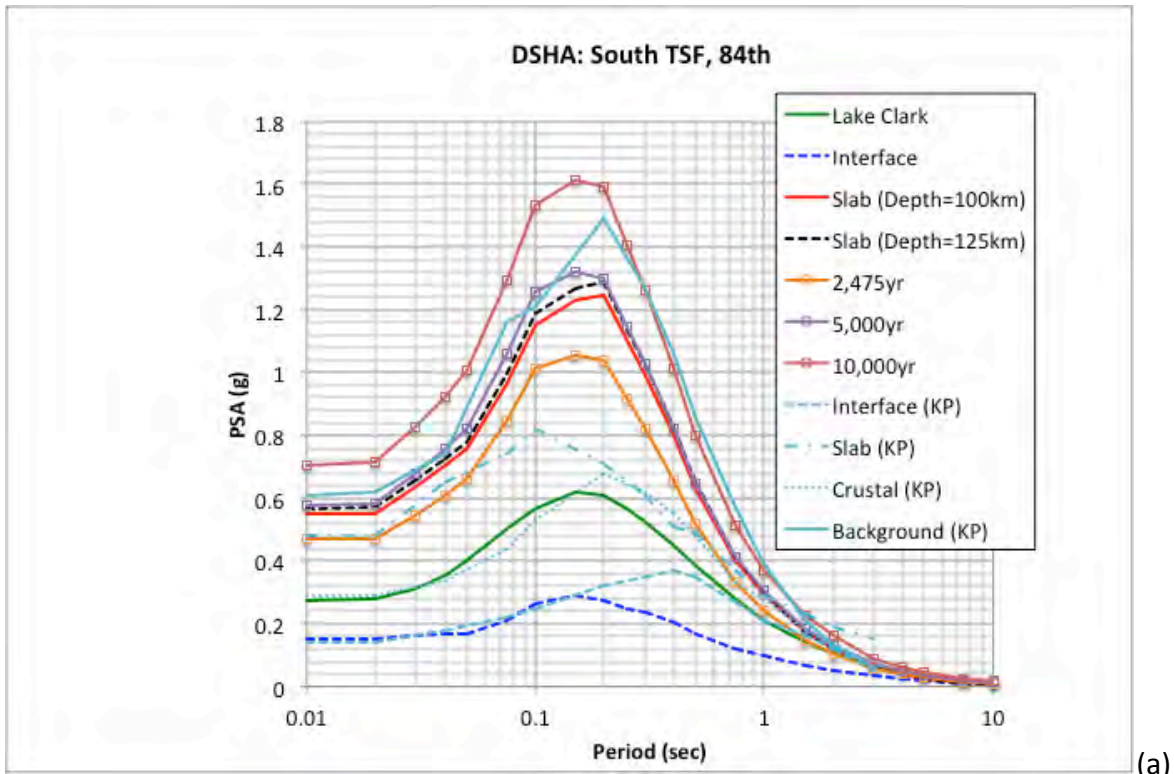


Figure 67. 84th percentile DSHA scenario events (South TSF) spectra from the Knight-Piesold (2013) study and the current study plotted log-linear (a) and log-log (b).

5.5 DSHA Summary

Given the close proximity of the three TSF site locations, the calculated DSHA are similar with variations for individual scenario events based on the relative distances from each site location to the source. For the controlling slab events, the ground motions from the Pyritic TSF site location are larger than the ground motions at the Main TSF site location by approximately 3% or less. As shown of the Main TSF site location, the 84th percentile DSHA spectra from the controlling slab seismic sources from this study are approximately equal to the 5,000-yr UHS from the PSHA calculations for spectral periods from PGA to approximately 1 sec. For longer spectral periods, the slab spectra falls closer to the 2,475-yr UHS and the deterministic spectra from the Lake Clark fault exceeds the slab spectra and is approximately equal to the 10,000-yr UHS for the Main and Pyritic TSF site locations and the 5,000-yr UHS for the South TSF site location.

The enveloping DSHA 84th percentile spectrum from this study is lower than the controlling DSHA 84th percentile spectrum from the Knight-Piesold (2013) study which was based on a background M6.5 event directly at the site location. The background event 84th percentile spectral ground-motion values from the Knight-Piesold (2013) study are more similar to the 5,000-yr UHS from this current study for spectral periods up to about 0.15 sec and closer to the 10,000-yr UHS for spectral periods greater than 0.2 sec and less than 1.5 sec. For longer spectral periods, the slab 84th percentile spectrum from the Knight-Piesold (2013) study is similar to the 10,000-yr UHS from this study.

In comparing the reported 84th percentile PGA value from the slab source between the results of this study and the values provided in the Knight-Piesold (2013) report (i.e., 0.48g), the current PGA value is greater by about 15%. For intermediate periods, this difference increases to about 80% peaking about 0.2 sec and then reduces to about 2% at 1 sec. For longer spectral periods, the ground-motion values from this current study are lower than the values from the Knight-Piesold (2013) report, and as discussed earlier, these observed differences are expected to primarily be a result from the different ground-motion models and their respective modeling features. The two subduction GMMs used in this study are consistent in their empirical shapes with modern empirical databases from subduction events.

Similar to the results from the PSHA, the results from the Pyritic TSF site location could be taken as the envelop ground motions for the three sites if the use of the three individual site-specific ground motions is not necessary for future analyses.

6. Summary and Conclusions

A SHA study is performed for three TSF site locations for the Pebble Mine project in Southwest Alaska. Both PSHA and DSHA studies are performed using approaches and methodologies consistent with the international state of practice. As part of this SHA study, a regional SSC model is developed based on published literature and previous SHA studies that have been performed in Southwestern Alaska. This SSC model represents an update given more current information than the model implemented in the previous Knight-Piesold (2013) study and the USGS regional seismic hazard map for Alaska (Wesson et al., 2007, 2008). As part of this update, an evaluation of the recent seismicity since 2004 is captured and incorporated into the SSC model. No site-specific geologic mapping was conducted as part of this study and if potential seismic sources in the project region are identified and characterized in the future, the hazard results and response spectra presented in this study should be re-evaluated.

In addition to the update of the SSC model, the GMC model is updated to include more current GMMs than were used in the previous studies. These newer models are incorporated for both crustal and subduction seismic events. All of the ground-motion results presented in this study are for the assumed reference site conditions with a V_{S30} value of 760 m/sec. The resulting 475-yr, 5,000-yr and 10,000-yr UHS and the envelop of the two controlling slab events (i.e., depths of 100 and 125 km) median and 84th percentile deterministic spectra are listed in Table 24 for the Main TSF site location. The results for the Pyritic TSF and South TSF site locations are listed in Tables 25 and 26. Before application of these computed ground-motion results as design spectra, the site conditions at the Pebble Mine project sites should be determined and the hazard results adjusted to the site-specific site condition if needed. Commonly, this is performed through the use of analytical site response modeling and should follow a standard state of practice in its methodology and application.

Table 24. PSHA UHS and controlling slab 84th percentile spectra for the reference site conditions of $V_{s30} = 760$ m/sec for the Main TSF site location.

Period (sec)	475-yr UHS (g)	5,000-yr UHS (g)	10,000-yr UHS (g)	Slab, Median (g)	Slab, 84th (g)
0.010	0.2653	0.5790	0.7067	0.2671	0.5614
0.020	0.2673	0.5849	0.7148	0.2688	0.5651
0.030	0.3089	0.6757	0.8248	0.3087	0.6499
0.040	0.3417	0.7586	0.9237	0.3395	0.7165
0.050	0.3695	0.8234	1.0084	0.3638	0.7690
0.075	0.4776	1.0591	1.2955	0.4638	0.9823
0.100	0.5653	1.2561	1.5334	0.5538	1.1732
0.150	0.5880	1.3186	1.6132	0.5915	1.2533
0.200	0.5771	1.2983	1.5889	0.6009	1.2711
0.250	0.5100	1.1442	1.4040	0.5312	1.1224
0.300	0.4563	1.0279	1.2603	0.4786	1.0097
0.400	0.3649	0.8235	1.0108	0.3879	0.8165
0.500	0.2882	0.6486	0.7989	0.3048	0.6409
0.750	0.1817	0.4151	0.5148	0.1936	0.4067
1.000	0.1310	0.3051	0.3724	0.1409	0.2960
1.500	0.0799	0.1839	0.2276	0.0816	0.1719
2.000	0.0567	0.1319	0.1641	0.0558	0.1177
3.000	0.0307	0.0737	0.0910	0.0300	0.0632
4.000	0.0213	0.0500	0.0616	0.0192	0.0403
5.000	0.0150	0.0355	0.0450	0.0125	0.0263
7.500	0.0080	0.0204	0.0261	0.0054	0.0111
10.000	0.0055	0.0141	0.0182	0.0032	0.0067

Table 25. PSHA UHS and controlling slab 84th percentile spectra for the reference site conditions of $V_{s30} = 760$ m/sec for the Pyritic TSF site location.

Period (sec)	475-yr UHS (g)	5,000-yr UHS (g)	10,000-yr UHS (g)	Slab, Median (g)	Slab, 84th (g)
0.010	0.2729	0.5949	0.7273	0.2732	0.5741
0.020	0.2751	0.6011	0.7360	0.2749	0.5780
0.030	0.3171	0.6954	0.8477	0.3156	0.6646
0.040	0.3511	0.7795	0.9507	0.3471	0.7326
0.050	0.3800	0.8467	1.0358	0.3719	0.7861
0.075	0.4925	1.0892	1.3323	0.4743	1.0045
0.100	0.5813	1.2913	1.5760	0.5663	1.1998
0.150	0.6054	1.3578	1.6607	0.6055	1.2831
0.200	0.5942	1.3368	1.6357	0.6154	1.3020
0.250	0.5245	1.1792	1.4470	0.5440	1.1494
0.300	0.4708	1.0580	1.2972	0.4899	1.0336
0.400	0.3756	0.8479	1.0396	0.3970	0.8357
0.500	0.2974	0.6688	0.8228	0.3119	0.6559
0.750	0.1878	0.4283	0.5300	0.1980	0.4161
1.000	0.1349	0.3137	0.3838	0.1441	0.3028
1.500	0.0821	0.1898	0.2344	0.0834	0.1756
2.000	0.0583	0.1357	0.1693	0.0573	0.1208
3.000	0.0316	0.0759	0.0939	0.0309	0.0651
4.000	0.0218	0.0515	0.0636	0.0197	0.0415
5.000	0.0154	0.0366	0.0466	0.0129	0.0270
7.500	0.0082	0.0209	0.0269	0.0055	0.0114
10.000	0.0056	0.0145	0.0187	0.0033	0.0069

Table 26. PSHA UHS and controlling slab 84th percentile spectra for the reference site conditions of $V_{s30} = 760$ m/sec for the South TSF site location.

Period (sec)	475-yr UHS (g)	5,000-yr UHS (g)	10,000-yr UHS (g)	Slab, Median (g)	Slab, 84th (g)
0.010	0.2646	0.5790	0.7072	0.2704	0.5684
0.020	0.2667	0.5849	0.7153	0.2722	0.5722
0.030	0.3082	0.6756	0.8254	0.3125	0.6580
0.040	0.3409	0.7585	0.9243	0.3437	0.7253
0.050	0.3686	0.8233	1.0089	0.3682	0.7783
0.075	0.4762	1.0590	1.2963	0.4696	0.9945
0.100	0.5639	1.2561	1.5343	0.5607	1.1878
0.150	0.5866	1.3188	1.6145	0.5992	1.2697
0.200	0.5757	1.2985	1.5904	0.6088	1.2880
0.250	0.5088	1.1443	1.4051	0.5382	1.1372
0.300	0.4551	1.0277	1.2610	0.4848	1.0229
0.400	0.3640	0.8231	1.0108	0.3929	0.8270
0.500	0.2873	0.6480	0.7985	0.3087	0.6491
0.750	0.1812	0.4145	0.5142	0.1961	0.4119
1.000	0.1307	0.3045	0.3717	0.1426	0.2998
1.500	0.0797	0.1833	0.2269	0.0826	0.1739
2.000	0.0566	0.1315	0.1635	0.0564	0.1190
3.000	0.0306	0.0733	0.0904	0.0304	0.0641
4.000	0.0213	0.0497	0.0611	0.0194	0.0408
5.000	0.0150	0.0351	0.0444	0.0127	0.0266
7.500	0.0080	0.0202	0.0256	0.0054	0.0112
10.000	0.0055	0.0140	0.0180	0.0033	0.0068

Based on the close proximity of the three site locations, the resulting ground-motion spectra are similar with the results from the Pyritic TSF site location being slightly higher given its closer distance to the controlling seismic sources. The observed differences are within the uncertainty of the ground-motion calculations. If a single representative set of PSHA and DSHA ground motions are requested from the project for analyses in the Pebble Mine project are, the results from Pyritic TSF site can be selected as representative for the ground motions given their enveloping level when compared to the results from the other two sites. If however, more site-specific analyses are requested for the three TSF site locations, the specific results provided in this report can be used.

7. References

- Abers, G.A. and M.E. Mann (2018). Earth Structure Effects on Wave Propagation of the Damaging 2016 M7.1 Iniskin Alaska Earthquake and other in-slab Earthquakes, Final Technical Report, USGS NEHRP award G17AP00065.
- Abrahamson, N.A. (2018). Seismic Hazard Software HAZ45.2, Piedmont, California.
- Abrahamson, N.A., N. Gregor and K. Addo (2016). BC Hydro Ground Motion Prediction Equations for Subduction Earthquakes, *Earthquake Spectra*, Vol. 32, No. 1, p. 23-44.
- Abrahamson, N.A., Silva, W.J., and R. Kamai (2014). Summary of the ASK14 ground motion relation for active crustal regions, *Earthquake Spectra*, Vol. 30, No. 3, p. 1025-1055.
- Ancheta, T.D., Darragh, R.B., Stewart, J.P., Seyhan, E., Silva, W.J., Chiou, B.S.-J., Wooddell, K.E., Graves, R.W., Kottke, A.R., Boore, D.M., Kishida, T., and Donahue, J.L. (2014). NGA-West2 database, *Earthquake Spectra*, Vol. 30, No. 3, p. 989–1005.
- Al Atik, L. and R.R. Youngs (2014). Epistemic uncertainty for NGA-West2 Models. *Earthquake Spectra*, Vol. 30, No. 3, p. 1301-1318.
- Amato, J.M., M.J. Bogar, G.E. Gehrels, G.L. Farmer and W.C. McIntosh (2007). The Tlikakila complex in southern Alaska: A suprasubduction-zone ophiolite between the Wrangellia Composite Terrane and North America, Geological Society of America, Special Paper 431.
- Atkinson, G.M., and Boore, D.M. (2003). Empirical ground-motion relationships for subduction-zone earthquakes and their application to Cascadia and other regions, *Bull. Seism. Soc. Am.*, Vol. 93, p. 1703–1729.
- Atkinson, G.M., and Boore, D.M. (2008). Erratum to empirical ground-motion relationships for subduction-zone earthquakes and their application to Cascadia and other regions, *Bull. Seism. Soc. Am.*, Vol. 98, p. 2567–2569.
- Barnes, F.F. (1966). Geology and coal resources of the Beluga–Yentna region, Alaska: U.S. Geological Survey Bulletin 1202-C, 54 p., 2 sheets, scale 1:250,000 and 1:63,360.
- Bazzurro, P., and C. A. Cornell (1999). Disaggregation of seismic hazard, *Bull. Seism. Soc. Am.*, Vol. 89, p. 501–520.
- BC Hydro (2012). Probabilistic Seismic Hazard Analysis (PSHA) Model, Engineering Report E658, November, 2012.
- Betka, P.M., R.J. Gillis and J.A. Benowitz (2017). Cenozoic sinistral transpression and polyphase slip within the Bruin Bay fault system, Iniskin-Tuxedni region, Cook Inlet, Alaska, *Geosphere*, Vol. 13, No. 6, p. 1806-1813.

- Boore, D.M. (2010). Orientation-independent, non geometric-mean measures of seismic intensity from two horizontal components of motion, *Bull. Seism. Soc. Am.*, Vol. 100, pp. 1830-1835.
- Boore, D.M, Stewart, J.P., Seyhan, E. and G.M. Atkinson (2014). NGA-West2 equations for predicting PGA, PGV, and 5% damped PSA for shallow crustal earthquakes. *Earthquake Spectra*, Vol. 30, No. 3, p. 1057-1085.
- Bozorgnia, Y., N. Abrahamson, L. Al Atik, T. D. Ancheta, G.M. Atkinson, J.W. Baker, A. Baltay, D.M. Boore, K.W. Campbell, B.S-J. Chiou, R. Darragh, S. Day, J. Donahue, R.W. Graves, N. Gregor, T. Hanks, I.M. Idriss, R. Kamai, T. Kishida, A. Kottke, S.A. Mahin, S. Rezaeian, B. Rowshandel, E. Seyhan, S. Shahi, T. Shantz, W. Silva, P. Spudich, J.P. Stewart, J. Watson-Lamprey, K. Wooddell, R. Youngs (2014). NGA-West2 Research Project, *Earthquake Spectra*, Vol. 30, No. 3, p. 973-987.
- Bozorgnia, Y., T. Kishida, N.A. Abrahamson, S.K. Ahdi, T.D. Ancheta, R.J. Archuleta, G. Atkinson, D.M. Boore, K.W. Campbell, B. Chiou, V. Contreras, R. Darragh, N. Gregor, Z. Gulerce, I.M. Idriss, C. Ji, R. Kamai, N. Kuehn, D.Y. Kwak, A. Kwok, P.S. Lin, H. Magistrale, S. Mazzone, S. Muin, S. Midorikawa, G. Parker, H. Si, W.J. Silva, J.P. Stewart, M. Walling, K.E. Wooddell, and R.R. Youngs (2018). NGA-Subduction Research Program, *Proceedings of the 11th US National Conference on Earthquake Engineering*, Paper 001705, Los Angeles, CA.
- Bozorgnia, Y. and J. P. Stewart (2020). Data Resources for NGA-Subduction Project, PEER Report 2020/02.
- Campbell, K.W. (2020). Proposed Methodology for Estimating the Magnitude at Which Subduction Megathrust Ground Motions and Source Dimensions Exhibit a Break in Magnitude Scaling: Example for 79 Global Subduction Zones, *Earthquake Spectra*, in press.
- Campbell, K.W. and Y. Bozorgnia (2014). NGA-West2 ground motion model for the average horizontal components of PGA, PGV, and 5% damped linear acceleration response spectra. *Earthquake Spectra*, Vol. 30, No. 3, p. 1087-1115.
- Carver, G., J. Sauber, W. Lettis, R. Witter, and B. Whitney (2008). Active Faults on Northeastern Kodiak Island, Alaska, American Geophysical Union, *Active Tectonics and Seismic Potential of Alaska*, Geophysical Monograph Series 179, p. 167-184.
- Chiou, B.S.-J., and R.R. Youngs (2014). Update of the Chiou and Youngs NGA model for the average horizontal component of peak ground motion and response spectra. *Earthquake Spectra*, Vol. 30, No. 3, p. 1117-1153.
- Chiou, B., R. Darragh, N. Gregor and W. Silva (2008). NGA Project Strong-Motion Database, *Earthquake Spectra*, Vol. 24, No. 1, p. 23-44.

- Decker, J., S.C. Bergman, R.B. Blodgett, S.E. Box, T.K. Bundtzen, J.G. Clough, W.L. Coonrad, W.G. Gilbert, M.L. Miller, J.M. Murphy, M.S. Robinson, and W.K. Wallace (1994). Geology of southwestern Alaska, *The Geology of North America, Vol. G-1, The Geology of Alaska*.
- Detterman, R.L.T. Hudson, G. Plakfer, R.G. Tysdal and J.M. Hoare (1976). Reconnaissance Geology Map along Bruin Bay and Lake Clark Faults in Kenai and Tyonek Quadangles, Alaska, USGS Open File Report 76-477.
- Detterman, R.L., and Reed, B.L. (1980). Stratigraphy, structure, and economic geology of the Iliamna Quadrangle, Alaska: U.S. Geological Survey Bulletin 1368-B, 86 p.
- DeMets, C., Gordon, R.G., Argus, D.F., and Stein, S. (1990). Current plate motions: *Geophysical Journal International*, v. 101, no. 2, p. 425–478.
- Doser, D.I., N.A. Ratchkovski, P.J. Haeussler, and R. Saltus (2004). Changes in Crustal Seismic Deformation Rates Associated with the 1964 Great Alaska Earthquake, *Bull. Seism. Soc. Am.*, Vol. 94, No. 1, p. 320-325.
- Earthquake Engineering Research Institute (1989). The basics of seismic risk analysis, *Earthquake Spectra*, Vol. 5, pp. 675–699.
- Elliot, J. and J. Freymueller (2018). Geodetic contributions to the Alaska Hazard Maps: Collaborative Research between the University of Alaska Fairbanks and Purdue University, USGS External Grants, Final Report, https://earthquake.usgs.gov/cfusion/external_grants/reports/G15AP00056.pdf.
- Field, E.H, G.P. Biasi, T.E. Dawson, K.R. Felzer, D.D. Jackson, K.M. Johnson, T.H. Jordan, C. Madden, A.J. Michael, K.R. Milner, M.T. Page, T. Parsons, P.M. Powers, B.E. Shaw, W.R. Thatcher, R.J. Weldon and Y. Zeng (2013). Uniform California Earthquake Rupture Forecast, Version 3 (UCERF3) – The Time-Independent Model, USGS Open File Report 2013-1165.
- Fugro (2012). Seismic Hazard Characterization and Ground Motion Analyses for the Susitna-Watana Dam Site Area, Report prepared for Alaska Energy Authority, February 24, 2012.
- Gardner, J.K. and L. Knopoff (1974). Is the sequence of earthquakes in Southern California with aftershocks removed, Poissonian?, *Bull. Seism. Soc. Am.*, Vol. 64, No. 5, p. 1363-1367.
- Gillis, R. J., D.L. LePain, K.D. Ridgway and E.S. Finzel (2009). A reconnaissance view of an unnamed fault near Capps Glacier, northwestern Cook Inlet Basin, and its potential as a regional-scale, basin-controlling structure, State of Alaska Division of Geological and Geophysical Surveys, Preliminary Interpretive Report 2009-03.
- Hale, C., N. Abrahamson, and Y. Bozorgnia (2018). Probabilistic Seismic Hazard Analysis Code Verification, PEER Report, Pacific Earthquake Engineering Research Center, University of California, Berkeley, California, PEER Report 2018/03.

- Hartstock, J. K. (1954). Geologic map and structure sections of the Iniskin Peninsula and adjacent area of Alaska, U.S. Geological Survey Open File Report 54-118.
- Haeussler, P.J., A. Matmon, D.P. Schwartz and G.G. Seitz (2016). Neotectonics of Interior Alaska and the late Quaternary slip rate along the Denali fault system, *Geosphere*, Vol. 13, No. 5., p. 1445 – 1463.
- Haeussler, P.J., Matmon, A., Schwartz, D.P., Seitz, G. (2014). The Denali fault slip rate and models of interior Alaska active deformation [abs.]: Seismological Society of America Annual Meeting, Anchorage, Alaska, April 30–May 2, 2014, Abstracts with Programs, v. 85, no. 2, p. 474.
- Haeussler, P.J., Bruhn, R.L., and Pratt, T.L. (2000). Potential seismic hazards and tectonics of the upper Cook Inlet basin, Alaska, based on analysis of Pliocene and younger deformation: *Geological Society of America Bulletin*, Vol. 112, No. 9, p. 1,414–1,429.
- Haeussler, P.J., Best, T.C., and Waythomas, C.F. (2002). Paleo- seismology at high latitudes; seismic disturbance of upper Quaternary deposits along the Castle Mountain Fault near Houston, Alaska: *Geological Society of America Bulletin*, Vol. 114, No. 10, p. 1296–1310.
- Haeussler, P. and R.W. Saltus (2004). 26 km of Offset on the Lake Clark Fault Since Late Eocene Time, U.S. Geological Survey Professional Paper 1709-A.
- Haeussler, P. and R.W. Saltus (2011). Location and Extent of Tertiary Structures in Cook Inlet Basin, Alaska, and Mantle Dynamics that Focus Deformation and Subsidence, U.S. Geological Survey, Professional Paper 1776-D.
- Hayes, G. (2018). Slab2 – A Comprehensive Subduction Zone Geometry Model, USGS data release, <https://doi.org/10.5066/F7PV6JNV>.
- Idriss, I.M. (2014). An NGA-West2 empirical model for estimating the horizontal spectral values generated by shallow crustal earthquakes. *Earthquake Spectra*, Vol. 30, No. 3, p. 1155-1177.
- Idriss, I.M., R.J. Archuleta, and N.A. Abrahamson (2018). Engineering Guidelines for the Evaluation of Hydropower Projects, Chapter 13 – Evaluation of Earthquake Ground Motions, Federal Energy Regulatory Commission (FERC), Washington D.C..
- Ktenidou, O.J. and N. A. Abrahamson (2016). Empirical Estimation of High-Frequency Ground Motion on Hard Rock, *Seism. Res. Letters*, Vol. 87, No. 6, p. 1465 – 1478.
- Knight-Piesold Ltd. (2013). Report on Seismicity Assessment and Seismic Design Parameters, Report prepared for Pebble Limited Partnership, August 14, 2013.
- Koehler, R.D. (2010). Technical Review of a Trench Across a Potential Fault Scarp Feature East of Lower Talarik Creek, Lake Iliamna Area, Southwestern Alaska, State of Alaska Division of Geological and Geophysical Surveys, Miscellaneous Publication 139.

- Koehler, R.D. and R.D. Reger (2011). Reconnaissance Evaluation of the Lake Clark Fault, Tyonek Area, Alaska, State of Alaska Division of Geological and Geophysical Surveys, Preliminary Interpretive Report 2011-1.
- Koehler, R.D., R.E. Farrell, P.A.C. Burns and R.A. Combellick (2012). Quaternary Faults and Folds in Alaska: A Digital Database, State of Alaska Division of Geological and Geophysical Surveys, Miscellaneous Publication 141.
- Koehler, R.D., P.A.C. Burns and J.R. Weakland (2013). Digitized Faults of the Neotectonic Map of Alaska (Plafker and Others, 1994), State of Alaska Division of Geological and Geophysical Surveys, Miscellaneous Publication 150.
- Koehler, R.D. and G.A. Carver (2018). Active faulting and seismic hazards in Alaska, State of Alaska Division of Geological and Geophysical Surveys, Miscellaneous Publication 160.
- Kuehn, N., Y. Bozorgnia, K. Campbell, and N. Gregor (2020). Partially Nonergodic Ground-Motion Model for Subduction Regions using the NGA-Subduction Database PEER Report 2020/XX, in press.
- Labay, K. and P.J. Haeussler (2001). GIS Coverages of the Castle Mountain Fault, South Central Alaska, USGS Open File Report 01-504.
- McGuire, R.K. (2004). Seismic Hazard and Risk Analysis, Monograph NMO-10, Earthquake Engineering Research Institute, Oakland, California.
- Parker, G.A., J.P. Stewart, D.M. Boore, G. Atkinson and B. Hassani (2020). NGA-Subduction Global Ground Motion Models with Regional Adjustment Factors, PEER report 2020/XX, in press.
- Parkington, T. (2018). Technical memorandum to Bill Craig, AECOM for the Pebble Project Review of Seismic Hazard Analysis, Letter dated September 17, 2018.
- Pavlis, T.L. and S.M. Roeske (2007). The Border Ranges Fault System, Southern Alaska, Geological Society of America, Special Paper 341.
- Pebble Partnership (2018). The Pebble Project, Project Description, December 2018.
- Plafker, G., R.L. Detterman, and T. Hudson (1975). New Data on Displacement History of the Lake Clark Fault, in Yount, M.E. ed., USGS Alaska Program, USGS Circular 722, p. 44-45.
- Plafker, G., Gilpin, L.M., and Lahr, J.C., (1994). Neotectonic map of Alaska, in Plafker, G., and Berg, H.C., eds., Geology of Alaska, Geology of North America, in Decade of North American Geology: Boulder, Geological Society of America, v. G-1, plate 12, 1 sheet, scale 1:2,500,000.
- Ratchkovski, N.A. and R.A. Hansen (2002). New Evidence for Segmentation of the Alaska Subduction Zone, Bull. Seism. Soc. Am., Vol. 92, No. 5, p. 1754-1765.

- Ruppert, N.A. and R.C. Witter (2020). Preface to the Focus Section on the 30 November 2018 Mw 7.1 Anchorage, Alaska, Earthquake, *Seism. Res. Letters*, Vol. 91, No. 1, p. 16 – 18.
- Sadigh, K., C.Y. Chang, J.A. Egan, F. Makdisi and R.R. Youngs (1997). Attenuation Relationships for Shallow Crustal Earthquakes Based on California Strong Motion Data, *Seism. Res. Letters*, Vol. 68, No. 1, p. 180-189.
- Schmoll, H.R., and Yehle, L.A. (1987). Surficial geologic map of the northwestern quarter of the Tyonek, A-4 Quadrangle, south-central Alaska: U.S. Geological Survey Miscellaneous Field Studies Map, MF-1934, scale 1:31,680, 1 sheet.
- Silwal, V., C. Tape, and A. Lomax (2018). Crustal earthquakes in the Cook Inlet and Susitna region of southern Alaska, *Tectonophysics*, p. 245-263.
- Sipkin, S.A. (2003). A Correction to Body-Wave Magnitude m_b based on Moment Magnitude M_w , *Seism. Res. Letters*, Vol. 74, No. 6, p. 739-742.
- Stevens, D.S.P. and P.A. Crow (2003). Geologic hazards in and near the Northern Portion of the Bristol Bay Basin, Alaska Division of Geological and Geophysical Surveys, Miscellaneous Publication 132.
- Utsu, T. (2002). Relationships between Magnitude Scales, in *International Handbook of Earthquake and Engineering Seismology, Part A*, IASPEI Handbook, edited by Lee, W. H. K., H. Kanamori, P. C. Jennings, and C. Kisslinger, Academic Press, New York, p. 733-746.
- Weichert, D.H. (1980). Estimation of the Earthquake Recurrence Parameters for unequal Observation Periods for Different Magnitude, *Bull. Seism. Soc. Am.*, Vol. 70, No. 4, p. 1337-1346.
- Wells, D.L. and K.J. Coppersmith (1994). New Empirical Relationships Among Magnitude, Rupture Length, Rupture Width, Rupture Area and Surface Displacement, *Bull. Seism. Soc. Am.*, Vol. 84, No. 4, p. 974-1002.
- Wesson, R.L., A.D. Frankel, C.S. Mueller and S. Harmsen (1999). Probabilistic Seismic Hazard Maps of Alaska, USGS Miscellaneous Investigation Series, I-2679.
- Wesson, R.L., O.S. Boyd, C.S. Mueller, C.G. Bufe, A.D. Frankel, and M.D. Petersen (2007). Revision of Time-Independent Probabilistic Seismic Hazard Maps for Alaska, USGS Open File Report 2007-1043.
- Wesson, R.L., O.S. Boyd, C.S. Mueller, and A.D. Frankel (2008). Challenges in Making a Seismic Hazard Map for Alaska and the Aleutians, in *Active Tectonics and Seismic Potential of Alaska*, Geophysical Monograph Series 179, American Geophysical Union.

Willis, J.B., Haeussler, P.J., Bruhn, R.L., and Willis, G.C., (2007). Holocene slip rate for the western segment of the Castle Mountain fault, Alaska, Bull, Seism. Soc. Am., Vol. 97, p. 1019-1024.

Woodward-Clyde Consultants (1978). Offshore Alaska Seismic Exposure Study, Woodward-Clyde Consultants, San Francisco, CA.

Youngs, R.R. and K.J. Coppersmith (1985). Implications of Fault Slip Rates and Earthquake Recurrence Models to Probabilistic Seismic Hazard Estimates, Bull. Seism. Soc. Am., Vol. 75, No. 4, p. 939-964.

Youngs, R., Chiou, S., Silva, W., and Humphrey, J., 1997. Strong ground motion attenuation relationships for subduction zone earthquakes, Seismic Research Letters Vol. 68, p. 58–73.

Appendix A – Modeling the Slab Seismic Source in Southern Alaska for PSHA programs

A-1. Introduction

The project region in Southern Alaska is located in the tectonically active Alaska-Aleutian subduction zone. Historically, seismic events have occurred along the shallow and deep parts of the subduction slab. The characterization of these seismic sources is presented in detail in the main part of this report. Typically for PSHA studies, the interface seismic source zone is geometrically represented by a planar fault source. This is consistent with the understanding of the rupture mechanism of these interface events, which tend to rupture along the subducting plate following the general down dip angle of the plate. However, the typical understanding of the rupture process for the deeper slab events is a normal mechanism event that ruptures through the cross section of the subducting plate rather than along the subducting plate.

Given this difference in the rupture process and the capabilities and limitations of PSHA programs, a wide range in the modeling approaches are currently used in practice. Hale et al. (2018) showed that these different approaches can lead to significant differences in the resulting hazard curves for a simple example. The main cause for these observed differences is in the distance metrics estimated from the different approaches. This is also accentuated given the strong depth dependence contained in slab ground motion models. This appendix summarizes the different approaches described in Hale et al. (2018) and also compares and discusses the approach used in this PSHA study and the USGS approach (Wesson et al., 2007), which was also applied in the Knight-Piesold (2013) study.

A-2. Slab Seismic Source Modeling Approaches

Given the current suite of available PSHA programs, four basic approaches are used for the modeling of slab subduction seismic sources. These are illustrated in Figure A-1 (from Hale et al., 2018). In approach (a) the slab source is modeled with multiple sub-source areal sources, each with a point source representation within a given areal sub-source. Together the collection of areal sub-sources attempts to represent the geometry of the subduction slab by varying the depth of these sources following the subducting plate geometry. The next approach (b) is similar to the representation for the shallower interface sources in which a planar fault source is used. This fault source can be assigned with the upper, middle (as shown in Figure A-1), or bottom part of the subduction slab. For the third approach (c), virtual faults are placed within the subducting slab to represent cross sections of the plate. Earthquakes are then defined on these virtual faults and this is the approach used in this current seismic hazard study. Finally, the last approach (d) is a variation on the first approach where the areal sub-source zones are represented by virtual faults centered on the point source locations within each area sub-zone.

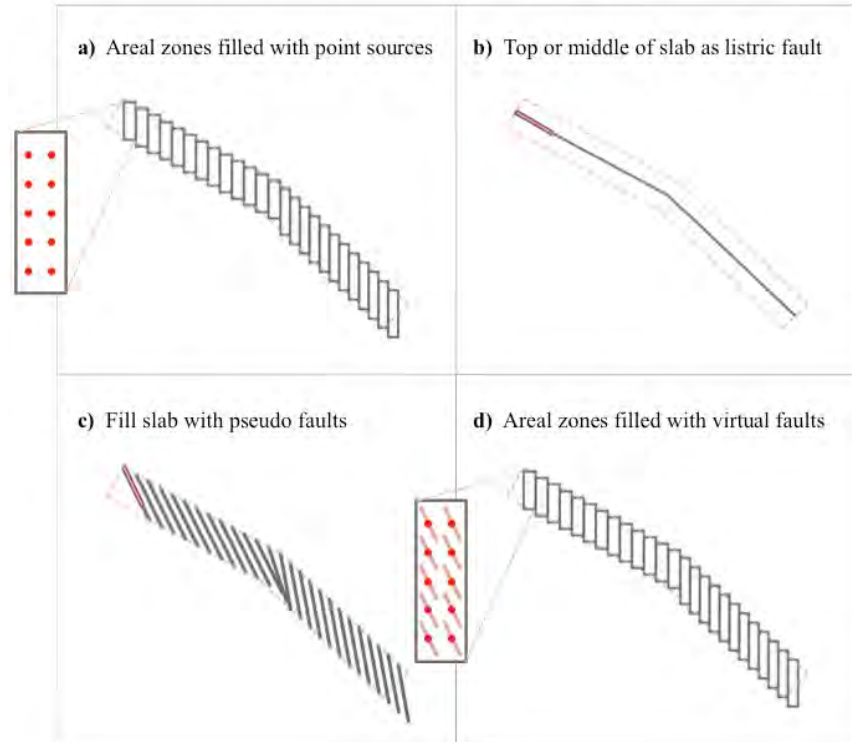


Figure A-1. Four representative approaches for the modeling of slab events in PSHA programs (Source: Hale et al., 2018).

Given these four modeling approaches, a simple example calculation using the same GMM model and with a **M**6.5 characteristic event assigned to the slab source was performed as part of the Hale et al. (2018) study. Three PSHA programs computed a hazard curve for approach (a), two for approach (b), seven for approach (c) and two for approach (d). The results of these calculations are shown in Figure A-2. As noted in Hale et al. (2018) a comparison of the results for a given approach (i.e., (a) through (d)) was favorable with differences between the results from different PSHA programs within 5%. However, it is observed in Figure A-2 and noted in Hale et al. (2018), that the differences in approach (a) relative to the other three approaches are more significant and lower than the other three approaches which are similar. Given that these differences are understood to be caused mainly by the different distance metrics computed using point sources (i.e., approach (a)) rather than virtual faults, it is expected that these differences would potentially increase for larger magnitudes given their larger rupture area and hence extended fault ruptures when compared to a point source. As is noted for the Hale et al. (2018) example calculation, the characteristic magnitude assigned to the sources was 6.5 whereas for this seismic hazard study the maximum magnitude assigned for the slab source is 7.5 and 8.0 and the differences observed in the Hale et al. (2018) example can be expected to be larger for this current study given the larger maximum magnitudes.

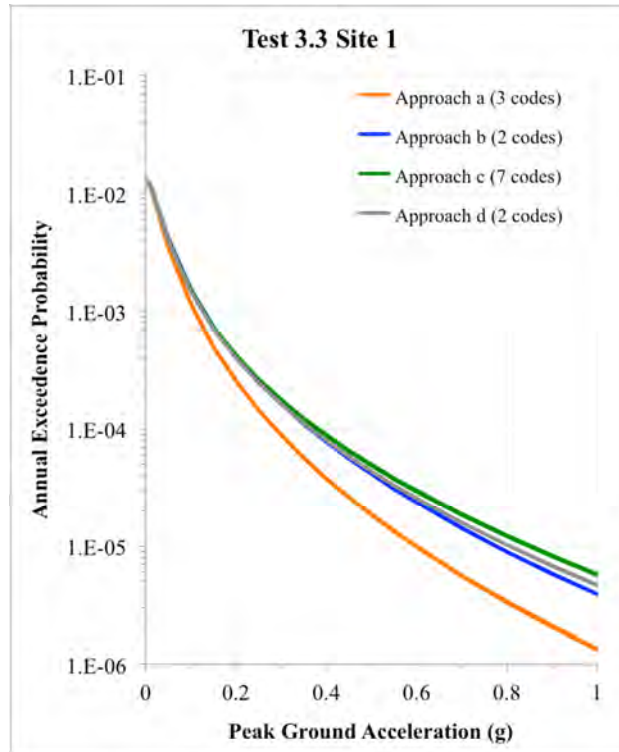
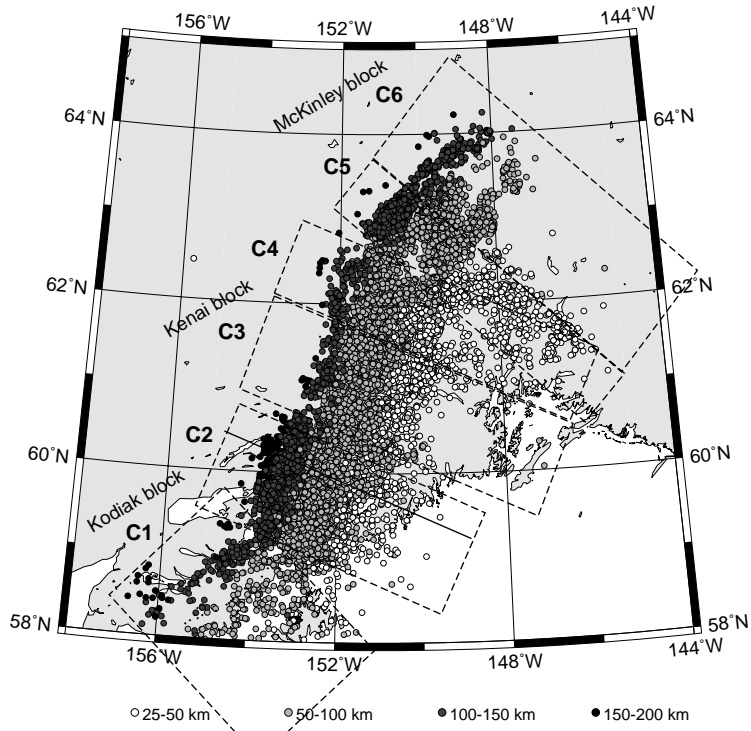


Figure A-2. Comparison of hazard curves from the four different slab modeling approaches presented in Hale et al. (2018). (Source: Hale et al., 2018).

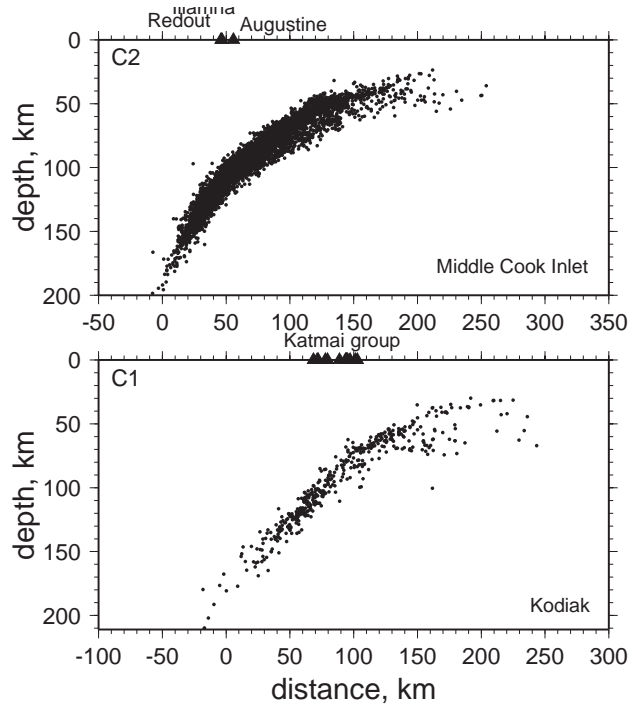
A-2. Application for Southern Alaska

The slab seismic source is shown in the main report to be the controlling seismic source from the PSHA calculations for high to intermediate spectral periods. For longer spectral periods, this slab source still contributes, but is equal in its contribution to the interface source. Thus, given its importance, the approach used in modeling the slab source can have strong impacts on the ground motions, especially given the sensitivity results presented in Hale et al. (2018).

The subduction slab associated with the Alaska-Aleutian subduction zone in the project region is a highly active seismic source with slab events occurring down to a depth of approximately 200 km which is about 30 km east of the project site locations. Ratchkovski and Hasen (2002) performed an earthquake relocation methodology in the region which allows for the image of the subducting slab as shown in Figure A-3. These relocated events in cross section C1 and C2 are the closest to the Pebble project site.



(a)



(b)

Figure A-3. Relocated earthquakes from Ratchkovski and Hansen (2002) shown in map view (a) and cross sections closest to the project site (b).

For the SSC model developed in this SHA study, virtual vertically dipping faults are placed at a series of depths ranging from 50 km to 200 km, every 25 km. This follows approach (c) from Hale et al. (2018). These virtual fault traces for the different depth range values are based on the depth contours of the subduction slab global model Version 2.0 (Hayes, 2018). The fault thickness is assumed to be 20 +/- 5 km to represent the thickness of the subducting plate given the cross sections from Ratchkovsi and Hansen (2002) shown in Figure A-3. These virtual faults are plotted in Figures A-4 through A-6 along with the project seismicity catalog for three depth ranges: 50 – 100 km (Figure A-4), 100 – 150 km (Figure A-5) and 150 – 250 km (Figure A-6). One feature observed with the seismicity associated with the slab events is a non-uniform spatial distribution of events. To capture this feature in the SSC model, the seismicity catalog is separated first by the three depth ranges. Next within a given depth range, subsections of seismicity based on the observed spatial distribution is selected. For the shallowest depth range of 50 – 100 km there are three selected subsections: SW, Central, and NE. The associated events with each of these subsections are plotted in Figure A-4 with different colors.

For the next depth range, a total of six subsections are selected starting with SW01 at the southwestern end of the source through SW06 at the northeastern end of the source. This depth range shows a larger variability in the spatial distribution of events than the previous shallower depth range. The seismicity associated with the six different subsections are indicated in Figure A-5 with the different colors. Finally in Figure A-6, the seismicity from the deepest depth range of 150 – 250 km is plotted in separate colors indicating the three subsections, SW, Central, and NE.

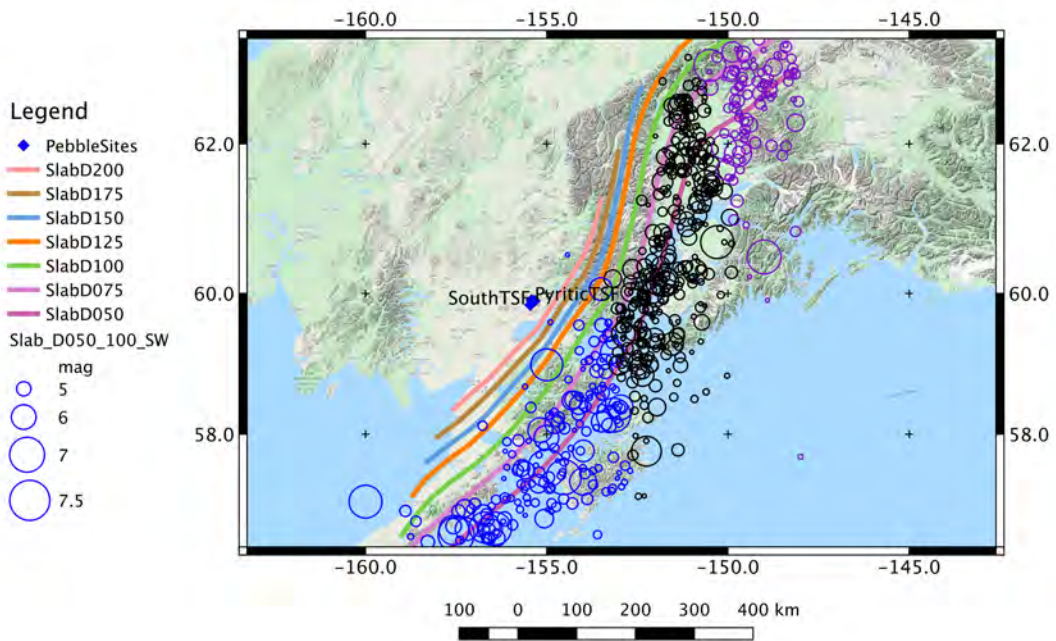


Figure A-4. Virtual slab faults and seismicity from the project catalog for events in the depth range of 50 – 100 km with color symbols separated based on geographical grouping.

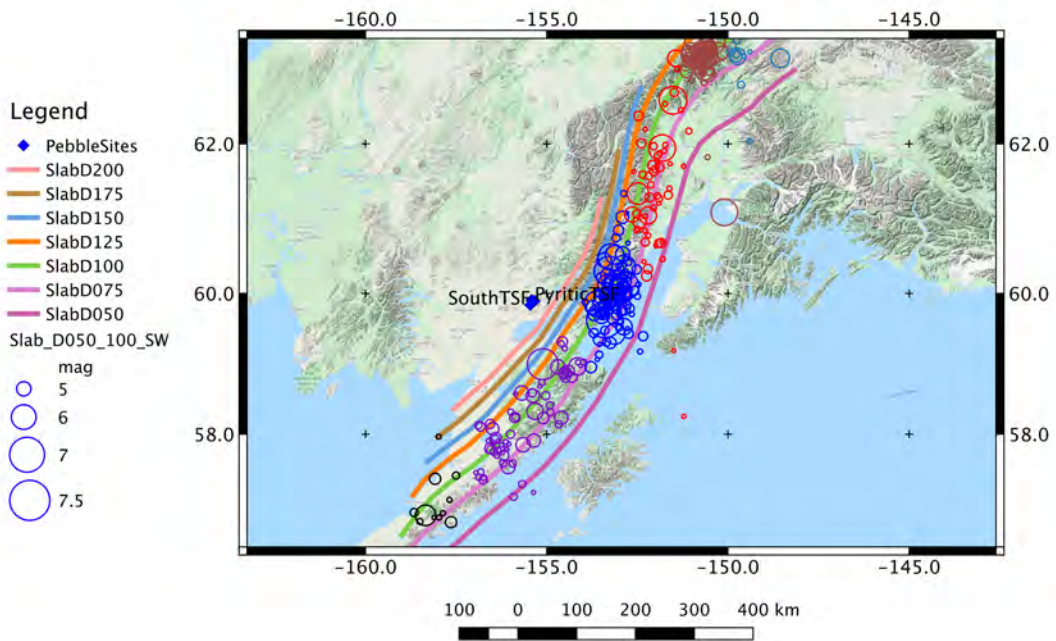


Figure A-5. Virtual slab faults and seismicity from the project catalog for events in the depth range of 100 – 150 km with color symbols separated based on geographical grouping.

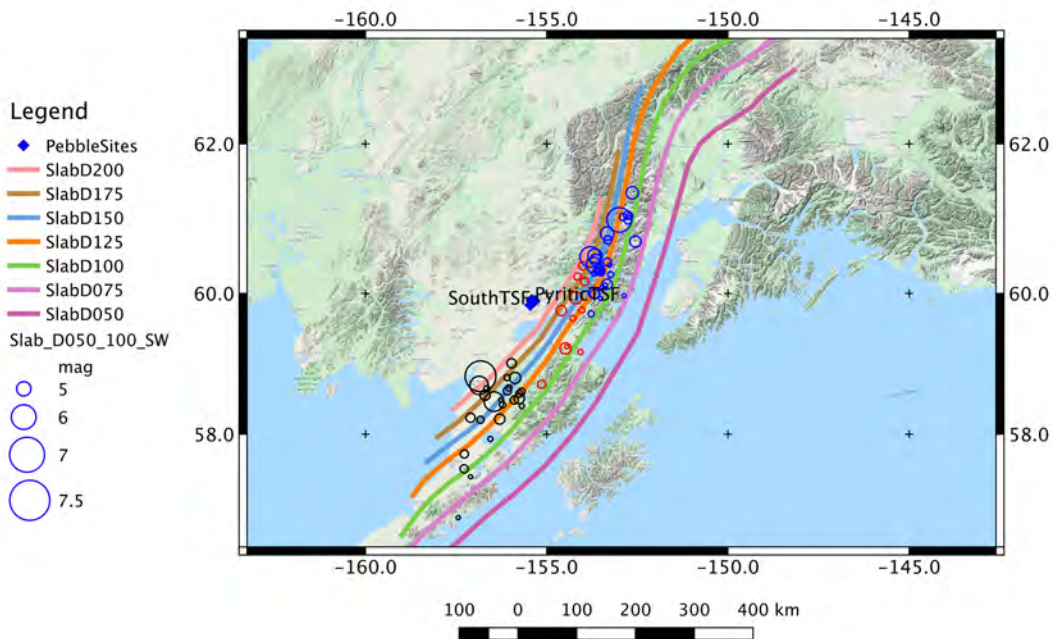


Figure A-6. Virtual slab faults and seismicity from the project catalog for events in the depth range of 150 – 250 km with color symbols separated based on geographical grouping.

For the current SSC model, earthquake recurrence rates are estimated following the Weichert (1980) approach using the project earthquake catalog separated by depth and an additional selection criterion of having events located within the longitudes of -148 to -160 degrees. Although events outside of these longitudes are observed, their greater distance from the project site locations does not necessitate their inclusion for the SSC model development.

Recurrence parameters are estimated for the three specific depth ranges of 50 – 100 km, 100 – 150 km, and 150 – 250 km based on the sorted earthquake catalog. Based on these estimated recurrence parameters, the activity rates for a given depth range were assigned to the corresponding virtual fault and partitioned based on the respective fault lengths for the associated depth range and number of events in each sub-source.

In contrast to the modeling approach used in this SHA study, the USGS modeling (Wesson et al., 2007), which was also used in the Knight-Piesold (2013) study, was a variation and simplification of approach (a) presented in Hale et al. (2018). Rather than model the subducting slab with sub-areal source zones, two regional areal source zones were developed for the depth ranges of 50 – 80 km and 80 – 120 km. Thus, the deeper part of the slab is not being modeled

within the USGS approach nor is the deepening of the slab in a northwesterly direction (i.e., toward the project sites) being directly modeled. This two-layer approximation is a simplified representation of the true geometry of the subducting slab in the region of Southern Alaska.

Within each of these two depth ranges, the seismicity catalog was processed to compute a smoothed grid of activity rates based on a 0.1x0.1 degree grid point spacing. The smoothing distance was 70 km (Wesson et al. 2007). Following this smoothing approach, the activity rate distribution is not uniform and more closely follows the historical seismicity in a similar approach that is implemented for this study.

The normalized activity rates for the two USGS grid files are plotted in Figure A-7 (50 – 80 km depth) and Figure A-8 (80 – 120 km). Also plotted are the virtual slab faults from the current SSC model. The shallow layer was placed at a depth of 60 km and the deeper depth at 90 km in the USGS analysis.

Based on a visual comparison of the normalized activity rates in Figure A-7 and the virtual slab faults which correlate with the top of the subducting plate, the highest activity from the USGS model is located slightly east of the 50 km depth virtual fault. This is assumed to be an artifact of the smoothing process implemented in the USGS methodology and the historical seismicity location distributions shown in Figure A-4. However, this relative eastern shift would result in lower ground motions at the project site locations given the larger distances from the sites to the source.

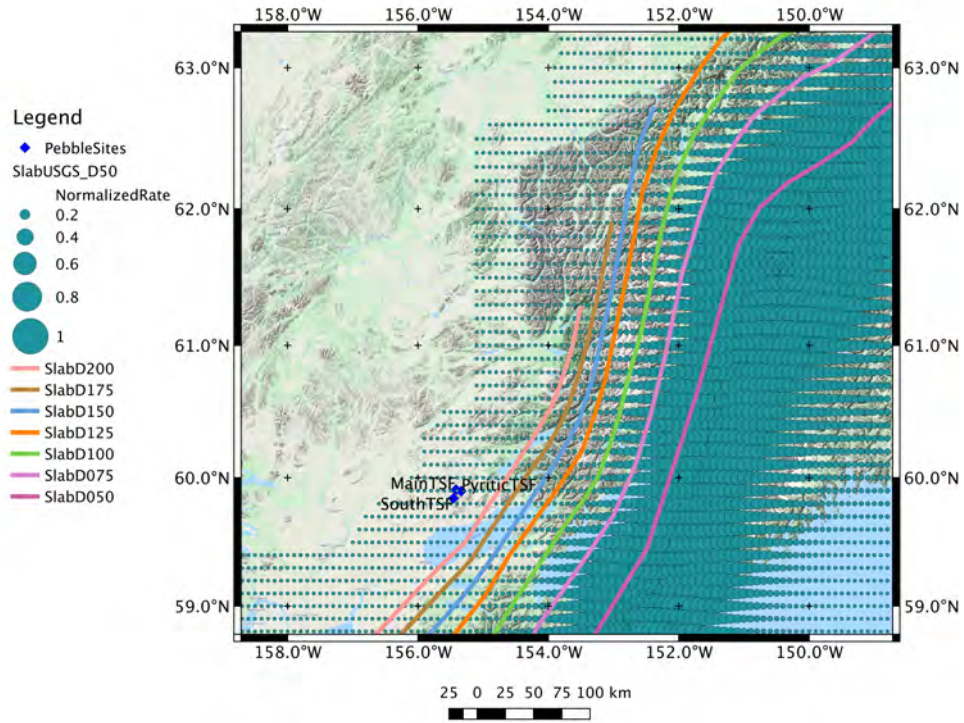


Figure A-7. Virtual slab faults and normalized seismicity activity rates from the USGS source model for events in the 50 – 80 km depth range.

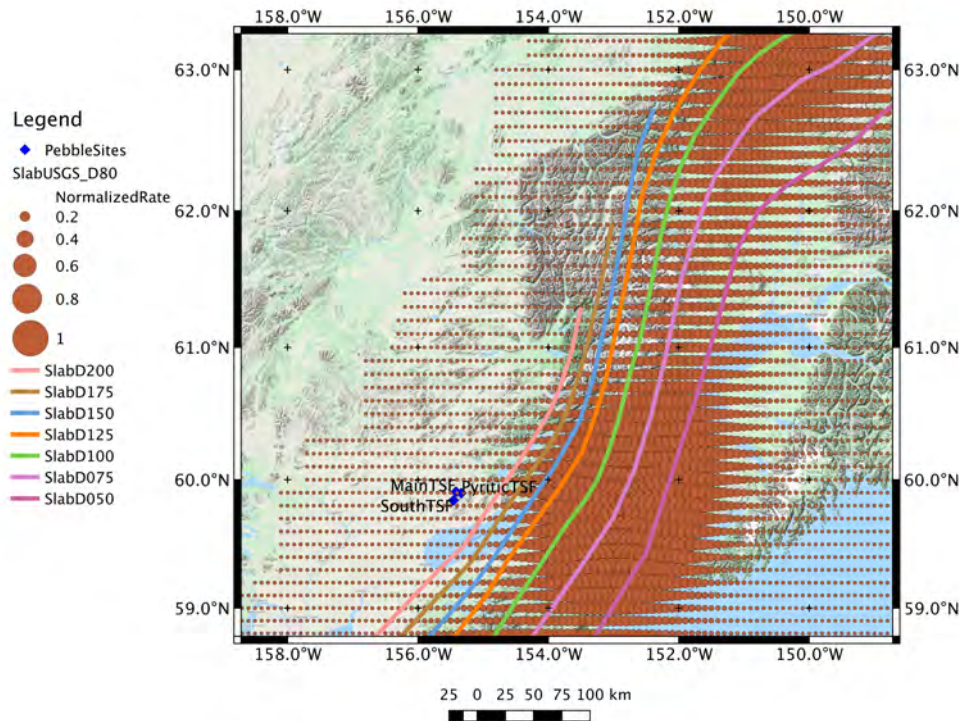


Figure A-8. Virtual slab faults and normalized seismicity activity rates from the USGS source model for events in the 80 – 120 km depth range.

For the deeper layer (80 – 120 km) there is a strong concentration of normalized activity rates east of the project site locations. This is in agreement with the observed seismicity shown in Figure A-5. However, similar to the previous shallow layer, the concentration of the normalized activity rates for the depth range of 80 – 120 km is slightly east of the faults associated with the 75 – 125 km depths. This observed shift would also have the expected impact of producing lower ground motions at the project site locations from the USGS model based on the larger separation distance. In addition, the depth of this layer was placed at 90 km and given the strong correlation of increasing ground motions as a function of depth, this shallower assigned depth would also be expected to cause lower ground motions at the project site location.

Given these noted differences and the expected differences based on the implementation and representation of the slab within a PSHA program (Hale et al., 2018), it is expected that the contribution from the slab sources from the current SSC model would be greater than the simplified model used by the USGS. However, given the observations and recommendations from Hale et al. (2018) for the modeling of slab sources, the current model, which follows approach (c), provides a better representation than the USGS model, which follows a variation of approach (a) from Hale et al. (2018). These differences in the implementation choices used in the two seismic hazard studies, indicates that the lower calculated ground motions from the Knight-Piesold (2013) study compared to the current study can be attributable to the

implementation methodology used for the slab seismic source and the inherent bias introduced by that representation.

A-3. References

- Hale, C., N. Abrahamson, and Y. Bozorgnia (2018). Probabilistic Seismic Hazard Analysis Code Verification, PEER Report, Pacific Earthquake Engineering Research Center, University of California, Berkeley, California, PEER Report 2018/03.
- Hayes, G. (2018). Slab2 – A Comprehensive Subduction Zone Geometry Model, USGS data release, <https://doi.org/10.5066/F7PV6JNV>.
- Knight-Piesold Ltd. (2013). Report on Seismicity Assessment and Seismic Design Parameters, Report prepared for Pebble Limited Partnership, August 14, 2013.
- Ratchkovski, N.A. and R.A. Hansen (2002). New Evidence for Segmentation of the Alaska Subduction Zone, *Bull. Seism. Soc. Am.*, Vol. 92, No. 5, p. 1754-1765.
- Weichert, D.H. (1980). Estimation of the Earthquake Recurrence Parameters for unequal Observation Periods for Different Magnitude, *Bull. Seism. Soc. Am.*, Vol. 70, No. 4, p. 1337-1346.
- Wesson, R.L., O.S. Boyd, C.S. Mueller, C.G. Bufe, A.D. Frankel, and M.D. Petersen (2007). Revision of Time-Independent Probabilistic Seismic Hazard Maps for Alaska, USGS Open File Report 2007-1043.

Dr. Thomas O'Rourke and Dr. Izzat M. Idriss, "Seismic Hazard and Stability Analysis Peer Review" (June 2020), with Curricula Vitae

EXHIBIT C

I. M. Idriss
Consulting Geotechnical Engineer
PO Box 32027
Santa Fe, New Mexico 87594
Cell: (505) 231-3111
email: imidriss@aol.com

T. D. O'Rourke
Geotechnical Consultant
10 Twin Glens Road
Ithaca, New York 14850
Cell: (607) 227-0644
email: tdo1@cornell.edu

June 19, 2020

Bristol Bay Reserve Association
Fishermen's Center Bldg.
1900 W. Nickerson, Ste. 320
Seattle, WA 98199

Gentlemen:

Subject: *Review of Seismic Hazard Studies*
Pebble Mine Project

1.0 INTRODUCTION

The purpose of this report is to summarize our review of seismic hazard reports relevant to the Pebble Mine Project currently under review by the U.S. Army Corps of Engineers (USACE) and other state, federal, and tribal entities. Initially, the following two documents were provided to us for this purpose:

- "Seismic Hazard Analysis for the Pebble Mine Project, Southwest Alaska (rev. 001d)", prepared by Dr. Nick Gregor and Dr. Linda Al Atik for K & L Gates, dated May 20,2020. For ease of reference, this report will be referenced as "2020 SHA Report".
- "Report on Seismicity Assessment and Seismic Design Parameters", prepared by Knight Piésold Ltd., Vancouver, Canada, for Pebble Limited Partnership, dated August 14, 2013. For ease of reference, this report will be referenced as "2013 KP Report".

We summarized the review of the 2020 SHA Report and the comparison with the results contained in the 2013 KP Report in a draft report that was submitted on June 5, 2020. Later that day, we received a file named "RFI 008g.pdf", which we were informed had been recently uploaded to the ACOE Website. File RFI 008g contains the two documents listed below:

- Report titled "Report on Seismicity Assessment and Seismic Design Parameters", prepared by Knight Piésold Ltd., Vancouver, Canada, for Pebble Limited Partnership, dated July 4, 2019. For ease of reference, this report will be referenced as "2019 KP Report".
- Memorandum covering "Main Embankment Stability Assessment – Static and Post-liquefaction", prepared by Knight Piésold Ltd., Vancouver, Canada, for Pebble Limited Partnership, dated July 8, 2019.

Our review of the 2019 KP Report, which is an update of the 2013 KP Report, is presented in Appendix A of this Report. Our review of the stability-assessment Memorandum is provided in a separate report.

Our review comments, observations, conclusions and recommendations are provided in this report, and cover the following topics:

- Seismic sources
- Earthquake ground motions models (GMMs)
- Probabilistic seismic hazard analysis (PSHA)
- Deterministic seismic hazard analysis (DSHA)
- Volcanism

We believe that Dr. Gregor and Dr. Al Atik have prepared a comprehensive report that provides seismic hazard results based on the current state of the art in completing such studies. The results of their report can be used to establish target earthquake ground motions for evaluating the seismic performance of all the components of the Pebble Mine.

Furthermore, we believe that the 2020 SHA Report supersedes both the 2013 and 2019 KP Reports for the following reasons:

- The assessment of the seismic sources in the 2020 SHA Report is more complete.
- The 2020 SHA Report includes up to date assignment of maximum magnitude, rupture distance, hypocentral distance and hypocentral depth for each seismic source. The 2013 and the 2019 KP Reports assigned same magnitudes to these sources, but chose to use epicentral distance¹ for the seismic characterization, which is inconsistent of how distance is defined in the earthquake ground motion models GMM used in the KP Reports.
- The 2020 SHA Report used the most currently available and applicable GMMs. The 2013 and the 2019 KP Reports used a number of GMMs that are out of date and not in use.
- The 2020 SHA Report placed no limitation on the maximum magnitude to use for calculating the spectral values for an earthquake occurring on the interplate. Both KP Reports used $M = 8.5$ to represent an $M = 9.2$ event. While this limitation had no effect of the selection of a "design" spectrum, it does reflect on the adequacy of the approach adopted for assessing the seismic hazard at this site.

Accordingly, we recommend that only the results of the probabilistic and deterministic hazard analyses included in the 2020 SHA Report be used for this project. The results presented in the 2013 and the 2019 KP Reports should not be used for this site.

2.0 SEISMIC SOURCES

The seismic sources identified in the 2020 SHA Report include crustal faults, interplate and intraslab subduction sources. The maximum magnitude, degree of activity, recurrence relationship, geometry, and other seismological parameters have been reasonably identified and the values assigned to each are appropriate.

The 2013 KP Report identified the same sources and included, in addition, a "background earthquake". Background earthquakes are often assigned to cover uncertainty associated with faults that may be present

¹ Epicentral distance, which represents a point on the earth's surface directly above what is considered to have been the initiating of the earthquake, which is defined as the hypocenter of the earthquake, has not been used in deriving earthquake ground motion models (GMMs) for several decades. Thus, although Knight Piésold use epicentral distance for the seismic source, the earthquake ground motions models selected by them use rupture distance and not epicentral distance.

at or near the site, but leave no surface expression and thus are assigned lower magnitudes, consistent with the absence of surface faulting. This background earthquake was assigned $M_w = 6.5$ in the 2013 KP Report.

The 2020 SHA Report calculated spectral values at the following three locations:

Tailings Storage Facility (TSF)	Latitude (N) – degrees	Longitude (W) – degrees
Main	59.908	155.417
Pyritic (Area E)	59.897	155.336
South	59.841	155.457

The 2013 KP Report calculated spectral values at a location at the mine site at Latitude 59.9 degrees north and Longitude 155.3 degrees west. This location is approximately 0.4 km north and 2 km east of the location at the Pyritic TSF considered in the 2020 SHA Report.

Both reports assigned a magnitude 9.2² earthquake to the interplate source and a magnitude 8 earthquake to the deep intraslab source. The key crustal source described in both reports is the Lake Clark fault; the 2013 KP Report assigns a magnitude 7.5 earthquake while the 2020 SHA Report assigns a magnitude 7.6 to this fault.

The 2013 KP Report used an epicentral³ distance of 120 miles (192 km) for the interplate earthquake and an epicentral distance of 50 miles (80 km) and a depth of 80 miles (128 km) to the deep intraslab earthquake. The 2020 SHA Report used a rupture distance of 222 km for the interplate earthquake and a hypocentral distance of 150 km and a depth of 135 km for the deep intraslab earthquake

There are two additional points to be addressed regarding the crustal source: (i) can this source be closer to the mine site; and (ii) should the Lake Clark fault be considered an extension of the Castle Mountain fault?

Regarding (i), the 2020 SHA Report states in page 16 that:

" ... we model the terminus of the Lake Clark fault at the southwest end of Lake Clark, consistent with the findings from Haeussler and Saltus (2004). ... future studies which would potentially extend this western terminus of the Lake Clark fault could impact the hazard results provided in this study, and we recommend that a re-analysis be performed in the future based on any updated characterizations of the Lake Clark fault."

It is also noteworthy that Knight Piésold had hypothesized an extension of the Lake Clark fault to place it as close as 7.5 miles (12 km) from the site, but indicated (in page 9 of the 2013 KP Report) that: *"Studies to examine the possible extent and alignment of the Lake Clark fault in the vicinity of the mine study area are ongoing."* It is not clear if such studies had continued beyond 2013 and, if continued, what the findings have been.

Regarding (ii), the information in Figure A below suggests that these two faults be considered as a single source. The 2020 SHA Report indicates that the Castle Mountain fault has a strike slip mechanism and that the Lake Clark fault has a reverse mechanism. The 2013 PK Report suggests that the two faults have the same mechanism.

² While the 2013 KP Report assigned $M = 9.2$ to the interplate source, page 17 of the report states: *"It should be noted that the level of ground shaking from a great earthquake of Magnitude 9+ is likely to be no larger than that from an event of about Magnitude 8 to 8.5."* Table 3-3 shows that $M = 8.5$ was used for calculating the earthquake ground motions

³ See footnote No. 1.

The discussion in the 2020 SHA Report provides reasonable support for treating them as separate sources. We concur with that discussion and with the conclusion, but note that future investigations may support a location closer to the mine site as well as considering the two faults as a single source.

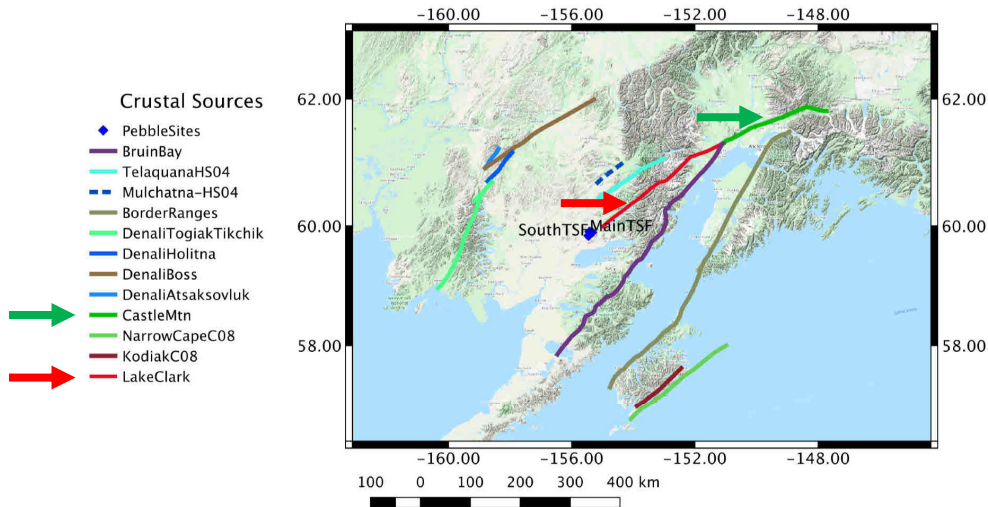


Figure 10. Characterized crustal fault used in the SHA.

**Figure A Crustal faults identified in the 2020 SHA Report
[Figure 10 in the 2020 SHA Report]**

3.0 EARTHQUAKE GROUND MOTIONS MODELS

The 2020 SHA Report used the NGA West2 earthquake ground motion models (GMMs) for crustal events, and the 2016 BC Hydro GMM for the subduction events for both the PSHA and the DSHA. For the PSHA, the NGA Subduction GMM recently developed by Kuehn et al. (2020) was also used; this GMM was assigned a weight of only 0.15 while the BC Hydro GMM was given a weight of 0.85. We concur with these selections.

The 2013 KP Report used the NGA West1 GMMs for the crustal events and the 1997 Youngs et al. GMM and the 2003 Atkinson and Boore GMM for the subduction events. Both the crustal and subduction GMMs have been superseded and neither set is currently in use.

4.0 PROBABILISTIC SEISMIC HAZARD ANALYSIS (PSHA)

The 2020 SHA Report calculated seismic hazard results for mean annual frequency of exceedance (MAFE) as low as 10^{-4} , which corresponds to a return period of about 10000 years. The report also provides uniform hazard spectra (UHS) for average return periods of 475, 1000, 2475, 5000 and 10000 years. The largest contribution to the seismic hazard, by far, is the Intraslab source, which contributed about 84% to the spectral values for spectral periods, $T \leq 1$ second and at average return periods, $ARP \geq 1000$ years.

The 2013 KP Report did not include a site specific probabilistic seismic hazard analysis. Instead, the United States Geological Survey (USGS) web site was used to obtain spectral values for a number of average return periods. The 2020 SHA Report shows a comparison of the PGA calculated in 2020 at the location of the

Main TSF and those included in the 2013 PK Report for average return periods of 475, 1000, 2475, 5000 and 10000 years; the ratio of the 2020 PGA divided by the 2013 PGA ranges from about 1.82 to 1.89.

The Pyritic TSF is the closest to the location used in the 2013 study. The values of PGA calculated at this location are listed below:

ARP* (years)	2020 PGA** (g)	2013 PGA*** (g)	Ratio: 2020/2013
475	0.2729	0.14	1.95
1000	0.3555	0.19	1.87
2475	0.4828	0.25	1.93
5000	0.5949	0.31	1.92
10000	0.7273	0.38	1.91

* Average return period; ** from Table 11 in the 2020 SHA Report; *** from Table 3.1 in the 2013 KP Report

The ratio at the Pyritic TSF location is comparable to the ratio obtained at the Main TSF location, but somewhat larger, ranging from about 1.87 to 1.95.

It is our experience that, while valuable for comparison purposes, the results obtained from the USGS website should not be used for design purposes for any critical structure. Our experience at other sites within the USA indicates that the results obtained from the USGS web site show comparatively high variability and provide spectral values: (i) somewhat larger than the results from a true site specific PSHA (such as that included in the 2020 SHA Report); (ii) about the same as the site specific PSHA; or (iii) smaller (sometimes significantly smaller, such as the case for this site as outlined above). It is emphasized that a true site specific PSHA is necessary for a critical project. A site specific PSHA was not provided in the Knight Piésold's reports.

5.0 DETERMINISTIC SEISMIC HAZARD ANALYSIS (DSHA)

Figure 66 in the 2020 SHA Report, part (a) of which is presented below in Figure B, presents the following spectra at the location of the Pyritic TSF:

- The 2020 UHS having average return periods 2475, 5000 and 10000 years.
- The deterministic 2020 84th-percentile spectra for the crustal events, the deep Intraslab event (depth = 125 km), the shallower Intraslab event (depth = 100 km), and the Interface event.
- The deterministic 84th-percentile spectra included in the 2013 KP Report for the Interface, Intraslab, crustal and background sources.

The deterministic 84th-percentile spectrum for the deep Intraslab event (depth = 125 km) for periods, $T \leq 2$ sec, and that for the crustal event for periods, $T > 2$ sec, are the largest spectra calculated in 2020. The 2013 spectrum for the background source is larger than either of the latter spectra for periods longer than about 0.15 sec. As listed in Table 3.3 in the 2013 KP Report, the magnitude of this background event is 6.5. The duration of the motions associated with either the 2020 crustal event ($M = 7.6$) or the Intraslab event ($M = 8$) are sufficiently longer than the duration of the 2013 background event ($M = 6.5$) that the 2020 events, particularly the Intraslab event, would control the design.

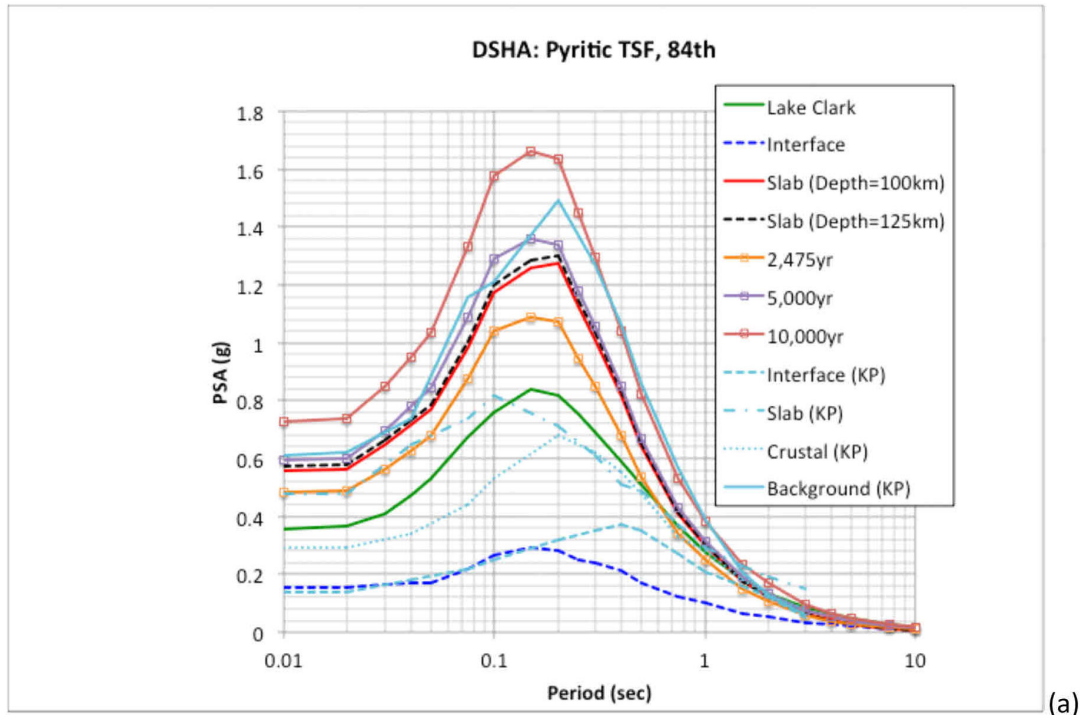


Figure 66. 84th percentile DSHA scenario events (Pyritic TSF) spectra from the Knight-Piesold (2013) study and the current study plotted log-linear (a)

Figure B Spectra calculated in 2020 and those calculated in 2013 at the location of the Pyritic TSF [Part (a) of Figure 66 in the 2020 SHA Report]

The duration of shaking is very important because longer durations of ground motion at comparable accelerations will cause greater damage, especially for earth structures. For example, in assessing the potential for triggering liquefaction, a magnitude scaling factor (MSF) is used to reflect the effect of duration and to act as an equalizer between two events having different magnitudes. The most recent reference⁴ on this issue has shown that MSF is not only a function of earthquake magnitude, but also depends on denseness of the soil being evaluated. For a medium dense sandy soil, having relative density of about 60%, this reference indicates that $MSF \approx 1.2$ for $M = 6.5$ and $MSF \approx 0.92$ for $M = 8$. Thus, for a magnitude 6.5 earthquake, it would require a $PGA = 1.2/0.92 \approx 1.3$ times the PGA for a magnitude 8 earthquake to trigger liquefaction in this medium dense sandy soil. This would indicate that the PGA associated with the background earthquake used in the 2013 PK Report is equivalent to having a magnitude 8 earthquake with a $PGA = 0.61/1.3 \approx 0.468$ g, which is significantly smaller than the PGA (0.574 g) reported in the 2020 SHA Report for the Intraslab event.

Not only is liquefaction triggered at lower acceleration levels for the deep Intraslab event, but the consequences of liquefaction in the form of ground deformation affecting TSF embankments and other mining facilities will be substantially more critical.

⁴ Boulanger, R. W. and Idriss, I. M. (2014). "CPT and SPT Based Liquefaction Triggering Procedures", Report No. UCD/CGM-14/01, Department of Civil & Environmental Engineering, College of Engineering, University of California at Davis, April.

Liquefaction triggering and ensuing ground deformation are important issues that need to be part of the assessment of the proposed Pebble Mine site, lifelines, and port facilities. This issue is addressed further in our report covering our review of the aforementioned stability-assessment Memorandum by KP.

The two 2020 spectra identified above are presented in Figure C for the site of the Pyritic TSF. The spectrum for the deep Intraslab event (depth = 125 km)⁵ is significantly larger than the spectrum for the crustal events for periods shorter than about one second. The spectrum for the crustal event is significantly larger than that for the deep intraslab event for periods longer than about 3 sec. The latter difference could be easily accommodated in the analyses by adjusting the spectrum-compatible time histories that will need to be constructed when evaluating the seismic performance of the various TSFs.

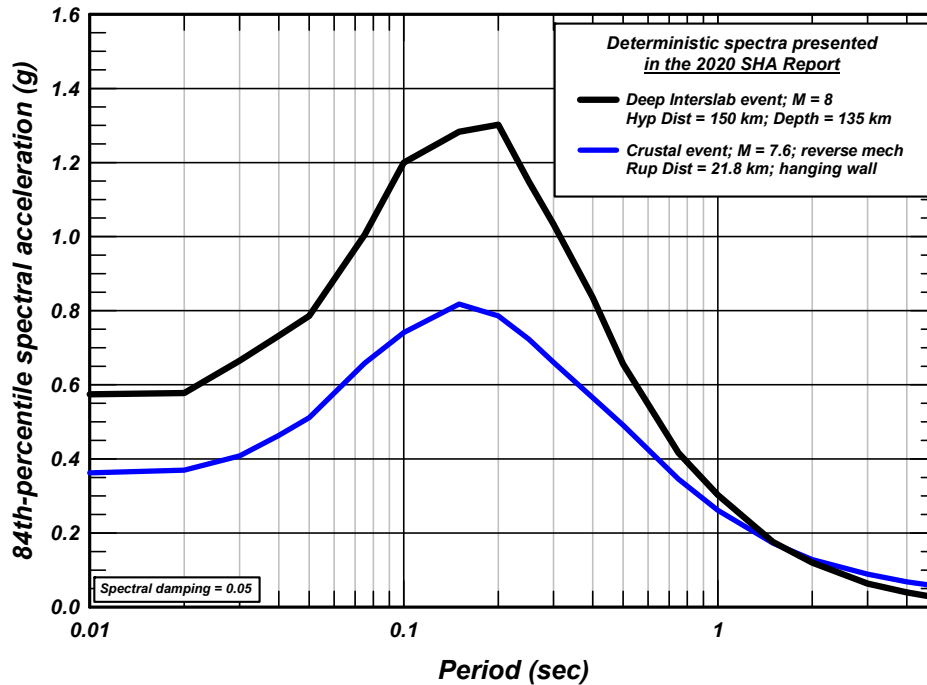


Figure C The 84th-percentile spectra calculated

Finally, it is useful to compare the results of the DSHA for the three sites considered in the 2020 SHA Report. The three spectra for the crustal event are shown in Figure D, and those for the deep Intraslab event are presented in Figure E. The largest spectrum for the crustal event is obtained at the location of the Pyritic TSF and the lowest at the South TSF. The spectra for the deep Intraslab event (Depth = 125 km) are essentially the same; the spectrum at the location of the Pyritic TSF has the largest values. Given the larger spectral values for both the deep Intraslab and crustal events, we suggest that the spectrum calculated for the Pyritic TSF be used as the unified design spectrum for all three sites.

⁵ The actual depth for this event, as listed in Table 19 in the 2020 SHA Report, is 135 km. The figures in the report designate this event with "Depth = 125 km", as shown in Figure B (Figure 66 in the 2020 SHA Report). It should be noted that the hypocentral depth used in the BC Hydro GMM is equal to "min[actual depth, 120 km]", that is, the value of the depth parameter used in the BC Hydro model is the actual depth or 120 km, whichever is smaller. Thus, if the actual depth is 90 km, the value used in the computation is 90 km, but if the actual depth is 135 km, then a value of 120 km is used in the calculation.

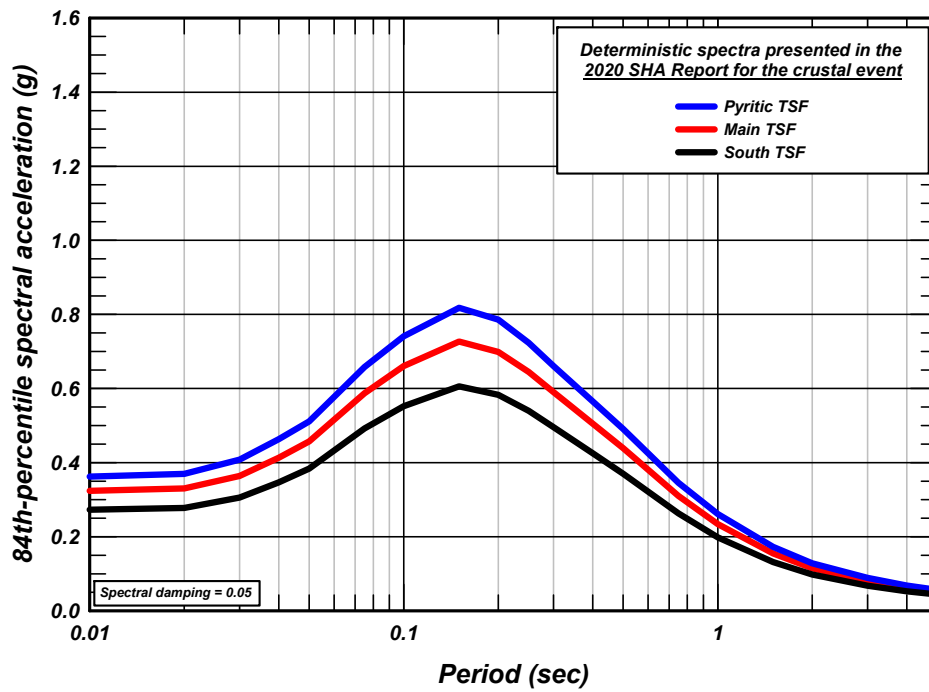


Figure D The 84th-percentile spectra for the crustal event calculated at the locations of each TSF

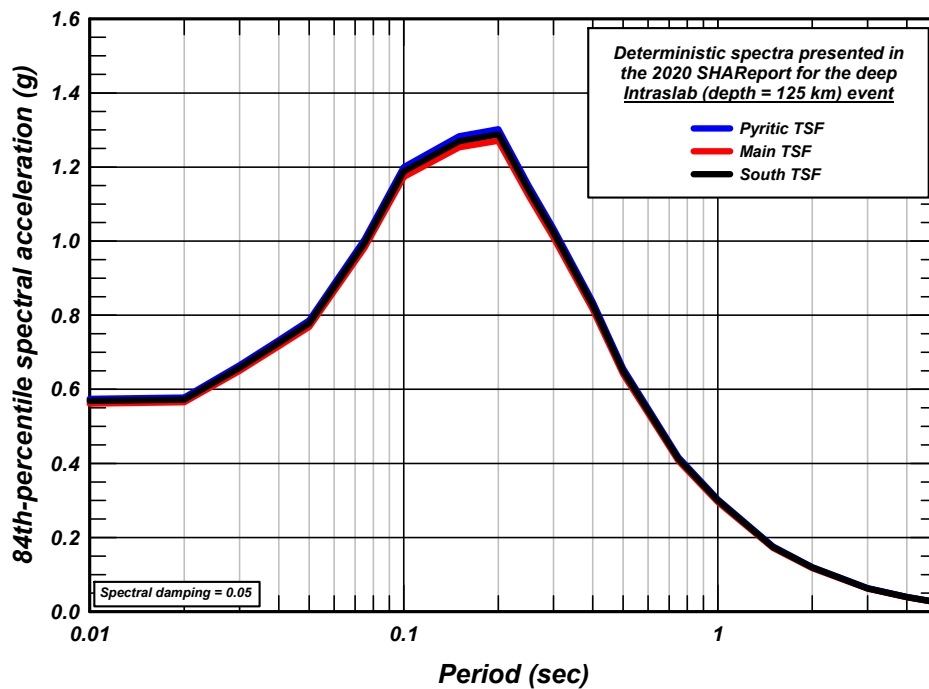


Figure E The 84th-percentile spectra for the deep Intraslab event (Depth = 125 km) calculated at the locations of each TSF

6.0 THE 2019 KP REPORT

The 2019 KP Report is an update of the 2013KP Report. A summary of the changes included in the 2019 Report and our review comments are presented in Appendix A of this report.

The spectrum recommended in the 2019 Report for the M8.0 deep Intraslab event is significantly greater than that recommended in the 2013 KP Report for the same event. This spectrum is compared to the spectra presented in the 2020 SHA Report for the three TSF locations in Figure F.

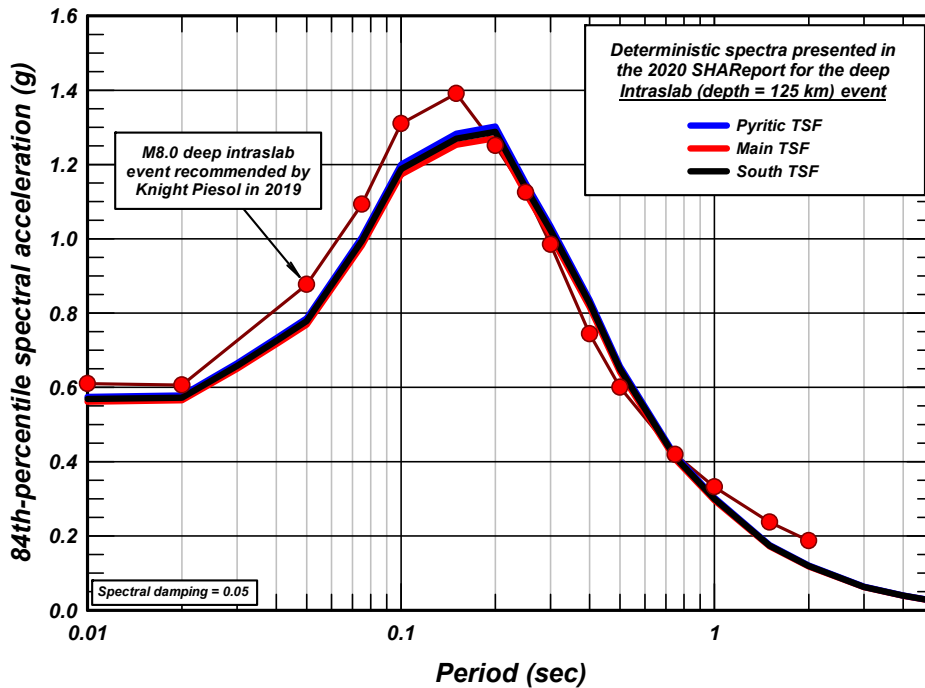


Figure F Comparison of the 84th-percentile spectra for the deep intraslab event presented in the 2020 SHA Report and shown in Figure E with the 84th-percentile spectrum recommended in the 2019 KP Report for the M8.0 deep intraslab event

The 2019 KP spectrum for the deep Intraslab event is about 6 to 11% larger than the spectrum presented in the 2020 SHA Report for the Pyritic TSF in the period range of 0.01 to 0.15 sec. The two spectra are practically identical over the period range from 0.2 to about 1 sec, and the KP spectrum is larger for longer periods.

As reported in Appendix A, however, we do not agree that the Atkinson and Boore (2003) GMM or the Zhao et al. (2006) GMM should be used for this site. Had Knight Piésold used the BC Hydro GMM, with the appropriate hypocentral depth and appropriate rupture depth, the two spectra would be practically the same.

As shown in Figure A-1d in Appendix A, the spectrum for the M6.5 background event recommended in the 2019 KP Report is slightly lower than that recommended in 2013. Therefore, as discussed in Section 5.0 above, the background event would not control the design.

7.0 VOLCANISM

The 2013 PK Report includes a section on volcanism (page 10) that is repeated in the 2019 KP Report (page 12), in which attention is drawn to volcanoes along the west shore of the Cook Inlet. In particular, a large volcano, Mount Saint Augustine, is located within ten miles of the locations of the potential Diamond Point and Amakdedori Ports. The volcanism section indicates that the 1883 eruption of Mount Saint Augustine produced a debris avalanche that resulted in a tsunami 33 ft high more than 62 miles from the volcano. Although the hazard from a tsunami generated by Mount Saint Augustine is considered minor in the KP Reports, this condition is qualified by the absence of a very large debris avalanche at high tide. The KP Reports also indicate that eruption of Mount Saint Augustine is likely to be repeated at any time, and that a tsunami could also occur as the result of a major earthquake around the Pacific Rim. A review undertaken for the current evaluation reveals eight eruptions of Mount Saint Augustine since and including the 1883 eruption and tsunami. The volcano erupted as recently as 2006.

In our opinion, the hazard of eruption, ensuing tsunami, and inundation and damage at the port sites represents a real threat, and should be considered as serious when planning the port and lifelines associated with the Pebble Mine. The American Society of Civil Engineers [ASCE] (Tsunami Loads and Effects Subcommittee of the ASCE/SEI Standards Committee, 2016) has developed a design standard⁶ that needs to be considered for facilities subject to tsunami effects. Based on what we reviewed, the design standard for tsunami effects has not been referenced or considered in either Knight Piésold report. We recommend that the ASCE Standard be addressed for this project.

8.0 CONCLUDING REMARKS

Our review of the seismic hazard studies completed for this site confirms that the report prepared by Dr. Gregor and Dr. Al Atik, with peer review by Dr. Norman Abrahamson, is comprehensive and provides seismic hazard results based on the current state of the art in completing such studies. Events occurring on the deep Intraslab source dominate the seismic hazard at this site, and the spectra derived for this source in the 2020 SHA Report can be used for the analysis, evaluation and design of the TSFs at the Pebble Mine site. In our opinion, the 2020 SHA Report supersedes both the 2013 and 2019 KP Reports because:

- The assessment of the seismic sources in the 2020 SHA Report is more complete.
- The 2020 SHA Report includes up to date assignment of maximum magnitude, rupture distance, hypocentral distance and hypocentral depth for each seismic source. The 2013 and the 2019 KP Reports assigned same magnitudes to these sources, but chose to use epicentral distance⁷, which is inconsistent of how distance is defined in the earthquake ground motion models GMM used in the KP Reports.
- The 2020 SHA Report used the most currently available and applicable GMMs. The 2013 and the 2019 KP Reports used a number of GMMs that are out of date and are not in use.
- The 2020 SHA Report placed no limitation on the maximum magnitude to use for calculating the spectral values for an earthquake occurring on the interplate. Both KP Reports used $M = 8.5$ to represent an $M = 9.2$ event. While this limitation had no effect of the selection of a "design" spectrum, it does reflect on the adequacy of the approach adopted for assessing the seismic hazard at this site.

It is extremely important to keep in mind that evaluating the seismic hazard and obtaining appropriate response spectra are only two of the critical steps in designing earthquake-resistant facilities. How these

⁶ ASCE Tsunami Loads and Effects Subcommittee of the ASCE/SEI Standards Committee, 2016, Chapter 6 in Minimum Design Loads for Buildings and Other Structures, ASCE Structural Engineering Institute, ASCE/SEI 7-16, Reston, VA.

⁷ See Footnote No. 1.

spectra and associated ground motions are used, types of analyses, material properties assigned to the embankment soils, foundation layers and tailings, location of the phreatic surface, construction control, etc. are critical for meeting the design criteria and achieving an appropriate design..

We find that the analyses presented in the Memorandum covering "Main Embankment Stability Assessment – Static and Post-liquefaction", prepared by Knight Piésold Ltd., Vancouver, Canada, for Pebble Limited Partnership, dated July 8, 2019 to be inadequate to evaluate the seismic performance of the Pebble Mine embankments. Those analyses provide an unsuitable basis for earthquake-resistant facilities and are not appropriate for making decisions about such a large and important development. As noted in Section 1.0 above, our review of the stability assessment Memorandum is provided in a separate report.

The probabilistic seismic hazard analysis (PSHA) included in the 2020 SHA Report is site specific and can be used in assessing the seismic risk. The results of the PSHA presented in the 2013 KP Report and in the 2019 KP Report are not site specific and should not be used for this site.

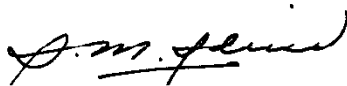
The following appendices are attached and complete this report:

- Appendix A Review Of "Report on Seismicity Assessment and Seismic Design Parameters",
Prepared by Knight Piésold, Dated July 4, 2019
- Appendix B Curricula Vitae of I. M. Idriss
- Appendix C Curricula Vitae of T. D. O'Rourke

As you requested, we have included the Curricula Vitae in Appendices B and C for your convenience.

We are pleased to be of assistance in making this review.

Sincerely,



I. M. Idriss



T. D. O'Rourke

APPENDIX A

REVIEW OF "REPORT ON SEISMICITY ASSESSMENT AND SEISMIC DESIGN PARAMETERS", PREPARED BY KNIGHT PIÉSOLD, DATED JULY 4, 2019

A.1 INTRODUCTORY REMARKS

For ease of reference, this report will be referenced as "2019 KP Report", which is an "update" of "the 2013 KP Report". The update consists of a minor change in the definition of the controlling crustal source and:

- replacing the 2008 NGA West1 earthquake ground motion models (GMMs) with the 2014 NGA West2 GMMs for calculating earthquake ground motions generated by crustal sources; and
- excluding the Youngs et al. (1997) GMM, retaining the Atkinson and Boore (2003) GMM and adding Zhao et al. (2006) GMM and the BC Hydro GMM (Abrahamson et al. 2016⁸) for calculating earthquake ground motions generated by crustal sources

There was no change in the approach used for the probabilistic seismic hazard analysis. The values of PGA presented in the 2019 KP Report, however, are slightly larger as summarized below:

Average Return Period (years)	PGA (g) presented in the	
	2013 PK Report	2019 PK Report
475	0.14	0.16
1,000	0.19	0.21
2,475	0.25	0.29
5,000	0.31	0.36
10,000	0.38	0.43

A.2 CHANGES FROM 2013 TO 2019

The following events were included for the mine site in the 2013 KP Report:

- *"Magnitude 9.2 interface subduction earthquake associated with the Alaska-Aleutian Megathrust, peak ground acceleration = 0.14 g"*
- *"Magnitude 8.0 deep intraslab (in-slab) subduction earthquake, peak ground acceleration = 0.48 g"*
- *"Magnitude 7.5 shallow crustal earthquake on the Lake Clark fault, peak ground acceleration = 0.29 g"*
- *"Magnitude 6.5 maximum background earthquake (shallow crustal event assumed to occur directly beneath potential mine site facilities), peak ground acceleration = 0.61 g"*

In the 2019 KP Report, the above seismic conditions were replaced as follows:

- *"M9.2 interface subduction earthquake associated with the Alaska-Aleutian Megathrust, peak ground acceleration = 0.16 g"*
- *"M8.0 deep intraslab (in-slab) subduction earthquake, peak ground acceleration = 0.61 g"*
- *"M7.5 shallow crustal earthquake on the Lake Clark fault, peak ground acceleration = 0.32 g"*
- *"M6.5 MBE shallow crustal event assumed to occur directly beneath potential mine site facilities, peak ground acceleration = 0.56 g"*

⁸ Section 6.0 (References) in the 2019 KP Report has the correct authorship and reference for the BC Hydro GMM in page 34. Beginning in page 18, however, the 2019 KP Report references this GMM as Addo et al. (2016) for which there is no publication in the reference list. The correct authorship is: Norman Abrahamson, Nick Gregor and Kofi Addo.

The 2013 and 2019 spectra recommended by Knight Piésold for the M9.2 interface event are presented in Figure A-1a. Those for the M8.0 deep intraslab event, the M7.5 shallow crustal event and the M6.5 background event are presented in Figures A-1b, A-1c, and A-1d, respectively.

Comparing the values listed for these four events in the 2013 KP Report (Table 3.3 Rev B – page 20 of 33) and in the 2019 KP Report (Table 3.3 – page 23 of 37), each event was assigned the same magnitude, mechanism fault. The mechanism for the Lake Clark fault was identified as reverse in 2013, but was changed to strike slip in 2019, with no specific explanation. Also, the distance for the crustal event to the Mine Site was listed as 15 miles in 2013, but was changed to 14 miles in 2019, again with no explanation.

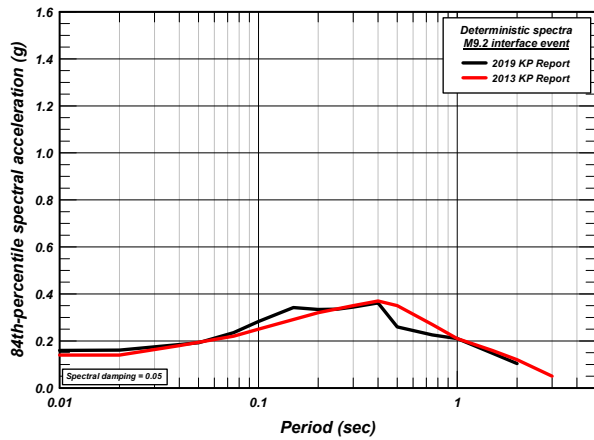
In this regard, it is noteworthy that both reports by Knight Piésold use a distance metric (epicentral distance) that has not been used in seismic hazard evaluations or in the development of earthquake ground motion models for decades. The GMMs that Knight Piésold used in 2013 and in 2019 have been derived in terms of "rupture distance", "hypocentral distance" and "Joyner-Boore distance". Other essential details regarding the parameters used by Knight Piésold for calculating the spectra presented in the 2013 or in the 2019 are missing.

A.3 REVIEW COMMENTS

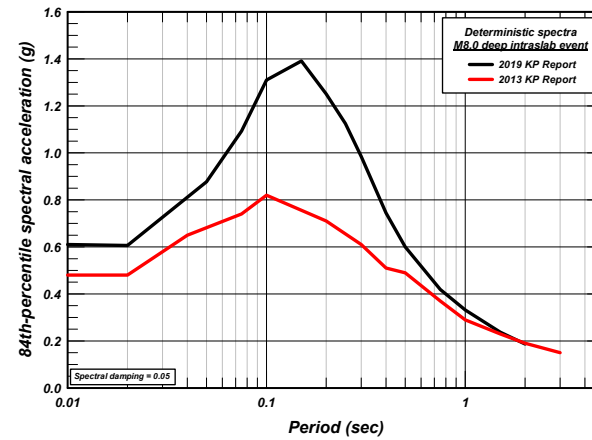
1. The spectra recommended in the 2019 KP Report are not much different from those recommended in the 2013 KP Report, except for the spectrum pertaining to the M8.0 deep Intraslab event.
2. The change from the 2013 spectrum for the M8.0 deep Intraslab event was due to dropping the Youngs et al. (1997) GMM and adding the Zhao et al. (2006) GMM and the BC Hydro GMM, as noted in Section A.1 above. The 2006 Zhou et al. GMM was superseded by the publication of two papers in 2016⁹.
3. We do not believe that it is appropriate to use the Atkinson and Boore (2003) GMM for this site. We also do not agree that the Zhao et al. (2006) or the 2016 GMMs should be used for this site.
4. We consider that the BC Hydro GMM, in the way it was used in the 2020 SHA Report, is currently the most appropriate approach for estimating earthquake ground motions at this site.
5. We do not agree that the spectral values for a magnitude 9.2 earthquake occurring on the interplate can be calculated using $M = 8.5$. There is absolutely no basis for this assumption. The BC Hydro GMM, which includes recordings from the 2010 M8.8 earthquake in Chile and 2011 M9.1 earthquake in Japan, suggests no such constraint.
6. The increase in spectral values for periods less than about 0.5 sec is of the order of 40% and about 60% in the period range of 1 to 5 sec for $M = 9.2$ compared to using $M = 8.5$ at a rupture distance of 190 km at a site with $V_{S30} = 760$ m/sec using the BC Hydro GMM.

⁹ The two papers published by Zhao et al. in 2016 are:

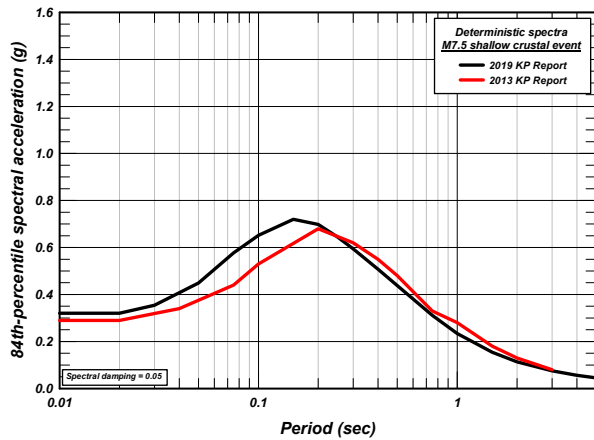
- Zhao, J. X., X. Liang, F. Jiang, H. Xing, M. Zhu, R. Hou, Y. Zhang, X. Lan, D. A. Rhoades, K. Irikura, Y. Fukushima, and P. G. Somerville (2016). "Ground-motion prediction equations for subduction interface earthquakes in Japan using site class and simple geometric attenuation functions", Bulletin of the Seismological Society of America, Vol. 106, No. 4, pp 1518–1534.
- Zhao, J. X., F. Jiang, P. Shi, H. Xing, H. Huang, R. Hou, Y. Zhang, P. Yu, X. Lan, D. A. Rhoades, P. G. Somerville, K. Irikura, and Y. Fukushima (2016). "Ground-motion prediction equations for subduction slab earthquakes in Japan using site class and simple geometric attenuation functions", Bulletin of the Seismological Society of America, Vol. 106, No. 4, pp 1535–1551.



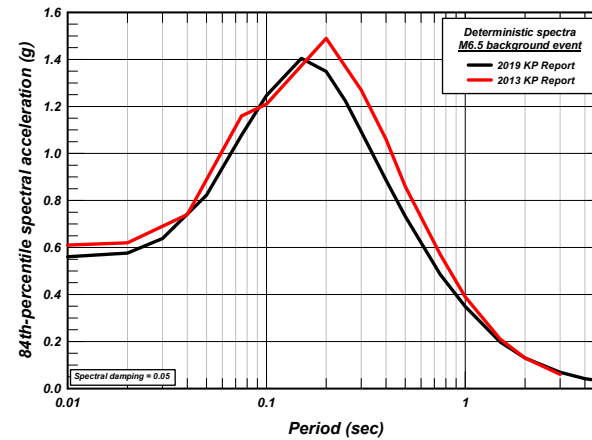
(a) M9.2 interplate event



(b) M8.0 deep intraslab event



(c) M7.5 shallow crustal event



(d) M6.5 background event

Figure A-1 Comparison of spectra recommended by Knight Piésold for the Mine Site in 2013 and in 2019

APPENDIX B

CURRICULA VITAE OF I. M. IDRIS

I. M. IDRIS

AREAS OF TEACHING, RESEARCH AND PRACTICE

*Geotechnical Earthquake Engineering; Geotechnical Engineering;
Embankment Dam Engineering; Numerical Modeling in Geotechnical Engineering.*

EDUCATION

B.C.E. Civil Engineering, Rensselaer Polytechnic Institute 1958
M.S. Civil Engineering, California Institute of Technology 1959
Ph.D. Civil Engineering, University of California, Berkeley 1966

REGISTRATION

Civil Engineer: California, 1969
Geotechnical Engineer: California, 1987

PROFESSIONAL HISTORY

Independent Consulting Geotechnical Engineer, 1989 – date.

University of California, Davis, Department of Civil and Environmental Engineering, Professor Emeritus of Civil Engineering, 2004- to date; Professor 1989 – 2004.

University of California, Davis, Director, Center for Geotechnical Modeling, 1989 - 1996

Woodward-Clyde Consultants, Senior Consulting Principal and Vice President, Oakland, California, 1987-1989

Woodward-Clyde Consultants, Managing Principal of the Orange County, Los Angeles and Santa Barbara area offices, and Vice President, 1982-1987

Woodward-Clyde Consultants, Project Engineer to Principal, Vice President and Director, Oakland and San Francisco, California, 1969-1982

UCLA, Department of Civil Engineering, Adjunct Professor, 1984-1986

Stanford University, Dept. of Civil Engineering, Consulting Professor, 1978-1982

University of California, Berkeley, Department of Civil Engineering, Lecturer and Research Engineer, 1966-1975

Consultant to several architect-engineers and other firms, 1966-1969

Dames & Moore, Field Engineer to Senior Engineer, 1959-1966; 1968-1969

Moran, Proctor, Meuser & Rutledge, Field Engineer, summer, 1958

HONORS

Terzaghi Lecture, American Society of Civil Engineers (ASCE), 2019
George W. Housner Medal, Earthquake Engineering Research Institute (EERI), 2018
The Nabor Carrillo Lecture, Mexican Society of Geotechnical Engineering, 2016
Honorary Member, Earthquake Engineering Research Institute (EERI), elected in 2012
Arthur Casagrande Memorial Lecture, Geo-Institute of the Boston Society Section of ASCE, 2010
Ralph B. Peck Award & Lecture, ASCE, 2010
Distinguished Member, American Society of Civil Engineers (ASCE), elected in 2008
Ishihara Lecture, International Society of Soil Mechanics and Geotechnical Engineering, 2007
Honorary Member, Japanese Geotechnical Society, elected in 2005
Kenneth L. Lee Lecture Award, Los Angeles Section of ASCE, 2004
Distinguished Public Service Award, University of California, Davis, 1999
H. Bolton Seed Medal, ASCE, 1995
Member, US National Academy of Engineering, elected in 1989

Special Lectures:

- The Woodward Lecture, *Woodward-Clyde Consultants, 1973*
- Theme Lecture on "Evaluating seismic risk in engineering practice," *XI International Conference on Soil Mechanics and Foundation Engineering, 1985*
- The Wilson Lecture, *Shannon & Wilson / University of Washington, Seattle, 2006*
- The Schiffman Lecture, *Cornell University, 2010*
- The GZA Lecture, New York City Chapter of the GI-Institute, ASCE, 2012
- The de Alba Lecture, University of New Hampshire, 2016

Norman Medal, ASCE, 1977

Walter L. Huber Civil Engineering Research Prize, ASCE, 1975

J. James Croes Medal, ASCE, 1972

The Thomas A. Middlebrooks Award, ASCE, 1971

Chi Epsilon (Honorary Member, Rensselaer Polytechnic Institute Chapter)

Tau Beta Pi

Sigma Xi

SPECIAL ASSIGNMENTS

Invited lecturer at various universities in the United States, Central and Latin America, Canada, Japan, United Kingdom, India, China, and the Middle East (since 1967).

Invited lecturer and state-of the-art speaker at specialty conferences and special courses in the United States, Canada, Latin America, Far East, Europe and the Middle East (since 1970).

On-going assignments (Partial List)

2019-date: Consultant, geotechnical engineering and geotechnical earthquake engineering issues, Pebble Mine Project, Bristol Bay Reserve Association and K & L Gates.

2018-date: Member, Independent Technical Review Board, Tailings Storage Facility (TSF) at the Hidden Valley Mine in Papua New Guinea, Harmony Gold.

2018-date: Member, Geotechnical Expert Advisory Panel for Iona Island Wastewater Treatment Plant Project Definition, Metro Vancouver, British Columbia, Canada.

2018-date: Consultant, geotechnical engineering and geotechnical earthquake engineering issues, Tailings Storage Facilities in Australia and in Canada, BHP Billiton.

2016-date: Member, External Advisory Panel, Las Bambas Dams, Las Bambas Tailings Storage Facilities, Peru, MMG.

2013-date: Member, Board of Consultants for LADWP Water Projects, Los Angeles Department of Water and Power, Kleinfelder.

2008-date: Member, Design Review Board, Tailings Dam Expansion, Kennecott's Magna Tailings Facility, Utah, Kennecott Utah Corporation.

2004-date: Member, Technical Review Panel, Calaveras Dam, San Francisco Public Utility Commission.

1998-date: Member, Seismic Safety Peer Review Panel for the design of the New East Spans of the San Francisco – Oakland Bay Bridge, California Department of Transportation, Sacramento.

1996-date: Consultant to the Federal Energy Regulatory Commission, Office of Energy Projects, on various dam projects throughout the United States.

1995-date: Chairman, Technical Review Board for the Cleveland Dam, Vancouver, British Columbia, Metro Vancouver (formerly, Greater Vancouver Regional District).

Completed assignments (Partial List)

2018-2019: Consultant, geotechnical engineering and geotechnical earthquake engineering issues, Padcal Tailings Storage Facility, Philippines, GHD Consulting (Australia).

2016-2017: Chairman, Technical Review Board, Annacis Water Supply Tunnel, Vancouver, British Columbia, Metro Vancouver (formerly Greater Vancouver Regional District).

2016 -2017: Consultant to McDowell, Rice, Smith & Buchanan, Kansas City, re: geotechnical earthquake engineering issues, site in Anchorage, Alaska.

2013-2016: Consultant, re: geotechnical earthquake engineering issues, North Spur, Lower Churchill Project, Labrador, Canada, SNC-Lavalin Inc., St. John's, NL.

2015: Member, Panel of Experts, Upper Tamakoshi Hydroelectric Project, Nepal, Upper Tamakoshi Hydropower Limited, Nepal Electricity Authority.

2012-2013: Member, Lihir Independent Cofferdam Review Board, Kapit Cofferdam Project, Lihir Mine, Lihir Island, Papua New Guinea, Newcrest Mining Limited.

2011-2016: Chairman, Technical Construction Review Board, Port Mann Tunnel, Vancouver, British Columbia, Metro Vancouver (formerly, Greater Vancouver Regional District).

2010-2017: Chairman, Technical Design Review Board, Second Narrows Water Supply Tunnel, Vancouver, British Columbia, Metro Vancouver (formerly Greater Vancouver Regional District).

2009-2012: Chairman, Technical Review Panel, Los Vaqueros Reservoir Expansion Project, Contra Costa Water District.

2008-2018: Member, Cerro Verde External Technical Review Board, Linga Tailings Storage Facility, Cerro Verde, Peru, Freeport McMoRan, MWH.

2006-2018: Member, Cerro Corona Independent Geotechnical Technical Review Board, Cerro Corona Tailings Dam, Peru, Gold Fields Co., MWH.

2006-2010: Chairman, Technical Design Review Board, Port Mann Tunnel, Vancouver, British Columbia, Metro Vancouver (formerly Greater Vancouver Regional District).

2005-2018: Member, Cerro Verde External Technical Review Board, Enlozada Tailings Storage Facility, Cerro Verde, Peru, Freeport McMoRan, MWH.

1991-2004: Member, Seismic Advisory Board, California Department of Transportation, Sacramento.

1995-2007: Chairman, Technical Review Boards for the Seymour Falls Dam, Vancouver, British Columbia, Metro Vancouver (formerly, Greater Vancouver Regional District).

1997-2003: Member, US Technical Coordination Committee, US-Japan Cooperative Research Program, National Science Foundation.

2001-2003: Member, Panel on Seismic Issues, Airfield Development Bureau, San Francisco International Airport.

2000-2003: Member, Embankment Technical Review Board, 3rd Runway at the Seattle-Tacoma International Airport, HNTB, Seattle, on behalf of the Port of Seattle.

1989-2003: Consultant to Pacific Gas & Electric Company (PG&E) – Diablo Canyon Nuclear Plant, Humboldt Bay Plant, and various dams in Northern California.

1989-2002: Member, Consulting Board for Earthquake Analysis for the Division of Safety of Dams, Department of Water Resources, State of California.

1993-2001: Member, Highway Seismic Research Council Technical Group, National Center for Earthquake Engineering Research (NCEER).

1993-2000: Member, Board of Consultants, Eastside Reservoir Project (renamed Diamond Valley Project in 2000), Metropolitan Water District of Southern California.

1999: Member, Review Panel, Seismic Design Criteria for the Cooper River Bridges in Charleston, South Carolina, Parsons Brinckerhoff, New York City.

1990-1999: Chairman, Seismic Research Advisory Panel, California Department of Transportation, Sacramento

1994-1999: Member, Peer Review Panel for the San Francisco-Oakland Bay Bridge and other Toll Bridges in Northern & Southern California, California Department of Transportation, Sacramento.

1991-1996: Member, Advisory Council, Southern California Earthquake Center, Los Angeles

1994-1995: Member, Advisory Panel for OTA Assessment of the ‘Federal Efforts to Reduce Earthquake Damage’, Office of Technology Assessment, Congress of the United States.

1992-1995: Member, Ad Hoc Working Group on the Probabilities of Future Large Earthquakes in Southern California, Southern California Earthquake Center, USGS, California Office of Emergency Services & CDMG.

1991-1994: Member, Blue Ribbon Panel on the Marina Soil Study, Bureau of Engineering, Department of Public Works, City & County of San Francisco.

1988-1992: Member, State of California Board of Mining and Geology; Chairman: Geohazard Committee of the Board; also Chairman, Ad Hoc Committee on Deterministic / Probabilistic Seismic Hazard Evaluations.

1989-1990: Member, Governor's Board of Inquiry to investigate the collapse of the Cypress section of I-880 and the damage to the Bay Bridge during the 17 October, 1989 Loma Prieta earthquake.

1984-1985: Participant, Workshop on Liquefaction, Committee on Earthquake Engineering, National Research Council.

1981-1982: Consultant to UNESCO in Paris, France on geotechnical and earthquake engineering issues in the Middle East and North Africa.

1971-1981: Seismology Committee, Structural Engineers Association of Northern California; Chairman, Soil Structure Interaction Subcommittee, 1971-72 and 1977-79; Chairman, Subcommittee on Sliding and Overturning, 1979-81.

1975-1980: Consultant to the International Atomic Energy Agency, Vienna; participated in preparation of IAEA's Safety Guide on "Seismic Analysis and Testing of Nuclear Power Plants".

1974-1979: Structural Division, ASCE; Nuclear Structures and Materials Committee; Chairman, Ad Hoc Group on Soil-Structure Interaction.

TEACHING AND RESEARCH

Dr. Idriss was a member of the faculty in the Department of Civil Engineering at the University of California at Davis (UCD) from 1989 to 2004. He taught courses on basic soil mechanics and foundation engineering, advanced soil mechanics and foundation engineering, an undergraduate course in statics, geotechnical earthquake engineering, and earthfill and rockfill dams,.

While he was at UCD, he conducted research related to: characteristics of earthquake ground motions; equivalent linear and nonlinear response of soil deposits during earthquakes; response of earth and rock fill dams and landfills during earthquakes; liquefaction; mitigation and remediation of liquefaction; and ground deformations due to earthquake loading conditions. He has continued his research on these topics since retiring from UCD.

RECENT AND CURRENT CONSULTING ASSIGNMENTS

Dr. Idriss has been since 1989, and continues to be, a consultant to several Consulting Engineering Firms, Architect/Engineering Firms, private and public Research Organizations, Owners, and various State and Federal Agencies. The consulting assignments have included:

Earth Dams, Rockfill Dams, Tailings Dams, and Dikes:

Costa Oriental Dikes in Venezuela
Sardis Dam, Mississippi
Diamond Valley Reservoir and Dams (Eastside Reservoir & Dams), Southern California
O'Neill Forebay, Central California
Devil Canyon Second Afterbay, Southern California
Garvey Reservoir, Southern California
Xiaolangdi Project (Yellow River Hydroelectric Project), China
North Tailings Dam near Salt Lake City, Utah
Dams, Power & Water Distribution Facilities in British Columbia
Los Vaqueros Dam in Contra Costa County, California
Little Dalton, Big Dalton, Santa Anita and Sawpit Debris Dams, Calif.
Sacramento-San Joaquin Delta Levees
Seven Oaks Dam, Southern California
Tarbela Dam, Pakistan
Prado Dam, Southern California
Lake Almador & Lake Francis Dams, Northern California
Butte Valley Dam, Northern California
Success Dam, Central California
Cleveland & Seymour Falls Dams, British Columbia
Matahina Dam, North Island, New Zealand
Karapiro Dam, North Island, New Zealand
Waitaki Dams, South Island, New Zealand
Lopez Dam, San Luis Obispo, California
Saluda Dam, South Carolina
Pardee Dam, Northern California
New Hogan Dam, Northern California
Santee-Cooper Project, South Carolina
Wateree Dam, North Carolina
Cushman, Wynoochee, Mayfield, & Mossyrock Dams, Washington
Clackamas River Project, Oregon
Claytor Dam, Virginia
Wickiup Dam, Oregon
Diversion Dam, New York
Skookumchuck Dam, Washington
Calaveras Existing & Replacement Dams, California
Lafayette Dam, California
Cerro Verde Enlozada Tailings Dam, Peru
Cerro Verde Linga Tailings Dam, Peru
Crane Valley Dam, California
Wells, Rocky Reach & Rock Island Dams, Washington
Boundary Dam, Washington
Priest Rapids Dam, Washington
Wanapum Dam, Washington
Upper Reservoir of Taum Sauk Dam, Missouri

Greens Creek Mine Tailings Pile, Alaska
Cerro Corona Tailings Dams, Peru
Hebgen Dam, Montana
San Pablo Dam, California
Dillon Dam, Colorado
Williams Fork Dam, Colorado
Comanche Dam, California
Kennecott's Magna Tailings Facility, Utah
El Dorado Forebay Dam, California
Scoggins Dam, Oregon
Los Vaqueros Reservoir Expansion Project, California
San Luis Tailings Dams, Peru
Lihir Cofferdam Project, Papua New Guinea
Anderson Dam, California
North Haiwee Dam, California
Upper Stone Canyon Reservoir, California
Stone Canyon Dam, California
Bouquet Dam, California
North Spur, Lower Churchill Project, Labrador, Canada
Upper Tamakoshi Hydroelectric Project, Nepal
Chuspiri Water Dam, Peru
Las Bambas Tailings Dam, Peru
Chilhowee Dam, Tennessee
Rampart Dam, Colorado
Gross Dam, Colorado
Cutler Dam, Utah
Padcal Tailings Storage Facility, Phillipines
Olympic Dam, Australia
Tailings Dam, Hidden Valley Mine in Papua New Guinea
Quirke Dikes, Canada
Pebble Mine Tailings Facilities, Alaska

Industrial Projects:

Getty Fine Arts Center
San Francisco Marina
Treasure Island
Metro Bay Center
Port of Los Angeles
Bayer's Project Site in Taiwan
Third Runway at the Seattle-Tacoma International Airport
Airport Expansion at the San Francisco International Airport
Port of Anchorage
Iona Island Wastewater Treatment Plant

Landfill Projects:

Acme Landfill
Ox Mountain Landfill
Pacheco Landfill
Operating Industries Inc. (OII) Landfill
Chiquita Landfill
Edom Landfill

Sunshine Landfill
Elsmere Canyon Landfill
Western Regional Sanitary Landfill, Placer County, California

Nuclear Plants and Facilities:

CESSAR (Combustion Engineering Standard Plant)
Long Term Seismic Program (LTSP) for Diablo Canyon
Seismic Margin Assessment – Hatch Plant, Georgia
Seismic Margin Assessment (SMA) Methodology
LOTUNG experimental and analytical study
New Production Reactors
Ground Motion Guidelines at Nuclear Plant Sites
Replacement Tritium Facility (RTF) at Savannah River
IPEEE Geotechnical Review for Limerick Plant
IPEEE Geotechnical Review for Peach Bottom Plant
Defense Waste Processing Facility (DWPF) at Savannah River
In-Tank Precipitation Facility (ITP) at Savannah River
Humboldt Power Plant (Hazard Evaluation & ISFSI)
Prairie Island Nuclear Generating Plant
Diablo Canyon Nuclear Plant (Hazard Evaluation & ISFSI)
Independent Spent Fuel Storage Installation (ISFSI) – Hatch Plant, Georgia
Independent Spent Fuel Storage Installation (ISFSI) – Farley Plant, Alabama
Grand Gulf Nuclear Plant
PDCF at Savannah River Site (SSI analyses; Liquefaction Studies; Geotechnical Issues)
Salt Waste Processing Facility at Savannah River Site (Geotechnical Issues)
Yucca Mountain Project (Site Response Studies; Earthquake Ground Motions)
River Bend Nuclear Plant, COLA Application
Fermi Nuclear Plant, COLA Application
Dry Fuel Storage Facility, Crystal River 3 Nuclear Plant, Florida
Seismic Hazard Assessment Program, SONGS, Southern California
FLEX Dome Storage Building, Vogtle Nuclear Plant, Georgia

Bridges:

Seismic Vulnerability of Bridges for the Illinois Department of Transportation
Seismic Hazard Evaluation and Site Response for the Benicia and the Carquinez Bridges
Seismic Hazard Evaluation for Bridge Crossings in Southern California
Seismic Hazard Evaluation for Bridge Crossings in Northern California
Liquefaction & Remediation Assessment at the I-5/Route 56 Interchange in S. Calif.
I-880 Reconstruction in Oakland
Route 24/580/980 Interchange in Oakland
San Francisco-Oakland Bay Bridge (existing bridge)
Route 8/805 Interchange in San Diego
California State Toll Bridges in the San Francisco Bay Area
California State Toll Bridges in Southern California
New East Span of the San Francisco-Oakland Bay Bridge
Cooper River Bridges, Charleston, South Carolina

Other Projects:

Nonlinear behavior of soils
Geologic Hazards in the Summit Area of the Santa Cruz Mountains
Marina and South of Market Street Liquefaction Study

Watsonville Liquefaction & Remediation Assessment
The King Dome in Seattle
International Arrival Building at JFK in New York
Pacific Telephone Building, Oakland
Bel Marin Keys, Novato, California
Gas Pipeline Earthquake Performance R&D Project
Webster Street & Posey Tunnels, Alameda, California
BART Trans Bay Tube
Port Mann Water Supply Tunnel, Vancouver
Second Narrows Water Supply Tunnel, Vancouver
Annacis Water Supply Tunnel, Vancouver

for:

ABB Combustion Engineering
ABB Impell
Automated Engineering Services Corp
Bayer AG
BHP Billiton
Black & Veatch
B. C. Hydro
Brookhaven National Laboratory
Bristol Bay Reserve Association
CDM Federal Programs Corporation
CH2M HILL
City of San Francisco
Clean Water Services
Comartin-Reis
County of San Luis Obispo, California
Department of Transportation of the State of California
Department of Water Resources of the State of California
Division of Safety of Dams of the State of California
J. M. Duncan
Emcon Associates
Electric Power Research Institute (EPRI)
Electricity Corporation of New Zealand, Ltd (ECNZ)
EQE
Federal Energy Regulatory Commission
Flour of Canada
Forell / Elsesser Engineers, Inc.
Freeport McMoRan
GEI Consultants
Geomatrix Consultants
GeoPentech Consultants
GHD Consulting (Australia)
Golder Associates
Gold Fields
Harding Lawson Associates
Harmony Gold
HNTB
Hushmand Associates
RPK Structural Mechanics

King County, State of Washington
Kleinfelder, Inc.
Klohn Crippen Berger Ltd.
Lawrence Livermore National Laboratory
McDowell, Rice, Smith & Buchanan
Metro Vancouver (formerly Greater Vancouver Regional District)
Miller Pacific Engineering Group
MMG Mining, Lima, Peru
Morrison Knudsen Corporation
Newcrest Mining Limited
Parsons
Pacific Gas & Electric Co.
Parsons Brinckerhoff, New York City
Parsons Brinckerhoff, San Francisco
Port Authority of New York & New Jersey
Port of Los Angeles
Progress Energy, North Carolina
San Francisco Public Utility Commission
SNC-Lavalin Inc., St. John's, NL, Canada
Southern Company Services, Inc.
STS Consultants Ltd.
TAMS
Treadwell & Rollo
Upper Tamakoshi Hydropower Limited, Nepal Electricity Authority
URS Corporation (became part of AECOM in 2016)
US Army Corps of Engineers, Los Angeles District
US Army Corps of Engineers, Sacramento District
US Army Corps of Engineers' Waterways Experiment Station
US Bureau of Reclamation
US Department of Energy
VECTRA Technologies, Inc.
Washington Group International
Woodward-Clyde Consultants (became part of URS in 1997)
World Bank
Yellow River Conservancy Commission, China
Yucca Mountain Project

TEACHING, CONSULTING AND RESEARCH EXPERIENCE PRIOR TO 1989

Dr. Idriss taught undergraduate courses in soil mechanics and foundation engineering from 1967 until 1970 at the University of California in Berkeley. He also lectured at various seminars and graduate courses dealing with geotechnical earthquake engineering at UC Berkeley, UCLA and the University of Arizona from 1968 through 1975. He taught a graduate course on earthquake engineering at Stanford University from 1978 through 1982 and undergraduate courses in soil mechanics and foundation engineering in 1986 and 1987 at the University of California in Irvine. Dr. Idriss has also taught at special courses on earth- and rock-fill dams, soil dynamics, soil-structure interaction, site response, earthquake ground motions, liquefaction evaluations ... etc. throughout the United States, in Europe, Central and Latin America and Japan from 1970 to-date.

Prior to joining the faculty of the Civil Engineering Department at the University of California in Davis, Dr. Idriss had about 30 years of experience in soil mechanics and foundation engineering,

with emphasis in geotechnical earthquake engineering during the latter 25 years. He developed or co-developed several analytical and empirical procedures to evaluate liquefaction potential, behavior of soil masses during earthquakes, seismic behavior of earth and rock fill dams (including post-earthquake considerations), and deterministic and probabilistic assessment of earthquake ground motions.

For a period of about 22 years, Dr. Idriss conducted and directed consulting assignments involving geotechnical earthquake engineering studies for earth, rock fill, and tailing dams, nuclear power plant sites, high-rise buildings, offshore platforms, and industrial facilities.

He also conducted and directed applied research studies. From 1973 through 1989, he directed and participated in multi-disciplinary projects for dams (earth, rock fill, tailings and concrete), commercial and industrial facilities, offshore platforms, nuclear power plant and LNG sites, pipelines, and generic multi-disciplinary projects.

From 1970 to 1989, Dr. Idriss conducted and directed geotechnical earthquake engineering studies for over 50 earth, rock fill, and tailing dams in California, Alaska, Alabama, North Carolina, New Mexico, Tennessee, Utah, Mexico, Guatemala, Costa Rica, Colombia, Argentina, Ecuador, Egypt, Morocco, and Algeria; and earthquake engineering studies (including ground motion characterization, assessment of liquefaction potential, evaluation of soil-structure interaction, and cyclic soil characterization) at over 25 nuclear plant sites in the United States, Europe, and the Middle East. Other geotechnical earthquake engineering projects include offshore platforms in California, Alaska, and New Zealand; and waterfront facilities, fossil plants, and hospital and office buildings in California, Idaho, Alaska, New Jersey, Texas, Italy, Puerto Rico, Iran, Guatemala, Nicaragua, Venezuela, Egypt, Saudi Arabia, Lebanon, and other locations.

Applied research and non-site-specific consulting assignments, during the period 1970 to 1989, included: *Soil-structure interaction studies for GESSAR and for General Electric's Standard Plant; Behavior of marine clay sediment during earthquake loading conditions; Behavior of marine clay sediments during wave loading conditions; Behavior of soil-pile-structure systems during earthquake; Soil-structure interaction studies and correlation with model field tests; Offshore Alaska seismic exposure studies; Probabilistic and deterministic assessment of ground motions; Engineering characterization of earthquake ground motions to develop guide-lines for seismic inputs for nuclear plants; Program for assessment and mitigation of earthquake risk in the Arab Region; Seismic margin assessment (SMA) methodology; Evaluation of the behavior of the Molikpaq due to ice loading conditions; Development of earthquake ground motions and dynamic soil properties for CESSAR (Combustion Engineering standard nuclear plant)*

Multi-disciplinary projects included:

- *Proposed Boruca Dam in Costa Rica*
- *San Onofre Nuclear Generating Station in southern California*
- *Seismic exposure studies for offshore Alaska*
- *Proposed offshore platform in southern California*
- *Bullards Bar Dam in northern California*
- *Bolsa Chica Development in southern California*
- *State Office Building in Anchorage, Alaska*
- *Honda Headquarters in southern California*
- *Costa Oriental Dikes in Lake Maracaibo Region, Venezuela*
- *Getty Fine Arts Center in Brentwood, California*

He conducted research related to the nonlinear behavior of soils under cyclic loading conditions. The results of this research have been applied to assessing performance of soft sediments during earthquakes. He has been engaged in other research activities that relate to significant duration of earthquakes, simplified procedures for assessment of soil-structure interaction, probabilistic review and assessment of recorded ground motions and associated spectra, and application of probabilistic techniques in geotechnical practice.

MEMBERSHIPS IN TECHNICAL SOCIETIES

American Society of Civil Engineers
Earthquake Engineering Research Institute
Canadian Dam Association
Canadian Geotechnical Society
Seismological Society of America
United States Society on Dams

PUBLICATIONS

Dr. Idriss has authored or co-authored about 240 technical papers and research reports on subjects related to the geotechnical aspects of earthquake engineering (seismic response of soil deposits; earth structures including slopes, earth and rock fill dams; dynamic soil material properties; liquefaction; soil-structure interaction; and probabilistic deterministic assessment of characteristics of ground motions). These papers have been published in the Journals of the Geotechnical Engineering Division, the Structural Engineering Division, and Proceedings of Specialty Conferences of the American Society of Civil Engineers; Bulletin of the Seismological Society of America; International Journal of Earthquake Engineering and Structural Dynamics; proceedings of World Conference on Earthquake Engineering, proceedings of the US National Conference on Earthquake Engineering, proceedings of the International Conference on Soil Mechanics and Foundation Engineering, proceedings of the Offshore Technology Conference, and proceedings of other international engineering meetings.

APPENDIX C

CURRICULA VITAE OF T. D. O'ROURKE

THOMAS D. O'ROURKE CURRICULLUM VITAE

Current Position: Thomas R. Briggs Professor of Engineering, Civil and Environmental Engineering, Cornell University, 422 Hollister Hall, Ithaca, NY 14853-3501.

Education: Ph.D., University of Illinois at Urbana-Champaign, 1975; M.S.C.E., University of Illinois at Urbana-Champaign, 1973; B.S.C.E., Cornell University, 1970.

Academic Positions: Thomas R. Briggs Professor of Engineering, Cornell Univ. (1999-date); Member, Graduate Faculty in Field of Systems Engineering, Cornell Univ. (2011-date); Fulbright Fellowship, Senior Specialist Program with Office of Prime Minister and Cabinet, Wellington, NZ (2007); Overseas Fellow, Churchill College, University of Cambridge (2006- date); By-Fellow, Churchill College, University of Cambridge (1999); Erskine Fellowship, University of Canterbury, Christchurch, NZ (1999, 2015, & 2020); Professor of Civil and Environmental Engineering, Cornell Univ. (1987-1999); Member, Graduate Faculty in Field of Textiles and Fiber Science, Cornell Univ., Ithaca, NY (1989-date); Associate Professor of Civil and Environmental Engr., Cornell Univ. (1981-1987); Member, Graduate Faculty in Field of Geological Sciences, Cornell Univ. (1981-date); Visiting Lecturer, Royal School of Mines, Imperial College of Science and Technology (1985); Assistant Professor of Civil and Environmental Eng., Cornell Univ. (1978-1981); Assistant Professor of Civil Engineering, Univ. of Illinois at Urbana (1975-1978).

Awards and Distinctions: *U.S. National Academy of Engineering* (1993); *Fellow of American Association for the Advancement of Science* (2000); *Distinguished Member of the American Society of Civil Engineers [ASCE]* (2014); *International Fellow of the Royal Academy of Engineering* (2014); *Corresponding Member of the Mexican Academy of Engineering* (2017). Other distinctions (chronological order): *C.A. Hogentogler Award*, Amer. Society for Testing & Materials (1976); *Collingwood Prize*, (1983); *Walter L. Huber Civil Engineering Research Prize*, ASCE (1988); *C. Martin Duke Award*, ASCE (1995); *Outstanding Earthquake Spectra Paper*, Earthquake Engr. Research Inst. [EERI] (1996); *Stephen D. Bechtel Pipeline Engineering Award*, ASCE (1997); *University of Illinois Distinguished Alumnus Award* (2000); *National Science Foundation Distinguished Lecturer* (2002); *Trevithick Prize*, Institution of Civil Engineers (2002); *Japan Gas Award*, Japan Gas Association (2003); *University of Illinois Distinguished Service Award* (2005); *Ralph B. Peck Award*, ASCE (2005); *Rankine Lecture*, British Geotechnical Association (2009); *Academy of Geo-Professionals Honorary Diplomate* [inaugural class], ASCE Geo-Institute (2009); *EERI Distinguished Lecturer*, EERI (2012); *EERI Honorary Membership*, EERI (2013); *Geo-Institute Touring Lecturer*, ASCE (2013); *Leval Lund Award*, ASCE (2014); *Terzaghi Lecture*, ASCE GeoInstitute (2016); *Housner Medal*, EERI (2016); *Outstanding Earthquake Spectra Paper*, EERI (2016), *IAEE Honorary Membership*, Int'l Assoc. for Earthquake Engr. [IAEE] (2017), *G.E.O. Widera Literature Award*, American Society of Mechanical Engineers [ASME] (2018); *Cross Canada Touring Lecturer* (2018), Canadian Geotechnical Society.

Teaching/Advising Awards and Distinctions: Kenneth A. Goldman '71 Excellence in Teaching Award (2003) and Daniel Lazar '29 Excellence in Teaching Award (1998), Cornell University; *ASCE Robert A. Ridgeway Award* (1983) Faculty Advisor, Cornell ASCE Student Chapter highest ranked U.S. student chapter, which designed and built a 50-m-long suspension bridge and wing-shaped children's pavilion in local parks, open to the public and providing service for more than 30 yrs.

Professional Experience: Geotechnical Engineer, Dames and Moore, Cranford, N.J. (1970); Field Instrumentation & Data Acquisition Specialist for Washington, DC Metro Construction, University of Illinois (1970-1975); Senior Research Associate, Transport and Road Research Laboratory, Crowthorne, U.K. (1976-1977); Geotechnical, Infrastructure, and Earthquake Engineering Consultant (1975-date).

Engineering Consultant: Consulting services on more than 130 projects in 13 different countries, including United States, United Kingdom, Angola, Canada, Ecuador, France, Mozambique, New Zealand, Nigeria, Russia, Trinidad, Turkey, and Venezuela. Chair or member of the consulting boards of many large underground construction projects, as well as peer reviews for projects associated with highway, rapid transit, water supply, and energy distribution systems. Many projects have included seismic design assessments. Representative projects include the Third NYC Water Tunnel, Bypass Tunnel for NYC Delaware Aqueduct, Boston Central Artery and Tunnel (CA/T), risk assessment for the First NYC Water Tunnel and NYC aqueducts, Tren Urbano Rapid Transit System, NYC Second Avenue

Subway and Fulton St. Transit Center, soft and hard rock tunneling for the Massachusetts Water Resources Authority, Dulles Airport underground expansion, San Francisco Transbay Transportation Center, TJPA Downtown Extension Project involving hard and soft ground tunneling, seismic design of tunnels in Turkey, Trans-Bay Tube Seismic Retrofit, seismic design for the San Francisco water supply (including the San Francisco Public Utilities Commission Crystal Springs By-Pass Tunnel, Bay Tunnel, Irvington Tunnel, and Bay Division Pipelines); Silicon Valley Rapid Transit System in San Jose, CA, geotechnical and seismic criteria for the Alaskan Way Viaduct in Seattle, WA; Los Angeles Headworks Reservoir, Stone Canyon and Bouquet Dams, Haiwee Reservoir, and Elizabeth Tunnel; San Francisco Auxiliary Water Supply System; Pacific Gas and Electric 270 kV electric transmission line in San Francisco. Peer review of earthquake redesign and recovery of Christchurch, NZ, including horizontal infrastructure (water supply, wastewater and drainage, roads and bridges) for Christchurch Earthquake Recovery Authority; liquefaction land damage for Earthquake Commission, NZ; foundation systems for residential structures for the Ministry of Business, Innovation, and Employment; and restoration of Lyttelton Port for the Lyttelton Port Company. Design contributions for foundations of LNG facilities in Trinidad, Angola, Nigeria, and Mozambique (for Bechtel). Boston CA/T: design/peer review of Bird Island Flats portion of Ted Williams Tunnel, Fort Point Channel deep soil mix ground stabilization and immersed tubes; excavation and tunneling effects on One Financial Center and Boston Metro Red Line. Chair, Board of Consultants for underground construction of Superconducting Super Collider, US DOE, as well as Energy Recovery Linac, Cornell Univ.

Teaching/Advising Experience: Supervision of 24 Ph.D. theses and doctoral students, 23 M.S. theses and masters students, and over 200 M. Eng. students and 10 M. Eng. design projects. Classes were taught to thousands of undergraduate and graduate students in the following courses: Planning and Engineering for Critical Infrastructure, Environmental Applications of Geotechnical Engineering, Retaining Structures and Slopes, Foundation Engineering, Introduction to Geotechnical Engineering, Civil and Environmental Engineering Design Project, Rock Engineering, Soil Dynamics, Graduate Soil Mechanics Laboratory, Geoenvironmental Engineering, and Tunnel Engineering. Courses jointly taught on sabbatical at Imperial College (1985) include Rock Dynamics and Graduate Tutorial in Rock Mechanics.

Professional Service: **President:** Earthquake Engineering Research Institute [EERI] (2003-04); ASCE Ithaca Section (1981-82). **Vice President:** EERI (2001-02). **Chair:** National Institute of Standards and Technology/Applied Technology Council Committee on National Lifelines Research and Implementation Roadmap (2013-2014); International Advisory Group, Center for Smart Infrastructure and Construction, University of Cambridge; EERI Honors Committee (2008-2010); EERI Development Committee (2005-07); Executive Committee, Institute for Civil Infrastructure Systems (1998-03); NSF COV Review of Civil Mechanical Systems Division (2001 and 2004); National Academy of Engineering, Section 4, Nomination Committee (2000-02); ASCE TCLEE Executive Committee (1998-01); Transportation Research Board (TRB) Subsurface Soil-Structure Interaction, A2K04 (1991-94); ASCE Earth Retaining Structures Committee (1986-90); ASCE TCLEE Executive Committee (1988-89); U.S. National Committee on Tunneling Technology (1987-88); ASCE TCLEE Gas and Liquid Fuel Lifelines Committee (1986-88); ASCE Underground Technology Research Council (1985-86). **Member:** International Committee of Visitors, Dept. of Engineering, University of Cambridge (2005- present); NIST Advisory Committee on Earthquake Hazard Reduction (2007-12); National Academies Board on Water Science and Technology (2008-10); National Academies Committee on New Orleans Regional Hurricane Protection Projects (2006-09); External Review Committee, Department of Civil and Environmental Engineering, University of California, Berkeley, CA (2005); International Committee to Review British Engineering Research, Royal Academy of Engineering and Engineering and Physical Sciences Research Council, U.K. (2004); Board of Directors, Consortium of Universities for Research in Earthquake Engineering (2001-06); International Evaluation Committee for College of Civil Engineering, Technion, Israel (2001); Advisory Board, Polytechnic University, Dept. of Civil and Environmental Engineering (1997-01); EERI Board of Directors (1998-2006); NSF Engineering Directorate Advisory Committee (1998-04); Executive Committee, Multidisciplinary Center for Earthquake Engineering Research [MCEER] (1997-08); National Institute of Building Sciences Utility Lifelines Subcommittee (1997-00); Mid-America Earthquake Center Board of Directors (1997-99); MCEER Research Committee (1996-1998); Southern Cayuga Lake Intermunicipal Water Commission (1996-97); National Research Council (NRC) Board on Energy and Environmental Systems (1994-96); NRC Energy Engineering Board (1993-94); NRC Committee for Infrastructure Technology Research Agenda (1992-94); NRC Geotechnical Board (1989-93); TRB

Committee on Subsurface Soil-Structure Interaction, A2KO4 (1985-90); ASCE Committee on Pipeline Crossings of Railroads and Highways (1984-2000); ASME Technical Subcommittee on Lifeline Earthquake Engineering (1982-83); Committee on Management of Construction, Building Futures Council (1983-85); ASCE Committee on Earth Retaining Structures (1982-86); ASCE TCLEE] Water and Sewage Committee (1981-92); ASCE TCLEE Gas and Liquid Fuel Lifelines Committee (1981-86); U.S. National Committee on Tunneling Technology, Subcommittee on Tunnel Design (1981-86); Construction Research Council Management of Construction Programs (1981-83); NRC BRAB Committee on Management of Urban Construction Programs (1979-81).

U.S. Congressional Testimony: before U.S. House of Representatives Science Committee on "National Earthquake Hazards Reduction Program: Disaster Resilient Communities" (2009), "National Earthquake Hazards Reduction Program" (2003), "The Turkey, Taiwan, and Mexico Earthquakes: Lessons Learned" (1999), and "Earthquakes in the Eastern United States" (1985).

Earthquake Reconnaissance Missions: Ecuador earthquake (1987); Armenia earthquake (1989) at invitation of USSR Academy of Science; Loma Prieta earthquake, CA (1989); Northridge earthquake, CA, (1994), Kobe earthquake, Japan (1995), Kocaeli earthquake, Turkey (1999), Chi-chi earthquake, Taiwan (1999), Canterbury Earthquake Sequence [after all 4 main shocks: Sept., 2010, Feb., 2011, 13 June, 2011 and 23 Dec., 2011]; and Tohoku earthquake, Japan (2011).

Patents: US Patents No. 5713393 for "frictionless pipe", Feb. 1998, and No. 8701469 for flexible substrate sensor system for environmental & infrastructure monitoring, Apr. 2014.

Research: Principal or co-principal investigator on more than 80 research projects, totaling over \$30 million. Select programs and projects include: **1)** Co-principal investigator and member of Executive Committee of NSF Engineering Research Center, Multidisciplinary Center for Earthquake Engineering Research (1997-2008) with oversight responsibility for an 11-year research program exceeding \$ 50 million. Personal research accomplishments include development of hydraulic network analyses of the earthquake response of water supplies, including applications for decision support by the Los Angeles Department of Water and Power (LADWP) for the Los Angeles water supply and the San Francisco Public Utilities Commission (SFPUC) and San Francisco Fire Department for the San Francisco auxiliary water supply; advanced geographical information systems (GIS) for earthquake effects on geographically distributed infrastructure, including the use of the LADWP water distribution system as a 1200 km² "strain gage" for the effects of the 1994 Northridge earthquake; and large-scale experiments on critical water and energy infrastructure to characterize earthquake performance and reduce seismic effects through fiber-reinforced polymeric reinforcement and special geotextile wrap to reduce shear transfer from soil in underground pipelines to near-zero conditions. **2)** Principal investigator for research team supported by the Gas Research Institute (GRI) on cased and uncased pipelines under highways and railroads (1987-93) that designed, built, and installed by auger boring 300-mm and 1000-mm nominal diameter high pressure (7 MPa) highly instrumented pipelines under the test railroad track at the U.S. Transportation Test Center, Pueblo, CO to collect data for scores of thousands of repetitive train loads; developed software packages for the design of pipeline crossings of highways and railroads distributed by GRI; and changed US practice for pipeline crossings through revisions in railroad standards and guidelines. **3)** Principal investigator (PI) supported by NSF to construct the Cornell Large Scale Lifelines Testing Facility as part of the George E. Brown, Jr. Network for Earthquake Engineering Simulation (NEES), including PI for several multi-institutional research projects using the facility, and co-PI for the maintenance, operation and management of the facility (2002-current). This unique research facility has hosted scores of researchers and developed advanced databases, innovative sensors, and substantially improved characterization of underground infrastructure response to large ground deformation, including the performance of high density polyethylene pipelines being applied by LADWP and the Christchurch City Council in the reconstruction of the Christchurch, NZ water and wastewater distribution systems, unique design of the SFPUC Bay Division Pipeline (30% of San Francisco water supply) crossing of the Hayward Fault, and verification and quantification of the capabilities of in situ trenchless pipe lining technologies to retrofit existing lifelines against earthquake effects. **4)** Co-principal investigator and Chair of Executive Committee of Institute for Civil Infrastructure Systems (1998-03), supported by NSF. The Institute was headquartered at the Wagner School of Public Service at New York University, and developed guidelines and policy for infrastructure planning and construction through multi-disciplinary interaction among engineers and applied social scientists, including planners

and economists. Research was undertaken for the Institute on the effects of the World Trade Center Disaster (9/11) on the New York City (NYC) water supply, electric power, telecommunication, and underground transportation networks, which revealed interdependencies among these systems that had never been recognized, contributing to protective measures for infrastructure in New York City and London. **5)** Principal investigator, supported by NSF, of a team of US and Japanese researchers for 20 years (1986-2006) on the effects of earthquake-induced ground failures on underground infrastructure. The collaboration resulted in 7 major workshops with published proceedings containing over 300 papers, 2 volumes of case histories, and many new modeling procedures and experimental findings that have improved the earthquake resistant design of lifeline systems worldwide.

Publications: First or co-author of over 400 papers and published reports, of which approximately 1/3 are in refereed journals. Select published papers include the 2009 Rankine Lecture: "Geohazards and large geographically distributed systems", *Geotechnique*, LX (7), 503-543 and 2005 Peck Lecture: "Lessons learned for ground movements and soil stabilization from the Boston Central Artery", *J. Geotech. & GeoEnviron. ASCE*, 132(8), 966-989. Several papers were selected for awards, including Japan Gas Association Japan Gas Award (2003) for "Large scale experiments on buried steel pipelines with elbows subjected to permanent ground deformation", *J. Str. Mech. & Earthquake Engr.*, JSCE, 20(1), 1s-11s; ICE Trevithick Prize (2002) for "Geotechnical aspects of lifeline engineering", *Proc. Inst. Civil Engrs. Geotech. Engr.*, 149(1), 13-26; EERI Outstanding Paper (1996) for "Earthquake performance of gas transmission pipelines", *Earthquake Spectra*, 13(3), 493-527; ASCE Collingwood Prize (1983) for "Ground movements caused by braced excavations", *J. Geotech. Engr. Div.*, 107(9), 1159-1178; ASTM C.A. Hogentogler Award (1976) for "Measurement of strut loads by means of vibrating-wire strain gages", *Performance Monitoring for Geotechnical Construction*, STP 584, 58-77.

Lectures and Presentations: Since 1995 delivered 180 invited lectures, keynote and conference presentations worldwide. Examples include: EERI Distinguished Lecture "The New Normal for Natural Disasters" presented at 2012 EERI Annual Meeting and 14 other locations, including University of Cambridge and Imperial College. Since 2009, named lectures include Rankine Lecture (British Geotechnical Association), Terzaghi Lecture (ASCE Geo-Institute), UC Berkeley Distinguished Geotechnical Lecture, Sowers Distinguished Lecture (Georgia Tech), Keiwi Lecture (Oregon State Univ.), Milligan Lecture (Queens University), Haley & Aldrich Lecture (Univ. of Massachusetts), Martin S. Kapp Lecture (ASCE NYC Met Section), Lovell Lecture (Purdue Univ.), Lee Lecture (ASCE Los Angeles Section), UC Davis Distinguished Lecture, Hilf Lecture (Univ. of Colorado), Shaw Lecture (Stanford Univ.), Richart Lecture (University of Michigan). Kersten Lecture (University of Minnesota), and 25 keynote lectures at conferences. Presented on behalf of NAE, CEATS Convocation (2011), and gave a lecture at RAE (2011) on "Critical Infrastructure, Hazards, and Sustainability" and keynote address at Royal Bank of England (2005) on "Complex Network Interdependence". Selected as 2013 ASCE Geotechnical Touring Lecturer and 2018 Cross Canada Lecturer.

I. M. Idriss
Consulting Geotechnical Engineer
PO Box 32027
Santa Fe, New Mexico 87594
Cell: (505) 231-3111
email: imidriss@aol.com

T. D. O'Rourke
Geotechnical Consultant
10 Twin Glens Road
Ithaca, New York 14850
Cell: (607) 227-0644
email: tdo1@cornell.edu

June 23, 2020

Bristol Bay Reserve Association
Fishermen's Center Bldg.
1900 W. Nickerson, Ste. 320
Seattle, WA 98199

Gentlemen:

Subject: *Review of Stability Analyses of the Main Embankment completed by Knight Piésold
Pebble Mine Project*

1.0 INTRODUCTION

The purpose of this report is to summarize our review of portions of the material included in the file named "RFI 008g.pdf" pertaining to the Pebble Mine Project currently under review by the U.S. Army Corps of Engineers (USACE) and other state, federal, and tribal entities.

File "RFI 008g.pdf", which we received on June 5, 2020, included the material listed below:

- Memorandum covering "Main Embankment Stability Assessment – Static and Post-liquefaction", prepared by Knight Piésold Ltd., Vancouver, Canada, for Pebble Limited Partnership, dated July 8, 2019. For ease of reference, this memorandum will be referenced as "2019 KP Memo".
- Knight Piésold's responses to questions and/or requests for information by the USACE. For ease of reference, this memorandum will be referenced as "2019 KP Responses".

Our reviews of the 2019 KP Memo and the 2019 KP Responses are presented below in Section 2.0 and Section 3.0, respectively.

2.0 REVIEW OF THE 2019 KP MEMO

This memorandum presents the results of stability analyses for the Main Embankment considering the section shown in Figure 1. In the Knight Piésold's analyses, the embankment is considered to have the same properties throughout, i.e., no zoning. It is noteworthy that the properties of the triangular portions of Zone U ("*part of upstream shell founded on the starter dam*", as stated in page 1 in the 2019 KP Memo) cannot be assumed to be the same as the main body of the embankment. These triangular portions will be placed and then compacted over the tailings beach, which will preclude, especially in the lower lifts, achieving the same degree of compaction as the main parts of the embankment. Therefore, the shear strength parameters for these triangular zones will be less than those assumed by Knight Piésold (Table 3.1 in the 2019 KP Memo).

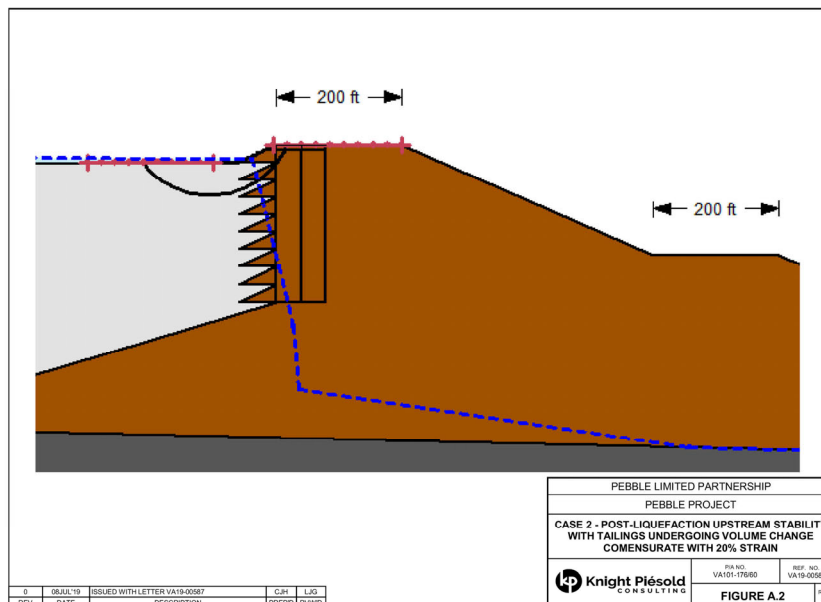


Figure 1 Cross section of main embankment showing critical surface calculated by KP
[Figure A-2 in the 2019 KP Memo; note that the title is not correct!]

Similarly, the phreatic surface (shown as the dashed blue line in all the figures in the 2019 KP Memo, including Figure A-2 above) is difficult to justify. The 2019 KP Responses includes the following statement: "The current embankment concept is a flow through rockfill embankment with filter and transition zones within the embankment." However, no information is provided about the characteristics of either the filter or the transition zone. Knight Piésold needs to provide justification as to why the phreatic surface is not far closer to a horizontal line and much closer to the crest of the embankment if the design will result in "a flow through rockfill embankment".

The overestimation of shear strength in the triangular portions of Zone U as well as the unsupported phreatic surface increases the safety factor against sliding in ways that are misleading and counterproductive for the Tailings Storage Facilities design. In our opinion the results of the stability analyses presented in the 2019 KP Memo are unusable to assess the safety of the proposed design.

Furthermore, we have not seen results of any geochemical waste rock investigation. Waste rock is proposed as rockfill to build the embankment. It is essential that investigations be completed to assess whether the waste rock is a potential acid generating material, thus making its use as rockfill unacceptable without major revisions in the design.

3.0 REVIEW OF THE 2019 KP RESPONSES

Part of File RFI 008g.pdf includes questions and/or requests for information that had been raised by the USACE as well as Knight Piésold's response to each. The questions/requests and responses pertain to:

1. Seismic analyses
2. Tailings liquefaction and seismic stability of upstream face
3. Future studies

¹ The title in Figure A-2 in the 2019 KP Responses document actually applies to what is presented in Figure A-1. The correct title for Figure A-2 is the title used in Figure A-1.

With respect to item 1, the 2019 KP Responses document uses the earthquake ground motions Knight Piésold had obtained in the seismic hazard analyses (SHA) inappropriately. The earthquake ground motions obtained in the SHA represent the motions at a rock outcrop at the mine site and definitely not the seismic response of the embankment. The large embankments will alter dynamically the bedrock motions so that the embankment seismic response will differ significantly from the motions used by Knight Piésold.

Even more problematic, Knight Piésold considered the PGA obtained in the SHA to represent seismic coefficients to be used in evaluating the potential deformations of the embankment.

In response to the USACE request: "Provide information regarding propagation of bedrock acceleration through the embankment and tailings for each of the four design earthquakes", Knight Piésold provided the following response:

"Seismic displacement analysis were performed using the Bray method. The Bray method considers the earthquake magnitude, the natural period of the dam structure (related to dam height and stiffness) and the spectral acceleration of the earthquake motion when estimating the seismic deformations. Therefore, the unique response spectrum defined for each design earthquake is considered in the analyses ..."

This response does not address the request for information.

To use the Bray and Travasarou² method requires calculating the yield coefficient, k_y , which is the seismic coefficient that results in a factor of safety of one when applied to a selected segment (sometimes referred to as a wedge or sliding mass like the green portion shown in Figure 2 below). The last 8 pages of the 2019 KP responses include calculations of the yield coefficient for the wedge shown in Figure 2.

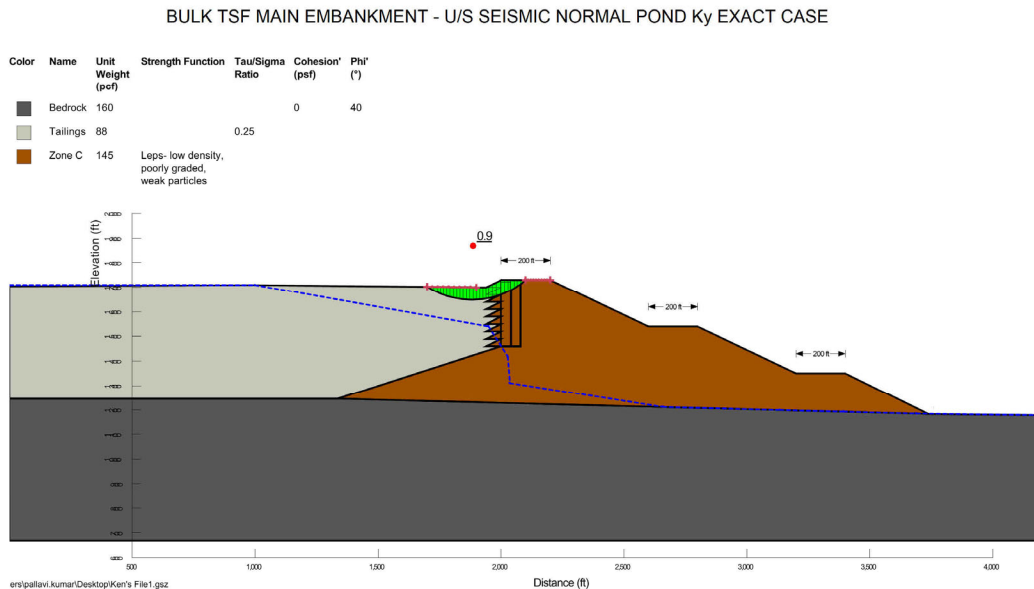


**Figure 2 Wedge for which k_y is calculated by KP
[from the 2019 KP Responses document]**

² Bray, J. D. and Travasarou, T. (2007). "Simplified procedure for estimating earthquake induced deviatoric slope displacements", Journal of Geotechnical and Geoenvironmental Engineering, ASCE, Vol. 133, No. 4, April 2007.

The phreatic surface (the blue dashed line in Figure 2) used in this calculation is impossible to justify. In addition, the use of the same shear strength parameters for the entire embankment is not justifiable, as noted in Section 2 above. These aspects render these calculations unusable to obtain values of k_y for this or any other wedge in the embankment-tailings.

Item 2 of the Knight Piésold responses above has been addressed in part by Section 2 of this report. Another item to consider for the embankments is deformation caused by liquefaction. As discussed in our report of June 19, 2020 on the subject of "*Review of Seismic Hazard Studies, Pebble Mine Project*", liquefaction triggering and ensuing ground deformation are important issues that need to be part of the assessment of the proposed Pebble Mine site, lifelines, and port facilities. Based on what we have reviewed, we have not seen evidence that liquefaction triggering and ground deformation after liquefaction have been considered appropriately in any of Knight Piésold's reports and responses.

With respect to item 3 above, the 2019 Knight Piésold responses outline a number of studies to be completed as part of future studies. In particular, the responses indicate that an "*Initial Design Package*" for the tailings facilities would be submitted by the end of 2019. We are not aware that such a submittal had been made.

4.0 EMBANKMENT MATERIALS

We were provided on June 22, 2020 with a copy of the document titled "Pebble Project Definition", prepared by Pebble Limited Partnership and updated December 2019. This document provides description of the project and includes the following statement, in Section 3.4.4, that is particularly relevant to the stability of the embankments.

"The embankments will be constructed using suitable rockfill or earthfill materials, including quarried rock, NPAG and non-ML waste rock excavated from the open pit, if available, and stripped overburden." NPAG is "non-potentially acid generating" and ML is "metal leaching", as defined in the Acronyms and Abbreviations Section of the Pebble Project Definition Report.

Thus, it is possible that major portions of the embankment may consist of earthfill and entirely of rockfill as had been used in the 2019 KP Memo and the 2019 KP Responses documents covered in Sections 2 and 3 of this report. Thus, not only the strength of the rockfill in the triangular zones but also in other major parts of the embankment can be lower than assumed by Knight Piésold, thus rendering the stability analyses even less supportable.

The statement in Section 3.4.4 the Pebble Project Definition Report emphasizes the need to complete appropriate geochemical investigations of the rock to be obtained from quarries and the pit to assess whether these rocks are potentially acid generating or metal leaching. These investigations are important during the permit review process and should not be delayed until construction, as intimated in Section 6 of the Pebble Project Definition Report.

5.0 CONCLUDING REMARKS

The information included in the 2019 KP Memo and in the 2019 KP Responses have serious limitations:

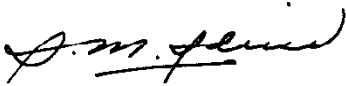
1. The same shear strength parameters are assigned to the entire embankment, including the triangular portions of the upstream face of the embankment. This results in an overestimate of the shear strength of these triangular portions.
2. The phreatic line used in the static and post-liquefaction stability calculations is unsupportable.
3. The phreatic line used in the yield coefficient, k_y , calculations is likewise unsupportable.
4. Major portions of the embankment could consist of earthfill whose shear strength would be overestimated using the strength parameters for rockfill.

Because of these limitations, we do not believe that these two documents provide sufficient information to judge the stability of the proposed tailings facility under static or earthquake loading conditions.

Furthermore, we have not seen results of any geochemical investigations. It is essential that appropriate geochemical investigations be completed to assess whether the quarried and waste rock are potential acid generating and/or metal leaching materials, thus making its use as rockfill unacceptable without major revisions in the design. These investigations are important during the permit review process and should not be delayed until construction, as intimated in Section 6 of the Pebble Project Definition Report.

We are pleased to be of assistance in making this review.

Sincerely,



I. M. Idriss



T. D. O'Rourke